Nonlinear Evolution in High Energy QCD

Emil Avsar

Department of Theoretical Physics
Lund University

Thesis for the degree of Doctor of Philosophy

Thesis Advisor: *Gösta Gustafson*
Faculty Opponent: *Larry McLerran*

To be presented, with the permission of the Faculty of Science of Lund University, for public criticism in lecture hall F of the Department of Theoretical Physics on Friday, the 26th of October 2007, at 10.15.

Organization
LUND UNIVERSITY
Department of Theoretical Physics
Sölvegatan 14A
SE–223 62 LUND
Sweden

Document name
DOCTORAL DISSERTATION
Date of issue
September 2007
Subject designator
Project name
Sponsoring organization

Author
Emil Avsar

Document title
Nonlinear Evolution in High Energy QCD

Abstract
QCD at very high energies is still not very well understood. Difficulties arise from a strong non-linear dynamics and also from nonperturbative physics. Detailed analytic calculations are often only possible either for simple toy models, or for asymptotically high energies.
In this thesis we investigate the high energy dynamics, with the goal of finding a realistic, working model for high energy QCD. We develop a phenomenological model based on the QCD dipole formalism. The model includes contributions both from saturation and unitarisation, and also from non-leading effects such as energy conservation and running coupling. The model is implemented in a Monte Carlo simulation, and is able to reproduce data from high energy processes relevant for the LHC.

Summary in Swedish

QCD vid höga energier är fortfarande inte väl förstådd. Svårigheter uppkommer ifrån en starkt icke-linjär dynamik, samt från icke-strörningsmässiga fenomen. Analytiska beräkningar är oftast möjliga enbart för enkla leksaksmodeller, eller för asymptotiska energier.
I denna avhandling undersöker vi dynamiken i högenergiprocesser, med målet att finna en fungerande och realistisk modell för högenergi-QCD. Vi utvecklar en fenomenologisk modell för högenergi-QCD baserad på QCD-dipolformalismen. Modellen inkluderar bidrag både från saturering och unitarisering, samt från icke-ledande effekter såsom energibevaring och löpande koppling. Modellen implementeras i en datorsimulering, och lyckas reproducera högenergidata.

Key words
Small-x physics, saturation, unitarity, dipole model, DIS

Classification system and/or index terms

Supplementary bibliographical information
Language
English

ISSN and key title
ISBN
978-91-628-7224-3

Recipent's notes
Number of pages
228
Price
Security class

DOKUMENTDATABLAD
enl SIS 61 41 21

Distributor
Emil Avsar
Department of Theoretical Physics, Sölvegatan 14A, SE–223 62 Lund, Sweden

Signature _____ Date 2007-09-12

This thesis is based on the following publications:

I Emil Avsar, Gösta Gustafson and Leif Lönnblad,
Energy Conservation and Saturation in Small-x Evolution
JHEP **07** (2005) 062, hep-ph/0503181.

II Emil Avsar, Gösta Gustafson and Leif Lönnblad,
Small-x Dipole Evolution Beyond the Large N_c Limit
JHEP **01** (2007) 012, hep-ph/0610157.

III Emil Avsar and Gösta Gustafson,
Geometric Scaling and QCD Dynamics in DIS
JHEP **04** (2007) 067, hep-ph/0702087.

IV Emil Avsar,
On the Dipole Swing and the Search for Frame Independence in the Dipole Model
Submitted to JHEP, arXiv:0709.1371, LU-TP 07-09.

V Emil Avsar, Gösta Gustafson and Leif Lönnblad,
Diffractive Excitation in DIS and pp Collisions
Submitted to JHEP, arXiv:0709.1368, LU-TP 07-25.

Contents

The history of a physicist's life was very simple. He was born; he became interested in physics in some way, either through reading or through the personal influence of a teacher or a lecturer; he wrote his thesis and received his PhD degree; he died. The rest and essential part of this biography could be read only in the scientific journals, in which were described his own work and the work of his students and colleagues. It was an eminently satisfactory life, to my mind the only serious occupation for a gentleman. The drama in which he played his role was epic in quality: the drama of man's unfolding discovery of the world in which he finds himself... The stage on which he played his role was the globe...He had no counterpart to the art critic, the music critic, the literary critic, or the dramatic critic to plague him. No one stood between him and his public because his public were his colleagues. With all the fringe benefits I have tried to describe so alluringly, you will not be surprised to find out that his actual take-home pay was not large. Plain living and high thinking were the order of the day.

— Isidor Isaac Rabi

i

Introduction

i.1 Introduction to QCD

This thesis deals with phenomena within the high energy limit of Quantum Chromodynamics (QCD). QCD is the quantum theory of the so-called strong force (or sometimes strong nuclear force) which is one of the four fundamental forces of nature. Despite the fact that there is no longer any doubt whether QCD, which was formulated some three decades ago, is the correct theory for the strong force, there is nevertheless good reason for why there still exists so many people working in the field. The problem is that QCD is still not a theory which is completely understood and it is extremely difficult, if not impossible, to derive some of the fundamental properties of the strong force directly from the basic principles of the theory.

In many cases one has to resort to so-called phenomenological models, which are models based on principles believed to hold (principles derived from what we observe) in the theory but which cannot be rigorously derived from first principles. The main objective of such models is to describe the various phenomena which we observe, and in order to fulfill this objective one has to make simplifying assumptions which, strictly speaking, cannot be proven from the fundamental theory. One example is the celebrated Lund string fragmentation model [1] which describes how the basic constituents of QCD (quarks and gluons) regroup themselves into the particles (such as protons and neutrons etc.) which we observe in our detectors.

Another possibility is to use effective theories which are theories constructed to work only in a certain energy range, or distance scale. One example is Chiral Perturbation Theory which describes strong phenomena in the low energy limit. Another possibility is to use the so-called Lattice Gauge Theory where one discretizes spacetime into a four dimensional lattice.

All the theories mentioned above have the property that they are either entirely based on, or that they contain, physics which we cannot calculate using standard perturbation theory. With standard perturbation theory we mean approximate calculations based on expanding the relevant quantities in

the coupling strength of the theory. For such calculations to be reliable, the coupling constant, denoted α, must be a small quantity. For example, in the quantum theory of electromagnetism (Quantum Electrodynamics, or QED for short) the coupling constant, also called the fine structure constant, is given by $\alpha_{em} = \frac{e^2}{4\pi\hbar c} \approx \frac{1}{137}$ where e is the fundamental electric charge, $\hbar$ is Planck's constant and c is the speed of light in vacuum. This is indeed a small number, and predictions from perturbative QED are experimentally verified to an astonishing accuracy.

QCD is however a much more complicated theory than QED. Here the nonperturbative physics plays an important role, which is why there are so many additional models we have to use if we want to make any reliable predictions.

One of the cornerstones in the understanding of the strong force was the discovery of asymptotic freedom by Gross, Wilzcek and Politzer. Asymptotic freedom states that the strong coupling strength α_s vanishes asymptotically as the relevant energy scale of a process gets very large. In other words, for very small distances, the quarks will behave as if they were free particles, despite the fact that they interact "strongly" with each other. This means that one can actually use perturbation theory for processes involving large momentum transfers, *i.e.* processes occurring at short distance scales. Such calculations have indeed been able to describe strong phenomena rather well, as is evident from the success of the so-called DGLAP equations in perturbative QCD, although we are still far away from the precision levels offered by QED.

For large distance scales, the strong force exhibits a behaviour known as confinement. Confinement is the property that the basic quantities of the strong force are confined in colourless objects, hadrons, which implies that it is not possible to observe any free quarks. Confinement is yet to be proven from QCD, but all experimental evidence collected so far support this picture. The key feature of confinement is that the colour electric field between two colour charges has the shape of a flux tube stretched between the charges. This is to be contrasted to the usual electromagnetic field which stretches out over all space. Confinement would follow in case the field strength between two charges is a constant, since this implies that the potential increases linearly with the distance, and it would consequently require an infinite amount of energy to completely separate two colour charges.

One possible explanation for confinement is that the QCD vacuum (the gluon condensate) forms a dual superconductor. A dual superconductor is a superconductor in which the roles of the electric and magnetic fields are reversed. Consider a static $q\bar{q}$ pair inside such a dual superconductor. The Meissner effect then attempts to expel the colour-electric field, just as it tends to expel the magnetic field in a usual superconductor. Due to Gauss' law, however, the colour-electric field cannot be completely expelled. The field would

instead be compressed into a narrow flux tube, occupying a minimal space, which joins the quark and the antiquark along a line. The colour-electric field runs parallel to the flux tube, maintaining a constant profile in the transverse direction, while the colour-magnetic field circulates around the flux tube. This would then give rise to the confining force mentioned above, thus providing a mechanism for confinement. There are, however, various other problems with this approach, but this is not really the subject of this thesis.

i.2 High Energy Particle Reactions

After a brief introduction to the general concepts in QCD and the strong force, we now move on to study the strong interaction in more detail. We will start by giving an historical introduction to the strong interactions and to the theories which were developed before the advent of QCD.

In order to account for the short range of the strong interactions, Hideki Yukawa proposed [2] the existence of the meson which was subsequently discovered in 1947. During the 50's and the 60's, a great zoo of strongly interacting particles emerged from experiments. These discoveries led to the ideas of quarks, gluons and eventually, the formulation of QCD. Before the discovery of asymptotic freedom, and the successful formulation of non-Abelian gauge theories however, it was not at all clear how one could formulate a gauge field theory for the strong interactions.

In those pre-QCD days, lacking an understanding of the underlying dynamics of the strong interactions, people rather tried to formulate phenomenological theories based on a set of fairly reasonable postulates. The hope was then to extract as much information as possible about the strong dynamics using these postulates. The central quantity in this approach is the so-called scattering matrix, or S-matrix. Let us therefore give a definition and brief overview of this quantity. A more detailed account can be found in [3].

i.2.1 The S-Matrix Approach

What happens in collider experiments is that a state is at time $-\infty$ prepared to have some definite particle content, and a measurement is made at time $+\infty$ to see what the outcoming state is. The "in" and "out" states, $|i^{in}\rangle$ and $|f^{out}\rangle$ respectively, are obtained by applying the time evolution operator on the free particle states $|i\rangle$ and $|f\rangle$,

$$|i^{in}\rangle = U(-\infty, 0)|i\rangle, \tag{i.1}$$
$$|f^{out}\rangle = U(\infty, 0)|f\rangle. \tag{i.2}$$

The S-matrix is then the linear operator defined as

$$S_{if} = \langle f^{out}|i^{in}\rangle = \langle f|U(-\infty, \infty)|i\rangle = \langle f|\boldsymbol{S}|i\rangle. \tag{i.3}$$

The probability for the transition $|i\rangle \to |f\rangle$ is given by

$$P_{i\to f} = |\langle f|\boldsymbol{S}|i\rangle|^2, \tag{i.4}$$

and since the sum over all the possibilities must add up to unity, we have

$$\sum_f P_{i\to f} = \sum_f |\langle f|\boldsymbol{S}|i\rangle|^2 = 1. \tag{i.5}$$

Using now the completeness of the free particle states we obtain

$$\sum_f \langle i|\boldsymbol{S}^\dagger|f\rangle\langle f|\boldsymbol{S}|i\rangle = \langle i|\boldsymbol{S}^\dagger\boldsymbol{S}|i\rangle = 1 = \langle i|i\rangle \tag{i.6}$$

for all states $|i\rangle$. Similarly we have $\langle i|\boldsymbol{S}\boldsymbol{S}^\dagger|i\rangle = 1 = \langle i|i\rangle$, and from this we conclude that

$$\boldsymbol{S}^\dagger\boldsymbol{S} = \boldsymbol{S}\boldsymbol{S}^\dagger = \mathbf{1}. \tag{i.7}$$

$\boldsymbol{S}$ is therefore a unitary matrix, which is thus a consequence of the conservation of probability.

The first postulate is the Lorentz invariance of the S-matrix. This means that the S-matrix can be expressed in terms of Lorentz invariant variables. For 2-particle scattering processes, $1+2 \to 3+4$, these are the usual Mandelstam variables u, t and s defined by

$$s = (p_1+p_2)^2 = (p_3+p_4)^2, \tag{i.8}$$
$$t = (p_1-p_3)^2 = (p_2-p_4)^2, \tag{i.9}$$
$$u = (p_1-p_4)^2 = (p_2-p_3)^2. \tag{i.10}$$

From the S-matrix one usually defines two other quantities. The first one is the transition matrix, or T-matrix which is defined as

$$\boldsymbol{S} = \mathbf{1} - i\boldsymbol{T}. \tag{i.11}$$

The unit operator above corresponds to the trivial situation where no interaction takes place. T is therefore a direct measure of the scattering process. The other quantity is called the relativistic scattering amplitude, and is defined by

$$T_{if} = (2\pi)^4\delta(p_f^{tot} - p_i^{tot})A(i \to f), \tag{i.12}$$

where we have thus extracted the total four momenta conserving delta function from T.

From the unitarity of the S-matrix it now follows immediately that

$$\begin{aligned}(\mathbf{1} - i\boldsymbol{T})(\mathbf{1} + i\boldsymbol{T}^\dagger) &= \mathbf{1}\\ \Rightarrow i(\boldsymbol{T}^\dagger - \boldsymbol{T}) &= \boldsymbol{T}^\dagger\boldsymbol{T}.\end{aligned} \tag{i.13}$$

Taking the matrix elements with respect to $\langle f|$ and $|i\rangle$ we obtain

$$\langle f|i(\boldsymbol{T}^\dagger - \boldsymbol{T})|i\rangle = \sum_n \langle f|\boldsymbol{T}^\dagger|n\rangle\langle n|\boldsymbol{T}|i\rangle, \tag{i.14}$$

that is

$$2\mathrm{Im}T_{if} = \sum_n T^*_{fn} T_{in}. \qquad (i.15)$$

For the scattering amplitude A we instead get

$$2\mathrm{Im}A(i \to f) = (2\pi)^4 \sum_n A^*(f \to n) A(i \to n) \delta(p_n^{tot} - p_i^{tot}). \qquad (i.16)$$

If now the initial and final states are the same we obtain

$$2\mathrm{Im}A(i \to i) = (2\pi)^4 \sum_n |A(i \to n)|^2 \delta(p_n^{tot} - p_i^{tot}) = \mathcal{F}\sigma_{tot}, \qquad (i.17)$$

where $\mathcal{F}$ is the incoming flux and σ_{tot} is the total cross section. This is the famous optical theorem which states that the total cross section is given by (modulo the flux factor) the imaginary part of the forward scattering amplitude, *i.e.* the elastic amplitude. Thus, in order to calculate the total cross section, one does not need to sum all possible matrix elements, but it is enough to only calculate a single matrix element, namely the elastic part of the scattering amplitude.

The second postulate is that the S-matrix is an analytic function of Lorentz invariant variables. This is a nontrivial property and it turns out to have important consequences. In quantum mechanics it can be shown that the analyticity of the S-matrix follows from causality, but this has not really been proven in relativistic S-matrix theory.

The amplitude A is usually written as a function of s and t, $A(s,t)$, and one can then study the singularity structure of A in the complex s plane. The singularities of the scattering amplitude on the real axis corresponds to the physical thresholds for real particle production. For example, there will be simple poles corresponding to the exchange of physical particles. In perturbation theory, such singularities arise from the propagator

$$\frac{1}{s - m^2 + i\epsilon}. \qquad (i.18)$$

In addition to this, there will be branch points corresponding to exchange of two or more particles.

As seen above, unitarity relates the imaginary part of the amplitude to a sum over other amplitudes, and using analyticity one can reproduce the real part of the amplitude from the imaginary part (via so-called dispersion relations).

In a similar way one can study the singularity structure in the complex t and u planes. All these planes are related to each other via the so-called

crossing symmetry which is an additional postulate in S-matrix theory, but is known to hold in perturbative field theory.

There are two very important consequences of the S-matrix approach. The first one is the Froissart-Martin Theorem [5, 6] which states that:
Assume that there exists a positive integer N such that the scattering amplitude, $A(s,t)$, satisfies $A/s^N \to 0$ as $s \to \infty$. It then follows that the total cross section cannot grow faster than $\ln^2 s$ as $s \to \infty$.
This means that we have

$$\sigma_{tot} \leqslant C \cdot \ln^2 s \quad \text{as} \quad s \to \infty. \tag{i.19}$$

It can be shown that

$$C \approx \frac{\pi}{m_\pi^2} \approx 60\text{mb}, \tag{i.20}$$

with m_π being the pion mass.

The second theorem is the Pomeranchuk theorem [7] which states that:
In any scattering process where there is a charge exchange the cross section vanishes as $s \to \infty$. Conversely, if for a scattering process σ_{tot} does not fall as s increases, then that process must be dominated by the exchange of vacuum quantum numbers.
Thus, if the cross sections are not falling as s increases, this is equivalent to saying that, asymptotically, the total cross sections for particle-particle and particle-antiparticle reactions must become equal, that is

$$\frac{\sigma_{tot}(PP)}{\sigma_{tot}(P\bar{P})} \to 1 \quad as \quad s \to \infty. \tag{i.21}$$

From this theorem we now move on to the idea of Regge poles.

i.2.2 Regge Theory

Consider the scattering of an incident particle on some arbitrary potential V. For a spherically symmetric V, it is in non-relativistic quantum mechanics well known that one can expand the scattering amplitude f in a partial wave series,

$$f(k,\theta) = \sum_{l=0}^{\infty} (2l+1) a_l(k) P_l(\cos\theta). \tag{i.22}$$

Here θ is the polar angle of the outgoing wave, k is the wave vector and P_l are the Legendre polynomials. The coefficients $a_l(k)$ are called the partial wave amplitudes. The bound states of the potential V then appear as the singularities of these amplitudes.

The idea in Regge theory is that one can analytically continue $a_l(k)$ to complex values of l. The emerging function $a(l,k)$ reduces to $a_l(k)$ for positive

integer values of l. For most potentials, the singularities of $a(l,k)$ turn out to be simple poles which depend on k,

$$l_{\text{pole}} = \alpha(k). \tag{i.23}$$

As k varies these poles trace out trajectories in the complex l plane, known as *Regge trajectories*.

Of course, for scattering off a potential, we know in non-relativistic quantum mechanics the underlying dynamics of the scattering process. This is given by the Schrödinger equation from which we can deduce the partial wave amplitudes, and study the singularity structure for a given potential. In Regge theory (and the S-matrix approach) on the other hand, we do not have knowledge about the underlying dynamics of the strong force, and we can therefore strictly speaking not prove the existence of Regge poles.

The existence of Regge poles is therefore a conjecture in this approach. However, this "simple" conjecture turns out to have some far reaching consequences. In the S-matrix approach we can similarly expand $A(s,t)$ in a partial wave series. For a $2 \to 2$ scattering event where all four particles have equal masses m, the relation between t and the angle θ is given by $\cos\theta = 1 + \frac{2t}{s-4m^2}$. Under the assumption that we can analytically continue $A(s,t)$ from positive t ($t = 2k \cdot m$ in (i.23)) to negative [1] t, one can show that Regge theory predicts the following asymptotic form of the scattering amplitude

$$A(s,t) \to \beta(t) s^{\alpha(t)} \ \ as \ \ s \to \infty. \tag{i.24}$$

Here $\alpha(t)$ is the position of the leading Regge pole in the crossed reaction, *i.e.* the pole with the largest real part, and β is the residue of this pole. The exact calculation of this residue would require an understanding of the dynamics of the process, but it is rather amazing that one can come down to such a simple formula using a limited set of postulates! The result derived above is valid in the region where $s \to \infty$ for fixed t, and this is called the Regge limit.

The result in (i.24) can be attributed to the exchange of a particle with "angular momentum" $\alpha(t)$. Of course this cannot be a real particle since the angular momentum must be an integer, and it cannot depend on t. The result rather corresponds to the exchange of a family of resonances which we, using particle physics language, call a *Reggeon*.

Plotting the spins of the low lying mesons against the square of their masses, it is seen that they all lie in a straight lines, *i.e.* one can parameterize the Regge trajectory in the form

$$\alpha(t) = \alpha(0) + \alpha' t. \tag{i.25}$$

[1] According to the postulate of the crossing symmetry mentioned above, the process where s is positive and t negative is described by the same amplitude, $A(s,t)$, as for the process where s is negative and t is positive (the crossed reaction).

The value $\alpha(0)$ is called the Reggeon intercept. Using the optical theorem, this implies that

$$\sigma_{tot} \propto s^{\alpha(0)-1}, \tag{i.26}$$

where the extra factor s^{-1} comes from the flux factor in (*i*.17), which is approximately equal to $2s$ for large s.

Now, in light of the Pomeranchuk theorem stated in the previous section, we see that a Regge pole satisfying $\alpha(0) \geqslant 1$ must carry vacuum quantum numbers (isospin zero, even under charge conjugation). Such a Regge pole is called the *Pomeron*.

Finally we notice that Donnachie and Landshoff [8] found a good fit to the $p\bar{p}$ and pp total cross sections using the following parameterizations

$$\sigma_{tot}^{pp} = (21.7s^{0.08} + 56.1s^{-0.45})\text{mb} \tag{i.27}$$

$$\sigma_{tot}^{p\bar{p}} = (21.7s^{0.08} + 98.4s^{-0.45})\text{mb}. \tag{i.28}$$

Here s is measured in units of GeV^2. The first term on both fits corresponds to the Pomeron with an intercept $\alpha(0) = 1.08$ while the second term corresponds to a Reggeon with an intercept 0.55 which consequently gives a negligible contribution as $s \to \infty$.

i.2.3 The Impact Parameter Picture

So far we have used the Mandelstam variables to characterize the amplitudes and, via the optical theorem, the total cross section. Sometimes it is very useful to switch from a description in momentum space to a description in impact parameter space. This will especially be apparent when we go on to discuss the dipole model and the question of multiple interactions.

Let us first look at the classical scattering of light from an obstacle or, equivalently, the diffraction of light from a hole in an opaque screen. We assume the incoming wave to propagate in the positive z direction, and the screen to lie in the xy plane, centered at the origin. The classical field u_P of the diffracted wave at some point P is given by

$$u_P = \frac{k}{2\pi i} \int dxdy \; u \, \frac{e^{ikR}}{R} \tag{i.29}$$

Here u is the field value calculated at the area element $dxdy$, R is the distance from the area element to the point P, and the integration is performed over the extent of the screen in the xy plane. We refer to the xy plane as the transverse plane, and we will from now on denote $dxdy$ by $d^2\boldsymbol{b}$.

In the case of Fraunhofer diffraction, the distance to the screen on which we observe the light is assumed to be very much larger than the dimensions

of the hole, which in turn is assumed to be much larger than the wavelength of the incident wave. This is actually the most relevant case for high energy particle reactions.

Defining the momentum transfer $\boldsymbol{q} = \boldsymbol{k}' - \boldsymbol{k}$ and denoting the distance from the origin to the point P by r we get

$$u_P \approx \frac{u_0 k}{2\pi i}\frac{e^{ikr}}{r}\int d^2\boldsymbol{b} T(\boldsymbol{b}) e^{-i\boldsymbol{q}\cdot\boldsymbol{b}}. \tag{i.30}$$

Here u_0 denotes the field value at the origin, and we have defined the so-called profile function T, which in the simple case of a hole is just given by 1 inside the hole while it is equal to 0 outside the hole. For scattering through general obstacles it will, however, be a more complicated function.

To make the analogy to particle physics, we make use of *Babinet's principle*, which states that complementary screens give the same intensity distribution for the diffracted light [9]. The field u_P produced by an opaque disc of the same dimensions as our hole is therefore given by

$$\begin{aligned} u_P &= \frac{u_0 k}{2\pi i}\frac{e^{ikr}}{r}\int d^2\boldsymbol{b}(1 - T(\boldsymbol{b})) e^{-i\boldsymbol{q}\cdot\boldsymbol{b}} \\ &\equiv \frac{u_0 k}{2\pi i}\frac{e^{ikr}}{r}\int d^2\boldsymbol{b}\, S(\boldsymbol{b}) e^{-i\boldsymbol{q}\cdot\boldsymbol{b}}, \end{aligned} \tag{i.31}$$

since the sum of these waves adds up to give the incident wave, $u_0 e^{ikz}$. This can be seen by writing $r \approx z + (1/2z)(x^2 + y^2)$ in the exponent in (i.29). In (i.31), S is the analog of the S-matrix defined earlier, while T is the analog of the T-matrix (or rather iT). If all the light falling in on the obstacle is completely absorbed we have $S = 0$ and $T = 1$, while if we have a completely transparent screen $S = 1$ and $T = 0$.

We note that the scattered wave in (i.31) can be written as

$$u_P = u_{in} + u_0 \frac{e^{ikr}}{r} f(\boldsymbol{q}), \tag{i.32}$$

$$f(\boldsymbol{q}) \equiv -\frac{k}{2\pi i}\int d^2\boldsymbol{b}\, T(\boldsymbol{b}) e^{-i\boldsymbol{q}\cdot\boldsymbol{b}}. \tag{i.33}$$

Thus f corresponds to the scattering amplitude. The scattering cross section is then given by

$$\begin{aligned} \sigma_{scatter} &= \int d^2\boldsymbol{q}\, \frac{|f(\boldsymbol{q})|^2}{k^2} \\ &= \int d^2\boldsymbol{b}\, |T(\boldsymbol{b})|^2 = \int d^2\boldsymbol{b} |1 - S(\boldsymbol{b})|^2. \end{aligned} \tag{i.34}$$

This is not the total cross section, however, since the wave can also be absorbed, and the absorption cross section is given by

$$\sigma_{absorb} = \int d^2\boldsymbol{b}(1 - |S(\boldsymbol{b})|^2). \tag{i.35}$$

The total cross section is finally given by the sum of the scattering and absorption cross sections,

$$\sigma_{tot} = 2\int d^2\boldsymbol{b}\,\mathrm{Re}(1 - S(\boldsymbol{b})) = 2\int d^2\boldsymbol{b}\,\mathrm{Re}T(\boldsymbol{b}). \tag{i.36}$$

i.2.4 The Eikonal Approximation

In the limit of vanishing wavelengths, propagating waves can be described in terms of rays, and the laws of their propagation constitute the domain of geometrical optics. The field of a propagating wave can be written in the form

$$\phi = u(\boldsymbol{r}, t)e^{i\psi(\boldsymbol{r},t)}, \tag{i.37}$$

where ψ is the phase of the wave. This situation is realized in high energy particle interactions when the wavelength of the incoming particle is much smaller than the interaction range. Solving the Schrödinger equation one obtains, after a number of manipulations and definitions [10], a scattering amplitude of the form

$$f(k, \theta, \phi) = -\frac{k}{2\pi i}\int d^2\boldsymbol{b}\, e^{-i\boldsymbol{q}\cdot\boldsymbol{b}}(1 - e^{i\chi(\boldsymbol{b})}). \tag{i.38}$$

Here the phase $\chi(\boldsymbol{b})$ is called the eikonal function, and is given by the integral of the potential over the longitudinal direction. If we define S by

$$S(\boldsymbol{b}) \equiv e^{i\chi(\boldsymbol{b})}, \tag{i.39}$$

we obtain exactly the same formulas as for the diffractive (i.34) and the inelastic (i.35) cross sections above.

Before finishing this chapter we will give an example of the use of the eikonal approximation in particle physics. However, we first note that the optical theorem (i.17), and relation (i.15), show that every open inelastic channel contributes to the imaginary part of the scattering amplitude. As $s \to \infty$, more and more inelastic channels open up, contributing to the imaginary part of the amplitude. For the real part of the amplitude no similar relation exists, and it is then reasonable to expect that the imaginary part of the scattering amplitude dominates over the real part in the high energy limit. (This implies a predominantly real S-matrix) This assumption is indeed supported by experimental results.

Consider a high energy particle, say a hadron h, impinging on a nucleus A. In this case the hadron can undergo multiple rescatterings with the nucleons inside the nucleus. If we assume each hadron-nucleon collision to be uncorrelated we obtain

$$S_A = \exp(i\chi_A) = \exp(i\sum_{i=1}^{A}\chi_{N_i}) = \prod_{i=1}^{A} S_{N_i}. \tag{i.40}$$

Here S_{N_i} is the S-matrix for the collision between h and the nucleon N_i. In case S is real, as mentioned above, the phase factor χ will be purely imaginary. For high energy scattering one can write $\chi = i\Delta$, and in that case we have $S = \exp(-\Delta)$.

Denote the profile function of nucleon N_i by f_i, which is actually the Fourier transform of the imaginary part of the forward scattering amplitude. It can here be interpreted as the absorption probability of the projectile particle as it travels through the nucleon[2]. In the eikonal approximation we assume that h follows the same trajectory after each scattering. This means that the simultaneous scattering of h on nucleons i and j is given by $f_i f_j$.

Assume first, for simplicity, that the nucleus consist only of 3 nucleons. In that case the sum of the profile functions is given by $f_1 + f_2 + f_3$. In order to avoid double counting, however, we must from this expression subtract the events where h scatters off two of the nucleons. This means that we get $f_1 + f_2 + f_3 - f_1f_2 - f_1f_3 - f_2f_3$. However, we must also not oversubtract which is why we should add to this the possibility that h scatters off all three nucleons. For the total profile function $T(\boldsymbol{b})$ we then have

$$T = f_1 + f_2 + f_3 - f_1f_2 - f_1f_3 - f_2f_3 + f_1f_2f_3. \tag{i.41}$$

This expression is equal to

$$T = 1 - (1-f_1)(1-f_2)(1-f_3), \tag{i.42}$$

$$S = (1-f_1)(1-f_2)(1-f_3), \tag{i.43}$$

and if the f_i's are assumed to be small we have

$$S \approx \prod_i \exp(-f_i) = \exp(-\sum_i f_i). \tag{i.44}$$

This expression is equal to (i.39), with a purely imaginary eikonal function. Using expression (i.36) for the total cross section, we then get

$$\sigma_{tot} = 2\int d^2\boldsymbol{b}(1 - \exp(-\sum_i f_i)), \tag{i.45}$$

which is an expression we will run into several times.

[2]Note that the optical theorem (i.17) relates the imaginary part of the amplitude to a sum over probabilities so that this quantity can both be seen as an amplitude and as a probability.

i.3 The High Energy Limit of QCD

Having reviewed high energy reactions during pre-QCD times, we will in this section go on to review the advancements in the field made within the framework of QCD. First, however, we will briefly describe an experiment which has been providing us with a lot of data which offer many tests of perturbative QCD, namely DIS.

i.3.1 Deep Inelastic Scattering

Consider the scattering of electrons on protons. The reaction looks something like this:

$$e^-(k) + p(P) \to e^-(k') + X(P_X). \tag{i.46}$$

Here we have an incoming electron with momentum k which scatters off a proton with momentum P. What comes out is the electron with momentum k' and a hadronic system X with momentum P_X. In case X is just a proton, the process is elastic.

The momentum exchange between the electron and the proton is mediated via electromagnetic interactions, and what happens is that the electron emits a virtual photon γ^* with momentum $q = k - k'$, which is then absorbed by the proton.

Experiments of this type were first performed during the 60's at SLAC (the SLAC-MIT experiment), and it was observed that for most events the mass of the system X is much larger than the proton mass [11]. In this case we call the process Deep Inelastic Scattering (DIS). DIS offers a direct study of the structure of the proton, and therefore a great possibility to test many predictions from perturbative QCD. The constituents of the proton (the quarks and the gluons) are collectively referred to as *partons*. For the last decade or so, DIS experiments have been performed in great detail at the HERA accelerator at DESY, and many interesting results have emerged [12, 13]. A picture of a DIS process is shown in figure *i*.1.

DIS is usually described in terms of three variables. One of these is the energy of the incoming electron which is fixed by the experimental set up. The other two are usually chosen among the following variables[3]

$$Q^2 = -q^2 > 0, \tag{i.47}$$

$$W^2 = (P+q)^2, \tag{i.48}$$

$$x = \frac{Q^2}{2P\cdot q} = \frac{Q^2}{W^2 + Q^2 - m_p^2} \approx \frac{Q^2}{W^2}. \tag{i.49}$$

[3]There exists two more variables which one usually defines, but we will in this thesis never make use of them so we do not write them here.

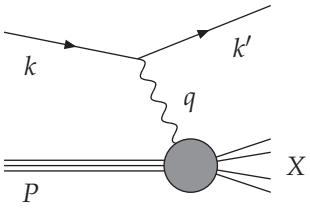

Figure *i*.1: Deep Inelastic Scattering.

Here W^2 is the cms energy of the $\gamma^* p$ system and Q^2 is the virtuality of the photon. The variable x is usually called the Bjorken variable and is sometimes denoted by x_{Bj}. In the last line we have neglected Q^2 and m_p^2 compared to W^2, which usually is a very good approximation, as for most experiments at HERA we have $W \approx 160 - 240$ GeV while $Q^2 < 100$ GeV^2.

The high energy limit, or Regge limit, corresponds to fixed Q^2 and large W^2 so that $x << 1$. This region is thus also referred to as the small-x region. The HERA accelerator has been able to probe values of x down to 10^{-4} for $Q^2 \approx$ few GeV^2. It is most common to describe DIS events in x and Q^2.

One of the most striking features of the small-x region in DIS is the observation that the gluon density in the proton, usually denoted $xg(x, Q^2)$, increases steeply as x gets smaller. We will below see that this is actually what QCD predicts.

i.3.2 QCD Reggeization

A particle is said to reggeize if the amplitude for a process involving the exchange of that particle goes like

$$A \propto s^{\alpha(t)} \quad as \quad s \to \infty, \tag{*i*.50}$$

and an interesting question in QCD is whether or not the gluon reggeizes.

Now, when calculating Feynman diagrams in the Regge limit care has to be taken to the fact the perturbation series may not converge very fast as one goes to higher orders in α_s [4]. The problem is that each factor α_s entering the result is accompanied by a factor $\ln(s/|t|)$, which can indeed be quite large in

[4] The coupling α_s should not be confused with the Regge trajectory $\alpha(t)$.

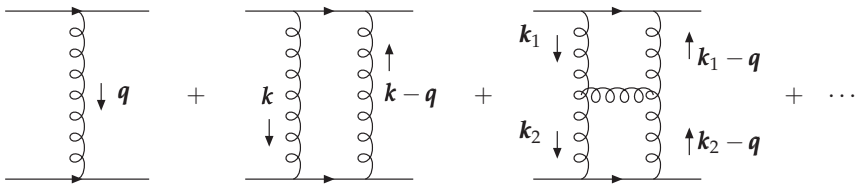

Figure *i*.2: . Feynman diagrams for quark–quark scattering via the exchange of gluons.

the Regge limit. Thus one can have $\alpha_s \ln(s/|t|) \sim 1$, and it is then not enough to stop the calculation at a fixed order in α_s.

These large logarithms come from the phase space integrations in the intermediate states. Such integrations originate from the unitarity relations given in (*i*.16), in which the sum over n also contains phase space integrations.

Obviously it is not possible to calculate the full diagrams to all orders in α_s so one has to make some approximations. The simplest choice is to only keep those terms, to a given order in α_s, which are accompanied by the largest power of $\ln(s/|t|)$. This procedure is known as the *Leading Logarithmic Approximation*, LLA. It turns out that the series one needs to sum up is of the form

$$\sum_n \frac{\ln^n(s/|t|)}{n!} a(t)^n \alpha_s^n = s^{a(t)\alpha_s}. \tag{*i*.51}$$

Summing up the diagrams shown in figure *i*.2 to all orders in perturbation theory, even in the LL approximation, is a formidable task. We will here only cite the result, and for a comprehensive derivation of the results to be presented in this section we refer the reader to [14].

Before quoting the result, we mention some interesting features of the LLA calculation. In this approximation, fermion loops inside the gluon ladder are completely absent. Actually, the only QCD vertex to enter the game, besides the quark-gluon vertices in the coupling to the external quarks, is the 3-gluon vertex. Thus also the 4-gluon vertex is suppressed in this approximation and never enters the calculations. Also, self-energy and vertex corrections do not produce the leading logarithms, and thus these diagrams do not enter the LLA calculations. In the LLA therefore, the coupling is a constant.

Calculating the relevant Feynman diagrams as in figure *i*.2 to all orders, and projecting out the colour octet contribution, it can be shown that the result for gluon exchange between two quarks does indeed behave as

$$A = A^{(0)} \cdot s^{\epsilon(t)} \propto s^{1+\epsilon(t)}, \tag{*i*.52}$$

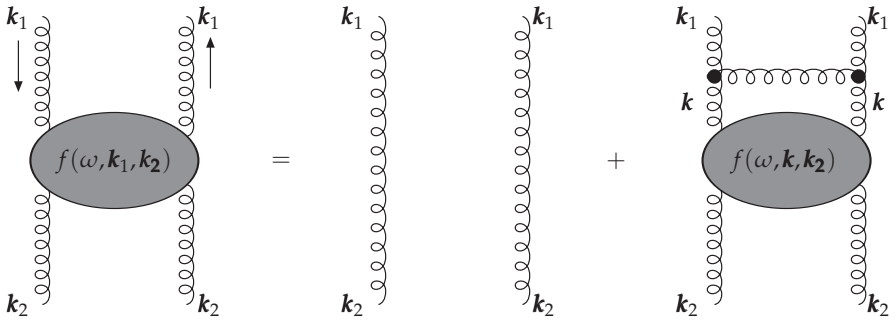

Figure *i*.3: Illustration of the evolution of the gluon ladder. The vertical gluons in the figure are actually *Reggeized gluons* which are obtained after summing over all virtual contributions with the result that the gluon propagator is modified as $1/\boldsymbol{k}^2 \rightarrow \frac{1}{\boldsymbol{k}^2}(\frac{s}{\boldsymbol{k}^2})^{\epsilon(\boldsymbol{k}^2)}$. The fat dots in the rightmost figure represent the so-called Lipatov effective vertex which is obtained after taking into account various Feynman diagrams for the gluon emission.

where

$$\epsilon(t) \equiv \frac{\bar{\alpha}}{2\pi}\int d^2\boldsymbol{k}\frac{t}{\boldsymbol{k}^2(\boldsymbol{k}-\boldsymbol{q})^2}, \quad \bar{\alpha} \equiv \frac{\alpha_s N_c}{\pi} \text{ and } t = -\boldsymbol{q}^2. \tag{i.53}$$

In (*i*.52) $A^{(0)}$ is the lowest order amplitude which is proportional to s. In (*i*.53) the boldface quantities denote two dimensional transverse momenta.

We thus see that the gluon ladder corresponds to a Reggeon with trajectory $\alpha(t) = 1 + \epsilon(t)$. Using the expression for $\epsilon(t)$ in (*i*.53) we see that the intercept is given by $\alpha(0) = 1 + \epsilon(0) = 1$, which means that the spin-1 gluon itself lies on this trajectory.

i.3.3 The BFKL Equation

Another interesting question is whether there is any analogy in QCD of the Pomeron which is responsible for the rising cross sections with s.

The simplest model for the Pomeron in QCD is offered by the two gluon model, in which Pomeron exchange corresponds to the exchange of two gluons in a colour singlet state. This is the Born approximation for the Pomeron, and the complete expression is given by summing the full gluon ladder, as in the case of the reggeized gluon, and projecting out the colour singlet contribution.

The easiest way to sum up contributions from all orders in α_s is to write down an integral equation for the evolution of the gluon ladder. We will here

only consider the simplest case of zero momentum transfer, *i.e.* $\boldsymbol{q} = 0$ in (*i*.53). The evolution is illustrated in figure *i*.3, and the equation reads

$$\omega f(\omega, \boldsymbol{k}_1, \boldsymbol{k_2}) = \delta(\boldsymbol{k}_1 - \boldsymbol{k}_2) + \frac{\bar{\alpha}}{\pi} \int \frac{d^2\boldsymbol{k}}{(\boldsymbol{k} - \boldsymbol{k}_1)^2} \Big\{ f(\omega, \boldsymbol{k}, \boldsymbol{k_2}) - \frac{\boldsymbol{k}_1^2}{\boldsymbol{k}^2 + (\boldsymbol{k} - \boldsymbol{k}_1)^2} f(\omega, \boldsymbol{k}_1, \boldsymbol{k_2}) \Big\}. \tag{*i*.54}$$

This is the celebrated BFKL [15, 16] (Balitsky, Fadin, Kuraev and Lipatov) equation (for zero-momentum transfer). The delta function corresponds to no evolution while the second part, which consists of one real and one virtual contribution, takes into account the evolution of the gluon ladder. The variable ω is the Mellin conjugate variable to $s/\boldsymbol{k}_0^2$, where $\boldsymbol{k}_0$ is some typical transverse momentum scale. To obtain the imaginary part of the scattering amplitude, ImA, one has to take the inverse Mellin transform of $f(\omega, \boldsymbol{k}_1, \boldsymbol{k_2})$, and then integrate the result over $\boldsymbol{k}_1$ and $\boldsymbol{k}_2$.

One can also write down the BFKL equation as an evolution equation for $f(s, \boldsymbol{k}_1, \boldsymbol{k_2})$ (the inverse Mellin transform of $f(\omega, \boldsymbol{k}_1, \boldsymbol{k_2})$). This is completely straightforward since the derivative w.r.t. $\ln(s/\boldsymbol{k}^2)$ brings down a factor ω as in the left side of (*i*.54). We thus get

$$\partial_y f(s, \boldsymbol{k}_1, \boldsymbol{k_2}) = \mathcal{K}_{BFKL} \otimes f(s, \boldsymbol{k}_1, \boldsymbol{k_2}) \tag{*i*.55}$$

where $y \equiv \ln(s/\boldsymbol{k}^2)$, and $\mathcal{K}_{BFKL}\otimes$ is the integral kernel in (*i*.54). The solution to the BFKL equation in the saddle point approximation reads

$$f(s, \boldsymbol{k}_1, \boldsymbol{k_2}) \approx \frac{1}{\sqrt{\boldsymbol{k}_1^2 \boldsymbol{k}_2^2}} \frac{1}{2\pi c} \frac{e^{\omega_0 y}}{\sqrt{\pi y}} \exp\left(\frac{-\kappa^2}{4c^2 y}\right), \tag{*i*.56}$$

where $c^2 = 14\,\bar{\alpha}\,\zeta(3)$, $\omega_0 = 4\,\bar{\alpha}\,\log 2$, and $\kappa \equiv \ln(\boldsymbol{k}_1^2/\boldsymbol{k}_2^2)$.

BFKL thus predicts a power like growth of the amplitude with energy, and the exponent is quite large, $\omega_0 \approx 0.55$ for $\bar{\alpha} = 0.2$ (which is a reasonable value for the coupling). This can be compared to the fits in (*i*.27) and (*i*.28) which give an exponent of 0.08 for pp and $p\bar{p}$ collisions. The terminology is such that the intercept calculated from perturbative QCD is referred to as the "hard Pomeron", while the Pomeron responsible for the rise in σ_{tot} in pp collisions is referred to as the "soft Pomeron".

What is seen at HERA is that the density does indeed grow like $x^{-\lambda}$, but the exponent λ is lower than 0.55, and it varies with Q^2, typically in values from around 0.3 for $Q^2 \sim 100$ GeV^2 down to values around 0.1 as $Q^2 \to 0$. We should also mention that the leading order BFKL growth is significantly reduced by non-leading and energy-momentum conservation effects. A numerical evaluation of these effects within the dipole formalism is the subject of paper 1.

i.3.4 Unitarity and Saturation

A growth of the cross section like $\exp(\omega_0 y)$ cannot continue indefinitely. The reason for this is simple; such a strong growth does not satisfy the Froissart-Martin (FM) bound in (*i*.19). This is of course not only a problem for the BFKL calculation but also for the fits in (*i*.27) and (*i*.28), which also violate this bound for very high s. (Although for these fits the violation would occur beyond the Planck scale!)

The FM bound specifies how fast a total cross section can grow asymptotically. In the classical analogy in section *i*.2.3, we considered the scattering of light on a disc and noted that $T(\boldsymbol{b}) = 1$ and $S(\boldsymbol{b}) = 0$ corresponds to the complete absorption of the wave at that $\boldsymbol{b}$. In that case the target is completely opaque, and this limit is referred to as the black disc limit. In this limit, it is seen from (*i*.34) and (*i*.35) that both the scattering and the absorption cross sections are given by πR^2, where R is the radius of the black disc. The total cross section is then equal to $2\pi R^2$.

The growth of the total cross section is then determined by the expansion of the black disc in the transverse plane. The growth of the black disc depends on how fast the partons proliferate at each $\boldsymbol{b}$, and also on the nature of the interaction. For example, the FM bound does not apply to the infinite range Coulomb potential as in this case the constant C in (*i*.19) is infinitely large (since the photon mass m_γ is zero). For a confining field on the other hand, the interaction probability falls off exponentially as a function of the interaction range. If one further assumes that the interaction probability at each fixed distance is bounded by a power of the energy (this was the assumption in the formulation of the FM theorem), then the probability for interaction at some distance r from the target is given by

$$P(E, r) \leqslant E^n e^{-mr}. \tag{*i*.57}$$

The interaction is then negligible outside the screening length $\frac{1}{m} n \ln E$, and the total cross section therefore satisfies

$$\sigma_{tot} \leqslant \frac{n^2}{m^2} \ln^2 E. \tag{*i*.58}$$

There must, however, also be a limit to how fast the interaction amplitude can increase at each $\boldsymbol{b}$, since the total reaction probability at any $\boldsymbol{b}$ must be bounded by unity, $T(\boldsymbol{b}) \leqslant 1$.

In QCD, the suppression of the growth at each $\boldsymbol{b}$ is provided within perturbation theory while the expansion in the transverse plane is determined both by the perturbative evolution and also by non-perturbative effects related to confinement.

From general arguments we expect the BFKL-like growth to be modified as the gluon density gets very high. Consider DIS where we probe the proton

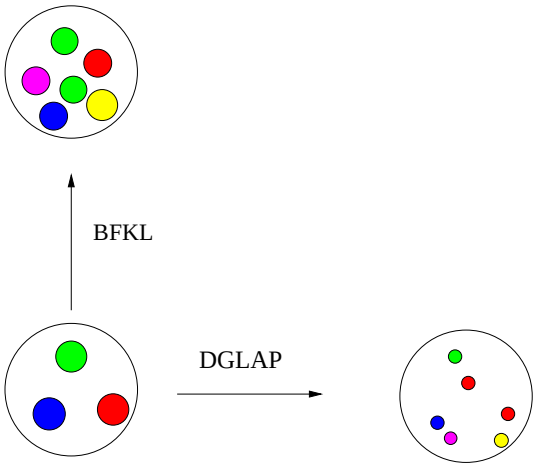

Figure *i*.4: A cartoon of the evolution of the proton in the transverse plane in the DGLAP and BFKL formalisms.

with a transverse resolution scale $\Delta x_\perp \sim 1/Q$. The proton travels at nearly the speed of light, and due to Lorentz contraction it will appear as a pancake, or a thin disc. As the proton is boosted to higher energies, gluons will be emitted at different transverse positions.

In figure *i*.4 we show a cartoon of how the proton appears at scale Q^2 for some x. The small discs represent the gluons inside the proton. If we now increase Q^2 at fixed $x = Q^2/s$, the evolution can be described by the QCD renormalization group equations, or the DGLAP [17–20] equations for short. In this domain the number of gluons increases but the density nevertheless decreases since Q^2 gets larger. Here the interaction probability stays below one (assuming it did so initially). In DGLAP evolution one can neglect interactions among the gluons inside the proton, and the linear evolution is therefore adequate in describing the physics.

Alternatively we can hold Q^2 fixed while we decrease x. We are then in the small-x region and BFKL evolution applies. In this case the number of gluons increases while their sizes (determined by Q^2) remain limited. Thus, at some sufficiently low x, one will fill up the entire proton, and the overlaps between the gluons are really large. At this point the interactions between the gluons cannot be neglected, and the linear BFKL evolution ceases to be valid.

The value of x at which the linear evolution has to be modified depends on Q^2. At large Q^2 the gluons probed by the projectile are smaller, and they will therefore start to overlap at smaller x as compared to the low Q^2 case. The line which separates the linear and non-linear regions is referred to as

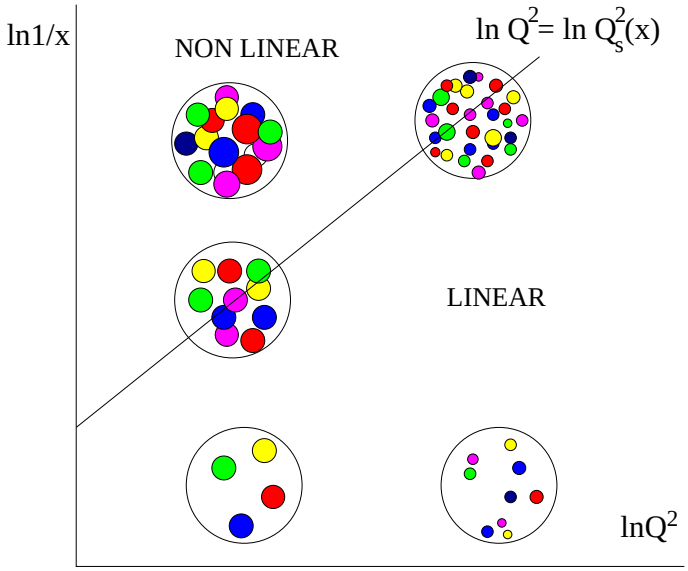

Figure *i*.5: The saturation line separates the linear and non-linear regions in the (x, Q^2) plane.

the "saturation momentum", and is denoted by $Q_s(x)$. Leading order QCD calculations predict that Q_s grows like a power of x [21] (an exponential in $y = \ln 1/x$).

In order to reduce the fast growth of the scattering amplitude there must be a mechanism which suppresses the growth of the gluon density. It was early suggested by Gribov, Levin and Ryskin [22] that parton saturation should tame the growth of the gluon density. They considered the evolution in the presence of $1 \to 2$ gluon splittings, as in the linear BFKL evolution, and $2 \to 1$ gluon mergings which are increasingly important as the gluon density grows. Such effects ought be proportional to the square of the gluon density, as opposed to the growth mechanism which is proportional to the density itself.

We note that the BFKL equation is a linear equation of the form

$$\partial_y f(y) = f(y), \tag{*i*.59}$$

which has the solution $f(y) = Ae^y$. If now we also take into account gluon mergings then we expect this equation to be modified into the following form

$$\partial_y f(y) = f(y) - f^2(y), \tag{*i*.60}$$

with the solution

$$f(y) = \frac{A}{A + e^{-y}}, \;\; f(0) = \frac{A}{A+1}. \tag{i.61}$$

From this expression we see that $f \to 1$ as $y \to \infty$. This is due to the non-linear term in (*i*.60) which becomes important as $f \to 1$, and exactly cancels the linear growth term when $f = 1$.

If initially f is small (in QCD f is of order α_s^2) then we see that, for small y, we can neglect A in the denominator in (*i*.61) in which case we obtain a BFKL type solution. Gluon mergings can thus be neglected initially but they become increasingly important as the density grows.

The equation derived by Gribov, Levin and Ryskin has a form similar to (*i*.60), and is known as the GLR equation. This equation was derived rather heuristically and it reads

$$\partial_y f(s, \boldsymbol{k}) = \mathcal{K}_{BFKL} \otimes f(s, \boldsymbol{k}) - \frac{81\alpha_s^2(\boldsymbol{k})}{16\boldsymbol{k}^2 R^2}(xg(x, \boldsymbol{k}))^2, \tag{i.62}$$

where R is an unknown parameter which is a measure of the size of a typical region where the gluon density is high. If the gluons are evenly distributed inside the proton then R is the proton radius. In that case recombination effects turn out to be negligible for $x \geqslant 10^{-4}$. However, due to fluctuations in the gluon number, there can be small regions inside the proton where the number of gluons is large in which case it could be possible to observe recombination effects for x values accessible at HERA. We should remark that also NLO effects reduce the growth of the gluon density, and it is therefore important to try to separate the effects of saturation from that of NLO effects.

Since the pioneering work by GLR, there has been much progress in understanding the non-linear evolution in high energy QCD, and in the forthcoming sections we will explore some of the evolution equations derived directly from perturbative QCD.

i.3.5 The Color Glass Condensate

During the recent years a new theory for the high energy limit of QCD has emerged. This theory predicts that all hadrons are at high energies described by a new type of matter called the Color Glass Condensate. We will here give a short summary of this theory and for a number of review articles we refer the reader to refs [21, 23, 24].

High energy QCD is conveniently formulated in light-cone (LC) coordi-

nates which are defined by

$$p^{\pm} = \frac{1}{\sqrt{2}}(E \pm p_z), \tag{i.63}$$

$$x^{\pm} = \frac{1}{\sqrt{2}}(t \pm z), \tag{i.64}$$

$$p \cdot x = p^{-}x^{+} + p^{+}x^{-} - p_{\perp} \cdot x_{\perp}, \tag{i.65}$$

where $p_\perp$ and $x_\perp$ are two-dimensional transverse vectors. Here x^+ is usually referred to as the LC "time", and its conjugate variable p^- is consequently referred to as the LC "energy". In hadron-hadron collisions the right (left) moving hadron has a large (small) p^+ and a small (large) p^- given by $p^- = \frac{m_\perp^2}{2p^+}$, with $m_\perp$ being the transverse mass defined by $m_\perp^2 = p_\perp^2 + m^2$.

Consider now a right moving hadron with total LC momentum P^+. The assumption is then that the hadron can be described by an effective theory in which the colour sources are given by high-x gluons which have momenta $p^+ > \Lambda = bP^+$. The small-x gluons on the other hand, have momenta $p^+ < \Lambda$. Here b is a number between 0 and 1 which is arbitrary, and x is the fraction of LC momentum carried by the gluon. The scale Λ, separating the high-x sources from the small-x gluons, is thus arbitrary, and in order to make the physics independent of this scale one has to introduce a Renormalization group procedure, in which layers of gluon fields are integrated out towards lower momenta[5].

The fields with $p^+ > \Lambda$ are no longer dynamical but are replaced by a classical colour source ρ_a. The quantum corrections renormalize the classical source without changing the effective formalism. The classical field equations are given by

$$D_\mu F_a^{\mu\nu}(x) = J_a^\nu = \delta^{\nu+}\rho_a(x). \tag{i.66}$$

Thus the sources move along the light-cone in the positive z direction, and it is assumed that they do not deviate from their trajectory after the emission of the small-x gluons (this is precisely the eikonal approximation encountered earlier).

The sources are thus sitting at $x^- \approx 0$ which implies that the classical density ρ_a is highly peaked around this value. The longitudinal extension of these sources can be approximated by $\Delta x^-_{fast} \sim \frac{1}{p^+_{fast}} << \frac{1}{p^+_{slow}} \sim \Delta x^-_{slow}$. This implies that, to the dynamical small-x gluons, the sources appear to be distributed on a thin sheet. Moreover we have $\Delta x^+_{fast} \sim \frac{1}{p^-_{fast}} >> \frac{1}{p^-_{slow}} \sim \Delta x^+_{slow}$ so that the sources appear to be frozen to the small-x gluons. For time scales

[5]This is done in the LLA as in sec *i*.3.3.

longer than Δx^+_{fast}, however, the source configuration will change, and ρ_a is therefore given by a random field with a normalized distribution $W_\Lambda[\rho]$, which depends on the scale Λ.

In the quantum theory, the small-x gluons are given by dynamical quantum fields, and one proceeds by integrating out these in layers starting from the initial scale Λ. The integrated fields are added to ρ_a which is renormalized. Correlation functions are then given by two averages, first an average over the dynamical quantum fields, and secondly an average over the classical random colour source ρ_a. Mathematically this can be written as

$$\begin{aligned}\langle A^\mu(x)A^\nu(y)\rangle &= \langle\langle A^\mu(x)A^\nu(y)\rangle^\Lambda_{quantum}\rangle_{\rho,classical} \\ &= \int \mathcal{D}\rho\, W_\Lambda[\rho]\,\langle A^\mu(x)A^\nu(y)\rangle^\Lambda_{quantum} \\ &= \int \mathcal{D}\rho\, W_\Lambda[\rho]\,\frac{\int^\Lambda \mathcal{D}A\, A^\mu(x)A^\nu(y)e^{iS[A,\rho]}\delta(G(A))}{\int^\Lambda \mathcal{D}A e^{iS[A,\rho]}\delta(G(A))} \qquad (i.67)\end{aligned}$$

where $G(A)$ is the gauge fixing condition. In covariant gauge $G(A) = \partial_\mu A^\mu$, and in this case the only non-trivial field component is $A^+_a \equiv \alpha_a$. The relation between α_a and ρ_a is given by the Poisson equation: $\nabla^2\alpha_a = -\rho_a$. Using this relation one can therefore specify W_Λ either as a function of α_a or ρ_a.

The weight function W_Λ satisfies a Renormalization Group Equation (RGE) which describes the evolution of the condensate in "rapidity" $Y \equiv \ln(P^+/\Lambda)$ (from now on we will instead of W_Λ use the notation W_Y). This RGE is known as the JIMWLK (Jalilian-Marian, Iancu, McLerran, Weigert, Leonidov and Kovner) equation [25–28], and it reads

$$\partial_Y W_Y[\alpha] = \frac{1}{2}\int d^2x_\perp d^2y_\perp \frac{\delta}{\delta\alpha_a(x_\perp)}\eta_{ab}(x_\perp,y_\perp)\frac{\delta}{\delta\alpha_b(y_\perp)}W_Y[\alpha], \qquad (i.68)$$

where

$$\begin{aligned}\eta_{ab}(x_\perp,y_\perp) = \frac{1}{4\pi^3}\int d^2z_\perp \frac{(x_\perp-z_\perp)\cdot(z_\perp-y_\perp)}{(x_\perp-z_\perp)^2(y_\perp-z_\perp)^2}\cdot \\ \cdot(1-\bar{V}^\dagger_{x_\perp}\bar{V}_{z_\perp})^{af}(1-\bar{V}^\dagger_{z_\perp}\bar{V}_{y_\perp})^{fb} \qquad (i.69)\end{aligned}$$

and

$$\alpha_a(x_\perp) \equiv \int dx^-\alpha_a(x^-,x_\perp). \qquad (i.70)$$

In (*i*.69), $\bar{V}$ denotes a Wilson line, to be defined below, which is non-linear in the fields α_a to all orders. One can notice that the JIMWLK equation is of

the Fokker-Planck type with η playing the role of the, spatially dependent, diffusion coefficient.

The average of an arbitrary observable $\mathcal{O}$ evolves according to

$$\partial_Y \langle \mathcal{O} \rangle = \int \mathcal{D}\alpha \, \mathcal{O}[\alpha] \, \partial_Y W_Y[\alpha] = \int \mathcal{D}\alpha \, \mathcal{O}[\alpha] \, H[\alpha] \, W_Y[\alpha] \, . \tag{i.71}$$

Here we have defined the JIMWLK "Hamiltonian" H. By using (i.68), and integrating by parts, this evolution can be rewritten in the following form

$$\partial_Y \langle \mathcal{O} \rangle = \left\langle \frac{1}{2} \int d^2x_\perp d^2y_\perp \frac{\delta}{\delta \alpha_b(x_\perp)} \eta_{ab}(x_\perp, y_\perp) \frac{\delta}{\delta \alpha_a(y_\perp)} \mathcal{O} \right\rangle. \tag{i.72}$$

Consider now an elementary projectile, a $q\bar{q}$ dipole, which scatters off a hadron. The scattering amplitude is denoted $T(x_\perp, y_\perp)$, where $x_\perp$ ($y_\perp$) is the transverse coordinate of the quark (antiquark). The explicit expression for T reads

$$T(x_\perp, y_\perp) = 1 - \frac{1}{N_c} \mathrm{Tr}(V^\dagger_{x_\perp} V_{y_\perp}) \tag{i.73}$$

where V is the Wilson line given by

$$V^\dagger_{x_\perp} = P \exp\left(ig \int dx^- \alpha_a(x^-, x_\perp) t^a \right). \tag{i.74}$$

Here t^a are the colour matrices in the fundamental representation. The reason we denoted the Wilson lines in (i.69) with $\bar{V}$ is because in that case the colour matrices are in the adjoint representation, *i.e* t^a is replaced by T^a. P in (i.74) denotes a path ordering of the colour matrices in the expansion of the exponential.

The Wilson lines describe the multiple scatterings of the quark and the antiquark off the classical colour fields $\alpha_a \equiv A^+_a$ in the eikonal approximation. Note that $V^\dagger$ can be rewritten in the following form

$$\begin{aligned} V^\dagger &= P \exp\left(i \int d\tau \, g \frac{dx^\mu}{d\tau} t_a A^a_\mu \right) = P \exp\left(i \int d^4y \int d\tau \, g \frac{dx^\mu}{d\tau} t_a \delta^4(x-y) A^a_\mu \right) \\ &= P \exp\left(i \int d^4y j^\mu_a A^a_\mu \right) = P \exp\left(i \int d^4y H_{int}(y) \right). \end{aligned} \tag{i.75}$$

In the last line we have identified the interaction Hamiltonian and we thus see that the Wilson line is nothing else but the S matrix for the particle. For the $q\bar{q}$ dipole we then get the gauge invariant expression $S = 1 - T$ with T given in (i.73).

By using equation (*i*.72) and (*i*.73) one can derive the following equation for $\langle T \rangle$,

$$\partial_Y \langle T(x_\perp, y_\perp) \rangle = \frac{\bar{\alpha}}{2\pi} \int d^2 z_\perp \frac{(x_\perp - y_\perp)^2}{(x_\perp - z_\perp)^2 (z_\perp - y_\perp)^2} \{ -\langle T(x_\perp, y_\perp) \rangle + \\ + \langle T(x_\perp, z_\perp) \rangle + \langle T(z_\perp, y_\perp) \rangle - \langle T(x_\perp, z_\perp) T(z_\perp, y_\perp) \rangle \}. \quad (i.76)$$

We see that the equation for $\langle T \rangle$ receives a contribution from $\langle TT \rangle$. The equation for $\langle TT \rangle$ will in turn receive a contribution from $\langle TTT \rangle$ and so on. Therefore the JIMWLK equation does not generate a closed equation for the dipole scattering amplitude, but it rather generates an infinite hierarchy of equations, of which (*i*.76) is the first. This hierarchy is commonly referred to as the Balitsky-JIMWLK (B-JIMWLK) hierarchy since the same set of equations were derived earlier by Balitsky [29], albeit in a different formalism.

In order to obtain a closed equation we can make a mean field approximation where we replace $\langle TT \rangle$ by $\langle T \rangle \langle T \rangle$. In that case we obtain the so-called Balitsky-Kovchegov (BK) equation [29, 30] which is probably the most simple non-linear evolution equation one can write down in perturbative QCD. The BK equation is similar to the GLR equation (*i*.62) but is, unlike the latter, well founded in perturbative QCD.

Let us now disregard all multiple scatterings in the evolution of the hadron, *i.e*. we disregard the higher order correlations encoded in the Wilson lines in (*i*.69). This means that we expand the Wilson lines to the lowest non-vanishing order in α_a, which is $\mathcal{O}(\alpha^2)$. This is justified if the associated fields are weak, so that we are outside the saturation region. In this case the last term in (*i*.76) is absent and the equation reduces to

$$\partial_Y \langle T(x_\perp, y_\perp) \rangle = \frac{\bar{\alpha}}{2\pi} \int d^2 z_\perp \frac{(x_\perp - y_\perp)^2}{(x_\perp - z_\perp)^2 (z_\perp - y_\perp)^2} \{ -\langle T(x_\perp, y_\perp) \rangle + \\ + \langle T(x_\perp, z_\perp) \rangle + \langle T(z_\perp, y_\perp) \rangle \}. \quad (i.77)$$

As demonstrated by Mueller [31], this is nothing else but the BFKL equation in transverse coordinate space. Thus the JIMWLK equation gives the BFKL equation in the weak field limit. We will later see that equations (*i*.76) and (*i*.77) can be easily derived within the dipole formalism.

The BFKL equation, which describes the evolution of a single colour singlet gluon ladder (the Pomeron), thus arises from the JIMWLK equation when η is expanded to $\mathcal{O}(\alpha^2)$. In this case we can write the Hamiltonian schematically as $H \sim \alpha^2 \frac{\delta^2}{\delta \alpha^2}$. This evolution is illustrated in figure *i*.6, and one can here interpret the fields α as annihilation operators which remove two gluons while the functional derivatives $\delta / \delta \alpha$ act as creation operators which add two gluons. In this way we see that H describes the evolution of a single gluon ladder as seen in the figure.

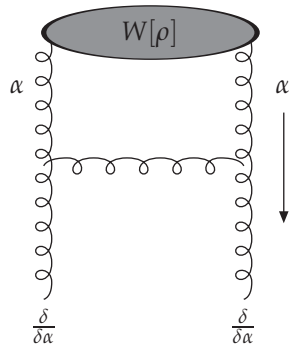

Figure *i*.6: The evolution generated with $H \sim \alpha^2 \frac{\delta^2}{\delta\alpha^2}$ which is equivalent to the BFKL evolution of the gluon ladder. The grey blob on the top denotes the classical source with weight $W[\rho]$ and the evolution proceeds in the direction of the arrow.

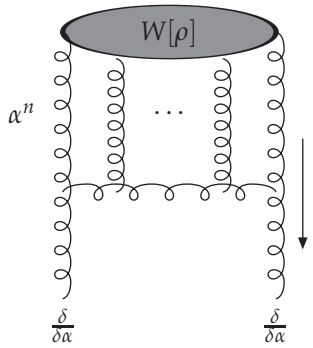

Figure *i*.7: One of diagrams generated from the full Hamiltonian $H \sim \sum_n c_n \alpha^n \frac{\delta^2}{\delta\alpha^2}$. In this case n gluons merge into 2 gluons.

The full Hamiltonian is given by $H \sim \sum_n c_n \alpha^n \frac{\delta^2}{\delta\alpha^2}$. Thus the higher order terms in α give rise to diagrams as in figure *i*.7, which describe the fusion of an arbitrary number of gluons into two gluons. However, since there are only two functional derivatives present in (*i*.68), this means that we cannot produce more than two t-channel gluons with which we can probe the target. Notice that this also implies that the B-JIMWLK hierarchy has the generic form[6]

$$\partial_Y \langle T^k \rangle = \mathcal{M} \otimes \{ \langle T^k \rangle - \langle T^{k+1} \rangle \}, \tag{*i*.78}$$

[6]For simplicity we here consider the large N_c version of these equations in which case complicated colour structures vanish and the evolution can be written in terms of dipole amplitudes only.

where T^k is thus coupled only to higher order amplitudes T^n, $n > k$. The presence of higher order functional derivatives in (*i*.68) would on the other hand generate equations of the form

$$\partial_Y \langle T^k \rangle = \mathcal{M} \otimes \{\langle T^k \rangle - \langle T^{k+1} \rangle\} + \mathcal{K}_1 \otimes \{\langle T^{k-1} \rangle - \langle T^k \rangle + \langle T^{k+1} \rangle\} \quad (i.79)$$

for $H \sim \sum_n c_n \alpha^n (\frac{\delta^2}{\delta \alpha^2} + \frac{\delta^4}{\delta \alpha^4})$ and some vertex $\mathcal{K}_1$, and

$$\begin{aligned} \partial_Y \langle T^k \rangle = \mathcal{M} \otimes \{\langle T^k \rangle - \langle T^{k+1} \rangle\} + \mathcal{K}_1 \otimes \{\langle T^{k-1} \rangle - \langle T^k \rangle\} + \\ \mathcal{K}_2 \otimes \{\langle T^{k-2} \rangle - \langle T^{k-1} \rangle + \langle T^k \rangle - \langle T^{k+1} \rangle\} \end{aligned} \quad (i.80)$$

for $H \sim \sum_n c_n \alpha^n (\frac{\delta^2}{\delta \alpha^2} + \frac{\delta^4}{\delta \alpha^4} + \frac{\delta^6}{\delta \alpha^6})$ and some vertex $\mathcal{K}_2$ and so on.

In terms of Pomeron interactions (we now restrict ourselves to the large N_c limit where two-gluon ladders dominate over higher order gluon ladders) such evolution equations describe processes where the Pomerons can evolve BFKL-like, split and merge. In that case one can obtain Pomeron loops during the evolution, and the modified equations above are therefore referred to as Pomeron loop equations. The B-JIMWLK equations on the other hand, only contain Pomeron mergings and therefore no Pomeron loops. This was realized quite recently, and there have since then been various attempts to modify the B-JIMWLK equations so that they can incorporate Pomeron loops [32–34].

i.4 The Dipole Picture of QCD

It is sometimes convenient to describe QCD in terms of colour dipoles [35,36], or colour antennas [37], rather than in terms of the quarks and the gluons themselves. Just as in electrodynamics, a colour dipole in QCD is formed by the separation of a colour electric charge–anti-charge pair. However, one difference is that while in electrodynamics there is only one type of electric charge, in QCD we have three colours, and in order to make a colour singlet the colour dipole needs to be the coherent sum of $r\bar{r}$, $b\bar{b}$ and $g\bar{g}$ colour charges.

Consider for example an e^+e^- annihilation event, as shown in figure *i*.8. The virtual photon splits into a $q\bar{q}$ pair which may then emit QCD radiation, and for short time scales asymptotic freedom enables us to use perturbation theory to make QCD calculations.

In QED, when the $q\bar{q}$ pair (or any other charge–anti-charge pair) emits a photon the electric current is not changed (apart from the recoils suffered by the emitters), since the photon does not carry electric charge. Thus the emission of the second photon proceeds in a similar way. In QCD, however, the gluons carry colour charges which means that the colour current is changed in a nontrivial way, and the emission of the second gluon is therefore not similar to the emission of the first.

The emission of gluons from the $q\bar{q}$ pair can, however, be understood in the colour dipole language in a very simple way. Assume that we have a $r\bar{r}$ pair formed from the virtual photon. Assume also that the red quark emits a $r\bar{b}$ gluon, which changes the colour of the quark into blue, as shown in figure *i*.8. After the emission we thus have two colour dipoles, a $b\bar{b}$ dipole stretched between the quark and the "antiquark" part of the gluon, and a $r\bar{r}$ dipole stretched between the antiquark and the "quark" part of the gluon. The same configuration also arises if we start with a $b\bar{b}$ pair and if the anti-blue antiquark emits a $\bar{b}r$ gluon, changing its colour to anti-red.

Since the original quark–antiquark pair is a colour singlet, *i.e.* a coherent sum of $r\bar{r}$, $b\bar{b}$ and $g\bar{g}$, there is no way we can distinguish the two processes from each other. Thus the quark and the antiquark in the pair emit the gluon coherently, and the result is that the original dipole splits into two new dipoles, one stretched between the quark and the "antiquark" part of the gluon, and the other one stretched between the "quark" part of the gluon and the antiquark.

If the gluons emitted in the cascade are ordered in energy in such a way that the last emitted gluon is much softer than the previous one, it can be shown that the emission of the second gluon can be described by the emission from two independent dipoles, modulo interference corrections which are suppressed by $1/N_c^2$. This picture holds for the entire cascade and the process can therefore be formulated as a classical branching process, where at

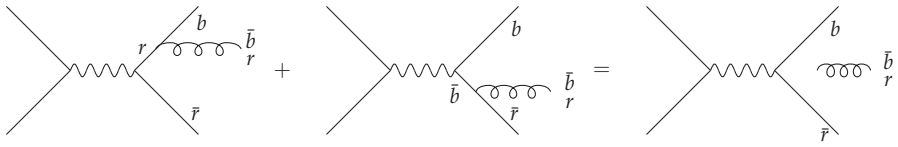

Figure *i*.8: Gluon radiation from an e^+e^- annihilation event.

each step a dipole can split into two new dipoles, both of which can further split, independently from each other and the rest of the cascade, apart from the $1/N_c^2$ corrections. It is here essential that the cascade is strongly ordered, and if we further assume N_c to be large, we obtain a cascade of independent dipoles.

As time goes on and the quarks and the gluons move further apart from each other, perturbation theory eventually breaks down. To further describe the evolution of the cascade one therefore needs to resort to phenomenological models, such as the Lund string fragmentation model. A further advantage of the perturbative dipole cascade is that it gives a smooth and natural transition to the non-perturbative Lund string.

In phenomenological applications the dipole formalism has been very successful. The dipole cascade model [35, 36], as implemented in the ARIADNE event generator [38], has been able to describe e^+e^- final states to a very good precision.

In DIS the situation is a bit more subtle. Here we are dealing with a space-like cascade initiated by the virtual photon, as opposed to the time-like e^+e^- cascade. Furthermore, DIS is much more complicated as there are two relevant scales, Q^2 and W^2, and in this case the QCD cascade determines both the final states and the total cross section. In e^+e^- annihilation on the other hand, the total cross section can easily be calculated perturbatively, while the dipole cascade determines the final states only.

A modified version of the dipole model for DIS is again implemented in ARIADNE. This model is referred to as the Soft-Radiation Model [39], and it is currently the most successful model in describing the final states at HERA. However, the model suffers from the fact that it does not predict the total cross section, and it is also not very well founded within perturbative QCD.

Another extension of the dipole model is called the Linked Dipole Chain Model (LDC) [40], which is a reformulation and a generalization of the so-called CCFM model [41, 42] which incorporates the features of both DGLAP and BFKL evolutions in their respective domains. The LDC and CCFM models have the ambition to describe both the total cross section and the final

states. They work reasonably well in describing both, although none of them is as successful as the abovementioned Soft-Radiation Model in describing the final states.

i.5 Dipoles In Coordinate Space

All dipole models described above have the property that they are formulated in transverse momentum space. This has the advantage that one can in a MC simulation easily take into account energy-momentum conservation effects which are not included in the leading order QCD calculations. For very dense systems, however, a formulation in transverse coordinate space is more appropriate as saturation effects are easier to take into account in this representation.

Actually in sec *i*.3.5 we have already introduced dipoles in the high energy region of QCD. In eq (*i*.76), we wrote down the evolution equation satisfied by an elementary dipole located at transverse coordinates $(\boldsymbol{x},\boldsymbol{y})$ (in this section we denote transverse vectors with $\boldsymbol{x}$ rather than with $x_\perp$). In that case the dipole was considered to be fixed while the target hadron evolved within the CGC formalism. However, we can formally interpret this equation in terms of dipole evolution, although we derived it from the JIMWLK equation which is not written in terms of dipole degrees of freedom.

i.5.1 The B-JIMWLK Equations in Dipole Language

To make the interpretation obvious, we rewrite the LHS of eq (*i*.76) as $\partial_Y T_Y = \frac{1}{dY}(T_{Y+dY} - T_Y)$ (for simplicity we drop all brackets). Moving over $T_Y(\boldsymbol{x},\boldsymbol{y})$ to the RHS, and multiplying both sides with dY, we get

$$T_{Y+dY}(\boldsymbol{x},\boldsymbol{y}) = T_Y(\boldsymbol{x},\boldsymbol{y}) \times \left(1 - dY\frac{\bar{\alpha}}{2\pi}\int_{\boldsymbol{z}} \mathcal{M}(\boldsymbol{x},\boldsymbol{y},\boldsymbol{z})\right) + \\ + dY\frac{\bar{\alpha}}{2\pi}\int_{\boldsymbol{z}} \mathcal{M}(\boldsymbol{x},\boldsymbol{y},\boldsymbol{z})\{T(\boldsymbol{x},\boldsymbol{z}) + T(\boldsymbol{z},\boldsymbol{y}) - T(\boldsymbol{x},\boldsymbol{z})T(\boldsymbol{z},\boldsymbol{y})\}. \qquad (i.81)$$

We have here defined the *dipole kernel* $\mathcal{M}$

$$\mathcal{M}(\boldsymbol{x},\boldsymbol{y},\boldsymbol{z}) \equiv \frac{(\boldsymbol{x}-\boldsymbol{y})^2}{(\boldsymbol{x}-\boldsymbol{z})^2(\boldsymbol{z}-\boldsymbol{y})^2}. \qquad (i.82)$$

The first term in the RHS of eq (*i*.81) suggests that the dipole $(\boldsymbol{x},\boldsymbol{y})$ might scatter off the hadron as it is, with a reduced probability given by expression in the parenthesis. The other terms take into account the possibility that only one of the two new dipoles $(\boldsymbol{x},\boldsymbol{z})$ and $(\boldsymbol{z},\boldsymbol{y})$ scatters off the target, while in the last term both of the new dipoles scatter.

The dipole splitting interpretation is actually more transparent if we rewrite (*i*.81) in terms of the S-matrix for the dipole, by using the relation $S = 1 - T$.

We then have

$$S_{Y+dY}(\boldsymbol{x},\boldsymbol{y}) = \left(1 - dY\frac{\bar{\alpha}}{2\pi}\int_{\boldsymbol{z}} \mathcal{M}(\boldsymbol{x},\boldsymbol{y},\boldsymbol{z})\right) \times S_Y(\boldsymbol{x},\boldsymbol{y}) + \\ + dY\frac{\bar{\alpha}}{2\pi}\int_{\boldsymbol{z}} \mathcal{M}(\boldsymbol{x},\boldsymbol{y},\boldsymbol{z})\, S_Y^{(2)}(\boldsymbol{x},\boldsymbol{z};\boldsymbol{z},\boldsymbol{y}), \qquad (i.83)$$

where $S_Y^{(2)}(\boldsymbol{x},\boldsymbol{z};\boldsymbol{z},\boldsymbol{y}) = \langle(1 - T(\boldsymbol{x},\boldsymbol{z}))(1 - T(\boldsymbol{z},\boldsymbol{y}))\rangle$. From this equation we clearly see that the dipole can remain as it is, with a reduced probability $1 - dY\frac{\bar{\alpha}}{2\pi}\int \mathcal{M}$, or it can evolve into two dipoles $(\boldsymbol{x},\boldsymbol{z})$ and $(\boldsymbol{z},\boldsymbol{y})$, with a differential probability given by $dY\frac{\bar{\alpha}}{2\pi}d^2\boldsymbol{z}\mathcal{M}$.

We should of course be a bit careful when we talk about the survival probability being equal to $1 - dY\frac{\bar{\alpha}}{2\pi}\int \mathcal{M}$, since the integral over $\mathcal{M}$ diverges which can be seen from (*i*.82). In the expressions above we therefore need a cutoff ρ such that $(\boldsymbol{x}-\boldsymbol{z})^2, (\boldsymbol{z}-\boldsymbol{y})^2 \geqslant \rho^2$. However, note also that the evolution equations in (*i*.76) and (*i*.77) are finite since the expression in the RHS vanish at $\boldsymbol{z} = \boldsymbol{x}$ and $\boldsymbol{z} = \boldsymbol{y}$. The fact that $T(\boldsymbol{x},\boldsymbol{x}) = 0$ is referred to as *colour transparency*, and it can easily be seen that (*i*.73) satisfies this condition.

The dipole interpretation given here can be extended to the complete B-JIMWLK hierarchy in case we neglect all N_c-subleading terms[7]. At each step one dipole can split into two new dipoles, both of which can continue to split independently from the rest of the cascade, just as in the discussion in sec *i*.4.

i.5.2 Mueller's Dipole Formulation

A dipole formulation of the leading order small-x evolution was given by Mueller [31, 43, 44]. Mueller's model is formulated in transverse coordinate space which makes it easy to take into account multiple scatterings as we discussed in sec *i*.2.4.

Starting from a $q\bar{q}$ pair, which might originate from the virtual photon in DIS, one can calculate the probability to emit a soft gluon from this pair (the process is illustrated in figure *i*.9). That the gluon is soft means that one can neglect the recoil in the emission (which is precisely the eikonal approximation), and in that case this probability is determined by the dipole kernel (*i*.82). In the leading logarithmic and large N_c approximations, further emissions factorize so that one gets a cascade of dipoles evolving according to the discussion above. The original $q\bar{q}$ along with the emitted soft gluons can be referred to as an onium (quarkonium).

The evolution of the dipole cascade can conveniently be formulated using the operator formalism introduced by Mueller [44]. We define the operators

[7] Again it is essential that the cascade is strongly ordered, which is true in the CGC approach since it is formulated in LLA as mentioned before.

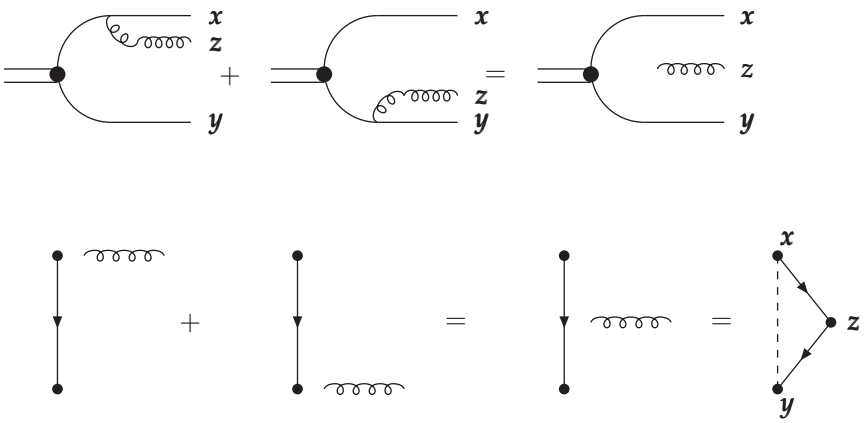

Figure *i*.9: The emission of a gluon from a colour dipole. The relevant Feynman diagrams are shown in the top figure. In the bottom figure we represent the dipole as a line stretched between the colour ends. The arrow indicates the direction of the colour flow, which goes from colour to anticolour. In the rightmost diagram we illustrate the splitting of the original dipole into two new dipoles.

$a(\boldsymbol{x},\boldsymbol{y})$ and $a^\dagger(\boldsymbol{x},\boldsymbol{y})$ which annihilate and create a dipole, respectively, at position $(\boldsymbol{x},\boldsymbol{y})$. These satisfy bosonic commutation relations

$$[a(\boldsymbol{x}_1,\boldsymbol{y}_1), a^\dagger(\boldsymbol{x}_2,\boldsymbol{y}_2)] = \delta^{(2)}(\boldsymbol{x}_1-\boldsymbol{x}_2)\delta^{(2)}(\boldsymbol{y}_1-\boldsymbol{y}_2). \tag{*i*.84}$$

The onium state $|\psi\rangle$ can then be expanded in the dipole states as

$$|\psi\rangle = \sum_N \int d\Gamma_N \psi_N(\{\boldsymbol{x}_i\boldsymbol{y}_i\}_N)|\{\boldsymbol{x}_i\boldsymbol{y}_i\}_N\rangle \tag{*i*.85}$$

$$\text{where}\quad d\Gamma_N = \frac{1}{\sqrt{N!}}\prod_{i=1}^N d^2\boldsymbol{x}_i d^2\boldsymbol{y}_i,\quad |\{\boldsymbol{x}_i\boldsymbol{y}_i\}_N\rangle = \prod_{i=1}^N a^\dagger(\boldsymbol{x}_i,\boldsymbol{y}_i)|0\rangle. \tag{*i*.86}$$

The evolution is driven by two vertices, one which includes the $1\to 2$ dipole splitting, and one which takes into account the virtual corrections which are

needed in order to ensure probability conservation. They read

$$\mathcal{V}_1 = \frac{\bar{\alpha}}{2\pi}\int_{\boldsymbol{x},\boldsymbol{y},\boldsymbol{z}} \mathcal{M}(\boldsymbol{x},\boldsymbol{y},\boldsymbol{z})a^\dagger(\boldsymbol{x},\boldsymbol{z})a^\dagger(\boldsymbol{z},\boldsymbol{y})a(\boldsymbol{x},\boldsymbol{y}), \tag{i.87}$$

$$\mathcal{V}_2 = -\frac{\bar{\alpha}}{2\pi}\int_{\boldsymbol{x},\boldsymbol{y},\boldsymbol{z}} \mathcal{M}(\boldsymbol{x},\boldsymbol{y},\boldsymbol{z})a^\dagger(\boldsymbol{x},\boldsymbol{y})a(\boldsymbol{x},\boldsymbol{y}). \tag{i.88}$$

Assume we start from a single dipole $(\boldsymbol{x}_0,\boldsymbol{y}_0)$ at rapidity 0. The probability that the system after a rapidity evolution of Y contains N dipoles is given by

$$\begin{aligned} P_N(Y) &= \langle N|e^{Y(\mathcal{V}_1+\mathcal{V}_2)}a^\dagger(\boldsymbol{x}_0,\boldsymbol{y}_0)|0\rangle & (i.89)\\ &= \int d\Gamma_N \langle 0|\prod_{i=1}^{N} a(\boldsymbol{x}_i,\boldsymbol{y}_i)e^{Y(\mathcal{V}_1+\mathcal{V}_2)}a^\dagger(\boldsymbol{x}_0,\boldsymbol{y}_0)|0\rangle \\ &= \int d\Gamma_N P_N(\{\boldsymbol{x}_i,\boldsymbol{y}_i\}|Y). & (i.90)\end{aligned}$$

In the last step we have defined the probability density to find N dipoles located at positions $\{(\boldsymbol{x}_i,\boldsymbol{y}_i)\}_{i=1}^N$. The interpretation of P_N as probabilities is due to the fact that they satisfy

$$\sum_N P_N(Y) = \sum_N \int d\Gamma_N P_N(\{\boldsymbol{x}_i,\boldsymbol{y}_i\}|Y) = 1 \tag{i.91}$$

for any Y.

The evolution can actually be formulated as a gain-loss type of equation. Starting from the elementary dipole $(\boldsymbol{x}_0,\boldsymbol{y}_0)$, the evolution generates a chain of colour dipoles $(\boldsymbol{x}_0,\boldsymbol{x}_1),(\boldsymbol{x}_1,\boldsymbol{x}_2),\ldots(\boldsymbol{x}_{N-1},\boldsymbol{y}_0)$ after the emission of $N-1$ gluons at transverse positions $\{\boldsymbol{x}_i\}_{i=1}^{N-1}$. Let us denote the probability density for this configuration by $P_N(\boldsymbol{x}_1,\boldsymbol{x}_2,\ldots,\boldsymbol{x}_{N-1}|Y)$. It can then be shown that it evolves according to

$$\begin{aligned}\partial_Y P_N(\boldsymbol{x}_1,\ldots,\boldsymbol{x}_{N-1}|Y) = &-\frac{\bar{\alpha}}{2\pi}\sum_{i=1}^{N}\int_{\boldsymbol{z}} \mathcal{M}(\boldsymbol{x}_{i-1},\boldsymbol{x}_i,\boldsymbol{z})P_N(\boldsymbol{x}_1,\ldots,\boldsymbol{x}_{N-1}|Y) + \\ &+\frac{\bar{\alpha}}{2\pi}\sum_{i=1}^{N-1}\mathcal{M}(\boldsymbol{x}_{i-1},\boldsymbol{x}_{i+1},\boldsymbol{x}_i)P^i_{N-1}(\boldsymbol{x}_1,\ldots,\boldsymbol{x}_{N-1}|Y)\end{aligned} \tag{i.92}$$

where in P^i_{N-1} the coordinate $\boldsymbol{x}_i$ is absent and we have defined $\boldsymbol{x}_N \equiv \boldsymbol{y}_0$.

Equation (i.92) is interpreted as follows. The negative contribution on the RHS is the loss term associated with the reduced probability that the original configuration remains as it is. The second term tells us that we can reach the

configuration on the LHS by emitting a gluon at position $\boldsymbol{x}_i$ from the configuration $(\boldsymbol{x}_0, \boldsymbol{x}_1), \ldots (\boldsymbol{x}_{i-1}, \boldsymbol{x}_{i+1}), \ldots, (\boldsymbol{x}_{N-1}, \boldsymbol{y}_0)$. This gives an increase in the probability density (a gain term).

The great advantage of the transverse coordinate space formulation is that the transverse coordinates of the gluons are frozen during the evolution (due to Lorentz contraction) and the scattering process. We can then construct the S-matrix much in the same way as we did in section *i*.2.4. Indeed, using the operator formalism, Mueller showed that the S-matrix is given by

$$\begin{aligned} S_Y &= \sum_{N,M} P_N(Y_0) P_M(Y - Y_0) \exp\Big(- \sum_{i=1}^{N} \sum_{j=1}^{M} f(\boldsymbol{x}_i, \boldsymbol{y}_i | \boldsymbol{x}_j, \boldsymbol{y}_j) \Big) \\ &= \Big\langle \exp\Big(- \sum_{i,j} f_{ij} \Big) \Big\rangle . \end{aligned} \tag{*i*.93}$$

Here f_{ij} is the basic dipole–dipole scattering amplitude given by

$$f_{ij} = f(\boldsymbol{x}_i, \boldsymbol{y}_i | \boldsymbol{x}_j, \boldsymbol{y}_j) = \frac{\alpha_s^2}{8} \ln^2 \Big(\frac{(\boldsymbol{x}_i - \boldsymbol{y}_j)^2 (\boldsymbol{y}_i - \boldsymbol{x}_j)^2}{(\boldsymbol{x}_i - \boldsymbol{x}_j)^2 (\boldsymbol{y}_i - \boldsymbol{y}_j)^2} \Big). \tag{*i*.94}$$

Note that (*i*.93) has exactly the same form as the expression in (*i*.44)[8]. The only difference between the two is that the dipole S-matrix is obtained after averaging over onium configurations. This is actually the relevant quantity physically since the dipole configuration would be different for each scattering event in a collider experiment.

Using this expression for the S-matrix, we get the total cross section as

$$\sigma_{tot} = 2 \int d^2\boldsymbol{b} \Big\langle 1 - \exp(- \sum_{ij} f_{ij}) \Big\rangle \tag{*i*.95}$$

where we note the similarity to (*i*.45).

Expanding the exponential in (*i*.95) one obtains the contribution from the multiple scattering series. The lowest one of these corresponds to the BFKL contribution, and we have already mentioned that eq (*i*.77) is the BFKL equation in transverse coordinate space. This equation follows immediately from the dipole model if we allow at most one dipole–dipole scattering in each event.

The higher order contributions generate the non-linear contributions in the B-JIMWLK equations, as we already mentioned above. We thus see that the dipole model takes us beyond the BFKL formalism since we can take into

[8]The similarity is even more obvious in a frame where the whole rapidity interval is given to one onium while the other one is just an elementary dipole.

account the exchange of an arbitrary number of Pomerons, even if we start the evolution from a single dipole. The fact that one can include the "many-body" correlations in a relatively simple way makes the transverse coordinate representation useful in high energy QCD.

We notice that eq (*i*.94) arises from the definition (*i*.73) in case we make a weak field expansion of the Wilson lines. The expression in (*i*.94) corresponds to the exchange of two gluons in a colour singlet state, which is the Born approximation for the Pomeron. The full Pomeron is thus generated by the evolution of the dipole cascades, plus the single scattering between two oppositely moving dipoles in the two gluon exchange approximation.

i.5.3 Saturation and Frame Independence

Multiple interactions induce correlations among different dipoles within the same cascade. Notice, however, that the evolution of the cascade is linear as there are no interactions between dipoles in the same cascade. Actually, since at each step each dipole can split independently from the rest of the cascade, the total number of dipoles increases exponentially. Therefore the cascade evolution is BFKL-like, while non-linearities only arise from multiple dipole interactions.

The treatment of non-linear saturation effects is therefore not fully consistent. However, in case the rapidity interval between the two cascades is shared equally, multiple scatterings become important at rapidities where one can still neglect saturation effects within the individual cascade evolutions. This can easily be understood from the following arguments. The scattering between two dipoles is of order α_s^2 and the total reaction probability goes like $\alpha_s^2 \cdot n(y) \cdot m(Y-y)$ for two cascades containing n and m dipoles respectively. Thus when this number is of order one, multiple scatterings become important.

If we assume that a dipole interacts with dipoles from the same cascade in the same way as it does with dipoles from another cascade, then the probability that it interacts with any other dipole in the cascade is given by $\alpha_s^2 \cdot n(y)$. The number of dipoles grows like $n(y) \sim e^{\omega y}$, with ω being the BFKL intercept, and we see that

$$\alpha_s^2 \cdot n(y) \cdot m(Y-y) \sim \alpha_s^2 e^{\omega y} e^{\omega(Y-y)} = \alpha_s^2 e^{\omega Y}. \tag{*i*.96}$$

Thus when $Y \sim \frac{1}{\omega}\ln(1/\alpha_s^2)$ multiple scatterings become important. On the other hand, saturation in the cascade evolution becomes important either when $y \sim \frac{1}{\omega}\ln(1/\alpha_s^2)$, or when $Y - y \sim \frac{1}{\omega}\ln(1/\alpha_s^2)$. In order to minimize the error the optimal choice is obviously $y = Y/2$. [9]

[9] Here we assume the initial states to be similar. If on the other hand we consider the collision between a dipole and a large nucleus, the optimal frame would be the rest frame of the nucleus.

At higher energies the approximation above becomes worse, and we then need to include saturation effects also during the evolution. Consider any process where we have multiple dipole interactions (multiple Pomeron exchanges). Assume now we make a Lorentz boost, which means that we change Y_0 in (*i*.93). We may for example choose $Y_0 \approx Y$ or $Y_0 \approx 0$, in which case one of the onia is just an elementary dipole.

In such a frame there must be Pomeron mergings inside the highly evolved onium, since there is now only one Pomeron exchange between the colliding onia. Since the evolution is linear, this process is not included in the dipole model. Thus, whether or not we include a non-linear interaction depends on the frame we use for the calculation. This implies that the formalism is frame dependent.

Mathematically, the condition that the formalism be frame independent means that the S-matrix (*i*.93) only depends on the total rapidity interval Y, and not on how we divide this interval between the two cascades. We must thus have $\partial_{Y_0} S = 0$.

Let us denote a generic dipole state containing $N-1$ gluons with $\mathscr{A}_N$. The state carries information on the transverse position of each gluon, and also on how these gluons are connected to each other via the dipoles. The evolution of the distribution $P(\mathscr{A}_N, Y)$ can then be written as

$$\begin{aligned}\partial_Y P(\mathscr{A}_N, Y) = &- \sum_{\mathscr{C}_{N+1}} \int_z \mathcal{R}(\mathscr{A}_N \to \mathscr{C}_{N+1}) P(\mathscr{A}_N, Y) \\ &+ \sum_{\mathscr{C}_{N-1}} \mathcal{R}(\mathscr{C}_{N-1} \to \mathscr{A}_N) P(\mathscr{C}_{N-1}, Y). \end{aligned} \tag{*i*.97}$$

Here we have assumed the dipole state to evolve through the addition of one gluon, with splitting rate $\mathcal{R}$, but we do not specify in which way the dipole configuration changes. The integral $\int_z$ specifies the integration over the transverse coordinates of the newly emitted gluon. We rewrite the S-matrix in the following way

$$S = \sum_{N,M=1}^{\infty} \sum_{\mathscr{A}_N} \sum_{\mathscr{B}_M} \int_{\{N,M\}} P(\mathscr{A}_N, Y_0) P(\mathscr{B}_M, Y - Y_0) \mathcal{S}(\mathscr{A}_N, \mathscr{B}_M), \tag{*i*.98}$$

where $\int_{\{N,M\}}$ denote the integration over the transverse coordinates of all the gluons in the respective cascades. Using eq (*i*.97), the condition $\partial_{Y_0} S = 0$ now reads

$$\begin{aligned}&\sum_{\mathscr{C}_{N+1}} \int_z \mathcal{R}(\mathscr{A}_N \to \mathscr{C}_{N+1}) \{\mathcal{S}(\mathscr{C}_{N+1}, \mathscr{B}_M) - \mathcal{S}(\mathscr{A}_N, \mathscr{B}_M)\} = \\ &= \sum_{\mathscr{D}_{M+1}} \int_z \mathcal{R}(\mathscr{B}_M \to \mathscr{D}_{M+1}) \{\mathcal{S}(\mathscr{A}_N, \mathscr{D}_{M+1}) - \mathcal{S}(\mathscr{A}_N, \mathscr{B}_M)\}. \end{aligned} \tag{*i*.99}$$

This equation is not satisfied for the dipole model in case one includes multiple scatterings. It was, however, shown in [45] that the equality does hold in the one pomeron approximation [10]. In that case the equation reduces to

$$\sum_{i=1}^{N}\sum_{j=1}^{M}\int_{\boldsymbol{z}}\mathcal{M}(\boldsymbol{x}_{i-1},\boldsymbol{x}_i,\boldsymbol{z})\{f(\boldsymbol{x}_{i-1},\boldsymbol{z}|\boldsymbol{y}_{j-1},\boldsymbol{y}_j)+f(\boldsymbol{z},\boldsymbol{x}_i|\boldsymbol{y}_{j-1},\boldsymbol{y}_j) \\ -f(\boldsymbol{x}_{i-1},\boldsymbol{x}_i|\boldsymbol{y}_{j-1},\boldsymbol{y}_j)\} = \\ =\sum_{i=1}^{N}\sum_{j=1}^{M}\int_{\boldsymbol{z}}\mathcal{M}(\boldsymbol{y}_{j-1},\boldsymbol{y}_j,\boldsymbol{z})\{f(\boldsymbol{y}_{j-1},\boldsymbol{z}|\boldsymbol{x}_{i-1},\boldsymbol{x}_i)+f(\boldsymbol{z},\boldsymbol{y}_j|\boldsymbol{x}_{i-1},\boldsymbol{x}_i) \\ -f(\boldsymbol{y}_{j-1},\boldsymbol{y}_j|\boldsymbol{x}_{i-1},\boldsymbol{x}_i)\}, \qquad (i.100)$$

where f was defined in (*i*.94). Here we have denoted the transverse coordinates of the dipoles in the left-moving (right-moving) onium with $\boldsymbol{y}_j$ ($\boldsymbol{x}_i$).

By making a Möbius transformation one can transform the coordinates $\boldsymbol{x}_i$ and $\boldsymbol{y}_i$ into one another, and using the Möbius invariance of the dipole kernel and f, each integral in the sum on both sides can be shown to be equal. Since there are $N \cdot M$ terms in each sum, the equality does indeed hold for the complete expression.

i.5.4 Dipole Swing

Identifying the interactions which give rise to the missing saturation effects mentioned above has been one of the tasks which the papers in this thesis are concerned with. Our proposal is to include the so-called *dipole swing* mechanism in the evolution.

Note that the evolution which starts from a single dipole generates a chain of dipoles which are all connected to each other via the gluons (this was discussed in sec *i*.4). When two dipole cascades collide, each dipole interaction implies a recoupling of the colour flow as indicated in figure *i*.10. A single dipole collision gives rise to two chains stretched between the right- and left-moving dipole ends, while multiple subcollisions give rise to colour loops.

If we now make a boost, these loops have to be formed inside one of the dipole cascades. It is then necessary that saturation effects give rise to such loops inside the cascades. The loops can be formed in two different ways.

First of all, if we wish to go beyond the leading N_c approximation we must take into account the fact that colour structures more complicated than dipoles, such as quadrupoles, are formed. Using the dipole basis one then has to decide how to represent such a quadrupole. The natural way to do this would be to approximate the quadrupole field by two dipoles formed by

[10] Note that eq (*i*.96), which corresponds to one pomeron exchange, does not depend on Y_0.

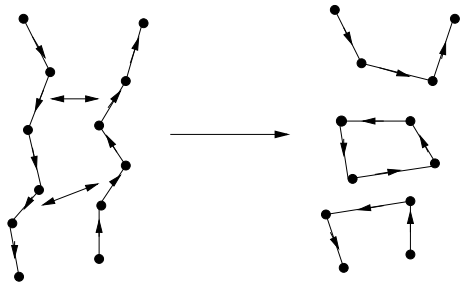

Figure *i*.10: Each dipole interaction among the dipole chains implies a recoupling of the colour flow as indicated in the figure. Each arrow indicates the colour flow which goes from colour to anti-colour.

the closest colour–anticolour pairs. Thus if we have two dipoles $(\boldsymbol{x}_i, \boldsymbol{y}_i)$ and $(\boldsymbol{x}_j, \boldsymbol{y}_j)$, we must take into account the fact that these may regroup themselves into two new dipoles $(\boldsymbol{x}_i, \boldsymbol{y}_j)$ and $(\boldsymbol{x}_j, \boldsymbol{y}_i)$. This process is called a dipole swing.

Secondly, dipoles inside the same cascade may interact with each other by exchanging gluons. As mentioned above, each interaction implies a recoupling of the colour flow, and therefore the two dipoles $(\boldsymbol{x}_i, \boldsymbol{y}_i)$ and $(\boldsymbol{x}_j, \boldsymbol{y}_j)$ will once more be transformed into $(\boldsymbol{x}_i, \boldsymbol{y}_j)$ and $(\boldsymbol{x}_j, \boldsymbol{y}_i)$.

If we see the dipole swing as a way to approximate colour quadrupoles, then it will be suppressed by[11] $1/N_c^2$. If on the other hand we view the swing as the result of a gluon exchange, then it must be proportional to α_s^2. However, notice that α_s is formally suppressed by a factor N_c when compared to $\bar{\alpha}$ which appears in the dipole splitting kernel in (*i*.82). Thus in both cases the process is suppressed by $1/N_c^2$.

In our Monte Carlo implementation each dipole is randomly assigned one of N_c^2 possible colours, and only dipoles of the same colour are allowed to swing. The weight for a swing is determined by the factor

$$\frac{(\boldsymbol{x}_i - \boldsymbol{y}_i)^2 (\boldsymbol{x}_j - \boldsymbol{y}_j)^2}{(\boldsymbol{x}_i - \boldsymbol{y}_j)^2 (\boldsymbol{x}_j - \boldsymbol{y}_i)^2}. \tag{*i*.101}$$

From this weight we see that the swing is more likely to replace two dipoles by two smaller dipoles, in accordance with the discussion above. It also retains the property that the total weight of a dipole chain is given by $\prod_i (1/\boldsymbol{r}_i^2)$ where the index i runs over all dipoles present in the cascade, and $\boldsymbol{r}_i$ the size of the dipole i.

[11] One may naively expect that the probability for a recoupling is proportional to $1/N_c$, but the correct factor is $1/N_c^2$ since this is the probability that a given colour–anticolour pair forms a colour singlet.

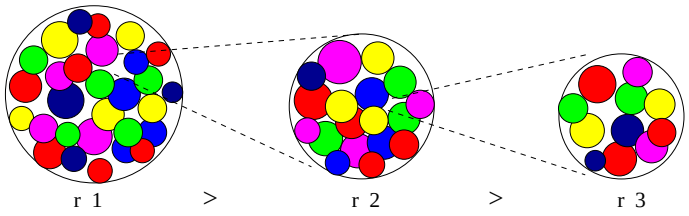

Figure *i*.11: At the leftmost figure, we see the proton at a certain resolution scale r_1. As we put more gluons inside the proton all avaliable holes with radius larger than r_1 get occupied. We can then put more gluons inside the proton by lowering our resolution scale to $r_2 < r_1$. We can continue to increase the gluon occupancy until there are no holes with radius larger than r_2. We can then continue by further lowering our resolution scale down to $r_3 < r_2$ and so on. Continously shrinking the length scale, we can always find avaliable space for more gluons.

We also note that the weight in eq (*i*.101) gives an analogy with the CGC formalism where it can be shown that the gluon occupation number at fixed impact parameter $\boldsymbol{b}$, and transverse momentum $\boldsymbol{k}$, satisfies

$$\frac{dN}{d^2\boldsymbol{b}d^2\boldsymbol{k}} \lesssim \frac{1}{\alpha_s^2} \tag{*i*.102}$$

due to saturation. In (*i*.102) we have integrated over rapidity y, and the occupation number density for each fixed y is bounded by $1/\alpha_s$. In the CGC formalism, there is no bound for the total number of gluons. The growth of the total number of gluons never stops, even in the saturation region. What happens is that the exponential growth in y (powerlike in s) in the dilute region is replaced by a linear growth in y (logarithmic in s) in the saturation region. What saturates is therefore the splitting rate of the gluons, rather than the total number of gluons.

This can be understood as follows. Let us again represent the proton as a thin disc in which the gluons appear as smaller discs with radii $r \sim 1/|\boldsymbol{k}|$. As we go to higher energies, the number of gluons inside the proton increases, and we can continue to put more gluons on top of each other until there are so many gluons overlapping that their mutual interaction is strong enough to prevent further occupation at that $\boldsymbol{b}$. If we thus hold the gluon sizes fixed, (fixed $\boldsymbol{k}$) then sooner or later we will reach a point where it is not possible to put in any more gluons of that size. In that case we have to increase $\boldsymbol{k}$, which in our classical picture corresponds to adding smaller discs into the proton, see figure *i*.11. At one stage those smaller discs will also fill up the avaliable holes, but there is then more room for even smaller discs and so on. We can continue in this way forever, and the total number of gluons therefore never

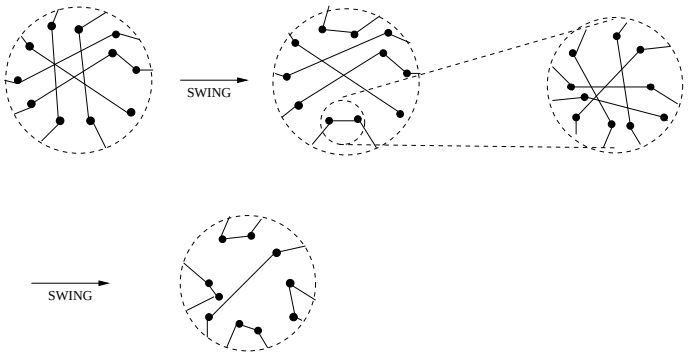

Figure *i*.12: At the leftmost figure, we see a certain region of the proton occupied by dipoles. When the number of dipoles around a certain $\boldsymbol{b}$ is large enough, there will be dipole swings. In the second figure we zoom into the region around one of the dipoles, which after some time gets occupied with more dipoles. When the density around this new $\boldsymbol{b}$ gets high, there will be more swings and so on.

ceases to grow. For fixed $\boldsymbol{k}$, however, the occupation number must saturate, as in (*i*.102).

The dipole swing works in a very similar way (see figure *i*.12). Since the evolution is driven by the $1 \to 2$ splitting plus the $2 \to 2$ swing, the total number of dipoles will continue to grow forever. Assume, however, that we wish to put many dipoles of similar size r around the same impact parameter $\boldsymbol{b}$. If the number of dipoles is less than N_c^2, there are no problems since the swing is not very likely. However, as soon as we have N_c^2 dipoles they can start to swing, and since in this case they sit on top of each other, they will do so as soon as the chance is given. When two dipoles swing they will be replaced by two smaller dipoles, with different impact parameters $\boldsymbol{b}'$. This implies that the dipole occupation number satisfies

$$\frac{dN}{d^2\boldsymbol{b}d^2\boldsymbol{r}} \lesssim N_c^2 \sim \frac{1}{\alpha_s^2}. \tag{*i*.103}$$

Here we assumed $\bar{\alpha}$ to be fixed and of order $1/\pi$ in which case we get $\alpha_s \sim 1/N_c$. When the number of smaller dipoles around $\boldsymbol{b}'$ gets large enough they will in turn start to swing to produce even smaller dipoles and so on. Thus we get a picture which is similar to that in the CGC formalism.

i.6 The Papers

In this section we shortly describe the 5 papers included in this thesis.

i.6.1 Paper 1

The small-x limit of QCD, where the momentum transfer is fixed and the energy is very large, is to leading order described by the BFKL equation. However, quantitative predictions from BFKL are made difficult due to the very large non-leading (NLO) corrections. Another problem comes from the fact that the linear BFKL equation does not contain saturation effects which are expected to be increasingly important as we go towards smaller x.

Non-linear effects such as saturation and unitarisation are easier to take into account in a formulation based on transverse coordinates, while non-leading corrections such as energy-momentum conservation are easier in a formulation based on transverse momenta. It has therefore been rather difficult to estimate the relative importance of these different effects.

In paper 1, we present a model for implementing both non-linear and non-leading effects, knowing that an important fraction of the NLO corrections to the BFKL equation are related to energy conservation. Our model is based on Mueller's dipole formulation which reproduces the leading order BFKL equation, and which in addition also takes into account saturation effects due to multiple scatterings. Mueller's model is formulated in transverse coordinate space, and does not include energy conservation. However, noting similarities between Mueller's model and the Linked Dipole Chain (LDC) model, we derive a scheme for implementing energy conservation in Mueller's model, and our ideas are tested in a Monte Carlo simulation.

We find that energy conservation has a large effect on the evolution, severely dampening the growth of the number of dipoles and, consequently, the total cross section. This also implies that saturation has a relatively small impact on the evolution at HERA, and we find a good semi-quantitative description of the effective slope $\lambda_{eff} = d\ln F_2/\ln x$, also without saturation.

i.6.2 Paper 2

Although Mueller's model includes saturation effects from multiple scatterings, the evolution of the dipole cascades satisfies the linear BFKL equation. There are consequently no saturation effects in the evolution of the individual dipole cascades, which also implies that the formalism is not Lorentz-frame independent.

In paper 2, we further improve our model from paper 1, to also include saturation effects during the cascade evolutions. We propose to take into account these effects by including a $2 \rightarrow 2$ dipole transition called the dipole

swing. Furthermore, we include effects from a running coupling and we also introduce a simple description of the initial proton in terms of three dipoles.

Implementing these improvements in our Monte Carlo simulation, we find a very good agreement with both the total $\gamma^* p$ cross section as measured at HERA, and the total pp cross section for energies ranging from the ISR to the Tevatron and beyond. Although we cannot show analytically whether or not the dipole swing would give a frame independent evolution, we find numerically for pp collisions that the resulting evolution is almost frame independent.

i.6.3 Paper 3

DIS data from HERA exhibits a remarkable property known as geometric scaling, which implies that the total cross section, $\sigma_{tot}^{\gamma^* p}$, is a function of the variable $\tau = Q^2/Q_s^2(x)$ only. Here $Q_s(x)$ is the so-called saturation momentum which is proportional to $x^{-\lambda}$, with λ having values around 0.3.

Geometric scaling is inherent in the Golec-Biernat Wüsthoff (GBW) dipole model (also called the saturation model) which successfully describes $\sigma_{tot}^{\gamma^* p}$ at HERA. The success of the GBW model, together with the fact that the scaling function shows a break around $\tau \approx 1$, has been taken as an indication for saturation. However, the analysis around the point $\tau \approx 1$ is made difficult due to the fact that small values of τ are at HERA only reached for $Q^2 < 1\text{GeV}^2$, meaning that non-perturbative physics plays an important role.

In paper 3, we show that, besides saturation, also the transition between the dominance of $k_\perp$-ordered (DGLAP) and $k_\perp$–non-ordered (BFKL) chains contributes to a break around $\tau \approx 1$, as well as the suppression for small Q^2 due to finite quark masses and confinement. We use the model developed in papers 1 and 2 to investigate the roles played by these different effects on the scaling properties. We also see that geometric scaling follows naturally from our dipole cascade model, when Q^2 is large compared to the quark masses, and that also the linear one-pomeron cross section exhibits scaling, so that geometric scaling alone cannot be taken as a proof for saturation.

Due to the limited energy range at HERA, there is little overlap between data at different Q^2 for fixed $\tau < 1$. It is therefore not experimentally excluded that scalebreaking effects would show up when a larger Q^2 range is avaliable. For small Q^2, the result is very sensitive to the assumed quark masses. The model can reproduce the data, but it also predicts a scale breaking behaviour, and as a consequence we predict that the scaling behaviour will be changed when data from a future machine will be avaliable.

We also investigate the scaling properties of the charm contribution, and we find that one can also here obtain a scaling function by a suitable transformation of x in $Q_s(x)$.

i.6.4 Paper 4

As we have already mentioned above, Mueller's model does not include saturation effects in a fully consistent way, meaning that the evolution is not frame independent.

In a simple model proposed by Mueller, one neglects all transverse coordinates, so that rapidity defines the only dimension. The model then describes a system of point-like "dipoles" which evolve through dipole splittings, as in a reaction-diffusion type model. In this model, explicit calculations are possible, and one can easily obtain an explicitely frame-independent formalism.

The resulting frame-independent evolution can be interpreted such that a new dipole is at each step emitted coherently from a "multi-dipole" state, with similarities to the saturation mechanism in the Color Glass Condensate. Recently, a 1+1 dimensional generalization of the simple toy model was presented. In this model, the assumption is again that a dipole state evolves by the addition of a new single dipole only, without changing the configuration of the emitting state. One can then easily obtain an explicitely frame independent evolution, in a fashion similar to the 1+0 dimensional toy model.

In paper 4, we show that the toy models mentioned above can be given a probabilistic formulation in terms of positive definite $k \to k+1$ transitions. Such transitions can in the real model be naturally generated by combining the dipole splitting with the dipole swing. In a $k \to k+1$ transition, a splitting is combined with $k-1$ simultaneous swings, so that k dipoles are replaced by $k+1$ new dipoles.

In an approximation where each dipole is restricted to single scattering only, a simple swing is shown to be enough to generate the necessary colour correlations, while one needs to include more than one swing at a time if individual dipoles are allowed to scatter multiply. In this case the evolution proceeds such that the newly produced dipoles swing multiply with the dipoles in the emitting cascade, giving rise to the $k \to k+1$ transitions mentioned above.

For a system consisting of N dipoles, we show that one needs at most $N-1$ swings in order to generate all colour correlations induced by the multiple dipole interactions. For spatially disconnected dipoles this is very easy to show. For the more relevant case of dipoles connected in chains, we have explicitely checked for a number of cases that this is also true, which leads us to conjecture that it is true for all cases.

The positive definite transition rates in the toy models are written in a form which suggests that they indeed describe such processes where a single splitting is combined with $k-1$ swings. However, one difference is in the saturation mechanisms. Due to the fact that the toy models have trivial topologies, it is difficult to directly compare the swing in the full model to the saturation mechanism present in the toy models. The results presented here may

hopefully help in the attempts to formulate an explicitely frame independent formalism for the full model.

i.6.5 Paper 5

In high energy pp collisions, the cross section for parton–parton subcollisions exceeds the total cross section, which implies that there are on average more than one subcollision in each event. Via unitarity and the AGK cutting rules, multiple subcollisions also have strong implications for diffraction.

In the quantum mechanical Good and Walker picture of diffraction, the diffractive excitation is determined by the fluctuations in the collision process. These fluctuations arise from the initial particle wave functions, from the cascade evolutions, from the impact parameter variation, and from the dipole–dipole scattering probabilities.

In paper 5, we use the model developed in papers 1-3 to study diffractive excitation in $\gamma^* p$ and pp collisions. We improve our model further to treat confinement effects by consistently replacing the infinite range colour-electric Coulomb potential by a screened Yukawa potential. This also turns out to have important consequences on the frame independence of $\gamma^* p$ collisions. Using the Good and Walker picture of diffraction, we can investigate the dependence of the cross sections on the mass of the diffractively excited system by studying the collision in different Lorentz frames.

Most models only include part of the fluctuations mentioned above, and this has the implication that different models give different results for the impact parameter profile of the cross section. In our model we include all fluctuations, and this implies among other things that our impact parameter profile is less steep as compared to models where not all fluctuations are included.

Investigating the role of the fluctuations from the different sources we conclude that there are important contributions from all of them, apart from the initial proton wave function, and we find a good agreement with data for both pp collisions and DIS. We also find that elastic data are best reproduced if we minimize the fluctuations in the initial proton state.

Acknowledgments

I am very grateful to my supervisor Gösta Gustafson for all his help and support during the past three years. It has been a very useful experience to be subjected to his amazingly intuitive approach to difficult QCD problems. I also feel lucky to have written four papers together with a person who truly knows the art of scientific writing. I am equally grateful to my "second supervisor" Leif Lönnblad who has been very helpful both in physical discussions, and in computer simulations. It is no exaggeration to say that much of the work presented in this thesis would not have been possible without his help.

I would also like to thank Johan Bijnens and Bo Söderberg for extensive, and very useful, discussions on various physical and mathematical topics. I am also thankful to Christoffer Flensburg for critical questions and comments on the thesis manuscript.

i References

[1] B. Andersson, G. Gustafson, G. Ingelman, and T. Sjostrand *Phys. Rept.* **97** (1983) 31.

[2] H. Yukawa *Proc. Phys. Math. Soc. Jap.* **17** (1935) 48–57.

[3] R. Eden, P. Landshoff, D. Olive, and J. Polkinghorne, *The Analytic S-Matrix*. Cambridge University Press, 1966.

[4] V. Barone and E. Predazzi, *High-Energy Particle Diffraction*. Springer-Verlag Berlin Heidelberg, 2002.

[5] M. Froissart *Phys. Rev.* **123** (1961) 1053–1057.

[6] A. Martin. *Phys. Rev.* **129** (1963) 1432.

[7] I. Pomeranchuk. *Sov. Phys.* **3** (1956) 306.

[8] A. Donnachie and P. V. Landshoff *Phys. Lett.* **B296** (1992) 227–232, `hep-ph/9209205`.

[9] L. D. Landau and E. M. Lifshitz, *The Classical Theory of Fields*. Elsevier Butterworth-Heinemann, 1975.

[10] J. J. Sakurai, *Modern Quantum Mechanics*. Addison-Wesley Publishing Company, Inc., 1994.

[11] M. Breidenbach *et al. Phys. Rev. Lett.* **23** (1969) 935–939.

[12] **H1** Collaboration, C. Adloff *et al. Eur. Phys. J.* **C21** (2001) 33–61, `hep-ex/0012053`.

[13] **ZEUS** Collaboration, J. Breitweg *et al. Z. Phys.* **C74** (1997) 207–220, `hep-ex/9702015`.

[14] J. R. Forshaw and D. A. Ross *Cambridge Lect. Notes Phys.* **9** (1997) 1–248.

[15] E. A. Kuraev, L. N. Lipatov, and V. S. Fadin *Sov. Phys. JETP* **45** (1977) 199–204.

[16] I. I. Balitsky and L. N. Lipatov *Sov. J. Nucl. Phys.* **28** (1978) 822–829.

[17] G. Altarelli and G. Parisi *Nucl. Phys.* **B126** (1977) 298.

[18] V. N. Gribov and L. N. Lipatov *Yad. Fiz.* **15** (1972) 781–807.

[19] L. N. Lipatov *Sov. J. Nucl. Phys.* **20** (1975) 94–102.

[20] Y. L. Dokshitzer *Sov. Phys. JETP* **46** (1977) 641–653.

[21] E. Iancu, A. Leonidov, and L. McLerran `hep-ph/0202270`.

[22] L. V. Gribov, E. M. Levin, and M. G. Ryskin *Phys. Rept.* **100** (1983) 1–150.

[23] E. Iancu and R. Venugopalan `hep-ph/0303204`.

[24] H. Weigert *Prog. Part. Nucl. Phys.* **55** (2005) 461–565, `hep-ph/0501087`.

[25] J. Jalilian-Marian, A. Kovner, A. Leonidov, and H. Weigert *Nucl. Phys.* **B504** (1997) 415–431, hep-ph/9701284.

[26] J. Jalilian-Marian, A. Kovner, A. Leonidov, and H. Weigert *Phys. Rev.* **D59** (1999) 014014, hep-ph/9706377.

[27] E. Iancu, A. Leonidov, and L. D. McLerran *Phys. Lett.* **B510** (2001) 133–144, hep-ph/0102009.

[28] H. Weigert *Nucl. Phys.* **A703** (2002) 823–860, hep-ph/0004044.

[29] I. Balitsky *Nucl. Phys.* **B463** (1996) 99–160, hep-ph/9509348.

[30] Y. V. Kovchegov *Phys. Rev.* **D60** (1999) 034008, hep-ph/9901281.

[31] A. H. Mueller *Nucl. Phys.* **B415** (1994) 373–385.

[32] E. Iancu and D. N. Triantafyllopoulos *Nucl. Phys.* **A756** (2005) 419–467, hep-ph/0411405.

[33] A. H. Mueller, A. I. Shoshi, and S. M. H. Wong *Nucl. Phys.* **B715** (2005) 440–460, hep-ph/0501088.

[34] E. Levin and M. Lublinsky *Nucl. Phys.* **A763** (2005) 172–196, hep-ph/0501173.

[35] G. Gustafson *Phys. Lett.* **B175** (1986) 453.

[36] G. Gustafson and U. Pettersson *Nucl. Phys.* **B306** (1988) 746.

[37] Y. L. Dokshitzer, V. A. Khoze, A. H. Mueller, and S. I. Troyan, *Basics of perturbative QCD*. Ed. Frontieres, Gif-sur-Yvette, France, 1991.

[38] L. Lönnblad *Comput. Phys. Commun.* **71** (1992) 15–31.

[39] B. Andersson, G. Gustafson, L. Lönnblad, and U. Pettersson *Z. Phys.* **C43** (1989) 625.

[40] B. Andersson, G. Gustafson, and J. Samuelsson *Nucl. Phys.* **B467** (1996) 443–478.

[41] S. Catani, F. Fiorani, and G. Marchesini *Phys. Lett.* **B234** (1990) 339.

[42] M. Ciafaloni *Nucl. Phys.* **B296** (1988) 49.

[43] A. H. Mueller and B. Patel *Nucl. Phys.* **B425** (1994) 471–488, hep-ph/9403256.

[44] A. H. Mueller *Nucl. Phys.* **B437** (1995) 107–126, hep-ph/9408245.

[45] A. H. Mueller and G. P. Salam *Nucl. Phys.* **B475** (1996) 293–320, hep-ph/9605302.

I

Energy Conservation and Saturation in Small-x Evolution

Emil Avsar, Gösta Gustafson and Leif Lönnblad

Dept. of Theoretical Physics, Sölvegatan 14A, S-223 62 Lund, Sweden

JHEP **07** (2005) 062, hep-ph/0503181.

Important corrections to BFKL evolution are obtained from non-leading contributions and from non-linear effects due to unitarisation or saturation. It has been difficult to estimate the relative importance of these effects, as NLO effects are most easily accounted for in momentum space while unitarisation and saturation are easier in transverse coordinate space. An essential component of the NLO contributions is due to energy conservation effects, and in this paper we present a model for implementing such effects together with saturation in Mueller's dipole evolution formalism. We find that energy conservation severely dampens the small-x rise of the gluon density and, as a consequence, the onset of saturation is delayed. Using a simple model for the proton we obtain a reasonable qualitative description of the x-dependence of F_2 at low Q^2 as measured at HERA even without saturation effects. We also give qualitative descriptions of the energy dependence of the cross section for $\gamma^\star\gamma^\star$ and $\gamma^\star-$nucleus scattering.

I.1 Introduction

In the asymptotical high-energy limit, QCD should be described by BFKL [1,2] evolution, at least to leading order and assuming a fixed coupling. Here terms of the form $(\alpha_s \log x)^n$ in a perturbative expansion are resummed to all orders. The result is a fast rise of any cross section with increasing energy or, equivalently, with decreasing x. The rise has the form $x^{-\lambda}$, where the power λ to leading order is given by $\bar{\alpha}\, 4 \log 2$, which is around one half for $\bar{\alpha} \equiv 3\alpha_s/\pi = 0.2$. Clearly such a behavior will violate the unitarity bound for large enough energies. To cure this problem Gribov, Levin and Ryskin [3] in pioneering works discussed non-linear effects from gluon recombination, which cause the gluon density to saturate before it becomes too high.

Because the transverse coordinates are unchanged in a high energy collision, unitarity constraints are generally more easy to take into account in a formalism based on the transverse coordinate space representation, and several suggestions for how to include saturation effects in such a formalism have been proposed. Golec–Biernat and Wüsthoff [4] formulated a dipole model, in which a virtual photon is treated as a $q\bar{q}$ or $q\bar{q}g$ system impinging on a proton, and this approach has been further developed by several authors (see e.g. [5] and [6]). Mueller [7–9] has formulated a dipole cascade model in transverse coordinate space, which reproduces the BFKL equation, and in which it is also possible to account for multiple sub-collisions. Within this formalism Balitsky and Kovchegov [10, 11] have derived a non-linear evolution equation, which also takes into account these saturation effects from multi-pomeron exchange. In an alternative approach a high density gluonic system is described by a so-called Color Glass Condensate [12, 13], where non-perturbative effects appear due to the high density, even though the coupling α_s is small.

There are, however, other effects which may dampen the growth of the structure function. One is the fact that the next-to-leading logarithmic corrections to the BFKL evolution turn out to be very large [14,15]. These corrections strongly suppress the growth for small x, and in fact, even for moderate values of $\bar{\alpha}$, the power λ becomes negative. It is well-known [16] that a major fraction of these higher order corrections is related to energy conservation. The large effect of energy-momentum conservation is also clearly demonstrated by the numerical analyses by Andersen–Stirling [17] and Orr–Stirling [18].

As a consequence there is currently some controversy over whether saturation has been observed in deeply inelastic scattering at HERA. Saturation effects have been studied in the coordinate space representation in which it has been difficult to include non-leading effects, and the non-leading effects have been studied in momentum space, where it is hard to include saturation. Therefore it has been difficult to estimate the relative importance of saturation and non-leading effects. To know if the dominant mechanism behind the re-

duced growth rate is due to energy conservation or to saturation is also very important for reliable extrapolations to higher energies at LHC and high energy cosmic ray events. Our aim in this paper is to find a formalism where it is possible to account for both unitarisation and energy-momentum conservation, knowing that the latter is a major part of the non-leading effects. An alternative approach to this problem is presented in [19, 20], in which a formalism to include saturation and conservation of energy (or rather the positive lightcone momentum component, p_+) is described. In our formalism we emphasize conservation of both lightcone components, p_+ and p_-.

We emphasize that the question concerning saturation is not whether it exists in general — clearly if the scale is small enough so that the transverse size of the gluons is as big as a nucleon there must be recombinations present — rather the debate is about whether effects of recombination of *perturbative* gluons at scales above a couple of GeV has been observed. The deviation from the linear BFKL evolution, as a consequence of saturation, is expected to be essential below a line $Q^2 = Q_s^2(x)$ in a (Q^2, x) diagram [4]. The effect can be viewed in two different ways, as a suppression of the logarithmic x-slope of the structure function, $d \log F_2 / d \log x \equiv \lambda_{\text{eff}}$, when x becomes small for fixed Q^2, or as a suppression when Q^2 becomes small for fixed x. HERA data show an almost linear dependence of λ_{eff} with $\log Q^2$, leveling off at ≈ 0.1 for Q^2 below 1 GeV^2, with the proviso that the x-interval used to determine the slope is not constant, but is shifted towards smaller x for smaller Q^2-values (see e.g. refs. [21, 22]). The suppression for small x and for small Q^2 also appears to satisfy a scaling property called geometric scaling, saying that F_2 is a function of a single variable $\tau = Q^2/Q_s^2(x)$. This scaling is satisfied by the HERA data to a high degree, and in an early study Golec–Biernat and Wüsthoff found a good fit to experiments with $Q_s^2(x) = (3.04 \cdot 10^{-4}/x)^{0.288}\,\text{GeV}^2$ [4]. In a more recent analysis Iancu, Itakura, and Munier [23] obtained a good fit to later HERA data with a model based on BFKL evolution including some non-leading effects[1] plus saturation, with $Q_s^2(x) = (0.267 \cdot 10^{-4}/x)^{0.253}\,\text{GeV}^2$. This value is smaller than the one in ref. [4], and therefore moves the saturation region closer to the non-perturbative regime.

The Mueller dipole evolution is formulated in rapidity ($\propto \log 1/x$) and transverse coordinate space, with rapidity acting as the evolution parameter. A DIS $\gamma^\star p$ scattering is typically viewed in the rest system of the proton, where the $\gamma^\star$ evolves into a $q\bar{q}$ pair, long before the interaction. This $q\bar{q}$ pair will then radiate off gluons, $q\bar{q} \to qg\bar{q} \to qgg\bar{q} \to \ldots$, a process which is formulated in terms of radiation from colour-dipoles. The initial dipole between the q and

[1] Basically, non-leading effects are taken into account by simply lowering the BFKL λ, or treating it as a free parameter, in which case it comes out close to the value predicted by the so-called renormalization-group improved [24] NLO BFKL. Also some non-leading effects are introduced by letting α_s run, typically with Q_s^2 as the scale.

$\bar{q}$ emits a gluon, splitting the dipole into two, one between the q and g and one between the g and $\bar{q}$, both of which can continue radiating gluons. In the end, one of these dipoles can interact with the proton, giving a cross section which increases as a power of $1/x$, and in leading order reproduces the BFKL result. Saturation comes in because when the density of dipoles becomes large there is a possibility that more than one of them interacts with the proton, thus slowing down the increase of the cross section. This effect can be interpreted as multi-pomeron exchange, and is taken into account in the non-linear BK equation.

The Mueller dipole evolution is very similar in spirit to the Dipole Cascade Model (DCM) [25,26], which describes time-like evolution of dipoles from e.g. an initial $q\bar{q}$ pair created in e^+e^- annihilation. However, here the evolution is formulated in momentum space. The transverse momentum is used as evolution parameter, and the conservation of energy and momentum is simple to implement, especially in a Monte Carlo Event Generator. This model gives a very good description of e^+e^- annihilation and the ARIADNE program [27], where it is implemented, describes almost all data from the four LEP collaborations to an astonishing precision (see e.g. [28]). Also with the so-called soft-radiation extension of the DCM, DIS final states as measured by HERA are well described using a simple semi-classical description of time-like dipole evolution (see e.g. [29]).

One problem in Mueller's formulation is the fact that, while the emission probability for a time-like cascade in the DCM is finite for a fixed value of the evolution parameter, the emission probability here diverges $\sim 1/r^2$ for very small dipole sizes r. However, the interactions from the colour charge and anti-charge interfere destructively, resulting in colour transparency, and for small r-values the dipole cross section is proportional to r^2, implying that the total cross section remains finite, and the Mueller dipole formulation can be shown to be equivalent to BFKL. Although σ_{tot} is finite, the singularities do cause problems. For a numerical analysis or a MC simulation it is necessary to introduce a cutoff for small dipoles, and for small cutoff values the number of dipoles becomes very large. In fact, the increase is so strong that a Monte Carlo simulation of the evolution, as is done e.g. in the OEDIPUS program [30–32], becomes extremely inefficient. It also implies that it is not possible to interpret the dipole chain as a real final state. If a small size in coordinate space corresponds to a large transverse momentum, the very large and diverging number of dipoles with very small sizes obviously violates energy-momentum conservation. Instead these emissions have to be regarded as virtual fluctuations, which in Mueller's approach are handled by appropriate Sudakov form factors.

An alternative approach to DIS is the so-called Linked Dipole Chain (LDC) [33,34] model, where an initial set of gluons is obtained using space-like par-

ton evolution, and then is evolved in time-like cascades into final-state gluons. LDC is a reformulation and generalization of CCFM evolution [35, 36], which reproduces BFKL in the asymptotic small-x limit but is also similar to DGLAP evolution [37–40] at larger x values. In addition to sequences of DGLAP evolution, where the *upward* gluon branchings with $k_{\perp i} \gg k_{\perp i-1}$ are strongly ordered in rapidity and in the $k_\perp$ of the propagating gluon, also *downward* splittings with $k_{\perp i} \ll k_{\perp i-1}$ may appear with a reduced weight. The result is an evolution which is totally symmetric, in the sense that it can be generated either from the projectile or from the target end with the same result. The LDC model is completely formulated in momentum space which makes it easy to implement in a Monte Carlo event generator [41], where energy and momentum conservation is easily accomplished.

In this paper we will identify some similarities between the LDC model and the Mueller dipoles, and use them to derive a scheme for implementing energy momentum conservation in the space-like dipole evolution. We conjecture that only gluon emissions which satisfy energy-momentum conservation can correspond to real final state gluons, and that keeping only these (with a corresponding modification of the Sudakov form factor) will not only give a better description of the final states, but also account for essential parts of the NLO corrections to the BFKL equation. Our approach is based on the observation that the emission of a dipole with a very small transverse size, r, corresponds to having two very well localized gluons, and such gluons must have large transverse momenta, of the order of $p_\perp \sim 1/r$. By in this way assigning a transverse momentum to each emitted gluon, and also taking into account the recoils of the emitting gluons, we can then make sure that each dipole splitting is kinematically allowed. However, as will be discussed in detail in section I.4.3, energy-momentum conservation is a *necessary* condition for a chain to correspond to a real final state, but it is not a *sufficient* condition. Therefore we will in this paper only discuss results for total cross sections, and postpone discussions of final state properties to a future publication.

The program described here is, of course, not easy to implement in an analytic formalism. Instead we have written a Monte Carlo program, similar to OEDIPUS, where the kinematics can be easily treated. This program can then be used to calculate cross sections for e.g. dipole–dipole scattering at different virtualities. We also introduce a simple model for nucleons as a distribution in dipole numbers and sizes, to investigate cross sections for dipole–A scattering. In principle this can also be used to study AA scattering, but such investigations will also be postponed for a future publication.

The layout of this paper is as follows. First we describe the dipole cascades formulated both in transverse momentum and in coordinate space in sections I.2 and I.3. In section I.4 we then describe the similarity between the LDC model and Mueller's cascade model, and how this guides us in the

introduction of energy-momentum conservation into the Mueller dipole formalism. In this section we also discuss some open questions related to final state properties and gluon recombination. In section I.5 we describe briefly the implementation in a Monte Carlo program we use to obtain the results presented in the following section I.6. Finally we arrive at our conclusions in section I.7.

I.2 Dipole Cascades in Momentum Space

The Dipole Cascade Model (DCM [25,26]) as implemented in the ARIADNE [27] event generator has been very successful in describing the bulk of the data on hadronic final states recorded at LEP. In this section we will first describe briefly this model and then go on to how it can be extended to also describe cross sections and hadronic final states in DIS by a reformulation of the CCFM evolution.

I.2.1 Time-like Cascades

In e^+e^- annihilation, the emission of a gluon from the initial $q\bar{q}$-pair can be described in terms of dipole radiation from the colour-dipole between the q and $\bar{q}$. Subsequent emission of a second gluon is then described as radiation from either of the two dipoles connecting the quark with the gluon and the gluon with the anti-quark. In the dipole rest frame the relative probability for such a dipole splitting is to leading logarithmic order given by the standard dipole radiation formula

$$d\mathcal{P} \propto \alpha_s \frac{dk_\perp^2}{k_\perp^2} dy. \tag{I.1}$$

The available phase space is a triangular region in the $(\log k_\perp^2, y)$ plane, $k_\perp e^{\pm y} < W$, where W is the invariant mass of the dipole.

Clearly this is very similar to the Mueller dipole formalism. The main differences are that here we have dipoles in momentum space rather than in transverse position, and the evolution is in decreasing transverse momentum rather than in increasing rapidity. Hence we here have a Sudakov form factor

$$-\log \Delta_S(k_{\perp\max}^2, k_\perp^2) = \int_{k_\perp^2}^{k_{\perp\max}^2} \frac{d\mathcal{P}}{dk_\perp'^2} dk_\perp'^2. \tag{I.2}$$

Also, we here deal only with real final-state emissions, while Mueller's formalism describe initial-state virtual dipoles.

The ordering in decreasing $k_\perp$ (measured in the rest frame of the emitting dipole) means that energy and momentum conservation is a relatively small

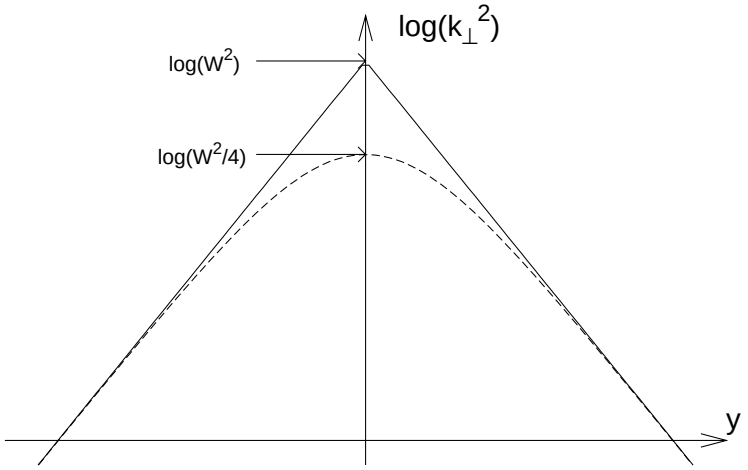

Figure I.1: The available phase space for a gluon emitted with some transverse momentum $k_\perp$ and rapidity y from a dipole with total invariant mass W. The full line represents the approximate phase space limits relevant for a leading log calculation, while the dashed line represents the modification when taking recoils of the emitting quarks into account.

correction. This formalism is easily implemented in a Monte Carlo generator, in which it is straight forward to take into account non-leading corrections to the emission probability in eq. (I.1) and energy-momentum conservation including proper recoils of the emitters, which modifies the triangular phase space region slightly as shown in figure I.1.

This formalism has many advantages as compared to conventional parton cascades. One very essential feature is that coherence effects, conventionally implemented as angular ordering, is automatically taken into account in a way which is more accurate than the conventional sharp angular cut.

I.2.2 Space-like Cascades

The dipole cascade model has been extended to also describe deeply inelastic lepton–hadron collisions in two different ways. The one which is implemented in ARIADNE relies on a semi-classical model [42] where all gluon emissions are treated as final-state radiation. This has been very successful in describing hadronic final states at HERA, but suffers from the fact that it does not predict the cross section. It is also difficult to relate to any standard evolution

equation, although it has qualitative similarities with BFKL and CCFM.

The other extension is called the Linked Dipole Chain (LDC) model [33] and uses a reformulation and generalization of CCFM evolution to build up an initial set of gluon emissions, which determines the cross section. These gluons define a chain of linked dipoles, which may initiate standard final-state dipole splittings, which then do not affect the cross section. The initial gluons are carefully selected to be purely real final-state gluons, i.e. only such emissions are considered which are not accompanied by large virtual corrections given by the so-called non-Sudakov form factor in CCFM (or Regge form factor in BFKL).

It turns out that these emissions are those where the gluons are ordered in both positive and negative light-cone momenta and with transverse momenta which are larger than the smaller of transverse momenta of the radiating propagator gluon before and after the emission: $p_{\perp i} > \min(k_{\perp i-1}, k_{\perp i})$. We are then left with simple splittings which either increase the $k_\perp$ of the propagator, given by

$$d\mathcal{P} = \bar{\alpha}\frac{dk^2_{\perp i}}{k^2_{\perp i}}\frac{dz_i}{z_i}, \tag{I.3}$$

or decreasing it, given by

$$d\mathcal{P} = \bar{\alpha}\frac{dk^2_{\perp i}}{k^2_{\perp i}}\frac{dz_i}{z_i}\frac{k^2_{\perp i}}{k^2_{\perp i-1}}. \tag{I.4}$$

The extra suppression $k^2_{\perp i}/k^2_{\perp i-1}$ for evolution with decreasing $k_\perp$ ensures that the evolution becomes symmetric, i.e. it does not matter whether we evolve from the proton or the virtual photon end. A local maximum, $k_{\perp\max}$, can be interpreted as evolutions from the projectile and target ends up to a central hard sub-collision. If treated as evolution from one end we then have a step up to $k_{\perp\max}$ followed by a step down in $k_\perp$, and from the weights in eqs. (I.3) and (I.4) this gives the correct factor $1/k^4_{\perp\max}$ expected from Rutherford scattering. If we instead have a local minimum, $k_{\perp\min}$, then there is no associated power of $k_\perp$, and such a minimum is therefore free of singularities.

Also the LDC model has been implemented in a Monte Carlo generator [41], which fairly well reproduces final states at HERA. However, there is a caveat, namely that crucial measurements sensitive to small-x dynamics, such as the rates of forward jets, can only be reproduced if non-singular parts of the gluon splitting function are omitted. For further discussions on this subject, we refer the reader to ref. [43].

I.3 Dipole Cascades in Coordinate Space

I.3.1 The Mueller Dipole Formulation

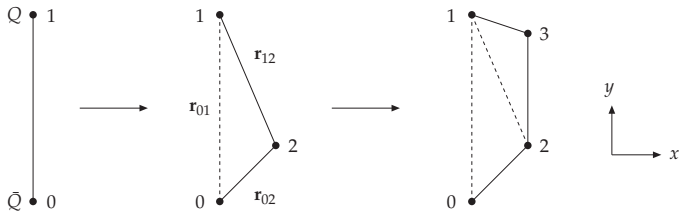

Figure I.2: A quark-antiquark dipole in transverse coordinate space is split into successively more dipoles via gluon emission.

Consider now the process of an evolving onium state or $\gamma^* \to Q\bar{Q} \to Qg\bar{Q} \to Qgg\bar{Q} \to \ldots$ in transverse coordinate space, as illustrated in figure I.2. Here a virtual photon is split into a $Q\bar{Q}$ colour dipole, which is first split into two dipoles by the emission of a gluon, then into three dipoles by a second gluon, etc. The probability for such a dipole splitting is given by the expression (for notation see figure I.2)

$$\frac{dP}{dy} = \frac{\bar{\alpha}}{2\pi} d^2\mathbf{r}_2 \frac{r_{01}^2}{r_{02}^2\, r_{12}^2} \cdot S$$
$$\text{where } S = \exp\left[-\frac{\bar{\alpha}}{2\pi} \int dy \int d^2\mathbf{r}_2 \frac{r_{01}^2}{r_{02}^2\, r_{12}^2} \right]. \tag{I.5}$$

Here S denotes a Sudakov form factor. When this dipole splitting is iterated it evolves into a cascade with with an exponentially increasing number of dipoles.

We note that the weight in eq. (I.5) is singular, and the integral over $d^2\mathbf{r}_2$ in the Sudakov form factor diverges for small values of r_{02} and r_{12}. Therefore Mueller introduced a cutoff ρ, such that the splitting has to satisfy $r_{02} > \rho$ and $r_{12} > \rho$. The integral in S is then also restricted in the same way. A small cutoff value ρ will here imply that we get very many dipoles with small r-values. However, as the cross section for a small dipole interacting with a target also gets small (see below), the total cross section is finite also in the limit $\rho \to 0$.

A proton target can be treated as a collection of dipoles. When two dipoles collide, there is a recoupling of the colour charges, forming new dipole chains. This is schematically illustrated in figure I.3 for the case of $\gamma^\star\gamma^\star$ scattering. Here we imagine the two virtual photons splitting up into quark-antiquark

pairs, which develop into two colliding dipole cascades. When the two central dipoles collide, it implies a recoupling, as indicated by the arrow. The weight for this interaction is given by the expression [32]

$$f = \frac{\alpha_s^2}{2}\left\{\log\left[\frac{|\mathbf{r}_1-\mathbf{r}_3|\cdot|\mathbf{r}_2-\mathbf{r}_4|}{|\mathbf{r}_1-\mathbf{r}_4|\cdot|\mathbf{r}_2-\mathbf{r}_3|}\right]\right\}^2. \tag{I.6}$$

An important property of this expression is that when e.g. the left of the interacting dipoles is small, the weight in eq. (I.6) can be shown to be proportional to $(\mathbf{r}_1-\mathbf{r}_2)^2$, which compensates the factor $(\mathbf{r}_1-\mathbf{r}_2)^{-2}$ in the evolution probability from eq. (I.5).

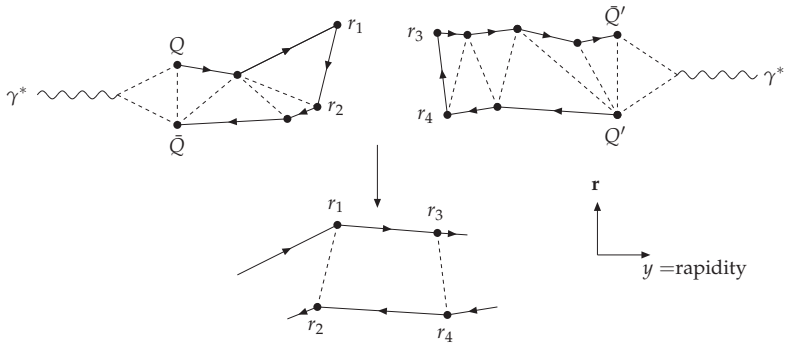

Figure I.3: A symbolic picture of a $\gamma^*\gamma^*$ collision in rapidity-$\mathbf{r}_\perp$-space. The two dipole chains interact and recouple with probability f given by eq. (I.6).

A $\gamma^\star p$ collision is frequently analyzed in the rest frame of the target proton. When the virtual photon hits the target, the number of dipoles present in this frame grows in accordance with the BFKL equation, and the total cross section increases proportional to $\exp(\lambda Y)$, where the total rapidity interval Y is given by $Y = \log(1/x) = \log(s/Q^2)$.

It is, however, also possible to study the collision in a frame different from the target rest frame. Then the target dipoles evolve in the same way a distance y in rapidity, while the projectile dipole evolves the shorter distance $Y - y$. As the evolution grows exponentially with rapidity, the cross section is proportional to $\exp(\lambda y)\cdot\exp(\lambda(Y-y)) = \exp(\lambda Y)$, which means that it is insensitive to the chosen frame, in which the collision is studied. This frame independence is, however, broken by multiple collision effects related to unitarity. This will be discussed further in section I.4.4.

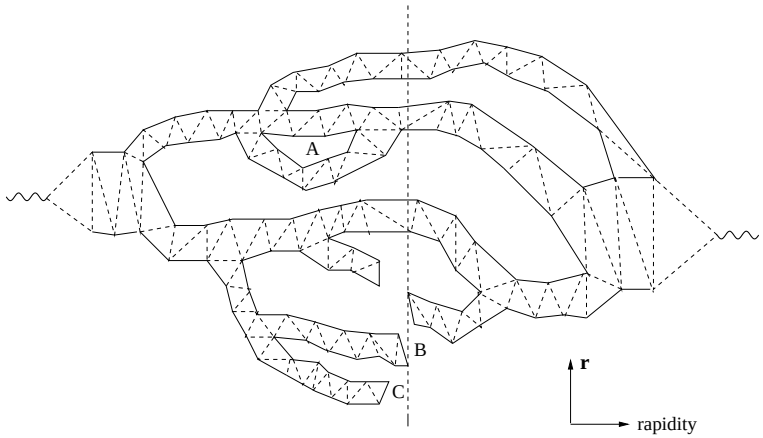

Figure I.4: A $\gamma^\star\gamma^\star$ collision event with multiple sub-collisions in rapidity-$\mathbf{r}_\perp$-space. At high energies several branches from the two colliding dipole systems may reconnect. The dashed vertical line symbolizes the Lorentz frame in which the collision is evaluated.

I.3.2 Unitarity and Saturation

A great advantage of the coordinate space representation is the fact that the transverse coordinate $\mathbf{r}$ is unchanged during the collision. This implies that unitarity can very easily be implemented by the replacement $f \to 1 - e^{-f}$. As the dipole cascades from the two virtual photons branch out, it is also possible to have *multiple interactions* with dipoles from the left and from the right, as illustrated in figure I.4. The total cross section is then given by

$$\sigma \propto \int d^2\mathbf{b}(1 - e^{-\sum f_{ij}}). \tag{I.7}$$

where $\mathbf{b}$ denotes the impact parameter separation between the two initial particles, and the sum runs over all pairs i and j of colliding dipoles. Here the factor $1 - e^{-\sum f_{ij}}$, where the exponent corresponds to a no-interaction probability, ensures that the unitarity constraint is satisfied. The first term in an expansion, $\sum f_{ij}$, corresponds to a single pomeron exchange, while the higher order terms are related to multi-pomeron exchanges.

Including these non-linear terms in the evolution equation leads to the Balitsky–Kovchegov (BK) equation [10, 11]. The BK equation governs the small-x evolution of the F_2 structure function of a large nucleus. In his original paper Kovchegov assumed a target nucleus at rest and an evolved projectile dipole. Using Mueller's dipole formulation for the evolution of the dipole and

summing pomeron exchanges of all orders he derived the following equation:

$$\frac{dN(\mathbf{r}_{01},Y)}{dY} = \frac{\bar{\alpha}}{2\pi}\int d^2\mathbf{r}_2 \frac{r_{01}^2}{r_{02}^2 r_{12}^2}\Big\{N(\mathbf{r}_{12},Y) + N(\mathbf{r}_{02},Y) - N(\mathbf{r}_{01},Y) - N(\mathbf{r}_{12},Y)N(\mathbf{r}_{02},Y)\Big\}. \quad \text{(I.8)}$$

Here $N(\mathbf{r}_{ij},Y)$ denotes the forward scattering amplitude (which also determines the total reaction probability) of the dipole $\mathbf{r}_{ij}$ on the target nucleus. The nucleus has been assumed to be large, which means that the impact parameter dependence of N is suppressed.

For small N-values the quadratic term can be neglected, and eq. (I.8) is reduced to Mueller's linear equation for the dipole cascade evolution. This equation is just the BFKL equation formulated in the dipole language. The first two terms correspond to the emission of a gluon forming two new dipoles, while the term with a minus sign accounts for the virtual corrections described by the Sudakov form factor in eq. (I.5). The quadratic term represents the effect of multiple collisions, which become more important when N becomes large. This suppresses the growth rate for larger Y-values and results in saturation when N approaches 1, thus preserving unitarity.

The BK equation (I.8) describes the development of the cascade before it hits a dense nuclear target. It can also be used to describe the evolution of two colliding cascades in a $\gamma^\star\gamma^\star$ collision, as illustrated in figure I.4. Here several branches from the two systems may reconnect as described in figure I.3 and eq. (I.6). We note here that the cascade evolution described by the linear terms in eq. (I.8) are only leading in colour, while the effect from multiple collisions is formally colour suppressed. Therefore this formalism includes corrections from multiple sub-collisions in the Lorentz frame in which the process is evaluated (denoted by the vertical dashed line in figure I.4), but does not take into account the possibility that two branches recombine before the collision. Such an event is indicated by the letter A in figure I.4. This effect is also colour suppressed and thus not included in the evolution. As a consequence the result depends on the Lorentz frame used, and this problem will be further discussed in section I.4.4.

I.4 Combining Energy-Momentum Conservation and Unitarity

With a small cutoff ρ ($r > \rho$) we get, as mentioned above, very many small dipoles. If these are interpreted as real emissions, with transverse momenta proportional to $1/r$, it would imply a catastrophic violation of energy-momentum conservation. As discussed above, the emission of these small dipoles

have a very limited effect on the total cross section, and they have to be interpreted as virtual fluctuations. Thus the result in eq. (I.7) will describe the inclusive cross section, but the many dipoles produced in all the branching chains will not correspond to the production of exclusive final states.

I.4.1 Relation Mueller's Dipole Cascade vs. LDC

Before a discussion of these virtual fluctuations we want to discuss the relation between Mueller's Dipole Cascade and the LDC model. Let us study the chain of emissions, which is illustrated in figure I.5. Apart from the Sudakov factors this chain gets the following weight:

$$\frac{d^2\mathbf{r}_2\, r_{01}^2}{r_{02}^2\, r_{12}^2}\cdot\frac{d^2\mathbf{r}_3\, r_{12}^2}{r_{13}^2\, r_{23}^2}\cdot\frac{d^2\mathbf{r}_4\, r_{23}^2}{r_{24}^2\, r_{34}^2}\cdot\frac{d^2\mathbf{r}_5\, r_{34}^2}{r_{35}^2\, r_{45}^2}\cdot\frac{d^2\mathbf{r}_6\, r_{35}^2}{r_{36}^2\, r_{56}^2} = \\ = r_{01}^2\,\frac{d^2\mathbf{r}_2\, d^2\mathbf{r}_3\, d^2\mathbf{r}_4\, d^2\mathbf{r}_5\, d^2\mathbf{r}_6}{r_{02}^2\, r_{13}^2\, r_{24}^2\, r_{45}^2\, r_{36}^2\, r_{56}^2} \tag{I.9}$$

We here note that the total weight is a product of factors $1/r_{ij}^2$ for all *"remaining dipoles"*, i.e. for those dipoles which have not been split by further gluon emission. They are marked by solid lines in figure I.5. All dependence on the size of *"intermediate"* dipoles, which have disappeared because they split in two daughter dipoles, is canceled in eq. (I.9), as they appear both in the numerator and in the denominator. (These dipoles are marked by dashed lines in figure I.5.)

If a dipole size, $\mathbf{r}$, is small, it means that the gluons are well localized, which must imply that transverse momenta are correspondingly large. This implies that not only the new gluon gets a large $k_\perp \sim 1/r$, but also that the original gluon, which is close in coordinate space, gets a corresponding recoil. For the special example in figure I.5 the emissions of the gluons marked 2, 3, and 4 give dipole sizes which become smaller and smaller, $a >> b >> c >> d$, in each step of the evolution. (This also implies that the "remaining" and the "intermediate" dipoles are pairwise equally large.) The corresponding $k_\perp$-values therefore become larger and larger in each step. After the minimum dipole, with size d, the subsequent emissions, 5, and 6, give again larger dipoles with correspondingly lower $k_\perp$ values. The probability for this chain is proportional to

$$\frac{d^2\mathbf{r}_2}{b^2}\cdot\frac{d^2\mathbf{r}_3}{c^2}\cdot\frac{d^2\mathbf{r}_4}{d^0}\cdot\frac{d^2\mathbf{r}_5}{e^2}\cdot\frac{d^2\mathbf{r}_6}{f^2}\cdot\frac{1}{f^2} \tag{I.10}$$

For the first emissions, 2 and 3, we in this expression recognize the product of factors $\prod d^2\mathbf{r}_i/r_i^2 \propto \prod d^2\mathbf{k}_i/k_i^2$, just as is expected from a "DGLAP evolution" of a chain with monotonically increasing $k_\perp$. Emission number 4 corresponds to the minimum dipole size, d, which should be associated with a

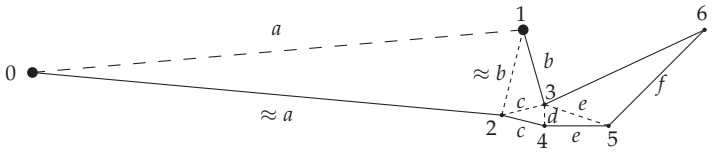

Figure I.5: A dipole cascade in rapidity-$\mathbf{r}_\perp$-space, where a chain of smaller and smaller dipoles is followed by a set of dipoles with increasing sizes. The initial dipole between points 0 and 1 is marked by long dashes, and those dipoles which have split into two new dipoles and disappeared from the chain are marked by short dashes. This chain is interpreted as one $k_\perp$-ordered cascade from one side and one from the other, evolving up to a central hard sub-collision, which is represented by the dipole with minimum size and therefore maximum $k_\perp$.

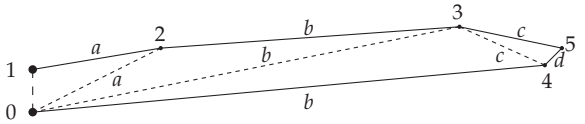

Figure I.6: A cascade where the dipoles increase to a maximum, and then decrease. Here the size of the largest dipole, denoted b, corresponds to the minimum $k_\perp$ in the chain.

maximum $k_\perp$. In the following evolution the dipole sizes get larger again, corresponding to successively smaller transverse momenta. In analogy with the evolution in the LDC model described in section I.2.2, this latter part can be interpreted as DGLAP evolution in the opposite direction, i.e. from the target end up to the central hard sub-collision. In this sub-collision the gluons 3 and 4 recoil against each other with transverse momenta $k_{\perp\max}$. In eq. (I.10) we see that the factors of d have canceled, which thus gives the weight $d^2\mathbf{r}_4 \propto d^2\mathbf{k}_{\max}/k_{\max}^4$. This reproduces the weight expected from a hard gluon–gluon scattering, and corresponds exactly to the result in the LDC model as discussed in section I.2.2.

Figure I.6 shows instead a chain with increasing dipole sizes up to a maximum value, $r_{\max}$, which thus corresponds to a minimum transverse momentum, $k_{\perp\min}$. Here we get the weight $d^2\mathbf{r}_{\max}/r_{\max}^4 \propto d^2\mathbf{k}_{\min}$. Therefore there is no singularity for the minimum $k_\perp$-value. This result is also directly analogous to the corresponding result in the LDC model.

I.4.2 Energy-Momentum Conservation

As discussed in section I.2.2, the main feature of the LDC model is the observation that both the total cross section and the final state structures are determined by chains consisting of a subset of the gluons appearing in the final state. These gluons were called "primary gluons" in ref. [33] and later called "backbone gluons" in ref. [44]. Remaining real final state gluons can be treated as final state radiation from the primary gluons. Such final state emissions do not modify the total cross sections, and give only small recoils to the parent emitters. The primary gluons have to satisfy energy-momentum conservation, and are ordered in both positive and negative light-cone momentum components, p_+ and p_-. We saw in the previous section that in Mueller's cascade the emission probabilities for gluons, which satisfy the conditions for primary gluons in LDC, have exactly the same weight, when the transverse momenta are identified with the inverse dipole size, $2/r$. This inspires the conjecture that with this identification an appropriate subset of the emissions in Mueller's cascade can correspond to the primary gluons in the momentum space cascade, meaning that they determine the cross sections while the other emissions can be regarded as either virtual fluctuations or final state radiation.

A necessary condition for this subset of gluons is that energy and momentum is conserved. (This is not a sufficient condition, as discussed further below.) Only emissions which satisfy energy-momentum conservation can correspond to real emissions, and keeping only these emissions (with a corresponding modification of the Sudakov form factor) gives a closer correspondence between the generated dipole chains and the observable final states. To leading order this does not change the total cross section. However, as it has been demonstrated that a large fraction of the next to leading corrections to the BFKL equation is related to energy conservation, we expect that taking this into account will improve the results also in this dipole formulation of the evolution.

A very important consequence of energy-momentum conservation is also that it implies a *dynamical cutoff*, $\rho(\Delta y)$, which is large for small steps in rapidity[2], Δy, but gets smaller for larger Δy. (Alternatively it could be described as a cutoff for Δy which depends on r.) The production of a small dipole with size r corresponds to the emission of a gluon with $k_\perp \approx 2/r$ and therefore $k_+ \approx (2/r)e^{-y}$. Thus conservation of positive light-cone momentum implies

$$r > 2e^{-\Delta y}/k_{\perp\text{parent}}. \tag{I.11}$$

Conserving also the negative light-cone momentum, p_-, implies that we in a similar way also get a maximum value for r in each emission. Here we note that while the projectile has a large p_+ component and a very small p_-

[2]Note that in our notation, y is rapidity and not $\log(1/x)$.

component, the target has small p_+ but contributes (almost) all p_-. Thus conservation of p_- means that in the evolution of the projectile cascade, the p_- components become steadily larger, presuming that in end the collision with the target will provide the total p_- needed to put the cascade on shell. (The kinematical details will be discussed further in section I.5.) Branches which do not interact must consequently be regarded as virtual fluctuations, which are not realized in the final state.

The net result of conservation of both p_+ and p_- is that the number of dipoles grows much more slowly with energy, and we will see in section I.6 that this also strongly reduces the total cross sections. Besides this physical effect, it also simplifies the implementation in a MC program, and implies that the severe numerical complications encountered in MC simulations without energy conservation, discussed in refs. [32] and [31], can be avoided.

I.4.3 Final States and Virtual Dipoles

However, even if we only include emissions which would be allowed by energy-momentum conservation, this does not fully correspond to the formation of a possible final state. As discussed above, the weight contains in the denominator the square of all "remaining dipoles". Even if the constraint from energy-momentum conservation implies a minimum rapidity gap for the emission of small dipoles, this suppression does not reproduce the weight $\propto d^2k_\perp/k_\perp^4$ for the smallest dipole in a sequence, needed to reproduce the cross section for a hard sub-collision. A possible solution is to interprete clusters of gluons, like those marked A, B, and C in figure I.7, as "effective gluons", where the small internal separations do not correspond to large transverse momenta for real final state gluons. These hard emissions have to be compensated by virtual corrections.

From the weight in eq. (I.5) we see that that the emission probability, where such a small dipole is the parent, is proportional to the square of its length, and therefore suppressed. However, if this dipole really does split by gluon emission, and starts a branch which interacts and gets coupled to a chain from the target (as illustrated in figure I.8) then the separation cannot be neglected. In this case the two gluons at the dipole ends have to be treated as independent, and can no longer be considered as a single effective gluon. This problem concerning the properties of exclusive final states will be further discussed in a forthcoming publication, and in the following we will here only discuss results for total cross sections.

A very important question concerns whether demanding energy conservation also for virtual emissions implies a serious overestimate of its consequences. The production of a small dipole implies large $p_\perp$ for the new gluon and also for its partner in the dipole, which suffers a recoil. Since the new

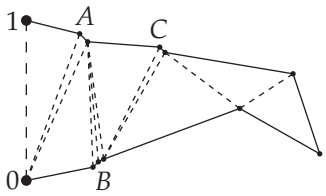

Figure I.7: The clusters of gluons marked A, B, and C must be interpreted as "effective gluons". The small dipole sizes do not correspond to large final state transverse momenta.

dipole can be virtual only if it does not interact further, this is a problem if the neighbouring dipoles are significantly changed by the emission. In the calculations of the effect of the recoil, the lightcone component $p_+ = e^{-y} \cdot p_\perp$ is conserved, which implies that the rapidity y is adjusted to a larger value. This implies that the emission of the virtual dipole does not significantly modify the p_+-component of the neighbouring dipoles. It does, however, have a large effect on the values of $p_- = e^{+y} \cdot p_\perp$, where the changes in $p_\perp$ and y do not compensate each other. In order not to overestimate the effect of p_--conservation, we therefore in this analysis implement the constraint from p_--conservation in such a way, that we neglect the size of the neighbouring dipoles. Thus we calculate this constraint assuming that the $p_\perp$ of the gluons in the dipole ends is determined only by the size of the emitting dipole. This does somewhat underestimate the effect of p_--conservation, but it avoids the large overestimate, which would be the consequence of including the unrealistic constraint from virtual dipole neighbours.

I.4.4 Gluon Recombination and Frame Dependence

As mentioned in section I.3.1 the resulting cross section is relatively insensitive to the reference frame in which a collision is studied. If the interaction is studied in a frame with rapidity y relative to the projectile, then (in leading order) the projectile cascade has evolved by a factor $e^{\lambda y}$ and the cascade from the target by a factor $e^{\lambda(Y-y)}$, where Y represents the total rapidity interval. The product is proportional to $e^{\lambda Y}$, and thus independent of y. It is also demonstrated in ref. [31] that the result for a single chain is the same in all frames, and independent of whether the cascades are developed from the projectile end or from the target end. This is a consequence of the Möbius invariance of the process, and is exactly true in the limit when the cutoff ρ goes to zero.

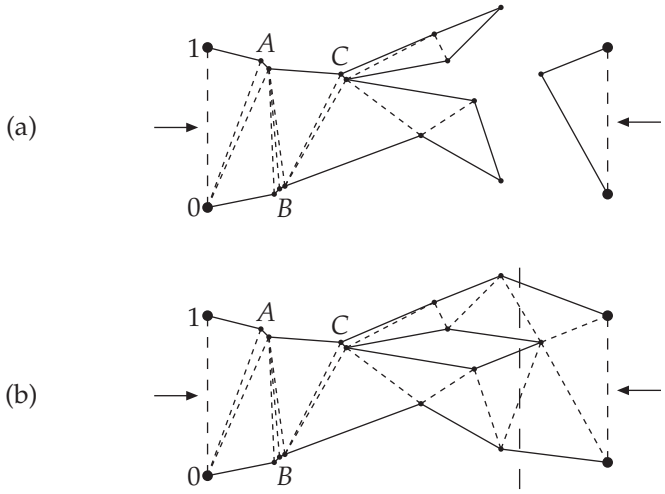

Figure I.8: (a) The emission of a new branch from a small dipole is suppressed, and proportional to the square of the small dipole size. However, if such a branch is emitted and interacts with a dipole from the target (b), then the small size has to correspond to a large $k_\perp$ in the final state.

However, including the unitarity corrections from multiple collisions also implies that the result is no longer frame independent. The contributions from multiple collisions in eq. (I.7) are formally colour suppressed $\sim 1/N_c^2$. What is treated as a multiple collision in figure I.4 or I.8 corresponds in the target rest frame to a process where two dipoles fuse to a single dipole (or two gluons fuse to a single gluon) before the collision with the target. Such recombinations[3] are consequently also colour suppressed, and they are not included in the dipole cascade evolution, which is only leading order in N_c. In the final state this process gives a closed dipole loop, which is colour disconnected from the rest of the system. In a string fragmentation scenario it gives a closed string, which fragments as a separate system. This implies that such loops are only taken into account if the collision is studied in a frame where they are appearing as multiple collisions between two branches coming from each direction, and not in a frame where they appear as gluon recombination, as e.g. in the target rest frame.

[3]In the terminology of ref. [31] the effect of multiple collisions is called a unitarisation effect, while the effect of gluon recombination is called saturation. As the separation between the two mechanisms is not dynamical, but only a question of bookkeeping depending on the particular frame of reference used in the analysis, we do in this paper not make this distinction.

We conclude that within this formalism the unitarisation corrections *do* depend on the Lorentz frame used. As discussed in ref. [31], for symmetric collisions the optimal frame should be the overall rest system, where both the projectile and the target may evolve, and the probability is largest that a dipole loop corresponds to a multiple collision event. This is illustrated in figure I.4, where in the overall rest system only one loop does not correspond to a multiple collision but to a gluon recombination. In a less central frame more loops would correspond to recombinations and there would be correspondingly fewer multiple sub-collisions.

The situation is different for onium scattering on a dense nuclear target. Here the target is treated as a large number of dipoles, and multiple collisions are most likely when different initial dipoles from the target are involved. Therefore multiple collisions are well accounted for in the target rest frame, where the projectile cascade is fully developed. This is also the approach taken in the BK equation, which similarly takes into account multi-pomeron exchange but not the gluon recombination process representing pomeron fusion.

The frame independence is a very essential feature of the LDC model, and we think it is important to develop a formalism in which multiple collisions and gluon recombinations appear on an equal footing, in a frame independent description. We will return to this problem in a future publication.

There is also another frame dependent effect, which has a more kinematic origin. For a finite cutoff ρ, or for the effective cutoff $\rho(\Delta y)$, the frame independence is only approximate, also for a single chain. Furthermore, in our scheme for energy conservation every new branch takes away energy, and therefore in a cascade with many branches the energy in each individual branch is reduced. As discussed in section I.4.2, a branch can only be realized if the interaction with the target can provide the necessary p_- momentum. The other branches are virtual and cannot be realized in the final state. This is e.g. the case for the branches marked B and C in figure I.4. As our constraint from energy-momentum conservation also includes the fractions needed to evolve the non-interacting branches the effect is somewhat overestimated. Quantitatively this bias turns out to be small. For dipole–dipole collisions, as described in section I.6.2, we find that the cross sections calculated in the cms at $y = 0.5\,Y$ or asymetrically at $y = 0.75\,Y$ differ by less than 4%.

I.5 The Monte Carlo Implementation

In this section we briefly describe the Monte Carlo scheme used to calculate the results presented in this paper. As we have mentioned before, the onium state is evolved in rapidity. For a given dipole one then generates y and $\mathbf{r}$ values for a possible gluon emission (dipole splitting) using (I.5).

I.5.1 Kinematics

To be able to study the effects of energy-momentum conservation we simply assign besides a transverse position and a rapidity, a positive light-cone momentum and a transverse momentum to each parton in the evolution, where $k_+ = k_\perp e^{-y} = (2/r)e^{-y}$. The dynamical cutoff is then given by

$$\rho = 2e^{-\Delta y}/k_{\perp\text{parent}}. \tag{I.12}$$

When a dipole emits a gluon the mother partons will receive recoils from the emitted gluon. Since a gluon belongs to two different dipoles one has to decide how the emission of a gluon effects the neighboring dipoles. We will simply assume that when a dipole emits a gluon the mother gluons need to supply all the needed energy. Thus the next time a neighboring dipole emits a gluon, the avaliable energy is reduced because one of its gluons has lost energy from the earlier emission.

Consider the emission of gluon n from the dipole ij between partons with light-cone momenta k_{+i} and k_{+j}. The transverse distances between the new gluon and partons i and j are denoted r_{in} and r_{jn} respectively. We then assume that the nearest parent gluon takes the dominant fraction of the recoil. Thus if k_{+n} is the momentum given to the emitted gluon, then the momenta left to the parents after the emission are given by

$$k'_{+i} = k_{+i} - \frac{r_{jn}}{r_{jn}+r_{in}}k_{+n} \text{ and } k'_{+j} = k_{+j} - \frac{r_{in}}{r_{jn}+r_{in}}k_{+n}. \tag{I.13}$$

Alternative formulas for sharing the recoils have also been studied, but the result does not depend sensitively on the exact formula. When an emission is generated we always make sure that $k'_+ \geq 0$.

As we in this paper are not investigating final state properties but only total cross sections, we will neglect the directions of the transverse momenta. Keeping only the lengths of the $\mathbf{k}_\perp$ vectors, we neglect the possibility that two contributions may be of approximately equal size in opposite directions, giving a much smaller vector sum. This approximation has to be improved in future analyses of final states, but should not be essential here. Thus in our approximation the transverse momentum of a parton will be decided by the shortest distance to another parton, with which it has formed a dipole, and when the gluon n is emitted from the dipole (ij), its transverse momentum is given by

$$k_{\perp n} = 2\max\left(\frac{1}{r_{in}}, \frac{1}{r_{jn}}\right). \tag{I.14}$$

In analogy the recoils on the emitting partons are given by

$$k'_{\perp i} = \max\left(k_{\perp i}, \frac{2}{r_{in}}\right) \qquad (I.15)$$
$$k'_{\perp j} = \max\left(k_{\perp j}, \frac{2}{r_{jn}}\right).$$

The recoil also implies that the rapidity is modified for the parents, and is determined by the relation $y' = \log \frac{k'_\perp}{k'_+}$. In some cases this could imply that an emitting parton ends up with rapidity larger than the rapidity of the emitted gluon. Since the cascade is assumed to be ordered in rapidity, such emissions are not allowed, and we demand that $y'_i, y'_j \leqslant y_n$. In this way we also avoid the situation where there are partons which have rapidities outside the allowed rapidity interval. As mentioned in section I.4.2, negative light-cone momentum is also conserved. This we do by imposing the condition $k_{-n} \geqslant \max(k_{-i}, k_{-j})$ during the evolution, where $k_{-i} = 2e^{y_i}/r_{ij}$ and $k_{-j} = 2e^{y_j}/r_{ij}$ according to the discussion in section I.4.3. For every generated gluon one checks the kinematical constraints described above, and in case one of them is not satisfied a new gluon is generated in a way which automatically includes the same phase-space restrictions in the integral of the Sudakov form factor.

The constraint on the negative light-cone momentum given above implies that k_- steadily increases. As also discussed in section I.4.2 we presume that in the end the collision with the target provides the necessary k_- to put the dipole chain on shell. To make sure that this indeed is possible, we impose the following constraint on the colliding dipoles

$$\frac{16}{r_{ab}^2} < k_{+a} \cdot k_{-b}. \qquad (I.16)$$

Here a and b denote two colliding gluons, which are connected in the recoupling as shown in figure I.3. The left moving onium is the one with larger k_- while the right moving onium has larger k_+. When two dipoles collide there is only one possible way to reconnect the gluons, which is consistent with the colour flow. The constraint in eq. (I.16) has to be satisfied for both pairs of connected gluons. If one of the constraints is not satisfied, the corresponding scattering amplitude is set to zero, which guarantees that only sub-collisions, which satisfy energy-momentum conservation, contribute to the cross section.

As a final remark we mention that all calculations are performed using a fixed coupling constant α_s, corresponding to $\bar{\alpha} = 0.2$. We intend to study the effects of a running coupling in future investigations.

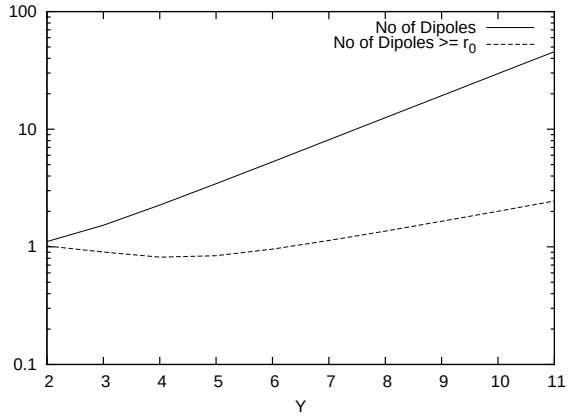

Figure I.9: The average total number of dipoles (full line) together with the average number of large dipoles (dashed line) in the onium state when evolved with energy conservation.

I.6 Results

I.6.1 Dipole Multiplicity

We will begin this section by describing some of the general properties of the dipole evolution, and we first study how the dipole multiplicity grows with energy. In figures I.9 and I.10 we show the average number of dipoles with and without energy conservation. As some dipoles have to be regarded as virtual, according to the discussion in section I.4.3, these results do not have a direct physical interpretation. They are interesting because they may be helpful, e.g. in estimates of effects of multiple collisions and the efficiency of the MC program. Without energy conservation a fixed cutoff, ρ, is needed for small dipole sizes, and in figure I.10 results are shown for $\rho = 0.04\, r_0$ and $\rho = 0.02\, r_0$, where r_0 is the size of the initial dipole starting the cascade. In all cases the total dipole multiplicity is growing exponentially with rapidity. A small cutoff favors the production of very many small dipoles, which is reflected in a very large dipole multiplicity, as seen in figure I.10. With energy conservation the dynamical cutoff $\rho(\Delta y)$, discussed in section I.4.2, is large for small values of Δy, and this feature effectively suppresses the production of many small dipoles in a small rapidity interval. Comparing the two figures we see that energy conservation indeed does have a very large effect. With energy conservation the multiplicity at $Y \approx 10$ is a factor 20 below the result obtained excluding energy conservation with the smaller cutoff value.

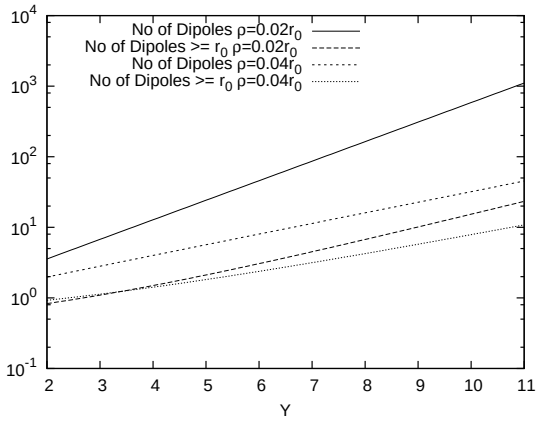

Figure I.10: The average total number of dipoles together with the average number of large dipoles in the onium state when evolved *without* energy conservation and using two different cutoffs. For the smaller cutoff, $\rho = 0.02$ the total number is given by the full line while the number of large dipoles is given by the dashed line. For the larger cutoff, $\rho = 0.04$ the total number is given by the short-dashed line while the number of large dipoles is given by the dotted line.

Without energy conservation the strong sensitivity to the small dipole cutoff reflects the large probability to emit very small dipoles (c.f. eq. (I.5)). As the small dipoles also have small cross section, one could imagine that the differences seen in the dipole multiplicity is rather unessential for total cross sections. This is, however, not the case. In figures I.9 and I.10 we also show the number of dipoles with sizes larger or equal to the initial dipole size. With energy conservation this number changes rather slowly and exceeds one first at $Y \sim 7$, while without energy conservation it is steadily increasing with energy. This is the case also for the larger cutoff value, although in this case the total multiplicity is not significantly larger than in the energy conserving case. This feature is further illustrated in figure I.11, which shows the distribution in dipole size at $Y = 6$ and $Y = 8$. Energy-momentum conservation does not only suppress small dipoles, which we understand as a result of conservation of the positive light-cone component, p_+, but there is also a suppression of large dipoles, as a consequence of p_--conservation. Thus we conclude that the implementation of energy conservation does not only have an effect on very small dipoles, which turns out to be less important for the total cross sections, but indeed also has a very strong effect on the main features of the evolution. This will be more clearly illustrated in the following subsections.

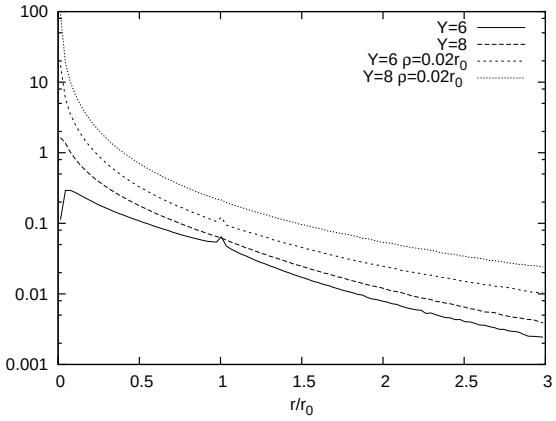

Figure I.11: The distribution in dipole size for $Y = 6$ and 8. The solid and longdashed lines show the result from evolution with energy conservation while the shortdashed and dotted lines show the same for evolution *without* energy conservation with the cutoff $\rho = 0.02\, r_0$.

I.6.2 Onium–Onium scattering.

We will here study the collision between two onium states, which we regard as two incoming dipoles. We denote the initial dipole sizes r_1 and r_2 respectively, and we imagine r_2 as the target dipole with fixed size, while we vary the projectile size $r_1 \propto 1/\sqrt{Q^2}$. We note that with energy conservation and fixed α_s there is no external scale, and therefore the result for the scaled cross section σ/r_2^2 does not depend on r_1 and r_2 separately, but only on their ratio.

Figure I.12 shows the total cross section as a function of the rapidity Y for different values of r_1/r_2, obtained including energy conservation and unitarisation in accordance with eq. (I.7). The result from single pomeron exchange, where the parenthesis in eq. (I.7) is replaced by $\sum f_{ij}$, is shown in figure I.13, and we see that these results are almost identical to those in figure I.12. We note in particular that the curves are not straight lines, as is expected from leading order BFKL. This implies that the effective slope, λ_{eff}, varies with rapidity, in a way expected as a result of saturation. We also note that λ_{eff} grows with larger values for the ratio between the dipole sizes. This effect is illustrated in figure I.14, and will be further discussed in section I.6.4.

For comparison, results obtained without energy conservation, with and without unitarisation, are shown in figure I.15. In this figure the ratio r_1/r_2 is chosen equal to 1. We see that here the one-pomeron cross section, without unitarisation, grows exponentially with rapidity, proportional to $e^{\lambda Y}$ with

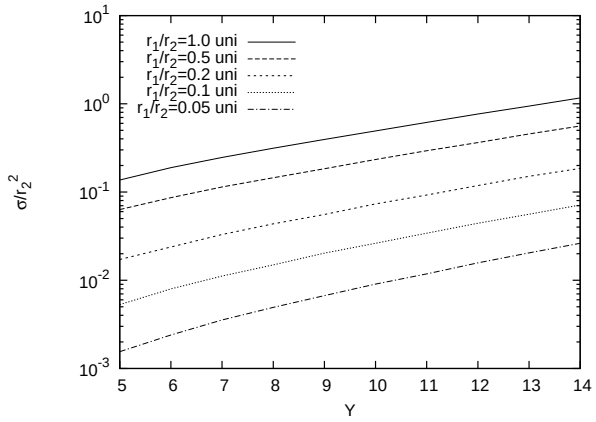

Figure I.12: The scaled unitarised dipole–dipole cross section as a function of Y for different initial conditions.

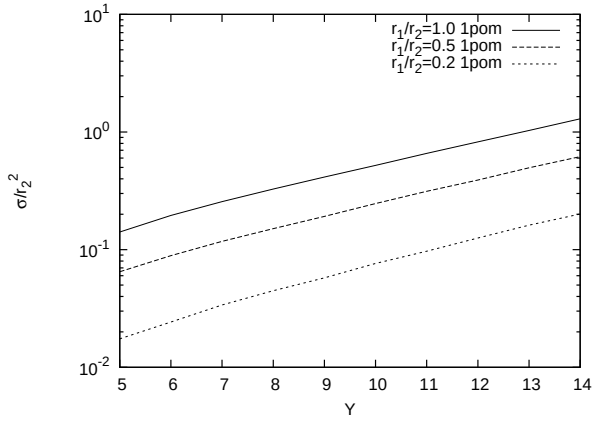

Figure I.13: The scaled one-pomeron dipole–dipole cross section as a function of Y for different initial conditions.

a constant slope λ. Including unitarisation gives here a noticeable suppression, which becomes stronger for larger rapidity and correspondingly higher dipole density. This has the expected effect that the growth rate is reduced for larger rapidities, with an effective slope parameter λ_{eff} which is decreasing for higher energies. Comparing figures I.12 and I.13 we note that already without unitarisation, the inclusion of energy conservation also results in an effective

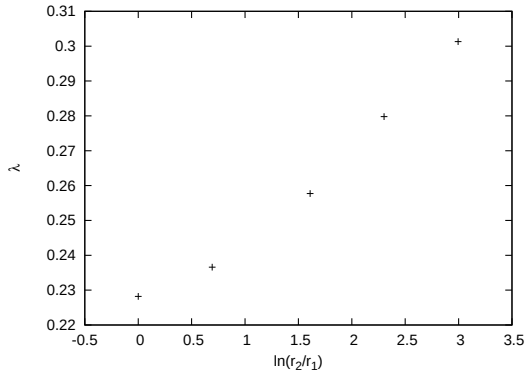

Figure I.14: The effective power λ_{eff} calculated from the unitarised dipole–dipole cross section where energy conservation has been included.

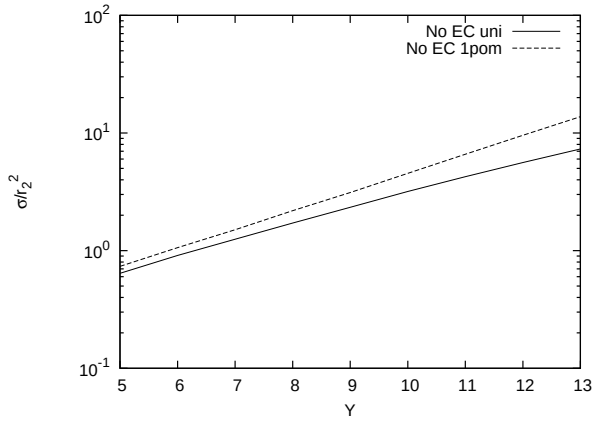

Figure I.15: The scaled unitarised (full line) and one-pomeron (dashed line) dipole–dipole cross sections calculated *without* energy conservation.

slope, which is varying with energy in much the same way.

I.6.3 Dipole–nucleus scattering.

Having studied dipole–dipole collisions we now apply our program to dipole–nucleus collisions. We will focus on the qualitative features and consider a toy model where the nucleus is given by a collection of colour dipoles, which are distributed with a Gaussian distribution in dipole size **r** and in impact pa-

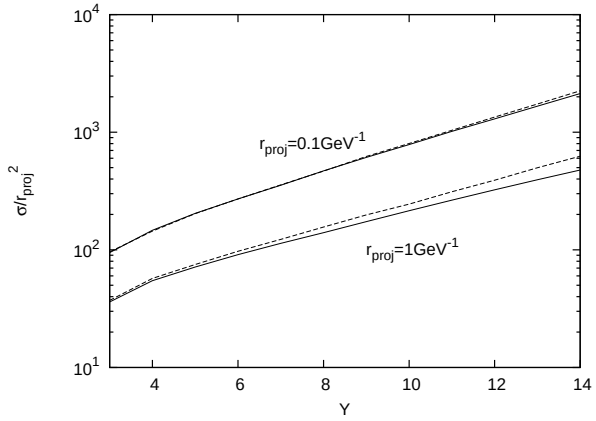

Figure I.16: The dipole–nucleus cross section for $r_{\text{proj}} = 0.1$ and 1 GeV^{-1} and $A = 200$. The unitarised result is shown by the solid lines, and the one-pomeron contribution by the dashed lines.

rameter **b** and with random relative angles. The number density of dipoles is given by

$$dN = B \cdot d^2\mathbf{r} e^{-\mathbf{r}^2/r_0^2} \cdot d^2\mathbf{b} e^{-\mathbf{b}^2/b_0^2} \tag{I.17}$$

The parameters r_0 and b_0 are related to the estimated primordial momentum in a proton and the nuclear radius respectively. As our model is rather crude we have not tried to optimize these parameters, but chosen the following canonical values: $r_0 = 1$ fm and $b_0 = A^{1/3} \cdot 1$ fm, A being the mass number for the nucleus. The normalization constant B is determined by the requirement that the transverse energy of the nucleus is set equal to $A \cdot 1$ GeV. To simplify the calculations, the interaction amplitude for a dipole–nucleus collision is calculated in the nucleus rest frame, by convoluting the basic dipole–dipole amplitude with the distribution in eq. (I.17). Although, as discussed in section I.4.4, the result is not exactly independent of the Lorentz frame, the differences are not large, and should not be essential for the qualitative studies in this section. For the application to ep scattering in the next section, where we will compare our results with data from HERA, we will perform our calculations in the hadronic rest system, which in that case should be more accurate.

The results for $A = 200$ and $r_{\text{proj}} = 0.1$ and 1 GeV^{-1} are shown in figure I.16. Results are presented both for single pomeron exchange and including unitarisation. The effect of unitarisation grows with nuclear size and with the size of the projectile. For a small projectile of size 0.1 GeV^{-1} we can see the effect of colour transparency, as the cross sections for the unitarised and the one pomeron calculations are almost identical. For a larger projectile we

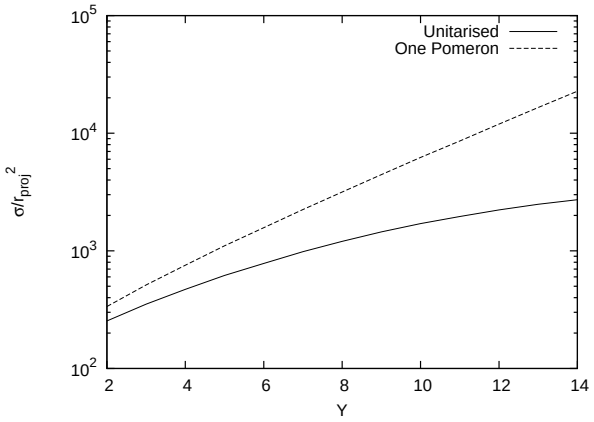

Figure I.17: The scaled dipole–nucleus cross section, *without* conservation of energy, for A = 200 with a projectile of size 1 GeV^{-1}. The full and dashed line shows the result with and without unitarisation respectively.

do see a clear effect from unitarisation, but even for $r_{\text{proj}} = 1$ GeV^{-1} and a nucleus with $A = 200$ this effect is only about 20 percent in the rapidity interval $10 - 14$. For smaller nuclei the effect will be correspondingly smaller.

It is also interesting to study our toy model without energy conservation, and figure I.17 shows results for $r_{\text{proj}} = 1$ GeV^{-1} and $A = 200$, corresponding to the larger projectile in figure I.16. The result is qualitatively similar to the corresponding results for dipole–dipole collisions, in the sense that the one-pomeron result is a straight line, while with unitarisation the suppression is increasing for larger Y-values, and the curve bends downwards. However, as expected the unitarisation effect is here quantitatively much larger.

Comparing the results in figures I.16 and I.17 we see that including energy conservation very strongly reduces the cross section. This suppression becomes larger for higher energies, which gives an effective slope, λ_{eff}, which decreases with energy in a way characteristic for saturation. The reduction of the gluon density due to energy conservation is also so large that the unitarity effects become comparatively small for available energies, even for large nuclei.

I.6.4 F_2 at HERA

When we apply our model to deep inelastic ep scattering we want to emphasize that we here only want to study the qualitative behavior. We postpone a quantitative comparison with HERA data to a future publication, where we

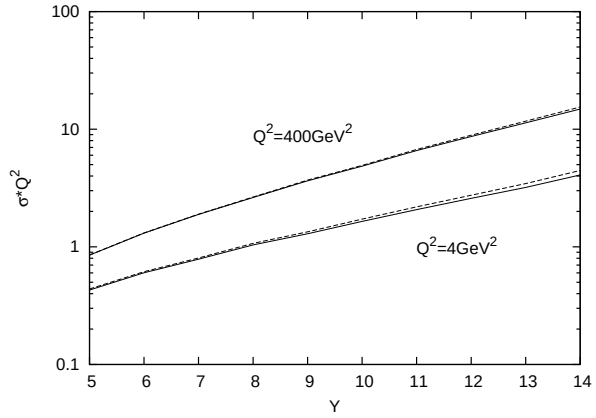

Figure I.18: The scaled dipole–p cross section as a function of $\log 1/x$, for $Q^2 = 4\,\mathrm{GeV}^2$ and $Q^2 = 400\,\mathrm{GeV}^2$. The unitarised results are shown by the solid lines while the dashed lines show the one-pomeron results.

can include effects of colour recombination and improve the simple toy model for the proton target.

For the application to DIS ep collisions we here use the same toy model described in section I.6.3, with $A = 1$. We also identify Q^2 directly with $4/r^2_{\mathrm{proj}}$ without taking into account the detailed effects of the photon wavefunction. This implies that the number of dipoles in the target is much smaller than the number of dipoles in an onium state developed to large Y-values as described in section I.6.1. Hence, the collision is more similar to the symmetric onium–onium scattering than to the very unsymmetric onium–nucleus collision. To reduce the frame dependent effects discussed in section I.4.4, we therefore study the dipole–proton collisions in the overall rest frame. We neglect possible correlations between the target dipoles, which thus are assumed to evolve independently. As the unitarisation effects turn out to be small, and we here only study the total cross section, it is also possible to neglect the fluctuations in the number of primary target dipoles.

The resulting dipole–nucleon cross section is shown in figure I.18 for two different projectile sizes, corresponding to $Q^2 = 4\,\mathrm{GeV}^2$ and $Q^2 = 400\,\mathrm{GeV}^2$. In this figure we also show the result for single pomeron exchange, i.e. without unitarisation corrections, and we here see that the effect from unitarisation is quite small.

Fig. I.19 shows the corresponding results without energy conservation. (The results presented here are obtained for the cutoff $\rho = 0.02\,\mathrm{GeV}^{-1}$, and

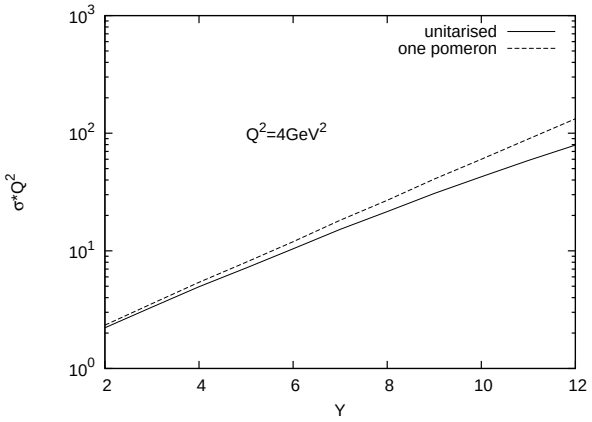

Figure I.19: The scaled dipole–p cross section as a function of $\log 1/x$ calculated *without* energy conservation using $\rho = 0.02\ \mathrm{GeV}^{-1}$. Both the unitarised (full line) and the one-pomeron (dashed line) calculations are shown.

therefore somewhat lower than the limiting values for $\rho \to 0$.) We see that without unitarisation and without energy conservation, the cross section grows exponentially with $Y = \log 1/x$, or as a power of x. With unitarisation (but without energy conservation) the growth rate is, as expected, reduced and becomes continuously smaller with decreasing x. We note, however, that energy conservation has a similar effect, also without unitarisation, and the reduction in the cross section due to energy conservation is so large that including unitarisation does not have a significant effect.

In figure I.18 we also see that the logarithmic slope

$$\lambda_{\mathrm{eff}} = \frac{d(\log \sigma)}{d(\log 1/x)}, \tag{I.18}$$

is increasing with increasing Q^2. As discussed above, λ_{eff} is not a constant for fixed Q^2, but depends on both Q^2 and x, when unitarisation and/or energy conservation is taken into account. To compare with experimental data we show in figure I.20 λ_{eff} determined in the x-interval used in the analysis by H1 [21], which varies from $x \approx 2 \times 10^{-5}$ for $Q^2 = 1.5\ \mathrm{GeV}^2$ to $x \approx 3 \times 10^{-2}$ for $Q^2 = 90\ \mathrm{GeV}^2$. We note that the result of our crude model is not far from the experimental data, although the dependence on Q^2 is somewhat weaker in the model calculations. As in figure I.18 we see that the effect of unitarisation is small, and, as expected, it gets further reduced for larger Q^2-values. From figure I.19 we see that the result without energy conservation and unitarisation corresponds to a much larger effective slope, and also including unitarisation

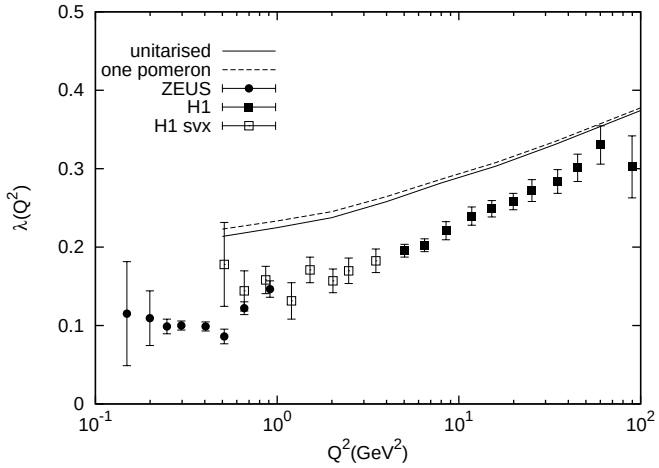

Figure I.20: The effective slope measured at different Q^2 compared to data from HERA. The full line is our model including unitarisation, while the dashed line is without. Filled circles are data from ZEUS [45], filled [46] and open [22] squares are data from H1.

the result for λ_{eff} is roughly a factor two larger than the corresponding result in figure I.18.

In conclusion we find that the result of our simple model is surprisingly close to experimental data from HERA. This is very encouraging, especially since we have not attempted to tune the model in any way. The effect of energy conservation is a suppression for small x-values and small Q^2, which is qualitatively similar to the effect expected from unitarisation. This suppression is so strong that the effect from adding unitarisation is only a very small correction, visible for small Q^2-values.

I.7 Conclusions

Including both higher-order corrections and unitarisation effects in the high-energy limit of QCD is not a simple task. Unitarisation effects are more easily included in a dipole picture formulation in transverse coordinate space, while higher-order corrections are more easily formulated in transverse momentum space. In this report we have used as a starting point that a large part of the NLO corrections to BFKL are due to effects of energy-momentum conservation, which again are more easily formulated in transverse momentum space. However, after noting similarities between the LDC and Mueller dipole for-

mulations of high energy QCD, we conjecture that also in the latter case, the essential contribution to the cross section comes from a subset of dipoles between real final-state gluons, which necessarily must respect energy and momentum conservation.

We have presented a way to implement energy and momentum conservation in the Mueller dipole model. This is a necessary, although not sufficient, requirement for selecting only final-state gluons, and should also include most NLO corrections to the BFKL evolution. Our way to implement energy-momentum conservation also eliminates the need for a cutoff for small dipoles in Mueller's formalism, in which the large number of small dipoles causes problems for a numerical treatment. Thus the number of dipoles produced in the evolution is drastically reduced. This applies not only to the number of very small dipoles, which do not much affect the resulting cross sections. Also the number of large dipoles is reduced, resulting in a drastic reduction of the cross section and in the effective slope $\lambda_{\text{eff}} = d \log F_2 / d \log x$.

Also in standard BFKL evolution one would expect a large reduction of the effective slope due to unitarisation effects. In our case the growth of the cross section is already damped, making the inclusion of unitarisation a rather small effect for the total cross section, even for deeply inelastic virtual photon scattering on large nuclei.

Comparing with the results of [20], we find a larger effect from energy-momentum conservation. One reason seems to be the inclusion of p_--conservation, which in our formalism is found to have an important effect. Thus we find that including only conservation of p_+, and not of p_-, increases the cross section by a factor 2 (3) for dipole–proton collisions at $Q^2 = 4\,(400)\text{GeV}^2$. Conservation of p_- is related to the so called consistency constraint [47], and in [20] this contribution to the NLO BFKL kernel is neglected, with the motivation that saturation effects suppress the gluon density so that this contribution is less important. Naturally, what is physically relevant is only the combined effect of both energy conservation and saturation. Including the contributions in different order, will also give different weights to the two effects. We feel that energy and momentum conservation is the more fundamental phenomenon, and hence obtain a much smaller effect from saturation.

To investigate the scattering on nuclei we have introduced a toy model, where the nucleons are treated as a collection of dipoles with a Gaussian distribution in sizes and impact parameter. We also use this to model the scattering on a single nucleon and compared our results with HERA data. Although we made no tuning of the parameters of our model, we obtain a good semi-quantitative description of the effective slope, λ_{eff}, measured at low x and Q^2 at HERA.

Thus encouraged we will now continue to develop our model, and there are several things which we would like to improve. A major development

would be to achieve a formalism which is completely frame independent. This would entail the inclusion of true gluon recombinations in the dipole evolution, and also a better understanding of the "effective" gluons with small transverse separation described in section I.4.3. In this way we hope to also be able to use our formalism to describe exclusive final-state properties. Another important development would be to include effects of a running α_s, and also to improve our nucleon toy model to investigate the impact of our formalism in nucleus–nucleus collisions. We intend to return to all these issues in forthcoming publications.

I References

[1] E. A. Kuraev, L. N. Lipatov, and V. S. Fadin *Sov. Phys. JETP* **45** (1977) 199–204.

[2] I. I. Balitsky and L. N. Lipatov *Sov. J. Nucl. Phys.* **28** (1978) 822–829.

[3] L. V. Gribov, E. M. Levin, and M. G. Ryskin *Phys. Rept.* **100** (1983) 1–150.

[4] K. Golec-Biernat and M. Wusthoff *Phys. Rev.* **D59** (1999) 014017, hep-ph/9807513.

[5] J. R. Forshaw, G. Kerley, and G. Shaw *Phys. Rev.* **D60** (1999) 074012, hep-ph/9903341.

[6] J. Bartels, K. Golec-Biernat, and H. Kowalski *Phys. Rev.* **D66** (2002) 014001, hep-ph/0203258.

[7] A. H. Mueller *Nucl. Phys.* **B415** (1994) 373–385.

[8] A. H. Mueller and B. Patel *Nucl. Phys.* **B425** (1994) 471–488, hep-ph/9403256.

[9] A. H. Mueller *Nucl. Phys.* **B437** (1995) 107–126, hep-ph/9408245.

[10] I. Balitsky *Nucl. Phys.* **B463** (1996) 99–160, hep-ph/9509348.

[11] Y. V. Kovchegov *Phys. Rev.* **D60** (1999) 034008, hep-ph/9901281.

[12] E. Iancu, A. Leonidov, and L. D. McLerran *Nucl. Phys.* **A692** (2001) 583–645, hep-ph/0011241.

[13] E. Ferreiro, E. Iancu, A. Leonidov, and L. McLerran *Nucl. Phys.* **A703** (2002) 489–538, hep-ph/0109115.

[14] V. S. Fadin and L. N. Lipatov *Phys. Lett.* **B429** (1998) 127–134, hep-ph/9802290.

[15] M. Ciafaloni and G. Camici *Phys. Lett.* **B430** (1998) 349–354, hep-ph/9803389.

[16] G. P. Salam *Acta Phys. Polon.* **B30** (1999) 3679–3705, hep-ph/9910492.

[17] J. R. Andersen and W. J. Stirling *JHEP* **02** (2003) 018, hep-ph/0301081.

[18] L. H. Orr and W. J. Stirling *Phys. Rev.* **D56** (1997) 5875–5884, hep-ph/9706529.

[19] E. Levin and K. Tuchin *Nucl. Phys.* **B573** (2000) 833–852, hep-ph/9908317.

[20] E. Gotsman, E. Levin, U. Maor, and E. Naftali hep-ph/0504040.

[21] **H1** Collaboration, C. Adloff *et al. Phys. Lett.* **B520** (2001) 183–190, hep-ex/0108035.

[22] A. Petrukhin, "New Measurement of the Structure Function $F_2(x, Q^2)$ at low Q^2 with Initial State Radiation Data." Proceedings of DIS04, Štrbské Pleso, Slovakia, 2004.

[23] E. Iancu, K. Itakura, and S. Munier *Phys. Lett.* **B590** (2004) 199–208, hep-ph/0310338.

[24] M. Ciafaloni, D. Colferai, and G. P. Salam *Phys. Rev.* **D60** (1999) 114036, hep-ph/9905566.

[25] G. Gustafson *Phys. Lett.* **B175** (1986) 453.

[26] G. Gustafson and U. Pettersson *Nucl. Phys.* **B306** (1988) 746.

[27] L. Lönnblad *Comput. Phys. Commun.* **71** (1992) 15–31.

[28] K. Hamacher and M. Weierstall hep-ex/9511011.

[29] N. Brook, R. G. Waugh, T. Carli, R. Mohr, and M. Sutton. Prepared for Workshop on Future Physics at HERA (Preceded by meetings 25-26 Sep 1995 and 7-9 Feb 1996 at DESY), Hamburg, Germany, 30-31 May 1996.

[30] G. P. Salam *Comput. Phys. Commun.* **105** (1997) 62–76, hep-ph/9601220.

[31] A. H. Mueller and G. P. Salam *Nucl. Phys.* **B475** (1996) 293–320, hep-ph/9605302.

[32] G. P. Salam *Nucl. Phys.* **B461** (1996) 512–538, hep-ph/9509353.

[33] B. Andersson, G. Gustafson, and J. Samuelsson *Nucl. Phys.* **B467** (1996) 443–478.

[34] B. Andersson, G. Gustafson, and H. Kharraziha *Phys. Rev.* **D57** (1998) 5543–5554, hep-ph/9711403.

[35] S. Catani, F. Fiorani, and G. Marchesini *Phys. Lett.* **B234** (1990) 339.

[36] M. Ciafaloni *Nucl. Phys.* **B296** (1988) 49.

[37] G. Altarelli and G. Parisi *Nucl. Phys.* **B126** (1977) 298.

[38] V. N. Gribov and L. N. Lipatov *Yad. Fiz.* **15** (1972) 781–807.

[39] L. N. Lipatov *Sov. J. Nucl. Phys.* **20** (1975) 94–102.

[40] Y. L. Dokshitzer *Sov. Phys. JETP* **46** (1977) 641–653.

[41] H. Kharraziha and L. Lönnblad *JHEP* **03** (1998) 006, hep-ph/9709424.

[42] B. Andersson, G. Gustafson, L. Lönnblad, and U. Pettersson *Z. Phys.* **C43** (1989) 625.

[43] **Small x** Collaboration, B. Andersson *et al. Eur. Phys. J.* **C25** (2002) 77–101, hep-ph/0204115.

[44] G. P. Salam *JHEP* **03** (1999) 009, hep-ph/9902324.

[45] **ZEUS** Collaboration, J. Breitweg *et al. Phys. Lett.* **B487** (2000) 53–73, hep-ex/0005018.

[46] **H1** Collaboration, C. Adloff *et al. Eur. Phys. J.* **C21** (2001) 33–61, hep-ex/0012053.

[47] J. Kwiecinski, A. D. Martin, and P. J. Sutton *Z. Phys.* **C71** (1996) 585–594, hep-ph/9602320.

II

Small-x Dipole Evolution Beyond the Large-N_c Limit

Emil Avsar, Gösta Gustafson and Leif Lönnblad

Dept. of Theoretical Physics, Sölvegatan 14A, S-223 62 Lund, Sweden

JHEP **01** (2007) 012, hep-ph/0610157.

We present a method to include colour-suppressed effects in the Mueller dipole picture. The model consistently includes saturation effects both in the evolution of dipoles and in the interactions of dipoles with a target in a frame-independent way. When implemented in a Monte Carlo simulation together with our previous model of energy–momentum conservation and a simple dipole description of initial state protons and virtual photons, the model is able to reproduce to a satisfactory degree both the $\gamma^* p$ cross sections as measured at HERA as well as the total pp cross section all the way from ISR energies to the Tevatron and beyond.

II.1 Introduction

Parton evolution at small x is a difficult problem. It is interesting because of the strong nonlinear effects and the interplay between perturbative and non-perturbative physics, and it is an important problem, as it is necessary to have a good understanding of the dominant effects from the strong interaction in the analyses of results from LHC and the interpretation of possible signals for new physics.

Although it cannot be possible to include all quantum interference effects in a classical branching process, such a stochastic evolution has been extremely successful to describe parton cascades in e^+e^--annihilation. This is also the case in the DGLAP regime of DIS (high Q^2 and large x). In these cases the virtuality or transverse momentum acts as a well-defined evolution parameter, and the perturbative cascade can be well separated from the non-perturbative effects in the hadronization or the input distributions in the DGLAP evolution. We note, however, that important for the good agreement with LEP data is both a description of the hardest gluons by fixed order matrix elements, and implementation of energy–momentum conservation in the event simulation procedure.

DIS at small x is more difficult. To LL or NLL accuracy the cross section is determined by the BFKL equation, which describes an evolution in x instead of the $k_\perp$-ordering in the DGLAP evolution. A big problem is here that the NLL corrections are so large, that it in practice only can give a qualitative description of experimental data.

Part of the NLL corrections originate from the running coupling α_s. Including a running coupling in the evolution implies that the parton chain spreads into the non-perturbative region, and a soft cutoff is needed for small $k_\perp$. This problem is avoided in studies of collisions between highly virtual photons or massive onium states. Another possibility is to study events with two high $p_\perp$ jets separated by a large rapidity interval. Also here it is demonstrated that the energy–momentum conservation constraint has a very large effect on the theoretical calculations [1]. In ep and pp scattering the influence of non-perturbative effects cannot be avoided, however, and has to be included in the analysis.

A most essential feature of the e^+e^--cascades is the so-called "soft colour interference" or angular ordering [2–5]. A colour charge in one parton has always a corresponding anti-charge in an accompanying parton, and it is important to account for the interference in the radiation from these emitters. An efficient way to treat this effect is offered by the dipole cascade model described in refs. [6, 7], in which the QCD state is described as a chain of colour dipoles formed by a charge–anti-charge pair, rather than a chain of gluons. In the large N_c limit the dipoles radiate independently, and analyses of experi-

mental data from LEP [8–11] indicate that the interference between different dipoles is very weak. (In contrast to the other three LEP experiments, DELPHI [11] does indeed favour some weak effects from interaction.)

In DIS a formulation with coherent colour dipoles was presented by Golec-Biernat–Wüsthoff [12, 13], and a space-like dipole cascade model was formulated by Mueller [14–16]. While the time-like dipole cascade model in ref. [7] is formulated in momentum space, the dipoles in these models are specified in transverse coordinate (or impact parameter) space. As the transverse coordinate is little affected in a high energy interaction, this makes it possible to account for multiple parton sub-collisions in a natural way.

Mueller's dipole cascade model is valid in the large N_c limit, and is demonstrated to satisfy the BFKL equation to LL accuracy. In this picture one starts with a $q\bar{q}$ colour singlet state (a quarkonium or simply onium state), and when the system is boosted to higher energy more and more soft gluons are emitted, forming a chain of colour dipoles. As mentioned this approach leads to the BFKL equation, but it also goes beyond the BFKL formalism. When two cascades collide it is possible to take into account multiple scattering to all orders, and it is thus possible to obtain a unitarised expression for the S-matrix. The probabilistic nature of the cascades implies that the evolution can be simulated in a Monte Carlo program, and the effects of unitarisation be studied numerically [17, 18] (see also [19]).

The dipole model contains a vertex in which a dipole splits into two new dipoles, originating when a soft gluon is emitted from the original colour dipole. The evolution can then be formulated as a typical birth–death process, where a dipole can decay into two new dipoles with a specified differential probability, proportional to dY, with $Y = \log 1/x$ which here acts as a time variable for the evolution process.

There are some problems with the dipole evolution as formulated in [14–16]. One problem comes from the fact that the cascade cannot correspond to real gluon emissions. The splitting vertex diverges as the size of one of the new dipoles goes to zero. The many small dipoles interact, however, very weakly with a target, a phenomenon referred to as colour transparency. Thus, even if the number of small dipoles diverges, the total cross section remains finite. Although we thus get a finite cross section, the divergence causes problems: i) Dipoles which do not interact should be regarded as virtual. Therefore the dipole model in this formulation can be used to study fully inclusive quantities like the total cross section, but not the properties of exclusive final states. ii) In numerical calculations the divergence has to be regulated by a cutoff for small dipoles. Although the cutoff does not show up in the cross section, it makes it extremely time consuming to run a simulation program with a cutoff, which is small enough to simulate the physics with good accuracy.

As mentioned above, the constraint from energy–momentum conservation

is very important in order to achieve agreement between theory and experiment in e^+e^--annihilation, and in [1] it is demonstrated that it also has a large effect in space-like cascades. This constraint goes beyond the LL approximation, and is not included in the formalism in [14, 15]. This is related to the problem with small dipoles discussed above. A very small dipole corresponds to well localized partons, which thus must have large transverse momenta, which in turn implies also non-negligible longitudinal momentum and energy. Only real final state partons have to obey conservation of energy and momentum, and to fully solve this problem one must also solve the problem with specifying the final states.

Another problem is due to the fact that in this formalism dipoles in the same onium do not interact. Saturation effects are included in the collisions between two cascades, but not in the evolution of each cascade separately. This problem is related to the large N_c approximation in the evolution. Multiple collisions are formally colour suppressed, and in the Lorentz frame where the collision is studied they lead to the formation of pomeron loops. As the evolution is only leading in colour, such loops cannot be formed during the evolution itself. If one e.g. studies the collision in a very asymmetric frame, where one of the onia carries almost all the available energy and the other is almost at rest, then the possibility to have multiple collisions is strongly reduced. Only those pomeron loops are included, which are cut in the specific Lorentz frame used for the calculations, which obviously only forms a limited set of all possible pomeron loops. It implies that the dipole model is not frame independent, and the preferred Lorentz frame is the one where the two colliding systems have approximately the same density of dipoles [1]. This feature clearly limits the rapidity range of validity. It is apparent that a frame independent formulation must include colour suppressed interactions between the dipoles during the evolution of the cascades, but so far it has not been possible to formulate a model, which includes saturation effects and is explicitely frame independent.

There is also another related problem with the finite number of colour charges. The dipole degrees of freedom are natural only in the $N_c \to \infty$ limit. Consider for example a system of $r\bar{r}r\bar{r}$ charges. Using the dipole basis this system the colours can be combined in two different ways. Obviously, to go beyond large N_c one would need to take into account quadrupoles, as in the example above, and even higher multipoles. This makes the colour structure of the gluon cascade really non-trivial, and one loses the picture of a system of dipoles evolving through dipole splittings in a stochastic process. As the dipole approximation is so successful in e^+e^--annihilation, it may still be possible to find a working approximation using only dipoles. In the exam-

[1] The model is, however, frame independent at the level of one pomeron exchange as a consequence of the conformal invariance of the process.

ple above it may be possible to describe the quadrupole field as two dipoles formed by the closest charge–anti-charge pairs. Such an approximate scheme can be realized by introducing a $2 \to 2$ transition vertex in the dipole evolution.

In this paper we want to discuss ways to improve the dipole description of high energy interaction in DIS and hadronic collisions. Some effects of energy–momentum conservation were presented in ref. [20]. This constraint gives a dynamic cutoff for small dipoles, which strongly reduces some of the problems discussed above. The dipole multiplicity is reduced, which makes the Monte Carlo simulation much more efficient. The reduced dipole multiplicity also reduces the effect of saturation, which becomes rather small for DIS within the HERA kinematical region. Here we will further extend the model presented in [20], including colour suppressed effects related to pomeron loops by introducing a $2 \to 2$ transition vertex in the dipole evolution. Although not explicitely frame independent, the dependence on the Lorentz frame used is here much reduced.

The coupling of a virtual photon to a $q\bar{q}$ dipole is well known, but the proton is a much more complicated system. It was early suggested that semi-hard parton sub-collisions and minijets are important ingredients in high energy pp collisions, and responsible for the rising cross section [21–24]. This picture is supported by the successful description of Tevatron data [25] using the PYTHIA MC, which is based on perturbative parton–parton collisions [26]. These results encourages us to describe high energy $\gamma^* p$ and pp collisions in terms of perturbative dipole–dipole collisions, and we will in this paper also present a simple model for the initial dipole system in a proton. The ideas are implemented in a computer simulation program, and the results are compared with DIS data from HERA and with data from hadron–hadron colliders.

The paper is organized as follows. In the next section we describe the dipole picture of high energy collisions in QCD and its relation to the string picture. In section II.3 we briefly summarize the alternative approach to high energy QCD, the colour glass condensate, and recent results related to the formation of pomeron loops in the corresponding evolution equations. In section II.4 we describe the improvements we have made in the dipole model as was briefly described in this introduction, followed in section II.5 by a brief discussion of the model of the proton used to obtain quantitative results. In section II.6 we present some details about our Monte Carlo program and how we implement the improvements we have made. Then, in section II.7, we present the applications of these improvements and compare our results to experimental data for DIS and pp scattering. Finally, in section II.8, we arrive at our conclusions.

II.2 Dipole Picture of QCD

Higher order QCD diagrams are very difficult, and naturally it is not possible to formulate a quantum mechanical parton cascade as a classical branching process, including all interference effects. The great success for parton cascades in e^+e^--annihilation is therefore quite surprising. DIS is, however, significantly more complicated than e^+e^--annihilation.

II.2.1 Cascades in e^+e^--annihilation

In e^+e^- the main problem is to calculate the properties of the final states, while the total cross section is well determined by low order perturbative QCD calculations. Although the 1st order matrix element for gluon emission diverges for soft gluons, the total cross section is still finite and given by $\sigma_{tot} \approx \sigma_0 \left(1 + \alpha_s/\pi\right)$, where σ_0 is the cross section to 0th order in α_s. The divergence for soft gluon emission is compensated by virtual corrections, which can easily be taken into account by Sudakov form factors. This implies that the cascade has a probabilistic nature; the emission of one more gluon in the ordered cascade does not change the total reaction cross section.

The process $e^+e^- \to q\bar{q}gg$ does factorize in the limit when one gluon is much softer than the other. In the large N_c limit also the amplitude for a multigluon final state factorizes in the strongly ordered regime, where one gluon is much softer than the previous one. N_c is, however, not a big number (even if the non-factorizing correction terms are of order $1/N_c^2$ and not $1/N_c$). Also the value of α_s is so large that cascades which are *not* strongly ordered (and therefore do not factorize), are very important in analyses of experimental data.

The result depends quite strongly on the treatment of not well ordered cascades, where the description depends equally much on physical intuition as on analytic calculations. A very essential feature is what is called soft colour interference, which was mentioned in the introduction. A parton with e.g. a red colour has always a partner carrying anti-red colour charge. The interference between these two charges implies a suppression for emission of gluons with wavelengths larger than the separation between the emitters. Thus the colour charge and its anti-charge partner do not radiate independently, but must be treated as one unit.

In a fixed Lorentz frame this interference effect can be approximated by an angular ordering [2–5]. This means that emissions from the red and anti-red partons is restricted to angular cones with opening angles equal to the angle between the emitters. This angular constraint is not Lorentz invariant but frame dependent. It also overestimates the emission in some directions and underestimates it in other, but in such a way that it averages out to the

correct value.

A different approach to this effect is given by the dipole cascade model described in [6, 7]. In this model the QCD state is described as a chain of colour dipoles (with given momentum, energy, and orientation) rather than a chain of gluons (with momentum, energy, and polarization). This is similar to the relation between a lattice and its dual lattice. It is interesting to note that at the end of the cascade this dipole chain gives a smooth transition to the string in the Lund fragmentation model [27]. In the large N_c limit the dipoles radiate independently apart from recoils (which may be important when the emissions are not strongly ordered). The radiation from the dipole formed by the red and anti-red charges discussed above is studied in the rest frame of the two partons forming that dipole. Boosting to e.g. the overall rest frame this reproduces the angular ordering, but without the (unrealistic) sharp angular cutoff. A comparison between the dipole approximation and the exact 2nd order matrix element is given in [28].

The angular ordering constraint is implemented in the event generators Herwig [29] and Pythia [30], and the dipole cascade in the Ariadne event generator [31]. They all give very good descriptions of experimental data from LEP and other e^+e^- colliders, with the dipole model giving just a slightly better overall χ^2. (The overall structure of the final state depends strongly on the first hard emissions, and in all approaches the best agreement is obtained if these are described by fixed order matrix elements.)

II.2.2 Cascades in DIS

DIS is a more complicated process than e^+e^--annihilation. First, there are in DIS two different energy scales, W^2 and Q^2. Secondly, in DIS both the cross section and the final state properties are highly nontrivial problems. Only in the pure DGLAP region, with high Q^2 and large x, has the probabilistic description in terms of $k_\perp$-ordered cascades been really successful, in this case both for cross sections and final state properties. In the DGLAP region the real emissions are compensated by virtual corrections in a way similar to the time-like cascades in e^+e^--annihilation. Thus the virtual corrections can also here be treated by Sudakov form factors, and the cascade contains only the real emissions appearing in the final state. Thus the DGLAP evolution describes the probability for a given parton state with a fixed resolution determined by Q^2. The total cross section is determined by the reaction probability between the virtual photon and the quarks in the cascade. The final state is obtained by adding final state radiation to the partons in the initial cascade (within angular ordered regions).

For lower x and Q^2 separate approaches have been used to describe the total cross section and the final state properties. To LL or NLL accuracy the

cross section is determined by the BFKL equation. The BFKL evolution can be formulated in different ways. In its implementation in the Mueller dipole cascade it is not suited to describe the final state, as the evolution contains a very large number of virtual dipoles, which do not appear as final state particles. As mentioned, the BFKL equation has also the problem that the NLL corrections are so very large.

The presently best description of the final state properties at HERA is given by the soft radiation model (frequently called the Color Dipole Model, CDM, and implemented in the Ariadne event generator). In this model the gluon radiation from the separating colour charges in the kicked out quark and the proton remnant is described in a way analogous to emission in e^+e^--annihilation. The CDM model does not predict the cross section, but only the properties of the final state. It has also the drawback that it is not solidly founded in perturbative QCD.

The CCFM model [32, 33] represents an interpolation between the DGLAP and BFKL evolutions. In the DGLAP region the cascade contains, besides the real emissions in the DGLAP equation, also softer emissions which are treated as final state radiation in the DGLAP approach. This makes the regions where final state radiation should be added more complicated, and a description of final state properties more difficult. The CCFM model is reformulated and generalized in the Linked Dipole Chain (LDC) model [34], which is based on a different separation between initial and final state radiation. Both these models are implemented in MC event generators, Cascade [35, 36] and LDCMC [37, 38] respectively. The models have the ambition to describe *both* the cross section and the final state properties. They both work well with respect to the cross sections, but none is as successful as the abovementioned CDM model, when it comes to the properties of the final states.

II.2.3 Mueller's Dipole Formulation

The Mueller dipole model [14–16] is formulated in transverse coordinate space. Such a formulation has the advantage that the transverse coordinates of the partons are not changed during the evolution. This makes it easier to take into account saturation effects due to multiple scatterings. On the other hand, it is easier to take into account energy–momentum conservation in a model formulated in transverse momentum space.

In Mueller's model we start with a $q\bar{q}$ pair, heavy enough for perturbative calculations to be applicable, and calculate the probability to emit a soft gluon from this pair. Here the quark and the antiquark are assumed to follow light-cone trajectories and the emission of the gluon is calculated in the eikonal approximation in which the emitters do not suffer any recoil. Adding the contributions to the emission from the quark and the antiquark, including the

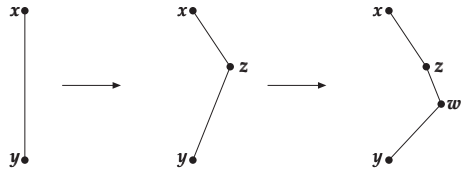

Figure II.1: The evolution of the dipole cascade. At each step, a dipole can split into two new dipoles with decay probability given by (II.1).

interference, one obtains the result (for notations, see figure II.1)

$$\frac{d\mathcal{P}}{dY} = \frac{\bar{\alpha}}{2\pi} d^2\boldsymbol{z} \frac{(\boldsymbol{x}-\boldsymbol{y})^2}{(\boldsymbol{x}-\boldsymbol{z})^2(\boldsymbol{z}-\boldsymbol{y})^2} \equiv \frac{\bar{\alpha}}{2\pi} d^2\boldsymbol{z}\mathcal{M}(\boldsymbol{x},\boldsymbol{y},\boldsymbol{z}). \tag{II.1}$$

Here $\boldsymbol{x}$, $\boldsymbol{y}$, and $\boldsymbol{z}$ are two-dimensional vectors in transverse coordinate space and Y denotes the rapidity, which acts as the time variable in the evolution process. This formula can be interpreted as the emission probability from a dipole located at $(\boldsymbol{x},\boldsymbol{y})$. In the large N_c limit the gluon can be seen as a quark–antiquark pair and the formula above can then be interpreted as the decay of the original dipole $(\boldsymbol{x},\boldsymbol{y})$ into two new dipoles, $(\boldsymbol{x},\boldsymbol{z})$ and $(\boldsymbol{z},\boldsymbol{y})$. In the same limit further emissions factorize, so that at each step one has a chain of dipoles where each dipole can decay into two new dipoles with the decay probability given by (II.1). In this way one obtains a cascade of dipoles which evolve through dipole splittings, and the number of dipoles grows exponentially with Y.

We note that the expression above has non-integrable singularities at $\boldsymbol{z} = \boldsymbol{x}$ and $\boldsymbol{z} = \boldsymbol{y}$. In numerical calculations it is therefore necessary to introduce a cutoff, ρ, such that $(\boldsymbol{x}-\boldsymbol{z})^2, (\boldsymbol{z}-\boldsymbol{y})^2 \geq \rho^2$. To obtain a meaningful probabilistic interpretation of (II.1) (note that $d\mathcal{P}/dY$ can become very large for small ρ) we also need to take into account virtual corrections to the real emissions. The effect of these corrections is described by a Sudakov form factor, $S = \exp(-\int dY d^2\boldsymbol{z} \cdot d\mathcal{P}/dY)$, which should multiply the splitting probability in (II.1).

II.2.4 Scattering of Dipoles

In Mueller's model each dipole interacts independently with some target via two-gluon exchange. In case of onium–onium scattering each onium evolves into a cascade of dipoles. We let f_{ij} denote the imaginary part of the elastic scattering amplitude for a dipole i, with coordinates $(\boldsymbol{x}_i,\boldsymbol{y}_i)$, in one of the onia and a dipole j, with coordinates $(\boldsymbol{x}_j,\boldsymbol{y}_j)$, in the other onium. The basic dipole–

dipole scattering amplitude from gluon exchange is given by

$$f_{ij} = \frac{\alpha_s^2}{8}\left[\log\left(\frac{(\boldsymbol{x}_i-\boldsymbol{y}_j)^2(\boldsymbol{y}_i-\boldsymbol{x}_j)^2}{(\boldsymbol{x}_i-\boldsymbol{x}_j)^2(\boldsymbol{y}_i-\boldsymbol{y}_j)^2}\right)\right]^2. \tag{II.2}$$

In the single pomeron approximation the onium–onium amplitude is then simply given by the sum of the basic dipole–dipole amplitudes, $\sum_{ij} f_{ij}$.

In the dipole model it is also possible to have *multiple scatterings*, i.e the simultaneous scatterings of several dipoles. Assuming that the individual dipole interactions are uncorrelated, summing multiple scatterings to all orders exponentiates, and the total amplitude for a single event is given by $1-\exp(-\sum_{ij} f_{ij})$. Thus, the expansion of the exponential in a power series corresponds directly to the contributions from the multiple scattering series, where the single pomeron cross section corresponding to the first term in this series is given by $2\int\langle\sum_{ij} f_{ij}\rangle$.

Consider the scattering of an elementary dipole $(\boldsymbol{x},\boldsymbol{y})$ off some arbitrary target. We denote the scattering matrix by $\mathcal{S}(\boldsymbol{x},\boldsymbol{y})$. After one step of evolution in rapidity the dipole $(\boldsymbol{x},\boldsymbol{y})$ has a chance to split into two new dipoles, $(\boldsymbol{x},\boldsymbol{z})$ and $(\boldsymbol{z},\boldsymbol{y})$, through the splitting kernel $\mathcal{M}_{\boldsymbol{xyz}} \equiv \mathcal{M}(\boldsymbol{x},\boldsymbol{y},\boldsymbol{z})$. The evolution of the S-matrix is then given by

$$\partial_Y \mathcal{S}(\boldsymbol{x},\boldsymbol{y}) = \frac{\bar{\alpha}}{2\pi}\int d^2\boldsymbol{z}\,\mathcal{M}_{\boldsymbol{xyz}}\{-\mathcal{S}(\boldsymbol{x},\boldsymbol{y}) + \mathcal{S}^{(2)}(\boldsymbol{x},\boldsymbol{z};\boldsymbol{z},\boldsymbol{y})\}. \tag{II.3}$$

The right hand side in this expression simply states that the dipole can remain as it is, with a reduced probability, $1-\bar{\alpha}/2\pi\int\mathcal{M}$, or that it can split into two new dipoles, $(\boldsymbol{x},\boldsymbol{z})$ and $(\boldsymbol{z},\boldsymbol{y})$, with a probability density given by (II.1). If we assume that $\mathcal{S}^{(2)}(\boldsymbol{x},\boldsymbol{z};\boldsymbol{z},\boldsymbol{y}) = \mathcal{S}(\boldsymbol{x},\boldsymbol{z})\mathcal{S}(\boldsymbol{z},\boldsymbol{y})$ and rewrite the equation in the scattering amplitude $T \equiv 1-\mathcal{S}$, we get

$$\partial_Y T(\boldsymbol{x},\boldsymbol{y}) = \frac{\bar{\alpha}}{2\pi}\int d^2\boldsymbol{z}\,\mathcal{M}_{\boldsymbol{xyz}}\{-T(\boldsymbol{x},\boldsymbol{y}) + T(\boldsymbol{x},\boldsymbol{z}) + T(\boldsymbol{z},\boldsymbol{y}) - T(\boldsymbol{x},\boldsymbol{z})T(\boldsymbol{z},\boldsymbol{y})\}. \tag{II.4}$$

This is the so called Balitsky–Kovchegov (BK) equation [39, 40]. The assumption that $\mathcal{S}^{(2)} = \mathcal{S}\mathcal{S}$, corresponds to a mean field approximation, which can be justified for a large target nucleus. As demonstrated in [14] the linear part of (II.4) reproduces the BFKL equation, while the inhomogeneous term describes the simultaneous scattering of the two new dipoles.

The S-matrix for a specific scattering event can be written as $\exp(-\sum_{ij} f_{ij})$. To obtain the physical cross section one has to perform an average over onium configurations, so that $\mathcal{S} = \langle\exp(-\sum_{ij} f_{ij})\rangle$. The total cross section is given by $2\int(1-\mathcal{S}(b))$, where b denotes the impact parameter, and for onium-onium

scattering we therefore get

$$\sigma_{tot} = 2 \int d^2\boldsymbol{b} \langle 1 - \exp(-\sum_{ij} f_{ij}) \rangle. \tag{II.5}$$

For $\gamma^*\gamma^*$ scattering one also needs to convolute the averaged amplitude with the virtual photon wave functions. The expression in (II.5) is also what we will use for $\gamma^* p$ and pp collisions, where we model the proton as a collection of colour dipoles. These points are explained in greater detail below.

II.2.5 Energy–Momentum Conservation

As we saw above, the probability to produce small dipoles diverges as the size of the dipoles goes to zero. To regulate this divergence a cutoff, ρ, was introduced. Even though this cutoff does not show up in the cross section (the divergence is canceled by virtual corrections, and σ_{tot} approaches a constant when $\rho \to 0$) it must still be kept in a Monte Carlo program. A small value of ρ, which is needed in order to simulate the physics with a good accuracy, will imply that we get very many small dipoles in the cascade. A small dipole means that we have two well localized gluons in the transverse plane, and these gluons must then have a correspondingly large transverse momentum of the order of the inverse dipole size, $p_\perp \sim 1/r$. Thus if these small dipoles are interpreted as corresponding to real emissions with $p_\perp \sim 1/r$, then the diverging number of such dipoles would imply the violation of energy–momentum conservation. This suggest that these dipoles should be interpreted as virtual fluctuations, which means that the dipole cascade will not correspond to the production of exclusive final states.

Similarities between Mueller's model and the Linked Dipole Chain (LDC) model [34] were used in ref. [20] to implement energy conservation in Mueller's model. This removes a dominant fraction of the virtual emissions. (It does, however, not remove all virtual emissions. That emissions must satisfy energy–momentum conservation if they are to be present in real final states is obviously a necessary condition, but as was discussed in [20], it is by itself not a sufficient condition.) The modified cascade is ordered in both light-cone variables, p_+ and p_-, and it was seen that this modification has a rather large effect on the cascade. One sees for example that the total number of dipoles, while still increasing exponentially, is greatly reduced, which implies that the onset of saturation is delayed. In fact it is found that in DIS the unitarity effects become quite small within the HERA energy regime, at least for $Q^2 \gtrsim 1\ \text{GeV}^2$. Naturally saturation is more important for dipole–nucleus or pp scattering. In particular we will in the following see that saturation effects have a large influence on pp collisions at the Tevatron.

II.3 The JIMWLK Approach

II.3.1 The Color Glass Condensate

A different approach to high energy QCD is called the Color Glass Condensate (CGC) (for review papers see [41–43]). This is an effective theory for QCD valid at high gluon densities. Here, the strong gluon fields present in the high energy particle (which might be a proton, a large nucleus etc.) emerge due to a classical random color source, ρ^a, and the classical fields satisfy the corresponding Yang–Mills equations of motion. These random sources are distributed according to a weight functional $W[\rho]$. As the particle evolves one proceeds by integrating out layers of quantum fields which are added to the classical source. This is a renormalization group procedure and the weight functional then satisfies a renormalization group equation which is known as the JIMWLK equation [44–47]. The JIMWLK evolution leads to the saturation of the gluon density[2] when the field strength is of order $1/\alpha_s$. The scale at which the hadron seems to saturate is called the saturation momentum, denoted by $Q_s(Y)$. The CGC formalism predicts that $Q_s(Y)$ grows exponentially with rapidity, defined by $Y = \log(1/x)$ in this case.

II.3.2 The Balitsky-JIMWLK Equations

When considering a scattering process within the CGC formalism, one usually thinks of the target as a highly evolved dense particle which can be described by the weight functional $W[\rho]$, satisfying the JIMWLK equation. The projectile, on the other hand, is usually a simple particle which is not so dense, such as an elementary dipole impinging on the target. The JIMWLK equation can be written as a Schrödinger equation for the weight functional, $\partial_Y W = H_{JIMWLK} W$, where H_{JIMWLK} denotes the "JIMWLK Hamiltonian". Operators corresponding to observables are averaged over with the weight $W[\rho]$, and one may then bring the action of H_{JIMWLK} on the operator, instead of on $W[\rho]$ itself. This is reminiscent of switching from the Schrödinger picture (evolution of the "wave function" $W[\rho]$) to the Heisenberg picture (evolution of an operator $\mathcal{O}$) in quantum mechanics. In particular, if one applies H_{JIMWLK} on $S(\boldsymbol{x},\boldsymbol{y})$, the S-matrix for the projectile dipole, an infinite hierarchy of equations emerge. This hierarchy of equations is now commonly referred to as the Balitsky–JIMWLK (B–JIMWLK) equations, since the same set of equations were some years earlier derived by Balitsky [40] within a different formalism. Taking the large N_c limit[3] the more complicated colour structures disappear,

[2] The growth does not cease completely, but it is only logarithmic as opposed to a power-like growth at lower energies.

[3] From now on, when we talk about the B–JIMWLK equations, we always mean the large N_c limit of these equations.

and the equations can be interpreted in terms of dipoles evolving according to the discussion in section II.2. Written in terms of the scattering amplitude $T(\boldsymbol{x},\boldsymbol{y}) = 1 - S(\boldsymbol{x},\boldsymbol{y})$, the equations in this hierarchy can formally be written as

$$\begin{aligned} \partial_Y \langle T \rangle &= \mathcal{K} \otimes (\langle T \rangle - \langle TT \rangle) \\ \partial_Y \langle TT \rangle &= \mathcal{K} \otimes (\langle TT \rangle - \langle TTT \rangle) \\ &\vdots \end{aligned} \tag{II.6}$$

where $\mathcal{K}$ is the evolution kernel. We see here that the equation for $\langle T \rangle$ contains a contribution from $\langle TT \rangle$. In turn, the equation for $\langle TT \rangle$ contains a term $\langle TTT \rangle$ and so on.

These equations simplify considerably when disregarding target correlations, i.e. making a mean field approximation where $\langle TT \rangle = \langle T \rangle \langle T \rangle$. As can be seen from (II.6) the hierarchy then boils down to a single, closed, nonlinear equation for $\langle T \rangle$, which turns out to be none other than the BK equation introduced in section 2.

II.3.3 Inclusion of Pomeron Loops

As we saw above the B–JIMWLK hierarchy couples the scattering amplitude $\langle T^k \rangle$ to all $\langle T^n \rangle$, with $n \geq k$. There are however no contributions from amplitudes $\langle T^n \rangle$ with $n < k$. The nonlinear term in the BK equation corresponds to pomeron splittings in the projectile; the projectile dipole splits into two dipoles and each of these two couples to the target through a single pomeron giving in total two pomerons coupling to the target. However, one can also assume that the target is given the rapidity increment, and in this case the two pomerons in the target must merge into one pomeron, which couples to the single dipole. Thus this term also corresponds to the merging of two pomerons inside the target (see figure II.2).

We therefore see that the B–JIMWLK equations describe either pomeron mergings, when the target is evolved, or pomeron splittings, in case the projectile is evolved, but not both. Thus, even though the CGC formalism correctly describes saturation effects, it nevertheless misses some essential physics as it cannot account for pomeron splittings. What is actually absent is gluon number fluctuations. Indeed, in the CGC approach the small-x gluons are radiated from the classical colour source ρ, but are themselves not allowed to split. They rather get absorbed into $W[\rho]$, and act as sources for gluons with even smaller x, as the evolution proceeds. The effects of fluctuations were demonstrated in numerical studies by Salam [48], and it is known that they are important for the approach towards the unitarity limit [49,50]. We note

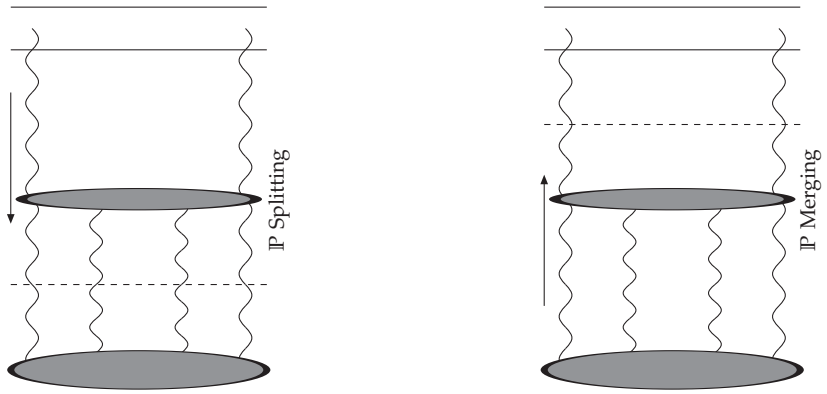

Figure II.2: Diagrams for pomeron splittings and mergings. On the left picture the projectile dipole is evolved, indicated by the down-going arrow, and one pomeron is split into two pomerons. The frame in which the collision is viewed is indicated by the horizontal dashed line. On the picture to the right, the target, the gray blob at the bottom, is evolved and two pomerons merge into one pomeron which couple to the projectile.

that these fluctuations are correctly taken into account in the dipole model, and in a Monte Carlo program based on it, as demonstrated by Salam.

Ever since it was realized that the B–JIMWLK equations are not complete, there has been a lot of effort to construct a model which contains both pomeron mergings and splittings, and, through iterations, pomeron loops. This has been formulated in the large N_c limit [51–53] where the dipole model has been used to add pomeron splittings to the B–JIMWLK equations in the dilute region. The extension to the dense region is then obtained by simply adding the remaining terms arising from the large N_c version of the B–JIMWLK hierarchy. The main principle is that the two kinds of pomeron interactions (splittings and mergings) are important in different, well separated, kinematical regions. The equations obtained in this way give the correct expressions in the two limits (dense and dilute systems), but it is not very clear how well they work in an intermediate region. The new equation for $\langle TT \rangle$ receives a contribution also from $\langle T \rangle$ and it can be written as

$$\partial_Y \langle TT \rangle = \mathcal{K} \otimes (\langle TT \rangle - \langle TTT \rangle) + \mathscr{F} \cdot \langle T \rangle, \tag{II.7}$$

where $\mathscr{F}$ is a quite complicated expression describing the fluctuations in the target (or saturation effects in the projectile).

II.4 Finite N_c Effects in Dipole Evolution

In this section we want to discuss what improvements can be made in order to obtain a more complete picture of high energy evolution using the dipole degrees of freedom. In a formalism where both the projectile and the target are considered within the dipole picture, the missing piece is saturation effects rather than fluctuations, which are fully accounted for in the dipole model.

In many approaches the dipoles in a cascade are treated as independent and without a specified direction. An important feature in our formalism is that our cascade consists of a *chain* of dipoles which are all connected to each other through the gluons. This chain has also a specified *direction*, with each dipole oriented from colour charge to anti-charge. Such a chain can only end in a quark or an antiquark. In this picture one therefore cannot simply take two arbitrary dipoles and merge them into one dipole, leaving loose ends behind. It is also necessary to specify how these ends afterwards get reconnected to other dipoles in the systems. We therefore begin this section by a discussion of colour structures, and a motivation why it is important, before engaging into the problems due to the finite number of colours. We end the section with a comparison between our formalism and other approaches to include colour suppressed effects in the dipole cascade formalism.

II.4.1 Colour Structures

In onium–onium scattering it is assumed that the probability for a dipole–dipole sub-collision is independent of the remaining dipoles in the cascades. The exchange of a gluon implies that the intermediate state corresponds to a recoupling of the colour flow, as is shown in fig. II.3. This interaction actually corresponds to the coherent sum of four different Feynman diagrams, illustrated in fig. II.4. Note in particular that in the dipole formalism a dipole is a colour singlet, i.e. a coherent sum of $r\bar{r}$, $b\bar{b}$, and $g\bar{g}$. Therefore the diagrams in figs. II.4c and II.4d have the same weight as those in figs. II.4a and II.4b. Summing and averaging over colours they are all of order α_s, and thus formally colour suppressed compared to the dipole splitting vertex in (II.1), which is proportional to $\bar{\alpha} = N_c\,\alpha_s/\pi$.

We see that the result of the interactions in figs. II.3 and II.4 is two new, directed and uniquely specified, dipole chains. The colour end from one initial dipole chain is connected to the anti-colour end from the other initial chain. There are actually two good reasons to keep track of the dipole orientations. First we note that given the orientation of the colliding dipoles the final dipoles are uniquely determined. There is only one possible way to connect the four involved gluons and only one possible orientation for the new dipoles. Thus keeping track of the orientation actually simplifies the formal-

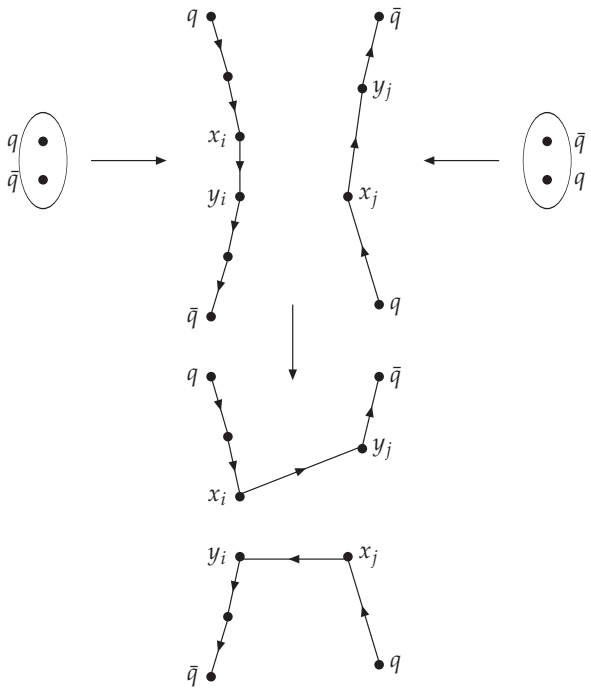

Figure II.3: Symbolic picture showing the interaction of two onia via a single sub-collision. The interaction between the dipoles $(\boldsymbol{x}_i, \boldsymbol{y}_i)$ and $(\boldsymbol{x}_j, \boldsymbol{y}_j)$ leads to a recoupling of the colour flow, with strength f_{ij} given by (II.2).

ism, as knowing which end of the dipole is the colour and which is the anti-colour reduces the number of contributing Feynman diagrams. Secondly we have the ambition to include analyses of exclusive final states in future work, and it is clearly necessary to keep track of the orientation of the dipole chains when we want to add final state radiation and hadronization.

Multiple dipole–dipole sub-collisions give more complicated final states, as illustrated in figs. II.5a and II.5b. When dipole 1 scatters against dipole 3 and dipole 2 against dipole 4, as shown in fig. II.5a, the result includes an isolated dipole loop in the center. If instead dipole 1 scatters against dipole 4 and dipole 2 against dipole 3, as in fig. II.5b, the result is two dipole chains, each connecting the two ends from one of the initial incoming chains. The lower figures give schematic pictures of the resulting dipole chains. Here the projectile and target remnants move to the right and left respectively. The dipole chains are stretched between these remnants and the gluons which have participated in the hard sub-collisions.

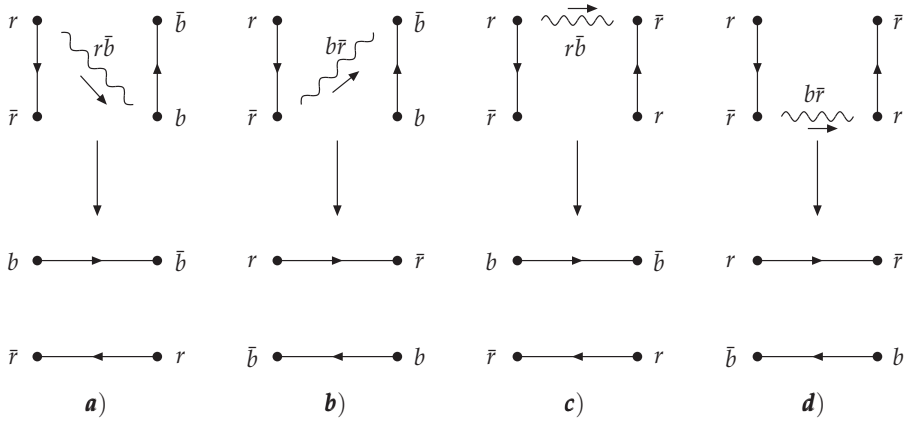

Figure II.4: Diagrams for dipole–dipole scattering. Each interaction implies a recoupling of the colour flow and the square of the sum of the four diagrams give f_{ij} in (II.2).

II.4.2 Effects of Finite N_c

As discussed in the introduction there are two different effects related to the finite number of colours. The first problem is due to the fact that the amplitude for a dipole–dipole collision is proportional to α_s, and therefore formally colour suppressed compared to the dipole splitting process proportional to $\bar{\alpha} = N_c\alpha_s/\pi$. Thus, while one takes into account colour-suppressed effects and saturation due to multiple dipole–dipole sub-collisions, the evolution itself does not contain such effects. The multiple collision events can lead to the formation of colour loops, as illustrated in fig. II.5a, or to pomeron loops in the elastic amplitude as shown in fig. II.6. Fig. II.7 shows an example with a more complicated event, where three dipole–dipole sub-collisions result in the formation of two loops. There is also one loop formed totally within one of the cascades, indicated by the letter A. Such a loop cannot be formed within Mueller's initial formalism, in which only dipole splitting is included within the cascade. It could, however, have been included if the reaction had been studied in a different Lorentz frame. We see that in order to achieve a boost invariant formalism we must allow dipoles to combine in the cascade. We note that the new terms that were included in the B–JIMWLK equations, discussed above, are also formally colour suppressed and are essential in order to obtain a frame independent formalism.

We should however point out that there is also another frame dependent effect, which is more kinematic in origin. For evolution with a finite cutoff, $\rho \neq 0$, frame independence is only approximative, even in the one pomeron

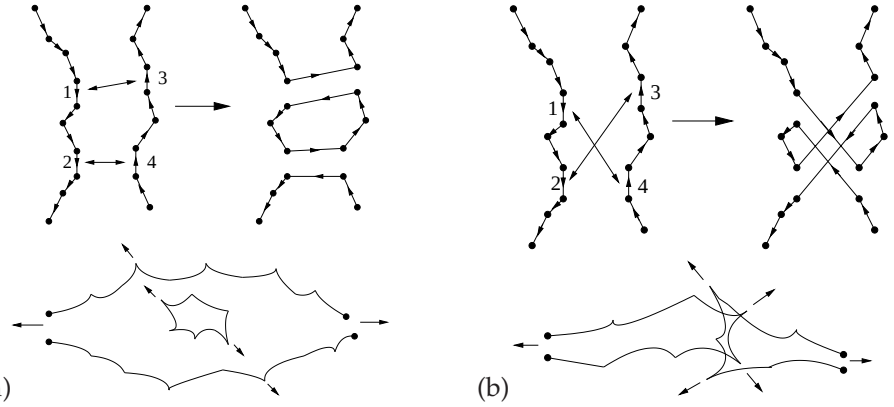

Figure II.5: The colour structure arising from two sub-collisions between the right- and left-moving onia. (a) The final configuration involves an isolated dipole loop together with two chains, each connecting the initial quark (antiquark) in the right moving onia with the initial antiquark (quark) in the left moving onia. (b) The final configuration obtained when dipole 1 collides with 4 and 2 with 3. The result is two "entangled" chains. The lower part of the pictures give a schematic view of the resulting dipole chains, with the projectile and target remnants moving to the right and left respectively. Gluons participating in the hard sub-collisions are also indicated by arrows.

approximation (only one branch coupling to the target). In our case we have a dynamical cutoff, $\rho(\Delta y)$ (see section II.6), and in our scheme every new branch takes away energy. This means that in a cascade with many branches the energy in each individual branch is reduced. We note that a branch can only be realized if it interacts with the target and branches which do not interact have to be regarded as virtual (such examples are shown in fig. II.7 where the branches marked B and C do not couple to the target). These branches should consequently be removed from the cascade and in the corresponding final state they should be replaced by their earlier ancestors. However, as our constraint from energy-momentum conservation also includes the fractions needed to evolve the non-interacting branches the effect is somewhat overestimated. Therefore we do not expect to find complete frame independence, but we will see in the following that the frame dependence is indeed very small.

The second problem is due to the possibility that two dipoles can have the same colour. The two charges and their corresponding anti-charges then form a colour quadrupole, which cannot be described as two independent dipoles.

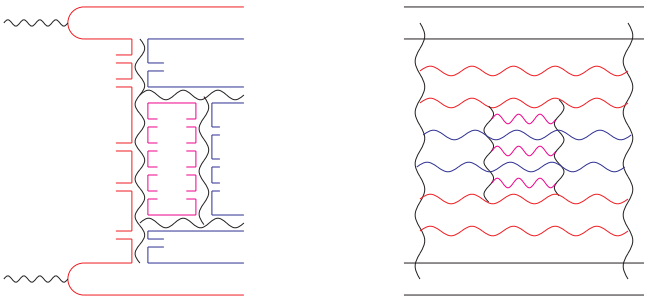

Figure II.6: A high energy collision showing the partonic sub-collisions inside the resolved photons. This figure shows the case of two sub-collisions and in the left figure there is a loop of dipoles at the center. To the right is the corresponding elastic diagram which shows the exchange of two pomerons.

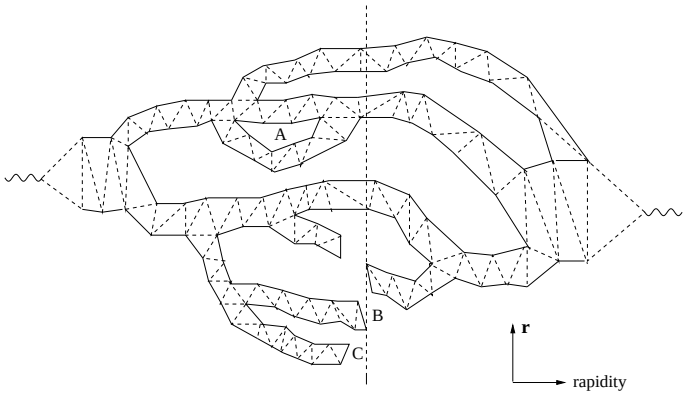

Figure II.7: Collision of two dipole cascades in $\boldsymbol{r}$-rapidity space. The dashed vertical line symbolizes the Lorentz frame in which the collision is viewed. The dipole splitting vertex can result in the formation of different dipole branches, and loops are formed due to multiple sub-collisions. The loop denoted by A can be formed via a dipole swing, which is further illustrated in fig II.9.

Gluon Exchange

The two dipole sub-collisions in fig. II.5a, which both are due to single gluon exchange, lead to a recoupling of the dipole chains and a closed dipole loop. Visualized in a different Lorentz frame this process must be interpreted as the result of gluon exchange between two dipoles in the cascade. It then corresponds to the replacement of two dipoles with two new dipoles within the

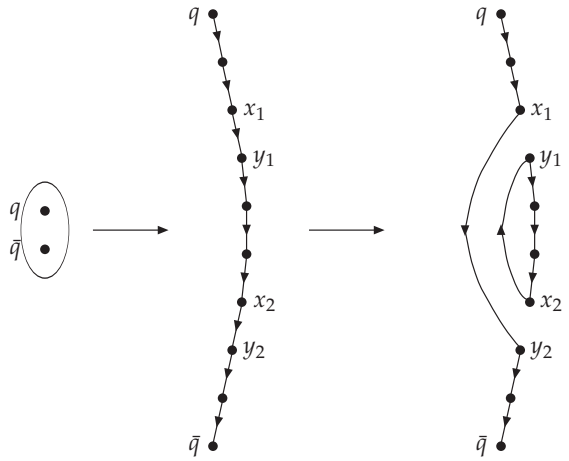

Figure II.8: Schematic picture of a dipole swing. The two dipoles $(\boldsymbol{x}_1, \boldsymbol{y}_1)$ and $(\boldsymbol{x}_2, \boldsymbol{y}_2)$ are transformed into two new dipoles $(\boldsymbol{x}_1, \boldsymbol{y}_2)$ and $(\boldsymbol{x}_2, \boldsymbol{y}_1)$ after a recoupling of the colour flow. The initial chain of dipoles is replaced by a new chain stretching between the original $q\bar{q}$ pair and a loop of dipoles.

evolution of the cascade. This process has been called a "dipole swing" and is illustrated in fig. II.8. As it represents the dipole–dipole scattering cross section in (II.2) it ought to be proportional to $\alpha_s^2/8$, and therefore effectively suppressed. We ought to point out that fig. II.8 is only a schematic picture showing how the dipoles are connected to each other, and does not represent the transverse size of the dipoles. In fact, the swing process is more likely to replace two dipoles with two smaller dipoles, as discussed below.

Including the dipole swing it is in fact possible to generate any kind of colour loop. Thus all loops formed when the expanding "tentacles" in fig. II.7 join can be generated by the original dipole splitting process together with the dipole swing. This is illustrated in fig. II.9, which shows how a dipole splitting process in the evolution towards the left can also be visualized as a pomeron fusion process generated by the dipole swing, when the process is evolved in the opposite direction.

Colour Multipoles

As mentioned above a second effect of finite N_c is the formation of colour quadrupoles and higher multipoles. In fact, it can be seen in the complete version of the B–JIMWLK equations that more complicated colour structures appear at each step of the evolution. Obviously these complicated colour struc-

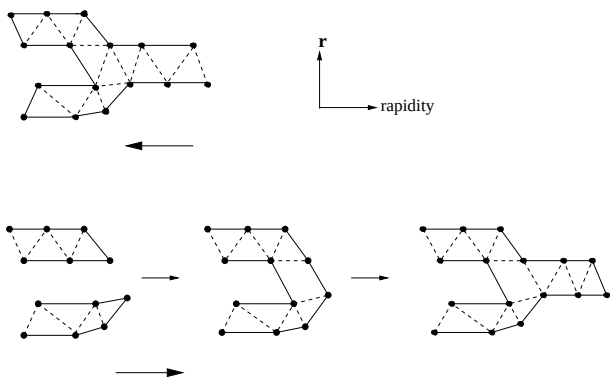

Figure II.9: Evolution of dipoles in $\boldsymbol{r}$-rapidity space. Going to the left we have evolution through dipole splittings and one dipole chain splits into two, corresponding to a $1 \longrightarrow 2$ pomeron splitting. If instead we evolve to the right then the two chains can be combined by a swing and only one of the chains continue evolving, corresponding to a $2 \longrightarrow 1$ pomeron merging.

tures imply that one loses the simple picture of a system of dipoles, which evolve through simple splittings. Nevertheless, in view of the success of the time-like dipole cascades in e^+e^--annihilation it may be possible to find a working approximation within the dipole framework also in this case. We may then try to approximate a quadrupole as two dipoles where those formed by the closest colour–anti-colour pairs should dominate. This means that we allow for a colour recoupling, in which two dipoles with coordinates $(\boldsymbol{x}_1, \boldsymbol{y}_1)$ and $(\boldsymbol{x}_2, \boldsymbol{y}_2)$, can be transformed into two new dipoles with coordinates $(\boldsymbol{x}_1, \boldsymbol{y}_2)$ and $(\boldsymbol{x}_2, \boldsymbol{y}_1)$.

We note that the result of this process also corresponds exactly to the dipole swing in fig. II.8, and consequently it has exactly the same effect as the gluon exchange process discussed above. The only difference we may expect is that the effect due to multipoles would be instantaneous, while the gluon exchange process ought to be proportional to the rapidity interval, Δy, in the evolution.

We have not (yet) found a weight for the dipole swing which makes the scattering process explicitely frame independent. We note, however, that the dipole splitting vertex in (II.1) gives a total weight for a specific dipole chain given by the product of factors $1/\mathbf{r}_i^2$ for all dipoles still present in the cascade. For dipoles which have already decayed (those denoted by dashed lines in figs. II.7 and II.9) the factor $\mathbf{r}_i^{-2}$ is exactly compensated by the factor $\mathbf{r}_i^2$ in the numerator of the splitting vertex factor. It may therefore seem natural that the swing $(\boldsymbol{x}_1, \boldsymbol{y}_1) + (\boldsymbol{x}_2, \boldsymbol{y}_2) \rightarrow (\boldsymbol{x}_1, \boldsymbol{y}_2) + (\boldsymbol{x}_2, \boldsymbol{y}_1)$ has a weight proportional to $(\boldsymbol{x}_1 - \boldsymbol{y}_1)^2(\boldsymbol{x}_2 - \boldsymbol{y}_2)^2/(\boldsymbol{x}_1 - \boldsymbol{y}_2)^2(\boldsymbol{x}_2 - \boldsymbol{y}_1)^2$. Such a weight would preserve

the feature that any dipole system has a weight proportional to $\prod \mathbf{r}_i^{-2}$. At the same time it also favours dipoles formed by close charge–anti-charge pairs in colour quadrupoles, in accordance with the discussion above.

Implementation of the Dipole Swing

When we include the dipole swing in the MC implementation we will therefore use a weight proportional to $(\boldsymbol{x}_1-\boldsymbol{y}_1)^2(\boldsymbol{x}_2-\boldsymbol{y}_2)^2/(\boldsymbol{x}_1-\boldsymbol{y}_2)^2(\boldsymbol{x}_2-\boldsymbol{y}_1)^2$, and the normalization should be adjusted so that the final result is approximately frame independent. This would show that there is the same probability to have a colour loop within the cascade evolution as formed by multiple subcollisions. Even if this is achieved it is, however, not possible to tell whether the dominant mechanism behind the swing is due to gluon exchange or to colour multipoles.

In the MC the probability for a swing $(\boldsymbol{x}_1,\boldsymbol{y}_1)+(\boldsymbol{x}_2,\boldsymbol{y}_2)\to(\boldsymbol{x}_1,\boldsymbol{y}_2)+(\boldsymbol{x}_2,\boldsymbol{y}_1)$ is formulated as if the main mechanism is colour multipoles. There is a probability $1/(N_c^2-1)$ that two dipoles have the same colour. Therefore we assume that two dipoles are allowed to swing with this probability. If they are allowed to swing, they do so during an evolution step Δy with a probability given by

$$\Delta P = \lambda\frac{(\boldsymbol{x}_1-\boldsymbol{y}_1)^2(\boldsymbol{x}_2-\boldsymbol{y}_2)^2}{(\boldsymbol{x}_1-\boldsymbol{y}_2)^2(\boldsymbol{x}_2-\boldsymbol{y}_1)^2}\Delta y. \tag{II.8}$$

If the normalization factor λ is large, the dipoles with the same colour will swing rapidly and adjust themselves to weights $\propto\prod\mathbf{r}_i^{-2}$ before the next dipole splitting. The applications presented in section II.7 are obtained using such a large λ-value, which implies that the swing can be regarded as instantaneous, as expected if colour multipoles is the dominant mechanism. This also means that the effective normalization is given by the number of different dipole colours $N_c^2-1=8$ and not by λ. We will see that this recipe does indeed give an almost frame independent result. This does, however, not imply that we also can conclude that colour multipoles is the dominant mechanism. It is actually possible to get approximately the same result allowing swings between more dipoles but with a smaller λ-value. In this case the swing does not occur instantaneously, but with a probability proportional to the step Δy in rapidity, as expected if the dominant mechanism is gluon exchange. It is therefore not possible to tell which mechanism is most important.

A more detailed description of how the swing is implemented in the simulation program is given in section II.6.

II.4.3 Comparison With Other Formalisms

There has been quite some effort to interpret pomeron mergings as dipole mergings, i.e. interpreting (II.7) in terms of a system of dipoles which can ei-

ther split (a $1 \to 2$ dipole vertex) or merge (a $2 \to 1$ vertex). While it is obvious that dipole mergings generate pomeron mergings, the opposite of this statement is not necessarily true. In fact there are also other dipole processes which generate pomeron mergings. In a formalism where the cascade is treated as a set of uncorrelated dipoles a $2 \to n$ dipole vertex, with $n \geq 2$, also leads to pomeron mergings. This follows because there is always the possibility that only one of the new dipoles interacts with the target, while the rest are spectators. Of course such a transition leads to all possible $2 \to m$ ($m = 1, \ldots, n$) pomeron transitions.

This argument can be illustrated by the following evolution equations. We denote the dipoles by the letters a, b and so on, and the S-matrix by $\mathcal{S}(a)$, for one dipole a, $\mathcal{S}(ab)$ for two dipoles a and b. The scattering amplitude is given by $T = 1 - \mathcal{S}$ and with $T(ab)$ we mean $\langle T(a)T(b)\rangle$. Assume now that there exist different vertices for different dipole transitions; $\beta(ab|c)$ for the merging of a and b into c, $\Gamma(ab|cd)$ for the transition $a + b \to c + d$ and so on. We then have the following evolution equations

$$\begin{aligned}\partial_Y \mathcal{S}(ab)_\beta &= \int_c \beta(ab|c)\Big\{-\mathcal{S}(ab) + \mathcal{S}(c)\Big\} \\ \partial_Y \mathcal{S}(ab)_\Gamma &= \int_{cd} \Gamma(ab|cd)\Big\{-\mathcal{S}(ab) + \mathcal{S}(cd)\Big\}. \end{aligned} \tag{II.9}$$

The negative contribution on the right hand side comes from the fact that the system can remain as it is, with a survival probability given by $(1 - \int \beta)$ or $(1 - \int \Gamma)$. Alternatively the system can evolve, with a probability density given by β or Γ, which corresponds to the positive contribution on the right hand side. Thus the evolution of the S-matrix has a clear probabilistic interpretation. One can now rewrite these equations for T, using the relation $T = 1 - \mathcal{S}$. We thus get

$$\begin{aligned}\partial_Y T(ab)_\beta &= \int_c \beta(ab|c)\Big\{-T(c) + T(a) + T(b) - T(ab)\Big\} \\ \partial_Y T(ab)_\Gamma &= \int_{cd} \Gamma(ab|cd)\Big\{-T(c) - T(d) + T(a) + T(b) - T(ab) + T(cd)\Big\}. \end{aligned} \tag{II.10}$$

Here we can see that both equations contain both pomeron mergings and also $2 \to 2$ pomeron transitions. It is straightforward to write the equations also for more general vertices. Indeed, for the general $2 \to n$ transition, with the vertex $\Gamma(ab|c_1c_2\ldots c_n)$, we get the following evolution equations

$$\partial_Y \mathcal{S}(ab)_\Gamma = \int_{c_i} \Gamma(ab|c_1c_2\ldots c_n)\Big\{-\mathcal{S}(ab) + \mathcal{S}(c_1c_2\ldots c_n)\Big\}$$

II

$$\partial_Y T(ab)_\Gamma = \int_{c_i} \Gamma(ab|c_1 c_2 \dots c_n) \Big\{ T(a) + T(b) - T(ab) + \\ + \sum_{k=1}^{n} (-1)^k \sum_{i_k > i_{k-1} > \dots > i_1}^{n} T(c_{i_1} c_{i_2} \dots c_{i_k}) \Big\}. \quad \text{(II.11)}$$

The interpretation of the equations for the amplitude T in terms of pomeron transitions can however be misleading, especially if a single dipole is allowed to couple to several pomerons. To find the equation for T, it is always safer to start with the corresponding equation for $\mathcal{S}$ and then use the relation $T = 1 - \mathcal{S}$ to deduce the equation for T, just as we have done above. The equation for $\mathcal{S}$ is determined by the structure of the corresponding dipole vertex and has a simple interpretation as described above.

Note that so far we have not asked whether equation (II.7) can be rewritten in a similar way. As mentioned above, this has been attempted by trying to write it with a contribution of the form $\partial_Y T(ab)_\beta$ in (II.10). However, it was shown in [54] that this approach has problems. Formally it is possible, but the problem is that the would-be dipole merging vertex (in this case the β-vertex above) has no fixed sign as is required in a proper probabilistic formalism.

We now want to demonstrate that the dipole swing discussed in the previous subsection can reproduce not only pomeron merging and loop formation, but also the more complicated transitions described in (II.11). Since the dipole model is just an effective picture it is likely that a more complete treatment will involve more general vertices, generating transitions involving an arbitrary number of pomerons. As discussed in section II.4.2, the weight for this process involves a phenomenological normalization parameter λ which determines the strength of the process, i.e. how fast this process happens in rapidity. In the applications presented in section II.7 the value of λ is such that the recouplings saturate in the sense that the recouplings lead to an equilibrium given by the weights proportional to $\prod \mathbf{r}_i^{-2}$. This means that effectively these recouplings happen instantaneously. After each gluon emission the cascade will evolve through recouplings back and forth until it settles in a preferred configuration (the weight in (II.8) here favours configurations where the dipoles are as small as possible) after which there is a new gluon emission (dipole splitting).

Assume that, at some rapidity, we have N partons, located at positions $(\boldsymbol{x}_0, \boldsymbol{x}_1, \dots, \boldsymbol{x}_{N-1})$ where $\boldsymbol{x}_0$ and $\boldsymbol{x}_{N-1}$ are the positions of the initial quark and antiquark respectively. Assume now that a gluon $\boldsymbol{z}$ is emitted from some dipole $(\boldsymbol{x}_i, \boldsymbol{x}_j)$ which means that this dipole is replaced by $(\boldsymbol{x}_i, \boldsymbol{z})$ and $(\boldsymbol{z}, \boldsymbol{x}_j)$. After this there will be a series of recouplings which transform the cascade into some new configuration involving N dipoles. From our discussion above, it follows that these recouplings will most likely involve the new dipoles which were produced after the emission of $\boldsymbol{z}$. This is so because the cascade, prior to

the emission of $\boldsymbol{z}$, already has settled in a preferred configuration and, apart from the replacement of $(\boldsymbol{x}_i, \boldsymbol{x}_j)$ with $(\boldsymbol{x}_i, \boldsymbol{z})$ and $(\boldsymbol{z}, \boldsymbol{x}_j)$, it keeps the same configuration after $\boldsymbol{z}$ is emitted. Therefore it is not so likely to have further recouplings among the other dipoles (if not, these would most likely have happened before the emission of $\boldsymbol{z}$). There will thus be a series of recouplings involving newly produced dipoles until the cascade once again settles in some preferred configuration, after which there will be a new emission.

The discussion above suggest that we may view the evolution as effectively being driven by vertices involving $k \to k+1$ dipole transitions, where k is determined by how many swings we have between the emissions. For a cascade evolving through such a general vertex we can write the evolution equations for $\mathcal{S}$ and T just as we did in above. Once again we denote the dipoles with letters a_i and the corresponding S-matrices with $\mathcal{S}(a_i)$ for a single dipole, $\mathcal{S}(a_i a_j)$ for two dipoles and so on. For a vertex $\Gamma_k(a_1 \dots a_k | b_1 \dots b_{k+1})$, giving rise to the transition $a_1 + \dots + a_k \to b_1 + \dots + b_{k+1}$ we then get the following evolution equations

$$\begin{aligned}
\partial_Y \mathcal{S}(a_1 \dots a_k)_{\Gamma_k} &= \int_{b_i} \Gamma_k(a_1 \dots a_k | b_1 \dots b_{k+1}) \Big\{ -\mathcal{S}(a_1 \dots a_k) + \mathcal{S}(b_1 \dots b_{k+1}) \Big\} \\
\partial_Y T(a_1 \dots a_k)_{\Gamma_k} &= \int_{b_i} \Gamma_k(a_1 \dots a_k | b_1 \dots b_{k+1}) \times \\
&\quad \times \Big\{ \sum_{m=1}^{k} (-1)^{k+m-1} \sum_{i_m > \dots > i_1}^{k} T(a_{i_1} \dots a_{i_m}) + \\
&\quad + \sum_{m=1}^{k+1} (-1)^{k+m} \sum_{i_m > \dots > i_1}^{k+1} T(b_{i_1} \dots b_{i_m}) \Big\}. \qquad \text{(II.12)}
\end{aligned}$$

Here one sees that T^k is coupled to T^m with $m = 1, \dots, k+1$ which means that there are pomeron mergings of the type $k \to i$, $i = 1, \dots, k-1$. We also note that similar type of equations involving some more general vertices have recently been presented in [55, 56] although the structure of the vertices are different. If we consider the process in zero transverse dimensions, which defines the toy model first presented in [16] (see also [57]), then for all dipoles a_i one replaces $T(a_i)$ by some t (and $T(a_1 \dots a_k)$ by t^k) which is the amplitude in the toy model. One can then see that the equations for t^k presented in [56] (equations (2.19) to (2.21)) can be understood in terms of the general transitions in (II.12).

II.5 The Initial States in the Cascade Evolutions

In the introduction we argued that results from the Tevatron supports a picture where high energy pp interactions are dominated by perturbative parton–

parton sub-collisions. This encourages us to interpret $\gamma^* p$ and pp collisions as a result of perturbative dipole interactions. We then also need an initial dipole state for a virtual photon and for a proton.

II.5.1 The Virtual Photon

The coupling of a virtual photon to a quark–antiquark pair is well known. In leading order and for the case of massless quarks the longitudinal and transverse wave functions, denoted ψ_L and ψ_T respectively, are given by

$$\begin{aligned} |\psi_L(z,r)|^2 &= \frac{6\alpha_{em}}{\pi^2}\sum_q e_q^2 Q^2 z^2 (1-z)^2 K_0^2(\sqrt{z(1-z)}Qr) \\ |\psi_T(z,r)|^2 &= \frac{3\alpha_{em}}{2\pi^2}\sum_q e_q^2 [z^2+(1-z)^2] z(1-z) Q^2 K_1^2(\sqrt{z(1-z)}Qr). \end{aligned} \tag{II.13}$$

Here z $(1-z)$ is the longitudinal momentum fraction of the quark (antiquark) and $\boldsymbol{r}$ is the transverse separation between them. Q^2 denotes the virtuality of the virtual photon and K_0 and K_1 are modified Bessel functions. The sum in (II.13) runs over all active quark flavours, and in our case we consider 3 massless flavours.

II.5.2 The Initial Proton

The initial state for the proton can naturally not be determined by pertubation theory, but has to be described by some model assumption, which can obviously never fully describe all features of the proton. We have tried a couple of different approaches based on the assumption that a proton at rest mainly consists of its three valence quarks. It is natural to think of these three quarks as the endpoints of dipoles and, assuming that the quarks all have different colours, this would give three different dipoles. One would not expect these dipoles to be completely independent, and indeed it was argued in [58] that they would be non-trivially correlated. We have tried two different approaches with varying degree of correlation[4]: completely uncorrelated dipoles or a "triangle" configuration. In the latter case each quark is connected by two dipoles to the other two quarks, ie. assuming that eg. a red quark behaves essentially as an anti-blue–anti-green colour compound to form dipoles with the other two (blue and green) quarks.

[4] In the original dipole formulation, all dipoles are independent and correlations can only be introduced through their relative placement in impact-parameter space. However, when introducing explicit energy conservation, neighboring dipoles will affect each other, thus introducing an additional correlation.

One could argue that a more natural choice would be to use a "Mercedes" star configuration, where all three dipoles are joined in a junction. However, a picture where the junction does not carry energy and momentum is then difficult to reconcile with the dipole formalism, and we have in the following settled for the triangle configuration with the dipole sizes distributed as Gaussians with an average size $\sim 3.1\ \mathrm{GeV}^{-1}$, which is determined by a fit to pp data.

II.6 Monte Carlo Simulation

Our calculations are performed with a simple simulation program written in C++, where there are gluons connected by dipoles and vice versa. A dipole state is described by a set of partons, each of which has a specified position in the transverse plane and a rapidity, y (which is the true rapidity and not $\log(1/x)$). In addition, each gluon is assigned a transverse momentum when it is emitted, corresponding to the inverse of the transverse size of the smallest dipole to which it is connected. Thus, if we have a splitting as in (II.1) we assign

$$p_\perp = \frac{2}{\min(|\boldsymbol{x}-\boldsymbol{z}|, |\boldsymbol{z}-\boldsymbol{y}|)}. \tag{II.14}$$

In this way we can implement ordering in $p_\pm = p_\perp e^{\pm y}$ separately. The transverse momentum of each of the emitting partons will be set to 2 times the inverse transverse distance to the emitted gluon if this is larger than the previously assigned $p_\perp$. In addition the rapidities of the emitting partons are changed so that the total positive light-cone momentum component is conserved in each emission. These recoils are distributed so that the emitting parton at $\boldsymbol{x}$ contributes a fraction $|\boldsymbol{z}-\boldsymbol{y}|/(|\boldsymbol{x}-\boldsymbol{z}|+|\boldsymbol{z}-\boldsymbol{y}|)$ to the p_+ of the emitted gluon. The assignment of the $p_\perp$ for the gluons as given above, and the conservation of the p_+ component, automatically gives a cutoff for small dipoles. Therefore we do not need to explicitely introduce a cutoff ρ, as described in section II.2.3, but we rather obtain a *dynamical cutoff*, $\rho(\Delta y)$, which is large for small steps in rapidity, Δy, but gets smaller for larger Δy.

In each step an emission is generated for each of the dipoles in a state according to (II.1) and the corresponding Sudakov form factor, allowing α_s to run according to the one-loop expression with the scale set to the $p_\perp$ of the emitted gluon[5]. The dipole which has generated the smallest step in rapidity is then allowed to radiate and is replaced by two new dipoles, and the procedure is reiterated until no dipole has generated a rapidity above (or below, depending of the direction of evolution) a minimum (or maximum) rapidity. Finally a cross section can be calculated by letting the dipoles from the target

[5]To avoid divergencies, α_s is frozen below the scale $p_\perp = 2/r_{\max}$.

II

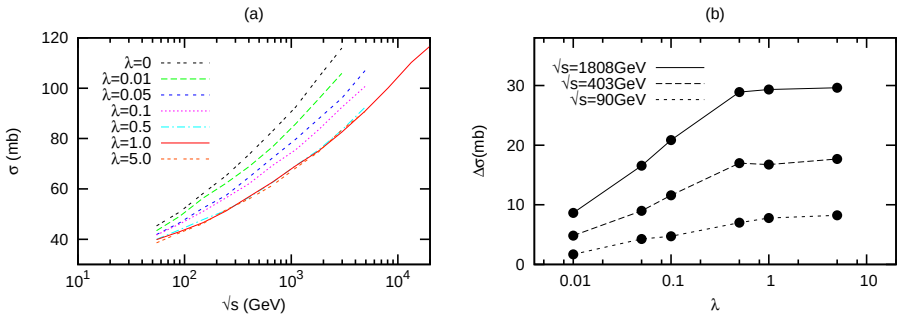

Figure II.10: The pp cross section for different values of the coefficient λ. It is seen in (a) that σ does not change for $\lambda \gtrsim 0.5$. This can also be seen from (b) which shows the difference in the cross section, $\Delta\sigma(\lambda) \equiv \sigma(\lambda = 0) - \sigma(\lambda)$,as a function of λ, and for different s.

and the projectile, both properly evolved, collide at a random impact parameter according to (II.2) and (II.5).

In the dipole model it is possible to create arbitrarily large dipoles. Even if the p_- ordering in our formalism sets a limit for how large a dipole can be, just as the p_+ ordering sets a limit for how small a dipole can be, there is no mechanism suppressing the formation of large dipoles. On the contrary they are enhanced by the running of α_s. Obviously confinement must suppress the formation of larger dipoles and we therefore choose a parameter r_{max} such that each emission is suppressed with a Gaussian of average size $\sim r_{max}$. This means that each emission, giving a new dipole of size r, is allowed with a probability $\exp(-r^2/r_{max}^2)$. We choose r_{max} to have the same value as the average size of the initial dipoles in the proton, i.e. $r_{max} = 3.1\text{GeV}^{-1}$, as this corresponds to the nonperturbative input for the proton.

When implementing the dipole swing mechanism we followed the strategy introduced in the Ariadne program [31,59] where each dipole is randomly assigned a colour index in the range $[1, N_c^2 - 1]$ in such a way that no neighboring dipoles have the same index.[6] In each step any pair of dipoles with the same index is allowed to generate a fictitious rapidity for a recoupling according to (II.8) modified with an appropriate Sudakov form factor. These generated recouplings are then allowed to compete with the generated emissions, so that in each step the process giving the smallest step in rapidity is performed. Because of the way colour indices are assigned we can ensure that no unphysical dipole chains (eg. with colour-singlet gluons) can occur.

[6] Naively one might expect there only to be three differently coloured dipoles, but the probability that two arbitraty dipoles are allowed to recouple is related to the number of different gluons rather than to the number of colours which is why we have $N_c^2 - 1$ different dipole indices.

Clearly if λ in (II.8) is very large, the evolution is swamped by recouplings back and forth, making the simulation very inefficient. In this way we also see that the effect of the recouplings must saturate at large enough λ. By chance it turns out that a value of $\lambda = 1$ is just large enough for saturation, see figure II.10.

It can be shown that two dipoles recoupling back and forth in this saturated way and colliding with a single dipole according to (II.2) corresponds exactly to a quadrupole–dipole scattering. Also higher multipole–multipole scatterings are in this way well approximated.

As discussed above these recouplings in some sense also give rise to pomeron mergings, as configurations where one dipole is very small is favored and this dipole has a smaller probability to interact with the target. In our program it is also possible to include explicit mergings of neighboring dipoles, a process which is necessary for the study of exclusive final states and will be studied in a future publication. It should be noted that the combined process of first splitting a dipole into two, then recoupling with a third dipole and finally merging one of them again, corresponds to the recoupling of two dipoles with different colour indices by the exchange of a gluon.

II.7 Results

In this section we compare results obtained from our model with experimental data from DIS at HERA and pp collisions at the Tevatron. As we yet have not a full control over the virtual dipoles we only study the total cross sections.

II.7.1 DIS

In [20] we obtained a reasonable qualitative agreement with HERA data for the F_2 structure function and the effective slope

$$\lambda_{\text{eff}}(Q^2) = d(\log F_2)/d(\log 1/x). \tag{II.15}$$

Having now improved our model further, we will see that we also obtain a good quantitative agreement with the data.

The $\gamma^* p$ total cross section is given by the sum of the two wave functions in (II.13), convoluted with the dipole–proton cross section, $\sigma(z, \boldsymbol{r})$,

$$\sigma^{tot}_{\gamma^* p} = \int d^2\boldsymbol{r} \int_0^1 dz \{|\psi_L(z,r)|^2 + |\psi_T(z,r)|^2\}\sigma(z,\boldsymbol{r}). \tag{II.16}$$

Here the dipole–proton cross section $\sigma(z, \boldsymbol{r})$ is obtained from equations (II.5) and by (II.2), when the initial proton state in section II.5 is evolved as described in section II.6.

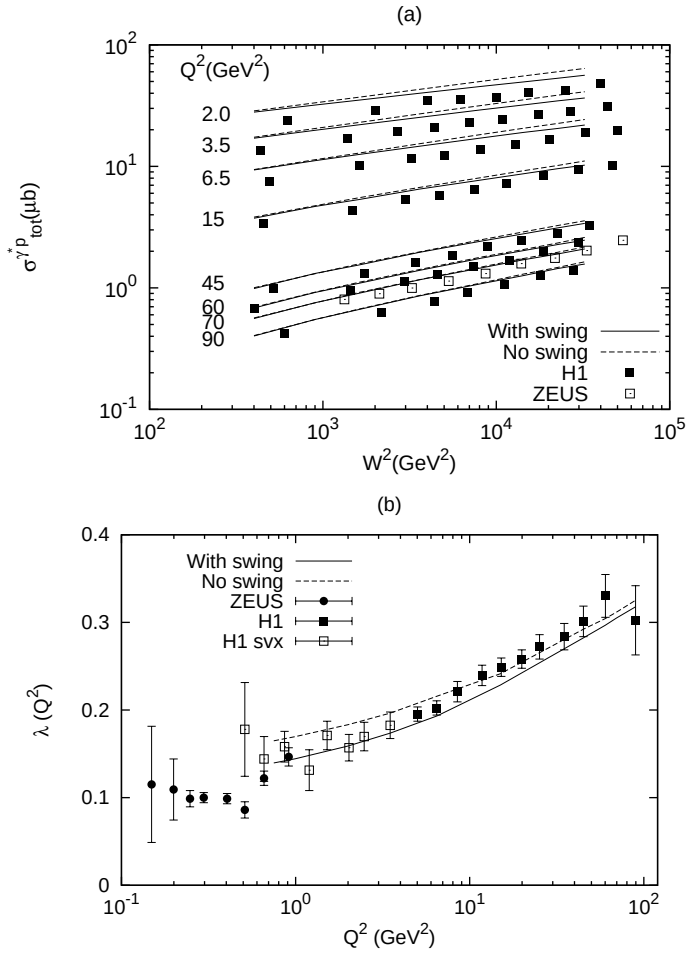

Figure II.11: (a) The $\gamma^* p$ total cross section shown for different Q^2. The solid lines include the dipole swing mechanism while the dashed lines do not. W denotes the cms energy. (b) The effective slope measured at different Q^2. The lines are the same as in (a). Filled circles are data from ZEUS [60] while filled [61] and open [62] squares are data from H1.

In figure II.11a we show the results for the $\gamma^* p$ total cross section. As we can see the results are in quite good agreement with data except for the fact that the normalization is around 10–15% too high for $Q^2 \lesssim 15\,\mathrm{GeV}^2$ while it is around 5–10% too high for $Q^2 \gtrsim 45\,\mathrm{GeV}^2$. Data points are taken from [60, 61]

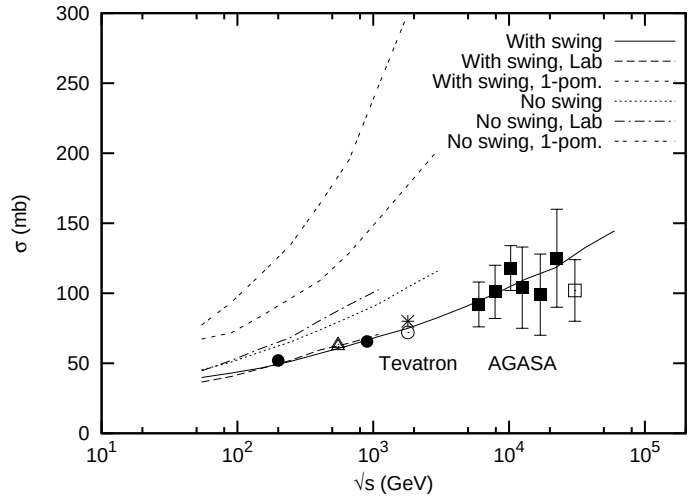

Figure II.12: The total cross section for pp scattering as a function of the cms energy $\sqrt{s}$. Here results are shown for evolution with and without the dipole swing mechanism. The results for the one pomeron contribution are also shown. Also shown are the results obtained in the "lab" frame where one of the protons is almost at rest.

II

and we also see that the effects of dipole swings are quite small, mainly visible for $Q^2 \lesssim 15\,\mathrm{GeV}^2$.

As seen from figure II.11a, our results seems to have the correct W dependence. This can be seen more clearly from figure II.11b, where we show the results for the logarithmic slope λ_{eff}. We see that there is a good agreement with data for all points lying in the interval $1\mathrm{GeV}^2 \lesssim Q^2 \lesssim 100\,\mathrm{GeV}^2$. Here the slope is determined within the same energy interval from which the experimental points, taken from [60–62], are determined.

II.7.2 Proton–Proton Collisions

The results obtained for the pp total cross section are presented in fig. II.12. Here we see that the dipole swing have a rather large effect, as expected. In the figure we also show the results for the one pomeron cross sections, and one can see the large effects of unitarisation. Our main results are calculated in the center of mass frame, where the colliding protons share the energy equally, but in the figure we also show results obtained in the "lab" frame, where one of the protons carries almost all avaliable energy, while the other one is essentially at rest. Due to the fact that the Monte Carlo simulation becomes very inefficient in such a frame (since the energetic proton has to be boosted to quite high

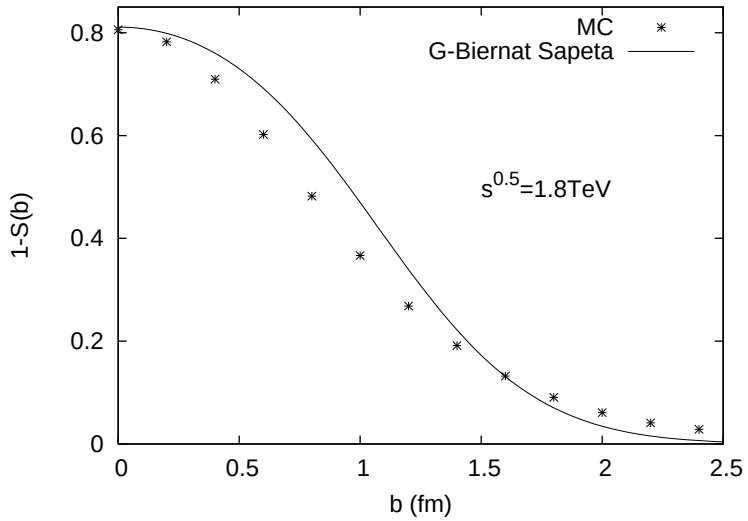

Figure II.13: The pp impact parameter profile, $(1/2)d\sigma_{tot}/d^2b$. The points are results obtained from our Monte Carlo while the line is a two parameter Gaussian fit from ref. [63].

rapidities) we have evaluated σ_{tot} only up to $\sqrt{s} \sim 1$ TeV. Although the result is not exactly frame independent we see that the frame dependence is reduced, and now very small.

The final result of this paper concerns the impact parameter dependence of the pp total cross section. The result is shown in figure II.13. Here we have plotted $(1/2)d\sigma_{tot}/d^2b$ as a function of b and for $\sqrt{s} = 1.8$TeV. The result is compared to a two parameter Gaussian fit from ref. [63]. There is a quite good agreement between the results. Our profile is more flat and has a somewhat longer tail, but a Gaussian fit to our result would be very similar to the fit in ref. [63].

II.8 Conclusions

The QCD description of high-energy scattering is clearly a complicated subject. Although a qualitative description of inclusive cross sections for $\gamma^* p$ and pp scatterings can be obtained in eg. the B–JIMWLK formalism, it is difficult to give quantitative predictions, and even more difficult to describe exclusive properties of the final states.

In this paper we have described a model of interacting colour dipoles based

on a limited set of fairly simple ingredients:

- The description of the initial-state virtual photon and proton as a (set of) dipole(s).
- Simple dipole splittings by gluon emissions according to the Mueller formalism.
- Energy–momentum conservation in each splitting, which gives a dynamic cutoff for small dipole sizes and introduces non-trivial correlations between neighboring dipoles.
- A mechanism for dipole reconnections (or "swing") corresponding to the introduction of pomeron loops in the evolution.
- A simple dipole–dipole scattering cross section, exponentiated to include multiple scattering and saturation effects.

Although each ingredient is fairly simple, it is prohibitively difficult to include them all in analytic calculations. However, implementing them in a Monte Carlo simulation program we are able to reproduce to a satisfactory degree both the $\gamma^* p$ cross sections as measured at HERA as well as the total pp cross section all the way from ISR energies to the Tevatron and beyond. It should be pointed out that this is achieved with effectively only two tuneable parameters, the basic QCD scale $\Lambda_{\rm QCD}$ and $r_{\rm max}$ giving the non-perturbative cutoff for large dipoles. There are two additional parameters involved in the dipole swing. One is λ and we have shown that as long as it is large enough to saturate the recouplings, the results are completely insensitive to this parameter. The other parameter is the number of colour indices, $N_c^2 - 1$, which we have fixed to 8, but could in principle be considered a free parameter to simulate the effect of recouplings between differently coloured dipoles by gluon exchange.

The resulting description is quite insensitive to the Lorentz frame chosen to perform the simulations, which shows that we have a consistent treatment of pomeron loops in the evolution and in the scattering of evolved dipole states.

Recently there has been a lot of activity in the subject of high energy evolution in QCD. Different, and very interesting, models have been proposed which are often based on analytical calculations in some toy limit or at asymptotically high energies. We here want to emphasize the importance of a working Monte Carlo simulation in order to confront QCD with real data at realistic energies.

We have also seen that the way the dipole swing is implemented in our model makes it possible to view the evolution as effectively being driven by more general vertices which give rise to more general pomeron transitions during the evolution. Some ideas with such vertices have recently been presented in [55, 56]. There is still more work to do with regard to explicit frame independence in the dipole model, and it is our intention to further study this

problem in future investigations.

Another advantage of our model is that it should be possible to also simulate exclusive properties of the final states. Confronting these with experimental observables will allow us to gain further insight into the QCD evolution at high energies. We will return to this problem in a future publication.

II References

[1] J. R. Andersen *Phys. Lett.* **B639** (2006) 290–293, hep-ph/0602182.

[2] A. H. Mueller *Phys. Lett.* **B104** (1981) 161–164.

[3] B. I. Ermolaev and V. S. Fadin *JETP Lett.* **33** (1981) 269–272.

[4] A. Bassetto, M. Ciafaloni, G. Marchesini, and A. H. Mueller *Nucl. Phys.* **B207** (1982) 189.

[5] G. Marchesini and B. R. Webber *Nucl. Phys.* **B238** (1984) 1.

[6] G. Gustafson *Phys. Lett.* **B175** (1986) 453.

[7] G. Gustafson and U. Pettersson *Nucl. Phys.* **B306** (1988) 746.

[8] **OPAL** Collaboration, G. Abbiendi *et al. Eur. Phys. J.* **C35** (2004) 293–312, hep-ex/0306021.

[9] **L3** Collaboration, P. Achard *et al. Phys. Lett.* **B581** (2004) 19–30, hep-ex/0312026.

[10] **ALEPH** Collaboration, S. Schael *et al.* hep-ex/0604042.

[11] M. Siebel hep-ex/0505080.

[12] K. Golec-Biernat and M. Wusthoff *Phys. Rev.* **D59** (1999) 014017, hep-ph/9807513.

[13] K. Golec-Biernat and M. Wusthoff *Phys. Rev.* **D60** (1999) 114023, hep-ph/9903358.

[14] A. H. Mueller *Nucl. Phys.* **B415** (1994) 373–385.

[15] A. H. Mueller and B. Patel *Nucl. Phys.* **B425** (1994) 471–488, hep-ph/9403256.

[16] A. H. Mueller *Nucl. Phys.* **B437** (1995) 107–126, hep-ph/9408245.

[17] G. P. Salam *Comput. Phys. Commun.* **105** (1997) 62–76, hep-ph/9601220.

[18] G. P. Salam *Nucl. Phys.* **B461** (1996) 512–538, hep-ph/9509353.

[19] E. Avsar hep-ph/0406150.

[20] E. Avsar, G. Gustafson, and L. Lönnblad *JHEP* **07** (2005) 062, hep-ph/0503181.

[21] G. Cohen-Tannoudji, A. Mantrach, H. Navelet, and R. Peschanski *Phys. Rev.* **D28** (1983) 1628.

[22] A. H. Mueller and H. Navelet *Nucl. Phys.* **B282** (1987) 727.

[23] L. V. Gribov, E. M. Levin, and M. G. Ryskin *Phys. Rept.* **100** (1983) 1–150.

[24] A. Capella, U. Sukhatme, C.-I. Tan, and J. Tran Thanh Van *Phys. Rept.* **236** (1994) 225–329.

[25] **CDF** Collaboration, R. Field *Acta Phys. Polon.* **B36** (2005) 167–178.

[26] T. Sjostrand and M. van Zijl *Phys. Rev.* **D36** (1987) 2019.

[27] B. Andersson, G. Gustafson, G. Ingelman, and T. Sjostrand *Phys. Rept.* **97** (1983) 31.

[28] B. Andersson, G. Gustafson, and C. Sjogren *Nucl. Phys.* **B380** (1992) 391–407.

[29] G. Corcella *et al. JHEP* **01** (2001) 010, hep-ph/0011363.

[30] T. Sjostrand, S. Mrenna, and P. Skands *JHEP* **05** (2006) 026, hep-ph/0603175.

[31] L. Lönnblad *Comput. Phys. Commun.* **71** (1992) 15–31.

[32] S. Catani, F. Fiorani, and G. Marchesini *Phys. Lett.* **B234** (1990) 339.

[33] M. Ciafaloni *Nucl. Phys.* **B296** (1988) 49.

[34] B. Andersson, G. Gustafson, and J. Samuelsson *Nucl. Phys.* **B467** (1996) 443–478.

[35] H. Jung and G. P. Salam *Eur. Phys. J.* **C19** (2001) 351–360, hep-ph/0012143.

[36] H. Jung *Comput. Phys. Commun.* **143** (2002) 100–111, hep-ph/0109102.

[37] H. Kharraziha and L. Lönnblad *JHEP* **03** (1998) 006, hep-ph/9709424.

[38] H. Kharraziha and L. Lönnblad *Comput. Phys. Commun.* **123** (1999) 153.

[39] Y. V. Kovchegov *Phys. Rev.* **D60** (1999) 034008, hep-ph/9901281.

[40] I. Balitsky *Nucl. Phys.* **B463** (1996) 99–160, hep-ph/9509348.

[41] E. Iancu, A. Leonidov, and L. McLerran hep-ph/0202270.

[42] E. Iancu and R. Venugopalan hep-ph/0303204.

[43] H. Weigert *Prog. Part. Nucl. Phys.* **55** (2005) 461–565, hep-ph/0501087.

[44] J. Jalilian-Marian, A. Kovner, A. Leonidov, and H. Weigert *Nucl. Phys.* **B504** (1997) 415–431, hep-ph/9701284.

[45] J. Jalilian-Marian, A. Kovner, A. Leonidov, and H. Weigert *Phys. Rev.* **D59** (1999) 014014, hep-ph/9706377.

[46] E. Iancu, A. Leonidov, and L. D. McLerran *Phys. Lett.* **B510** (2001) 133–144, hep-ph/0102009.

[47] H. Weigert *Nucl. Phys.* **A703** (2002) 823–860, hep-ph/0004044.

[48] A. H. Mueller and G. P. Salam *Nucl. Phys.* **B475** (1996) 293–320, hep-ph/9605302.

[49] E. Iancu, A. H. Mueller, and S. Munier *Phys. Lett.* **B606** (2005) 342–350, hep-ph/0410018.

[50] E. Iancu and A. H. Mueller *Nucl. Phys.* **A730** (2004) 494–513, hep-ph/0309276.

[51] E. Iancu and D. N. Triantafyllopoulos *Nucl. Phys.* **A756** (2005) 419–467, hep-ph/0411405.

[52] A. H. Mueller, A. I. Shoshi, and S. M. H. Wong *Nucl. Phys.* **B715** (2005) 440–460, hep-ph/0501088.

[53] E. Levin and M. Lublinsky *Nucl. Phys.* **A763** (2005) 172–196, hep-ph/0501173.

[54] E. Iancu, G. Soyez, and D. N. Triantafyllopoulos *Nucl. Phys.* **A768** (2006) 194–221, hep-ph/0510094.

[55] M. Kozlov, E. Levin, and A. Prygarin hep-ph/0606260.

[56] J. P. Blaizot, E. Iancu, and D. N. Triantafyllopoulos *Nucl. Phys.* **A784** (2007) 227–258, hep-ph/0606253.

[57] A. Kovner and M. Lublinsky *Nucl. Phys.* **A767** (2006) 171–188, hep-ph/0510047.

[58] M. Praszalowicz and A. Rostworowski *Acta Phys. Polon.* **B29** (1998) 745–753, hep-ph/9712313.

[59] L. Lönnblad *Z. Phys.* **C65** (1995) 285–292.

[60] **ZEUS** Collaboration, J. Breitweg *et al. Phys. Lett.* **B487** (2000) 53–73, hep-ex/0005018.

[61] **H1** Collaboration, C. Adloff *et al. Eur. Phys. J.* **C21** (2001) 33–61, hep-ex/0012053.

[62] A. Petrukhin, "New Measurement of the Structure Function $F_2(x, Q^2)$ at low Q^2 with Initial State Radiation Data." Proceedings of DIS04, Štrbské Pleso, Slovakia, 2004.

[63] S. Sapeta and K. Golec-Biernat *Phys. Lett.* **B613** (2005) 154–161, hep-ph/0502229.

III

Geometric Scaling and QCD Dynamics in DIS

Emil Avsar and Gösta Gustafson

Dept. of Theoretical Physics, Sölvegatan 14A, S-223 62 Lund, Sweden

JHEP **04** (2007) 067, hep-ph/0702087.

DIS data from HERA show a striking regularity as $\sigma^{\gamma^* p}$ is a function of the ratio $\tau = Q^2/Q_s^2(x)$ only. The scaling function shows a break at $\tau \approx 1$, which has been taken as an indication for saturation. However, besides saturation also the transition between dominance of $k_\perp$-ordered (DGLAP) and $k_\perp$-non-ordered (BFKL) evolution contributes to a break around this value of τ, as well as the suppression for small Q^2 due to finite quark masses and confinement. In this paper we use a dipole cascade model based on Mueller's dipole model, which also includes energy conservation and pomeron mergings, to investigate the contributions of these different effects to the scaling behaviour. As a result we predict that the scaling function for $\tau < 1$ will be modified when data for $Q^2 > 1\,\mathrm{GeV}^2$ become available. We also investigate the scaling properties of the charm contribution and the impact parameter dependence of the saturation scale.

III.1 Introduction

Data from deep inelastic scattering (DIS) experiments at small-x exhibits an interesting property called geometric scaling [1]. This means that the total $\gamma^* p$ cross section is not a function of the two variables x and Q^2 separately but rather a function of the combination $Q^2/Q_s^2(x)$ only, where the "saturation scale" Q_s is defined such that saturation is expected to occur at Q-values below Q_s.

DIS is quite successfully described by the Golec-Biernat–Wüsthoff (GBW) model [2, 3] in which the virtual photon splits into a $q\bar{q}$ dipole long before the interaction with the proton. The GBW model is also called the saturation model, since it explicitely assumes that the dipole-proton cross section, σ_{dp}, saturates to a constant value σ_0 as the dipole size, r, gets large. To be more precise, the GBW model assumes that

$$\sigma_{\mathrm{dp}} = \sigma_0\{1 - \exp(-r^2/4R_0^2(x))\}, \tag{III.1}$$

where the "saturation radius" $R_0(x)$, identified with $Q_s^{-1}(x)$, decreases with decreasing x. In the GBW fit Q_s^2 has the form

$$R_0^{-2} = Q_{s,GW}^2 = Q_0^2\left(\frac{x_0}{x}\right)^{\lambda} \quad \text{with} \quad Q_0 = 1\mathrm{GeV},\ x_0 = 3{\cdot}10^{-4},\ \lambda = 0.29. \tag{III.2}$$

We thus see that σ_{dp} is a function of $r/R_0(x)$ only, and consequently it satisfies "geometric scaling". For massless quarks this also implies that the $\gamma^* p$ cross section is a scaling function of $\tau = Q^2R_0^2 = Q^2/Q_{s,GW}^2$, and this feature is indeed confirmed by experimental data as demonstrated in ref. [1]. (This reference also finds scaling if the relation $\ln R_0^2 \sim \lambda \ln x$ is replaced by $\ln R_0^2 \sim -x^{-0.08}$.)

Plotting the observed $\gamma^* p$ cross section as a function of τ one can also see that the growth of the cross section towards smaller τ is reduced noticeably when $\tau \lesssim 1$, corresponding to values satisfying $Q^2 \lesssim Q_{s,GW}^2$. Later analyses including DGLAP evolution for larger Q^2 [4] improve the agreement with the HERA data, with the consequence that saturation is beginning at somewhat smaller τ-values. This good agreement together with the success of the GBW model in describing diffractive data, has been taken by some authors as a proof that saturation exists, and that it has been observed at HERA.

Including the finite quark mass in the wavefunction describing the $\gamma^* - q\bar{q}$ coupling introduces scale-breaking effects. In particular the charm quark gives a large contribution to the cross section, which is phased out for $Q^2 \lesssim 4m_c^2$. In ref. [2] a fit including the charm quark mass actually shifts the expected onset of saturation to much smaller x-values, with $x_0 = 0.4{\cdot}10^{-4}$ in the expression for R_0 or Q_s in eq. (III.2). Such a shift is confirmed in the analysis

in ref. [5], which includes the mass of the charm and beauty quarks into the DGLAP-improved formalism of ref. [4].

For small Q^2 also the mass of the light quarks becomes important. In refs. [1, 2] this is taken into account by replacing the variable $x = Q^2/W^2$ in the definition of R_0 or $Q_{s,GW}$ by

$$\bar{x} = x(1 + 4m_f^2/Q^2) = \frac{Q^2 + 4m_f^2}{W^2}. \qquad \text{(III.3)}$$

In this way the scaling relation can be studied also for very small Q^2 and for photoproduction.

The test of scaling in the region of small τ is, however, limited by the fact that small values of τ are reached *only* for small Q^2, since larger Q^2-values would need energies not accessible at the HERA accelerator. Thus the data for $\tau < 0.5 - 1$, where the change in the slope of the $\gamma^* p$ cross section is observed, are all obtained for Q^2-values smaller than 1 GeV^2, which means that they are all in the non-perturbative region. The limited kinematical range at HERA also implies that there is little overlap between data at different Q^2 for fixed τ, which implies that it is relatively easy to achieve a scaling result by adjusting the quark masses.

The question of scaling for $Q^2 > Q_s^2$ is discussed by Iancu et al. in ref. [6]. These authors argue that if Q_s^2 is defined as the scale where the scattering probability is of order 1, then the BFKL evolution equation implies that the quark and gluon distributions have to obey geometric scaling in the range $1 \lesssim \ln(Q^2/Q_s^2) \ll \ln(Q_s^2/\Lambda_{QCD}^2)$. This rather wide range in Q^2 results from the fast diffusion in $\ln k_\perp^2$ and the fast growth towards small x in the leading log BFKL evolution. Beyond this range in Q^2 the BFKL diffusion is gradually replaced by the (not explicitely scaling) double leading log result.

A numerical analysis of the diffusion in the BK equation is presented by Golec-Biernat et al. [7], including non-leading effects from a running coupling and from the so called kinematical constraint. The result from a running α_s is that $\ln Q_s^2$ for high energies grows $\sim \sqrt{Y}$, rather than proportional to Y, as assumed in eq. (III.2). It also significantly reduces the diffusion into the region of large $k_\perp^2$. The kinematical constraint reduces this diffusion further, and these results therefore put a question mark for the large scaling region dominated by BFKL dynamics obtained in ref. [6]. A related work is presented by Kwieciński and Staśto [8], where they study DGLAP evolution starting from scaling initial conditions on the line $Q^2 = Q_s^2$, with Q_s^2 determined by some unspecified dynamics. The result from this approach is also that scaling is approximately preserved in a large domain above the line $Q^2 = Q_s^2$.

In the past few years it has been observed that a scaling feature is inherent in the asymptotic solutions to the evolution equations in high energy QCD.

It was also realized that the non-linear Balitsky-Kovchegov (BK) equation, which is the mean field version of the more general Balitsky-JIMWLK hierarchy (B-JIMWLK), is similar to a certain type of equation, well known in statistical physics, called the Fisher-Kolmogorov-Petrovsky-Piscounov (FKPP) equation, which is known to have traveling wave solutions [9, 10]. Written for a function $u(x,t)$, which depends on x and the time t, the solution for large t has the form of a traveling wave, $u(x-vt)$, where v is the speed of the wave. The similarity is expressed by the fact that the BK equation lies in the same universality class as the FKPP equation.

More recently, the importance of fluctuations in small-x evolution has been better understood [11], and this has led to the modification of the original version of the B-JIMWLK hierarchy into a new hierarchy of equations, which include both fluctuations and saturation effects. These new equations are also referred to as pomeron loop equations, since they contain both pomeron splittings and pomeron mergings in the evolution. This hierarchy of equations can also be written as a single Langevin equation, which is very similar to what is called the stochastic-FKPP (s-FKPP) equation [11]. The study of the asymptotic behaviour of the solution to this equation leads to the prediction of a new type of scaling law, called diffusive scaling [12], which is expected to hold at very high energies. It ought to be emphasized that the traveling wave solutions discussed here are asymptotic solutions expected to be relevant at extremely high energies, and therefore cannot be used to explain the scaling observed in the HERA energy regime.

The above discussion raises three important questions:

i) What is the importance of saturation for the scaling behaviour?

ii) What is the dynamical mechanism behind the scaling observed for $\tau > 1$, i.e. for $Q^2 > Q_s^2$?

iii) Will the cross section still be scaling for $\tau \lesssim 1$, when data for larger Q^2 are available?

In this paper we will argue that geometric scaling is expected also in the absence of saturation, and not only in the region dominated by BFKL diffusion, but also in the double leading log domain, where $k_\perp$-ordered (DGLAP) evolution chains are most important. Scaling appears naturally in a dipole cascade model [13, 14], which is based on Mueller's dipole evolution [15–17] but also includes energy-momentum conservation, pomeron merging, and a simple model for the proton. The MC implementation of the model reproduces both F_2 data from HERA and the total cross section in proton-proton scattering. This model shows geometric scaling for Q^2 below as well as above $Q^2_{s,GW}$, and for the one pomeron contribution as well as for the full unitarized result. In the model the transition between BFKL diffusion and $k_\perp$-ordered evolution occurs for Q^2 quite close to $Q^2_{s,GW}$, and there are three different effects which all contribute to the change in the scaling curve for $\tau \approx 0.5 - 1$:

Saturation, the BFKL-DGLAP transition, and the finite effective masses for the light u-, d-, and s-quarks.

In order to get an intuitive understanding of the scaling feature we will besides the results of the MC simulations also discuss two simple approximations, which contain the basic features of DGLAP-BFKL evolution and the colour dipole cascades.

Diffractive excitation or rapidity gap events correspond to a large fraction of the events at HERA. Diffractive scattering is related to the impact parameter dependence of the interaction, and in section III.8 we will discuss how the speed of the traveling wave varies with impact parameter, averaging out to the velocity observed in the experimental data.

The paper is organized as follows. In the next two sections we briefly discuss the DIS cross section, the concept of geometric scaling, and the dipole cascade approach to DIS. In section III.4 we discuss the effect of the charm contribution together with the effect of saturation on the total cross section. In section III.5, we present the two simple approximations to the full model as mentioned above. The scaling properties of the charm structure function are studied in section III.6, and in section III.7 we concentrate on the region $Q^2 < Q_s^2$ and study the effects of confinement and finite quark masses for small Q^2 below 1 GeV^2 and the scaling properties of the cross section in this region. In section III.8 we investigate the behaviour of the scattering amplitude for different impact parameters and how the scaling feature varies with impact parameter. Finally, in section III.9, we reach at our conclusions.

III.2 DIS and Geometric Scaling

In the dipole description of DIS the virtual photon, long before the interaction with the proton, splits into a $q\bar{q}$ pair which then interacts with the proton. The transverse separation between the quark and the antiquark in such a dipole is denoted $\boldsymbol{r}$, and their fractions of the γ^* longitudinal momentum z and $1-z$. The coupling of the γ^* to the $q\bar{q}$ pair is well known and the leading order result reads

$$
\begin{aligned}
|\psi_L(z,r)|^2 &= \frac{6\alpha_{em}}{\pi^2}\sum_f e_f^2 Q^2 z^2 (1-z)^2 K_0^2\left(\sqrt{z(1-z)Q^2+m_f^2}\,r\right)\\
|\psi_T(z,r)|^2 &= \frac{3\alpha_{em}}{2\pi^2}\sum_f e_f^2\Big\{[z^2+(1-z)^2](z(1-z)Q^2+m_f^2)\times\\
&\qquad K_1^2\left(\sqrt{z(1-z)Q^2+m_f^2}\,r\right)+m_f^2 K_0^2\left(\sqrt{z(1-z)Q^2+m_f^2}\,r\right)\Big\}.
\end{aligned}
\tag{III.4}
$$

Here ψ_L and ψ_T denote the longitudinal and transverse wave functions respectively. K_0 and K_1 are modified Bessel functions and the sum $\sum_f$ runs over all active quarks flavours, with mass m_f and electric charge e_f. The $\gamma^* p$ total cross section can then be written as

$$\sigma^{tot}_{\gamma^* p} = \int d^2\boldsymbol{r} \int_0^1 dz \{|\psi_L(z,r)|^2 + |\psi_T(z,r)|^2\} \sigma_{dp}(z,\boldsymbol{r}). \tag{III.5}$$

This cross section is related to the F_2 structure function via the relation

$$F_2 = \frac{Q^2}{4\pi\alpha_{em}} \sigma^{tot}_{\gamma^* p}. \tag{III.6}$$

The factor $\sigma_{dp}(z,\boldsymbol{r})$ in (III.5) above denotes the dipole-proton cross section. In the GBW model this cross section is assumed to have the form given in eq. (III.1). If we only consider the three light quarks and neglect their masses, we see that the dipole size can be rescaled $r \to r/R_0$, which implies that the result only depends on the scaling variable $\tau \equiv Q^2/Q_s^2$.

The charm quark is known to give a significant contribution to the cross section, and the heavy charm quark must obviously have a large effect on the scaling properties. This will be discussed further in sections III.4 and III.6. However, also for the light quarks the finite masses will have significant effects for small Q^2, which will be discussed in section III.7.

III.3 The dipole cascade model for DIS

We will in this section shortly describe the model we use to study the effect on geometric scaling from different features in the QCD evolution.

DIS at small x is dominated by gluonic cascades due to the $1/z$ singularity in the gluon splitting function. At large Q^2 the cascade can be described by DGLAP evolution, where the gluons are strictly ordered in transverse momentum. For smaller Q^2 also non-ordered gluon chains are important, and the $k_\perp$-ordered DGLAP evolution is replaced by the x-ordered BFKL evolution. The ordering in $k_\perp$ when $Q^2 \to \infty$ and the ordering in energy when $x \to 0$ follow both from an ordering in angle or, equivalently, in rapidity. Such an ordering is a consequence of soft gluon interference, and is the basis for the CCFM model [18, 19], which reproduces DGLAP and BFKL evolution in their respective domains of applicability with a smooth transition in between. The CCFM model is reformulated and generalized in the Linked Dipole Chain (LDC) [20] model. Here some emissions, which are treated as initial state radiation in CCFM, are instead included as final state radiation, with the result that the "non-Sudakov" formfactors disappear, and the cascade becomes symmetric when exchanging the role of the projectile and the target. The remain-

ing gluons (called primary gluons in ref. [20] and backbone gluons in ref. [21]) define totally the structure of the final state.

At very high energies the density of gluons becomes very large, and non-linear effects are needed to tame the exponential growth in the above linear evolutions, which would otherwise break the unitarity limit. Saturation and multiple interactions are easier to take into account in a formulation in transverse coordinate space since at high energies the transverse coordinate does not change between repeated subcollisions, while these collisions do change the transverse momenta. This is exploited in the GBW dipole model and the dipole cascade model by Mueller [15–17].

The evolution in Mueller's model reproduces the leading order (linear) BFKL evolution. It starts from a colour singlet $q\bar{q}$ pair. The quark and the antiquark emit gluons coherently, forming a colour dipole. The original dipole is then split in two dipoles formed by the qg and $g\bar{q}$ systems. The new dipoles split repeatedly forming a dipole cascade. In the leading log approximation the probability per unit rapidity Y for a dipole with transverse coordinates $\boldsymbol{x}$ and $\boldsymbol{y}$ to split emitting a gluon at $\boldsymbol{z}$ is given by (to leading log accuracy $Y \equiv \ln 1/x$ and the true rapidity are equivalent)

$$\frac{d\mathcal{P}}{dY} = \frac{\bar{\alpha}}{2\pi} d^2\boldsymbol{z} \frac{(\boldsymbol{x}-\boldsymbol{y})^2}{(\boldsymbol{x}-\boldsymbol{z})^2(\boldsymbol{z}-\boldsymbol{y})^2} \tag{III.7}$$

The splitting probability in eq. (III.7) is singular for small dipole sizes $\boldsymbol{x}-\boldsymbol{z}$ or $\boldsymbol{z}-\boldsymbol{y}$. These singularities have to be screened by a cutoff, but the small dipoles have also a small probability to interact with the target, and therefore the total cross section is finite when the cutoff goes to zero. This implies that a lot of non-interacting virtual dipoles are created in the process, which also makes computer simulations difficult [22, 23].

It is well known that a significant part of next to leading corrections are related to energy-momentum conservation [24], and in refs. [25, 26] it is demonstrated that energy conservation has a large effect on the small x evolution. Relating the dipole size r to $1/k_\perp$ there are great similarities between Mueller's model and the LDC model. In ref. [13] these similarities were used to implement energy conservation in the dipole cascade formalism. The result is a dynamical cutoff for small dipoles, and the remaining emissions are ordered in both light cone variables p_+ and p_-, similar to the ordering in the LDC model. A dominant fraction of the virtual emissions is here eliminated, leaving mainly the "primary gluons" mentioned above. As a result the exponential growth for small x is significantly reduced. It also greatly improves the efficiency of the MC simulation, removing the difficulties encountered in refs. [22, 23].

Mueller's cascade includes saturation effects from multiple collisions in the Lorentz frame chosen for the calculation, but not the effects of pomeron merg-

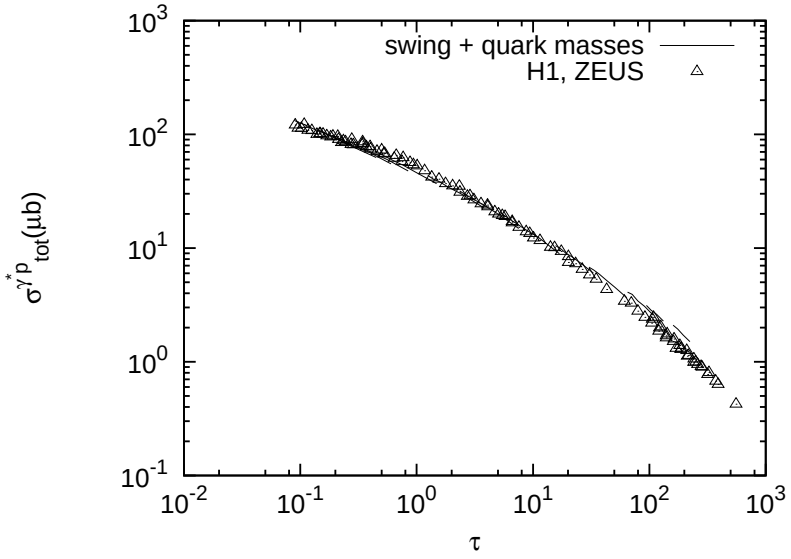

Figure III.1: Our full results for the $\gamma^* p$ total cross section plotted as a function of the scaling variable $\tau = Q^2/Q^2_{s,GW}$. Here saturation effects are included both in the collision between the γ^* and the proton cascades and within the evolution in each individual cascade, via the so called dipole swing. We have used a charm mass of 1.4 GeV and an effective light quark mass of 60 MeV for the u, d and s quarks. Data points are taken from [27] and [28]. Results are presented for Q^2 ranging from 0.3 GeV^2 to 90 GeV^2, and with the same kinematics for the data and the model.

ing in the cascades. The result is therefore not Lorentz frame independent. In ref. [14] we improved our model by allowing (colour suppressed) recouplings of the dipole chain during the evolution, a "dipole swing", which leads to an almost frame independent formalism. In this paper we also introduced a simple model for the proton in terms of three dipoles.

The dipole splitting is calculated in perturbative QCD, and therefore the model is meant to work in the perturbative regime, which means not too small Q^2. In figure III.1 we show results for $\sigma^{\gamma^* p}$ as a function of the scaling variable $\tau \equiv Q^2/Q_s^2$ for different Q^2 above 0.3 GeV^2. The results include both the dipole swing and multiple collisions and for $Q_s(x)$ we here use the definition by Golec-Biernat and Wüsthoff, given by (III.2). For these Q^2-values a scale-breaking effect is obtained from the charm mass, for which we use the value 1.4 GeV. The theoretical result is presented for the same kinematical variables as the experimental data, and we see that there is a very good agreement between theory and data. For small Q^2 the result is sensitive to confinement

effects and effective quark masses. These problems will be further discussed in sec. III.7.

III.4 Effects of saturation and the charm contribution

The effects of saturation and of the large charm quark mass are illustrated in figure III.2. The results correspond to Q^2 between 0.75 and 90 GeV^2, and therefore the light quark masses can be neglected. The dotted lines show the results of the full model, presented in fig. III.1. The solid lines show the result when the charm mass is set to zero. The deviation between these curves therefore shows the effect of the charm quark mass. Neglecting also the swing gives the long-dashed curves, and finally including only the single pomeron term in the collisions gives the short-dashed curves. The difference between these and the solid lines therefore represents the effect of saturation.

We first note that saturation effects from multiple collisions and the swing have a relatively small effect for $\tau > 1$, but grow for smaller τ, and reduce the cross section by approximately a factor 2.5 for $\tau = 0.1$. The effect of the charm quark mass is, as expected, also largest for smaller τ. The charm contribution is about 30% for $\tau = 100$ and 10% for $\tau = 1$, which should be compared with 40% for zero mass charm quarks.

We note in particular that also the one-pomeron result satisfies geometric scaling, even down to $\tau = 0.1$. Thus the scaling feature alone is not enough to prove the existence of saturation. The scale-breaking effect from the charm contribution will be further discussed in sec. III.6. The dominance of the light quark contributions, and the strong correlation between Q^2 and x due to the limited HERA energy, imply that this effect is not so evident in the results shown in figs. III.1 and III.2, although we can see a small shift between the curves for different Q^2 in fig. III.2.

Although saturation reduces the result for $\tau < 0.5$, there is a more clear break in the experimental data. We note, however, that the experimental points, which show this break, all correspond to small Q^2-values below 0.5 GeV^2. Here we expect also non-perturbative effects to be important. The wave functions in eq. (III.4) extend to very large transverse separations r, and such large dipoles must be suppressed by confinement effects. We also note that energy limitations imply that for fixed Q^2 the experimental points lie in a rather small x-interval, which implies that the points for different Q^2 have a limited overlap. The scaling features for small Q^2 will be further discussed in sec. III.7.

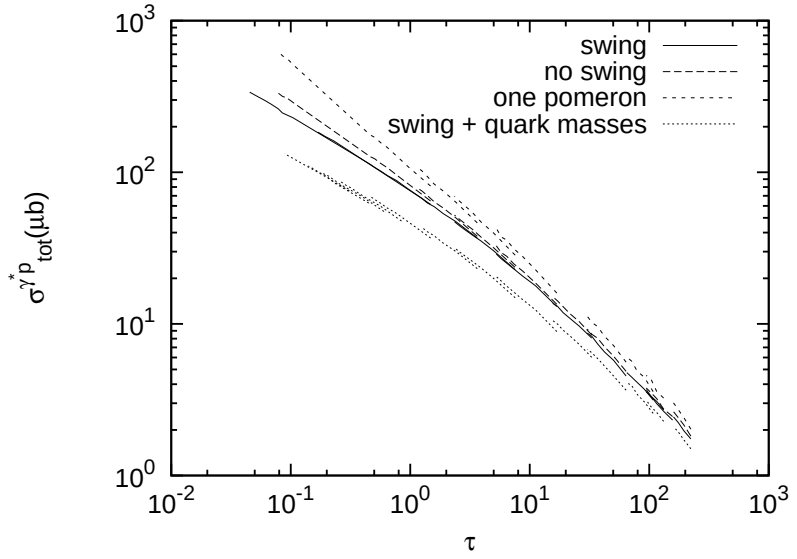

Figure III.2: The top three curves show the $\gamma^* p$ total cross section obtained from our Monte Carlo simulation for Q^2 ranging from 0.75GeV^2 to 90GeV^2 and for zero quark mass for 4 flavours. The solid lines show the results for evolution including the dipole swing and also multiple collisions, the long-dashed lines show the results without the swing but including multiple collisions, while the short-dashed lines are results without the swing and also without multiple collisions. It is seen that all three results satisfy geometric scaling. The bottom curve represents our full results shown in fig III.1.

III.5 Understanding geometric scaling in the linear evolution

The saturation model gives a motivation for geometric scaling in the kinematic range $Q^2 < Q_s^2$, but it does not give a reason for the observed scaling behaviour for $Q^2 > Q_s^2$ at experimentally feasible energies at current accelerators. The arguments in ref. [6] imply that the cross section should scale as a function of $Q^2/Q_s^2(x)$ within a wide kinematic region,

$$1 \lesssim \ln(Q^2/Q_s^2) \ll \ln(Q_s^2/\Lambda_{QCD}^2), \tag{III.8}$$

which is dominated by BFKL diffusion. Here $Q_s^2(x)$ is defined as the scale where the scattering probability is of order 1. As mentioned in the introduction this is a consequence of the fast growth towards small x and wide

diffusion to large $k_\perp$ in the leading log BFKL evolution. Both these effects are strongly damped by non-leading effects [7], which therefore reduce the region dominated by linear BFKL evolution. (We also note that both references [7] and [6] point out that with a running coupling the BFKL evolution leads to a saturation scale which satisfies $\ln Q_s^2 \sim \sqrt{Y}$ rather than $\ln Q_s^2 \sim Y$.) For larger Q^2, $k_\perp$-ordered evolution should be dominant and Kwieciński and Staśto [8] have assumed that DGLAP evolution is applicable in the whole region $Q^2 > Q_s^2$, with scaling initial conditions at $Q^2 = Q_s^2$. They then found that although not perfectly scaling, the result showed approximate scaling in the same kinematical domain specified by eq. (III.8). Their arguments do, however, not explain the shape of the saturation line.

We will below argue that scaling is expected both in the region dominated by BFKL diffusion and in the $k_\perp$-ordered double leading log (DLL) regime at larger Q^2. (In the DLL regime this is not obvious from the analytic expressions, but follows from a numerical analysis.) Furthermore we find that the transition between the DLL ($k_\perp$-ordered) and BFKL ($k_\perp$-non-ordered) regimes is given by $Q^2 = Q_{\text{limit}}^2 \propto x^{\lambda_{BFKL}}$, where λ_{BFKL} is the exponent in the solution to the BFKL evolution, estimated to be around 0.3. This implies that Q_{limit}^2 is very close to $Q_{s,GW}^2$, leaving only a very small region where the linear BFKL evolution is dominating.

The qualitative features of the QCD evolution at small x are present already in the leading log $1/x$ results, and we will in sec. III.5.1 discuss a toy model describing the BFKL-DLL transition [29]. Non-leading corrections from *e.g.* energy conservation and a running coupling are important for the quantitative result. In sec. III.5.2 we try to isolate the most important features of the full dipole cascade MC, to get an intuitive picture of geometric scaling in the non-saturated region.

III.5.1 Leading log approximation

When both $1/x$ and Q^2 are large the gluon distribution is given by ladders which are ordered in $k_\perp$ and where the splitting function is dominated by the $1/z$ pole. This corresponds to the double log approximation, and for a running coupling the gluon density is given by

$$g(x, Q^2) \sim \exp\left(2\sqrt{\alpha_0 \ln\ln Q^2 \ln 1/x}\right), \text{ where } \bar{\alpha}(Q^2) \equiv \frac{\alpha_0}{\ln(Q^2/\Lambda^2)}. \quad \text{(III.9)}$$

This expression does not scale exactly with $Q_s^2 \propto x^{-\lambda}$. Neglecting the very slow variation of $\ln\ln Q^2$ the cross section $\sim g/Q^2$ scales with

$$Q_s^2 \propto \exp(\lambda'\sqrt{\ln 1/x}), \quad \text{(III.10)}$$

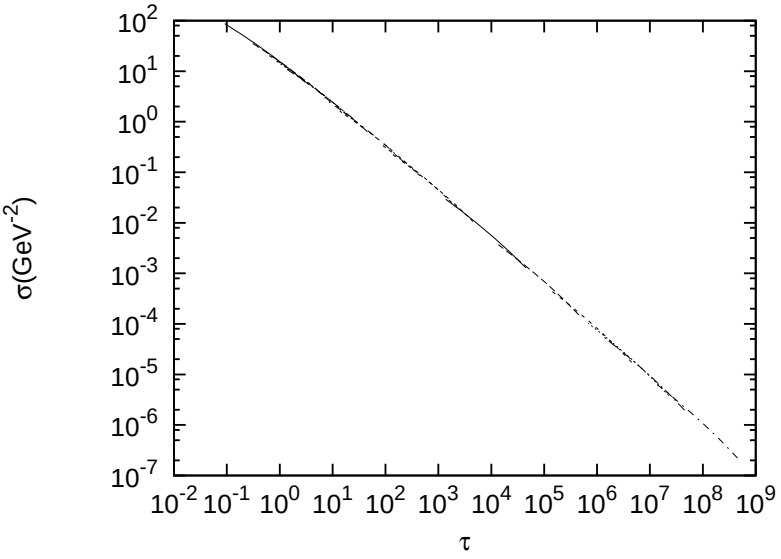

Figure III.3: The cross section $\sigma_{\gamma^* p} \sim g/Q^2$ with the gluon density g given by equation (III.9) for different Q^2, varying from $Q^2 = 100\text{GeV}^2$ to $Q^2 = 1.5 \cdot 10^{10}\text{GeV}^2$, and plotted as a function of Q^2/Q_s^2, with Q_s parametrized according to (III.2), but with λ equal to 0.7.

with some parameter λ', and in ref. [30] it is pointed out that the experimental data can be equally well fitted with both these expressions for Q_s. This is also seen in fig. III.3, which shows the cross section $\sigma^{\gamma^* p} \sim g/Q^2$ *vs.* τ with g from eq. (III.9) and τ defined from eq. (III.2) but with $\lambda = 0.7$.

For limited Q^2 we are instead in the BFKL regime dominated by $k_\perp$-non-ordered chains, where the gluon density is growing as a power $1/x^\lambda$ for small x, with λ of the order 0.3. Multiplying by $1/Q^2$ therefore gives directly the scaling cross section

$$\sigma^{\gamma^* p} \sim \frac{Q_s^2}{Q^2} = \tau^{-1} \tag{III.11}$$

with $Q_s^2 \propto 1/x^{0.3}$.

We now also want to argue that, as described in ref. [29], the line $Q^2 = Q^2_{\text{limit}}$ corresponding to the separation between ordered (DGLAP-like) chains and unordered (BFKL-like) chains, is also close to $Q^2_{s,GW}$. In the double log approximation the (non-integrated) gluon distribution G is given by the $k_\perp$-

ordered expression

$$G(x,k_\perp^2) \sim \sum_n \prod_i^n \left\{ \int \frac{4\alpha_s}{3\pi} \frac{dk_{\perp,i}^2}{k_{\perp,i}^2} \theta(k_{\perp,i} - k_{\perp,i-1}) \frac{dx_i}{x_i} \theta(x_{i-1} - x_i) \right\} \times \\ \times \delta(x - x_n) \delta(k_\perp^2 - k_{\perp,n}^2). \quad \text{(III.12)}$$

With the notation $l_i \equiv \ln(1/x_i)$ and $\kappa_i \equiv \ln(k_{\perp,i}^2/\Lambda^2)$ (and $\kappa = \ln(k_\perp^2/\Lambda^2)$, $l = \ln(1/x)$) we get for a fixed coupling the result

$$\begin{aligned} G &\sim \sum_n \left\{ \prod_i^n \int^\kappa \bar{\alpha} d\kappa_i \theta(\kappa_i - \kappa_{i-1}) \cdot \prod_i^n \int^{\ln 1/x} dl_i \theta(l_i - l_{i-1}) \right\} \\ &= \sum_n \bar{\alpha}^n \cdot \frac{\kappa^n}{n!} \cdot \frac{l^n}{n!} = I_0(2\sqrt{\bar{\alpha} \ln Q^2 \ln 1/x}) \\ &\sim \exp\left(2\sqrt{\bar{\alpha} \ln Q^2 \ln 1/x}\right). \end{aligned} \quad \text{(III.13)}$$

For a running α_s we have instead of $dk_{\perp,i}^2/k_{\perp,i}^2 = d\kappa_i$ a factor $d\kappa_i/\kappa_i = d\ln\kappa_i$, which then gives the result in eq. (III.9).

In the BFKL region with small x but not so large Q^2, the $k_\perp$-ordered phase space in eq. (III.12) becomes small, and chains which are not ordered in $k_\perp$ give important contributions. The BFKL evolution can be formulated in different ways. Expressed in terms of the primary [20] or backbone [21] gluons a step downwards in $k_\perp$ is suppressed by a factor $k_{\perp i}^2/k_{\perp i-1}^2$ [20,31]. We note that this implies that a maximum $k_\perp$-value in the chain will contain the factor $dk_{\perp\max}^2/k_{\perp\max}^4$ which can be interpreted as a hard parton-parton subcollision with the expected cross section proportional to $d\hat{t}/\hat{t}^2$. Expressed in the logarithmic variable κ, a step down is consequently suppressed by a factor $\exp(\kappa_i - \kappa_{i-1}) = \exp(-\delta\kappa)$. This implies that the effective range allowed for downward steps corresponds to approximately one unit in κ. Consequently we find that the phase space limits $\kappa_i \gtrsim \kappa_{i-1}$ in eq. (III.13) is replaced by [29,31]

$$\kappa_i \gtrsim \kappa_{i-1} - 1. \quad \text{(III.14)}$$

For a fixed α_s the transverse momentum integrals giving $\kappa^n/n!$ in eq. (III.13) will be replaced by

$$\int_0^\kappa \prod_i^n d\kappa_i \theta(\kappa_i - \kappa_{i-1} - 1) \approx \frac{(\kappa+n)^n}{n!}. \quad \text{(III.15)}$$

When κ is very large we recover the DLL result in eq. (III.13), but for smaller values of κ we find instead using Stirling's formula

$$\kappa \text{ small } \Rightarrow \frac{(\kappa+n)^n}{n!} \sim \frac{n^n}{n!} \sim e^n \quad \text{(III.16)}$$

which implies

$$G \sim \sum_n \frac{[\bar{\alpha}\, e \ln(1/x)]^n}{n!} = e^{e\,\bar{\alpha}\ln(1/x)} = \frac{1}{x^\lambda} \tag{III.17}$$

with

$$\lambda = e\,\bar{\alpha} \approx 2.72\,\bar{\alpha}. \tag{III.18}$$

In this range the chain corresponds to a random walk in $\ln k_\perp^2$. The result should be compared with the result from the leading order BFKL equation, which gives

$$\lambda = 4 \ln 2\,\bar{\alpha} \approx 2.77\,\bar{\alpha}. \tag{III.19}$$

We see that this simple picture describes the essential features of BFKL evolution.

We note here in particular that the boundary between the domains dominated by $k_\perp$-ordered chains (eq. (III.13)) and $k_\perp$-non-ordered chains (eq. (III.16)) is determined by the relation

$$\ln k_{\perp\text{limit}}^2 = e\,\bar{\alpha}\ln(1/x). \tag{III.20}$$

We see that if we replace the LL λ-value by a lower value ≈ 0.3, as indicated by the experimental data, then $k_{\perp\text{limit}}^2$ is similar to $Q_{s,GW}^2(x)$ from the early fit by Golec-Biernat and Wüsthoff [2,3]. This shows that the line $Q^2 = Q_{s,GW}^2(x)$ (corresponding to $\tau = 1$) is actually close to Q_{limit}^2, which represents the separation between $k_\perp$-ordered (DGLAP-like) chains and non-ordered (BFKL-like) chains.

III.5.2 The dipole cascade

The qualitative features in the LLA in sec. III.5.1 are modified by energy conservation and other non-leading effects. We will here study how the scaling behaviour can be seen in the dipole cascade model presented in sec. III.3, trying now to isolate the most important features of the full MC simulation.

Let us look at a dipole with size r, which after a rapidity interval Δy splits in two dipoles with sizes $r_>$ and $r_<$, with $r_>$ larger than $r_<$. Fig. III.4 shows the MC results for the average values of the ratios $r_>/r$ and $r_</r$ for different values for the "time", Δy, it takes from the formation of the dipole till it splits. The probability distribution $dP/d\Delta y$ is also shown. We see here that a dipole typically splits in two dipoles, where one has the same size as the parent while the other has just half its size. This result is independent of the step Δy and of the photon virtuality Q^2. This also shows that it is independent of the size of the parent dipole. We note that these results depend crucially on the energy-momentum conservation in the evolution. Without this constraint the typical splitting would occur within a very small rapidity step giving one

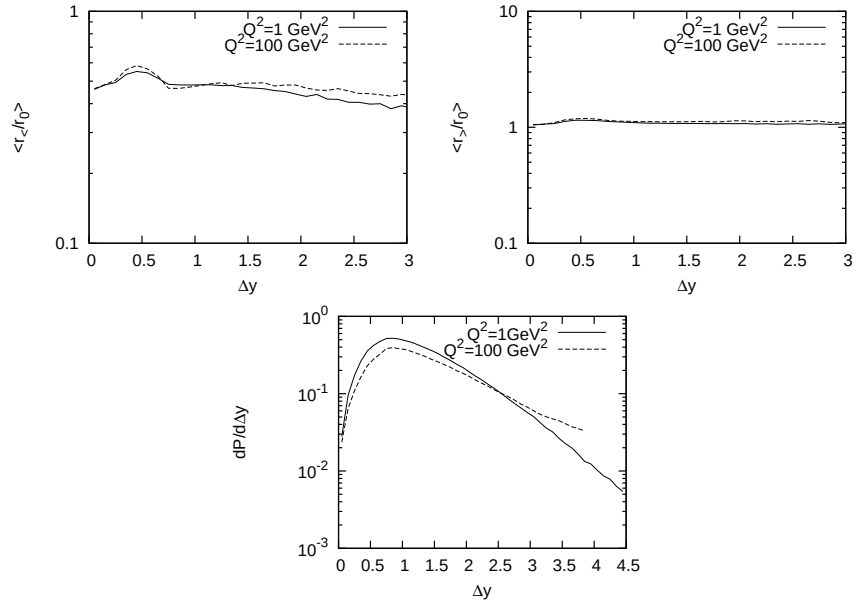

Figure III.4: The top figures show how the average values of the ratios $r_</r_0$ (left) and $r_>/r_0$ (right) for splitting events vary with the rapidity separation Δy. It is seen that both these ratios are approximately constant independent of Δy, and that $r_>/r_0$ is ≈ 1. The bottom figure presents the Δy-distribution $dP/d\Delta y$. This distribution has a peak around $\Delta y = 1$ and falls off exponentially for larger Δy-values.

virtual dipole with a size close to the necessary cutoff. When the cutoff goes to zero both Δy and $r_</r$ would also go to zero. Essential for the simple result in fig. III.4 is the conservation of both p_+ and p_-. This is seen in fig. III.5, which shows the corresponding result obtained with only p_+-conservation.

Let us then assume that each dipole r splits after a typical Δy, which from the distribution $dP/d\Delta y$ is found to be around 1.8 units, into two dipoles with sizes r and r/a, with the parameter a of the order of 2. If Y denotes the total rapidity range the number of steps will be $N = Y/\Delta y$ and the number of dipoles $2^N = 2^{(Y/\Delta y)}$. Starting from an initial dipole r_0 the number of dipoles having size r_0/a^n will be equal to $\binom{N}{n}$, with $n = 0, 1, \ldots, N$.

To study the scaling behaviour of the $\gamma^* p$ cross section within this approximation, we can treat the photon as a dipole with size $r_\gamma = 1/Q$. In the linear region the initial proton can also be treated as a single dipole with size $r_p = 1/\Lambda$. The cross section for the scattering of two dipoles, r_1 and r_2, is

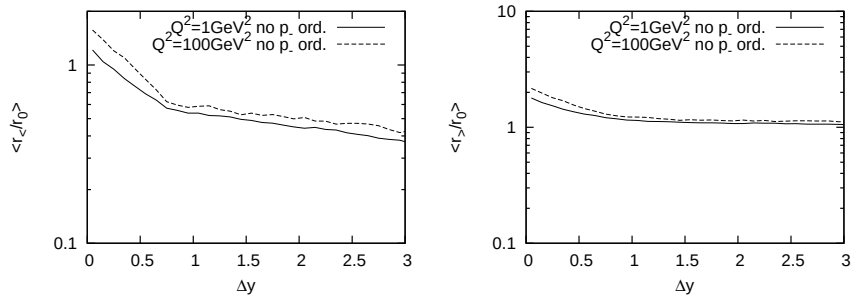

Figure III.5: The averaged ratios $\langle r_< / r_0 \rangle$ and $\langle r_> / r_0 \rangle$ as functions of Δy in a simulation where p_- is not conserved in the evolution. We see that p_+-conservation is not enough to get the almost constant ratios seen in figure III.4.

given by [17]

$$\sigma_{dd}(r_1, r_2) = 2\pi\alpha_s^2 r_{min}^2 \{1 + \ln(\frac{r_{max}}{r_{min}})\} \tag{III.21}$$

where r_{max} (r_{min}) is the largest (smallest) of the two colliding dipoles r_1 and r_2. We study the collision in a frame where only the proton is evolved, and the photon therefore treated as a single dipole.

When Q is larger than $a^N \cdot \Lambda$ the photon dipole is smaller than all dipoles in the proton cascade. The resulting cross section is then given by

$$\begin{aligned}
\sigma^{\gamma^* p}(Q^2, Y) &= 2\pi\alpha_s^2 \sum_{n=0}^{N} \binom{N}{n} Q^{-2} \left\{ 1 + \ln(\frac{Q}{a^n \Lambda}) \right\} \\
&= \pi\alpha_s^2 Q^{-2} 2^N \left\{ 2 - N \ln a + \ln \frac{Q^2}{\Lambda^2} \right\} \\
&\propto \frac{Q_{sc}^2}{Q^2} \left\{ 1 + \frac{1}{2} \ln(\frac{Q^2}{Q_{sc}^2}) \right\},
\end{aligned} \tag{III.22}$$

where in the last expression we have used $a = 2$, $N = Y/\Delta y$ and $Q_{sc}^2 = \Lambda^2 x^{-\ln 2/\Delta y} \approx \Lambda^2 x^{-0.38}$. The result is obviously scaling, and the exponent 0.38 is not far from the experimental fit around 0.3. We note also that in this case the dominating contribution comes from dipole chains where the dipoles are ordered in size and where the last dipole in the cascade is larger than the photon dipole. This just corresponds to the dominance of $k_\perp$-ordered DGLAP-type ladders.

For smaller Q-values the curly bracket in eq. (III.22) overestimate the contribution from small proton dipoles represented by n-values for which $a^n \cdot \Lambda >$

Q. The largest terms in the sum are obtained when the binomial factor has its maximum, *i.e.* for $n \approx N/2$. Therefore the result in eq. (III.22) is a good approximation as long as $Q > a^{N/2} \cdot \Lambda$. Indeed, using Stirling's formula we can write $\binom{N}{N/2} \approx 2^N$, and in the saddlepoint approximation we again arrive at the result given in eq. (III.22). We note that the constraint $Q > a^{N/2} \cdot \Lambda$ corresponds just to $Q^2 > Q_{sc}^2$, which thus is the limit for the dominance of $k_\perp$-ordered, DGLAP-type evolution chains.

Below this region, *i.e.* for $Q^2 < Q_{sc}^2$, it is not a good approximation to neglect the contributions from scatterings where the proton dipoles are smaller than the photon dipole. The full expression, including all contributions, can be written as

$$\sigma^{\gamma^* p}(Q^2, Y) \propto \sum_{n=0}^{m} \binom{N}{n} Q^{-2} \left\{ 1 + \ln(\frac{Q}{a^n \Lambda}) \right\} + \\ + \sum_{n=m+1}^{N} \binom{N}{n} a^{-2n} \Lambda^{-2} \left\{ 1 + \ln(\frac{a^n \Lambda}{Q}) \right\} \qquad \text{(III.23)}$$

where $m \equiv \frac{\ln Q/\Lambda}{\ln a}$. This expression is more complicated, but we show in figure III.6 the result of a numerical evaluation expressed with a scale $Q_{sc}^2 \propto x^{-0.4}$. We see that scaling is indeed satisfied for a large range of values for Q^2, also in the kinematic region dominated by chains which are not well ordered in dipole size or in transverse momentum.

We note that our toy model has important similarities with the empirical model presented in ref. [32]. In this paper it is demonstrated that geometric scaling follows from an assumption that the dipole cascade in the proton is dominated by dipoles with size Q_s^{-1} (while the virtual photon can be represented by a dipole with size Q^{-1}). Our toy model approximation of the full MC cascade has just this feature; the dipole multiplicity is given by the binomial coefficient $\binom{N}{n}$, with a maximum for $n = N/2$ corresponding to $r = 1/Q_{sc}$. The result in eq. (III.22), which is obtained for $Q > Q_{sc}$ using the saddlepoint approximation, is thus identical to the corresponding result in [32]. Ref. [32] also points out that if events with $Q < Q_s$ can be described by an analogous cascade evolution of the initial photon dipole, then the expression $Q/Q_s \sigma^{\gamma^* p}(Q/Q_s(x))$ is symmetric under the exchange $Q \leftrightarrow Q_s(x)$. This symmetry was initially observed in the HERA data by ref. [1]. For these smaller Q-values ($Q < Q_{sc}$) the dominant contributions from $n \approx N/2$ are contained in the second term in eq. (III.23). Using again the saddlepoint approximation we also obtain the symmetric result

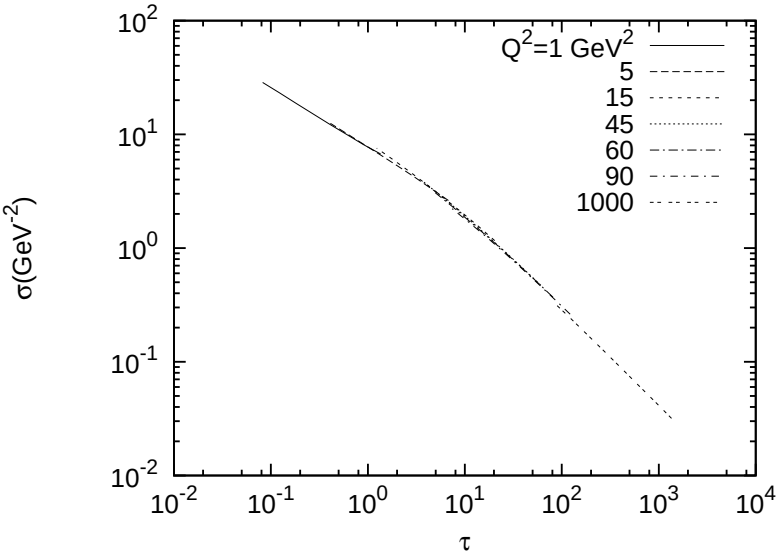

Figure III.6: The toy model cross section in (III.23) plotted as a function of the scaling variable with $Q_{sc}^2 = \Lambda^2 \cdot x^{-0.4}$, with $\Lambda^2 = 0.1\text{GeV}^2$, and for different Q^2. The normalization here is not of interest and all prefactors has been simply put to 1. We indeed see that the result shows scaling, for low and high Q^2 alike.

$$\begin{aligned}\sigma^{\gamma^* p}(Q^2, Y) &\approx 2\pi\alpha_s^2 2^N a^{-N}\Lambda^{-2}\left\{1+\ln(\frac{a^{N/2}\Lambda}{Q})\right\}\\ &\approx 2\pi\alpha_s^2\Lambda^{-2}\left\{1+\ln(\frac{Q_{sc}}{Q})\right\}. \qquad \text{(III.24)}\end{aligned}$$

In conclusion we find that $Q^2 = Q_{sc}^2 \propto x^{-\lambda}$, with λ approximately equal to the BFKL exponent, specifies the limit between dominance of $k_\perp$-ordered and $k_\perp$-non-ordered chains, and that a simple toy model having this property gives the qualitative features of the scaling dynamics for both large and small τ. We also see that the toy model approximation to the full MC simulation of the dipole cascade model have important similarities with the empirical model in ref. [32], and gives a scaling result with a scaling exponent not far from what is observed at HERA.

III.6 Scaling features in the charm contribution

It is well known from HERA data that charm quarks contribute a significant part to the total cross section. As discussed in sec. III.4, the large charm quark mass modifies the scaling properties, and it is seen that the HERA charm data do indeed not scale as a function of $\tau = Q^2/Q^2_{s,GW}(x)$. As pointed out in ref. [33] they do, however, scale quite well as a function of the modified scaling variable $\tau_c = (Q^2 + 4m_c^2)/Q_s^2$.

From the photon wave function in (III.4) we see that the term proportional to the Bessel function K_1^2 in $|\psi_T|^2$ only contains Q^2 and m_f in the combination $z(1-z)Q^2 + m_f^2$. If z-values around $1/2$ dominate, we would expect that the charm contribution is gradually switched off when Q^2 is of the order $4m_c^2$ or smaller, which necessarily leads to a breaking of geometric scaling. The sum of the terms proportional to K_0^2 in $|\psi_T|^2$ and $|\psi_L|^2$ is proportional to

$$[4z(1-z)]z(1-z)Q^2 + m_f^2,$$

and for z close to $1/2$ the square bracket equals 1, and we get the same factor $z(1-z)Q^2 + m_f^2$ as before. From these features we may expect that the charm contribution scales approximately with a modified scaling parameter where, for example, we replace Q^2 by $Q^2 + n \cdot m_c^2$ in the definition of τ, for some number n which should be close to or a little larger than 4.

In fig. III.7 we show data for the charm cross section from ZEUS [34] and our MC obtained for $m_c = 1.4\,\text{GeV}$. In this figure we have used the scaling variable

$$\tau_c = (Q^2 + 6m_c^2)/Q^2_{s,GW}(\bar{x}) \quad \text{with} \quad \bar{x} = (Q^2 + 6m_c^2)/W^2, \tag{III.25}$$

obtained with $n = 6$ in the definition of τ_c, which we find gives somewhat better scaling properties. This implies that $\tau_c = (1 + 6m_c^2/Q^2)^{1+\lambda} \cdot \tau_{GW}$. We here first note that the MC agrees quite well with the data, being only a little high for the largest τ-values. Secondly we confirm the observation in ref. [33] that the charm cross section does scale well as a function of such a modified scaling variable.

The value $n = 6$ chosen for the scaling variable in eq. (III.25) is not crucial for the scaling behaviour, which works rather well also for $n = 4$. We note, however, that replacing x by $\bar{x}$ in Q_s only contributes a minor part to the difference between τ_c and τ_{GW}, represented by the factor $(Q^2 + 6m_c^2)^\lambda$. More important is the replacement $Q^2 \to Q^2 + 6m_c^2$ in eq. (III.25). This is illustrated in fig. III.8, which shows that scaling does not hold if we replace τ by $Q^2/Q^2_{s,GW}(\bar{x})$.

We want here to point out that the effect of the charm mass is reduced very slowly for larger Q^2. Integrating over the dipole size, $\mathbf{r}$, we obtain from a

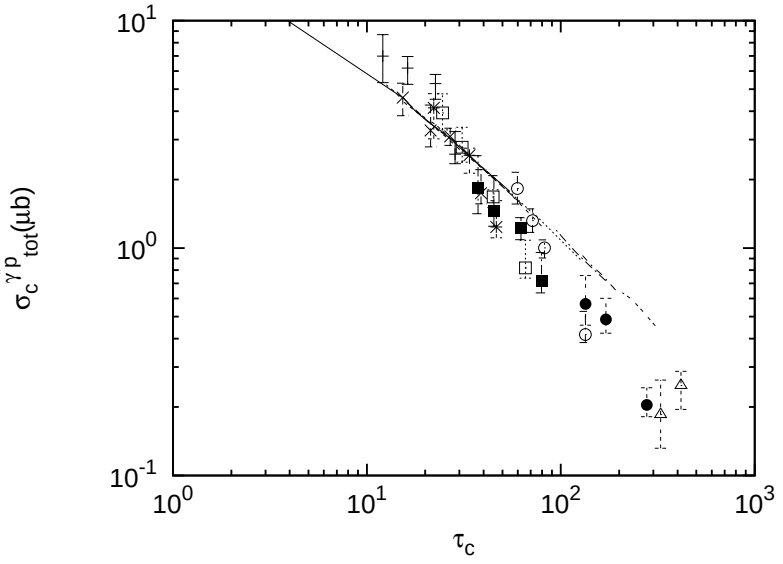

Figure III.7: The total charm cross section, $\sigma_T^c + \sigma_L^2$ plotted as a function of τ_c defined in (III.25) with $\lambda = 0.35$ and $m_c = 1.4$ GeV. Results are shown for Q^2 between 2 and 130 GeV^2. We see that the result scales fairly well with this scaling parameter. Data points are taken from ref [34].

dimensional analysis

$$\int d^2\boldsymbol{r} K_i^2(\epsilon r)\sigma(z,\boldsymbol{r}) \propto \frac{1}{\epsilon^4}\,, \qquad \epsilon = \sqrt{z(1-z)Q^2 + m_f^2}. \tag{III.26}$$

When $4Q^2$ is small compared to m_f^2 we have $\epsilon \approx m_f$, and the charm cross section ought to scale as

$$\sigma_T \propto \frac{1}{m_c^2}, \qquad \sigma_L \propto \frac{Q^2}{m_c^4}. \tag{III.27}$$

We see here that the longitudinal contribution depends on two separate scales Q^2 and m_c^2. In the other limit, when $z(1-z)Q^2 > m_c^2$ we can neglect m_c. However, since $z(1-z)$ can take on arbitrarily small values for fixed Q^2, we the effect of the charm mass can be important also for high Q^2. In the MC results presented in fig. III.7 the reduction due to the charm mass is about 30% for $Q^2 = 90\,\text{GeV}^2$ and 55% for $Q^2 = 15\,\text{GeV}^2$. This slow decrease of the mass effect is also seen in fig. III.2. (We should here also remark that the transverse wave function ψ_T is not normalizable due to the singularity $K_1^2(r) \sim 1/r^2$ at

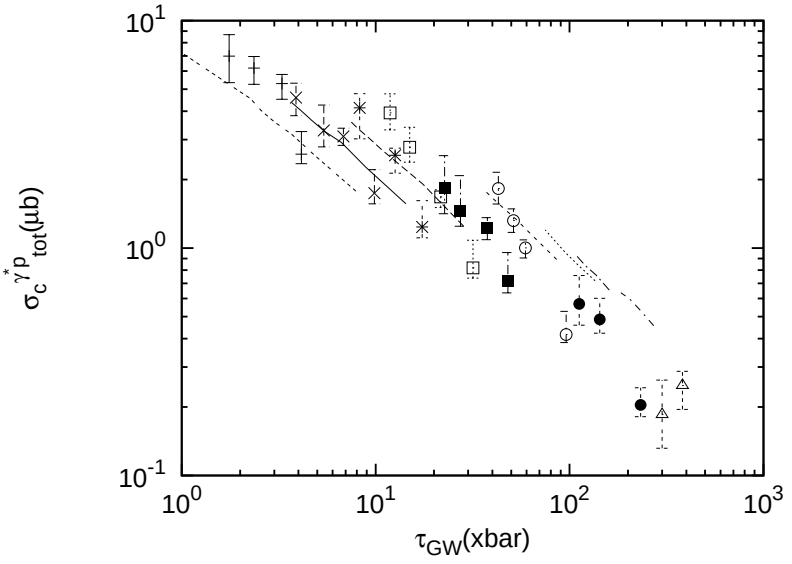

Figure III.8: Here we plot the charm cross section as a function of $Q^2/Q_s^2(\bar{x})$ with the same parameters as in fig. III.7. In this case we see that the result does not scale, which shows the importance of replacing Q^2 with $Q^2 + n \cdot m_c^2$, $n \sim 4$, as argued in the text.

small r. However, at small r the dipole-proton cross section behaves like r^2 and thus the result is still finite.)

III

III.7 Interaction at smaller Q^2

Due to the limited energy in the HERA accelerator the experimental data in the region $\tau < 0.5$ are all obtained for rather small virtualities Q^2, where non-perturbative effects must be expected.

III.7.1 Can the perturbative dipole formalism be used for Q^2 below 1 GeV^2?

For small Q^2 the wave functions in eq. (III.4) extend to very large transverse separations r, and such large dipoles must be suppressed by confinement effects. The interaction of these photons is usually described in terms of two separate components, a vector dominance contribution and a direct coupling to the quarks. We will here test if it is possible to represent the interaction of

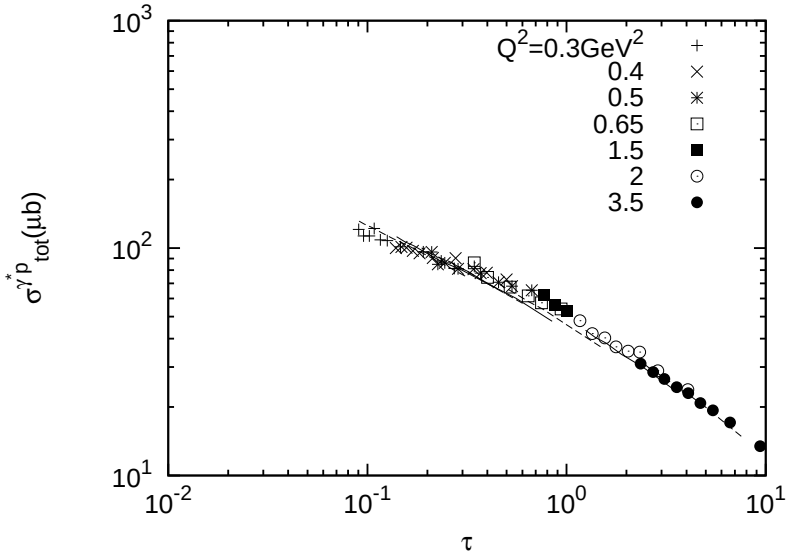

Figure III.9: The $\gamma^* p$ total cross section plotted as a function of the scaling variable τ for low Q^2 values. Points are data from the H1 [27] and ZEUS [28] collaborations, while the lines are results obtained from our Monte Carlo. We can here see a successive suppression of the cross section for smaller Q^2 as a result of the finite quark masses.

these photons with a finite mass for the light quarks, which effectively suppresses the contribution from the very large dipoles. Because the contribution from the strange quark is suppressed by its smaller electric charge, and therefore relatively small, it is not possible to study in any detail the effect of the strange quark mass. We therefore use a single quark mass, m_l, for all the light quarks, u, d, and s. The results in fig. III.9 for Q^2 in the range 0.3-3.5 GeV^2 are obtained for $m_l = 60$MeV and $m_c = 1.4$GeV, and we here show the model results for the same combinations of x- and Q^2-values as in the experimental data. We see that the experimental data are very well reproduced by the model calculations, which gives some support to the application of this perturbative description also for these small virtualities.

The effective quark mass is quite small, and we would have expected a larger suppression for small Q^2. The value 60 MeV is smaller than Λ_{QCD}, and also smaller than the effective mass obtained in ref. [35] in an analysis of the vector-current two-point function. Ref. [35] studies a model with an effective quark mass which varies with Q^2, becoming smaller when Q^2 is increased. The agreement in fig. III.9 would actually be improved by such a varying ef-

fective mass, but we do not believe that the accuracy of our model is sufficient to claim that this improvement is significant. We have therefore here only used a constant effective quark mass in the wave functions in (III.4).

III.7.2 Is geometric scaling obeyed for $Q^2/Q_s^2 < 1$?

The effect of a finite quark mass is approximately a multiplicative factor which suppresses the cross section for smaller Q^2. As discussed in sec. III.6 the result of the quark mass in the photon wave functions corresponds roughly to a suppression by a factor $Q^2/(Q^2 + 4m_f^2)$. The fact that the model results in fig. III.9 look as a scaling function is therefore a consequence of the strong correlation between x and Q^2 in the experimental data. The finite energy in the HERA accelerator implies that for small values of τ there are only data for (x, Q^2)-values within a very small interval. With a future accelerator with higher energy, one could also reach smaller τ-values keeping $Q^2 > 1\text{GeV}^2$. For these Q^2 we do not get much suppression from the light quark masses, and fig. III.10 shows that the scaling curve will lie somewhat above the present HERA results. In the figure we show the extend the curve for $Q^2 = 2\text{GeV}^2$ to $\tau \approx 0.07$. As can be seen, the difference is increasing for smaller τ-values and is about a factor 1.4 for $\tau \approx 0.07$. We also expect to see the scalebreaking effects of the charm mass for $1\text{GeV}^2 \lesssim Q^2 \lesssim 10\text{GeV}^2$, while for higher Q^2 these effects should be gradually switched off. This cannot, however, be observed at accelerators in the foreseeable future.

As a conclusion of this section we predict that at higher energies the data will scale at larger values for the cross section than the present HERA data for $\tau < 1$. We should, however, point out that the analysis in this section only holds for the particular value $\lambda = 0.3$ for the saturation scale in eq. (III.2). For a different λ the scaling behaviour will be different and it turns out that the deviation from the scaling behaviour would be somewhat reduced with a higher λ.

III.8 Impact parameter dependence of the traveling wave

In this section we will look at the impact parameter dependence of the dipole-proton scattering amplitude $T^{dp}(b)$, defined as $T = 1 - S$. We expect that the contribution from small dipoles is reduced for large impact parameters, which may result in different scaling behaviour for central and peripheral collisions. This feature may be of special interest in studies of diffraction.

The amplitude T^{dp} is related to the total dipole-proton cross section by the

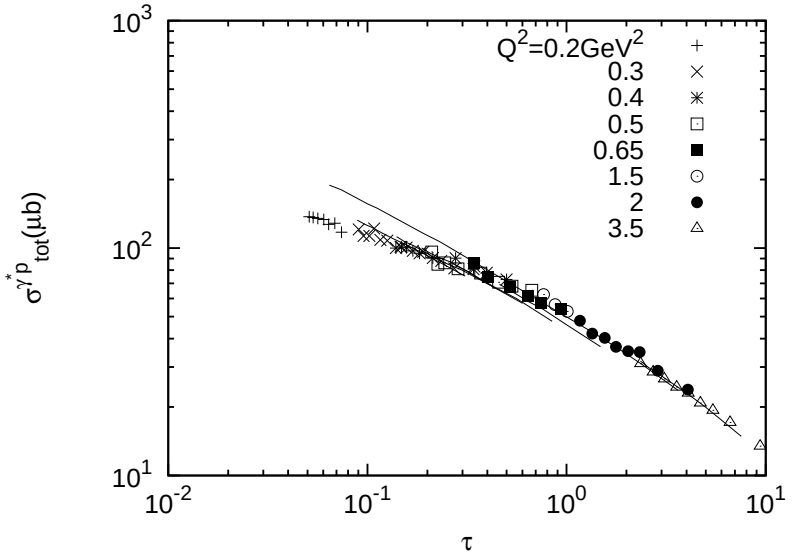

Figure III.10: In this figure we extend the result for $Q^2 = 2\text{GeV}^2$ to smaller τ-values. We can here see a deviation from the scaling behaviour at higher energies, about a factor 1.4 for $\tau \approx 0.07$ corresponding to $x \approx 3 \cdot 10^{-9}$ for $Q^2 = 2\text{GeV}^2$. In this plot the deviation from the scaling curve is to a large extent due to the effective light quark mass.

relation

$$\sigma^{dp}(z, \boldsymbol{r}) = 2 \int d^2\boldsymbol{b}\, T^{dp}(b). \tag{III.28}$$

To get the amplitude for photon-proton scattering, the amplitude $T^{dp}(b)$ has to be weighted by the photon wave function in eq. (III.4). The average value $\langle T \rangle$ will then depend on the virtuality Q^2 and the impact parameter b.

In the introduction we mentioned the similarity between the high energy evolution equations for T and a certain type of equation (or rather a class of equations) from statistical physics, known as the FKPP equation. Neglecting the impact parameter dependence, the BK equation for the amplitude $T(l, Y)$ (with $l \equiv \ln k^2$) is analogous to the FKPP equation for the function $u(x, t)$, with the identifications $l \leftrightarrow x$ and $\bar{\alpha} Y \leftrightarrow t$. The asymptotic solution, as $t \to \infty$, $u_{as}(x, t) = u(x - vt)$, then corresponds to $T_{as}(l, Y) = T(l - \lambda Y)$ in QCD. If we define $Q_s^2 = \exp(\lambda Y)$ as before the solution satisfies the geometric scaling relation $T(l, Y)_{as} = T(\ln k^2 / Q_s^2)$. There are a number of conditions which must be satisfied in order to obtain an asymptotic solution of this form, and for a short review on traveling wave solutions in QCD we refer to [36].

As our model satisfies geometric scaling we can expect that the function $\langle T \rangle(\ln Q^2)$ plotted for different Y-values looks like a traveling wave. This can be seen in fig. III.11 which shows results for $Y = 6, 8, 10$ and 12. In this figure we also show the result for different impact parameters b. If we look at different points with the same $\langle T \rangle$-value, the velocity is determined by the relation

$$v(b) = \frac{\Delta \ln Q^2}{\Delta Y} \tag{III.29}$$

The results in fig. III.11 correspond to the following velocities when saturation effects are included in the amplitude: $v(b = 0) = 0.28$, $v(b = 0.5fm) = 0.35$ and $v(b = 1fm) = 0.37$. (For the one pomeron amplitude we instead obtain $v(b = 0) = 0.41$, $v(b = 0.5fm) = 0.46$ and $v(b = 1fm) = 0.48$) Thus the velocity varies significantly with the impact parameter, being smaller for central collisions and larger for peripheral collisions. As the scattering probability is largest for the central collisions, these results seem to be reasonably consistent with weighted average over impact parameters corresponding to the velocity $v \approx 0.3$ observed for the total cross section.

In fig. III.11 we can see that also the one pomeron amplitude, which contains no saturation effects, seems to exhibit the form of a traveling wave. We also see that we need quite high energies, corresponding to $x \approx 6 \cdot 10^{-6}$ for $Q^2 \approx 4\text{GeV}^2$ and $b = 0$, before the one pomeron amplitude reaches the unitarity limit $T = 1$. However, it is also seen that saturation effects reduce the amplitude by about 10% for larger Q^2 and about 40% for small $Q^2 \sim 1\text{GeV}^2$ already at $x \sim 10^{-3}$ for $b = 0$. This result is consistent with the previous results presented in fig. III.2.

III.9 Conclusions

DIS data from HERA show a striking regularity as $\sigma^{\gamma^* p}$ is a function of the ratio $\tau = Q^2/Q_s^2(x)$ only, with $Q_s^2(x)$ given by eq. (III.2) [1–3]. Such a geometric scaling has been expected in the range $\tau < 1$, as a natural consequence of saturation when the gluon density becomes very high, and there has been a lot of discussion in the literature whether saturation has or has not been observed at HERA. Modifications of the saturation model including DGLAP evolution [4] improves the agreement with data for larger Q^2, but it has not been equally obvious how geometric scaling follows in a natural way from QCD evolution in the non-saturated domain. The traveling wave solutions to the nonlinear evolution equations in QCD do predict geometric scaling also for $\tau > 1$ [9,10], but these solutions are valid only at extremely high energies, far beyond what is available at the HERA accelerator.

In this paper we have tried to shed some light on these questions: What is the reason for scaling for $\tau > 1$, and is saturation indeed the reason for geometric scaling for $\tau < 1$? Supporting the saturation idea is the fact that the scaling curve seems to have a break just around $\tau = 1$. There are, however, also other effects which contribute to a break in this region. In ref. [29] it is shown that the transition between $k_\perp$-ordered (DGLAP-like) chains and $k_\perp$-non-ordered (BFKL-like) chains is expected close to Q_s^2. Secondly the finite energy in the HERA machine implies that experimental data for $\tau < 1$ are only available for $Q^2 < 1\text{GeV}^2$, where nonperturbative effects begin to be important.

To study the influence on the scaling from different dynamical effects we have used the dipole cascade model presented in ref. [14]. This model is based on Mueller's dipole cascade model, but includes energy-momentum conservation and saturation effects, not only from multiple subcollisions but also from pomeron mergings in the cascade evolution, and it does successfully reproduce the data from HERA.

Our conclusion is that scaling is a natural consequence of the dipole evolution in the linear region $\tau > 1$. Indeed, neglecting saturation the linear evolution exhibits geometric scaling at high energies for τ-values both larger and smaller than 1. The change from the DGLAP to the BFKL regime causes a change in the slope of the scaling curve, but this change is rather smooth, without a sharp break at $\tau = 1$. The break seen in the HERA data is to a significant part caused by saturation, but to an even larger extent by scalebreaking effects at low Q^2. The latter are partly due to the large c-quark mass and partly due to non-perturbative effects related to confinement for the light u-, d-, and s-quarks. Therefore we predict that the results from a future higher energy machine will show deviations from the scaling behaviour in the variable τ_{GW}. These results are expected to lie above the HERA results for $\tau_{GW} < 1$, and be represented by a curve which is more smooth around $\tau_{GW} = 1$. (Recently it has also been predicted that a new type of scaling, called diffusive scaling, will occur at very high energies, but we have in this paper concentrated on energies which might be within reach at some future accelerator.)

We study the charm contribution separately, and compare with data for the charm cross section. The charm contribution does not scale as the total cross section, but we see that it does scale rather well as a function of the variable $(Q^2 + 6m_c^2)/Q_s^2(\bar{x})$. Finally we have studied how the scaling feature varies with impact parameter. We here see that the effective power λ in (III.2) is somewhat smaller for central collisions and larger for peripheral collisions, averaging out to the observed value around 0.3. Such a variation may be of interest in studies of diffractive scattering.

Acknowledgments

We want to thank Leif Lönnblad for valuable discussions and help with the MC simulation. We are also grateful to Hannes Jung for pointing out to us the lack of scaling in the charm contribution, and to Edmond Iancu for useful comments on the manuscript.

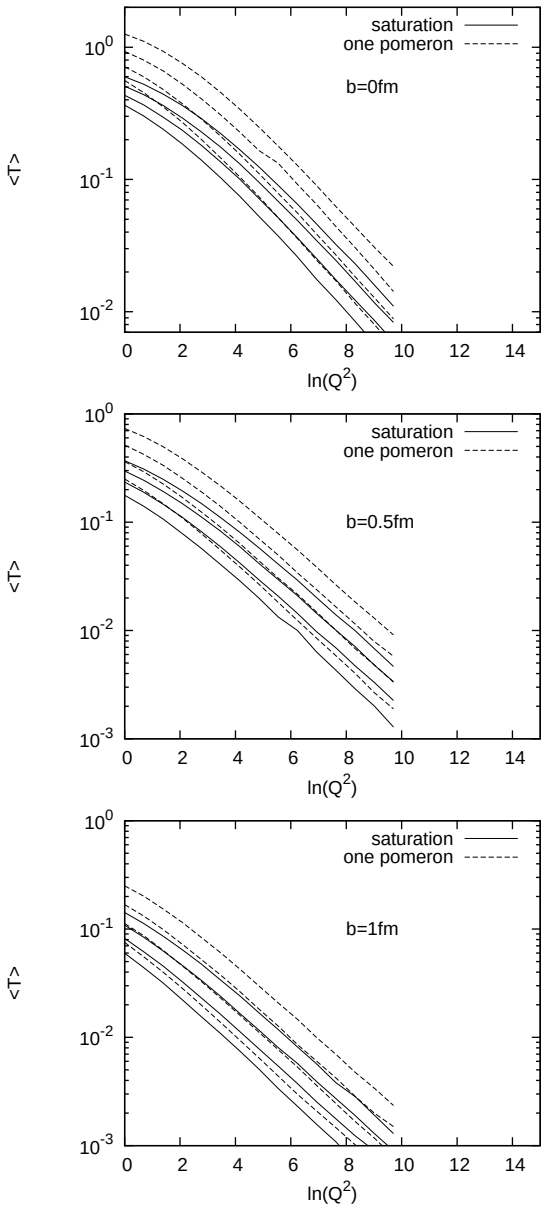

Figure III.11: The average scattering amplitude as a function of $\ln(Q^2/1\text{GeV}^2)$ for $Y = 6, 8, 10$ and 12 and impact parameters $b = 0, 0.5, 1$fm. Both the amplitude containing full saturation effects and the linear one pomeron amplitude are shown. For the amplitude including saturation we obtain from here the velocities $v(b = 0) = 0.28$, $v(b = 0.5fm) = 0.35$ and $v(b = 1fm) = 0.37$.

III References

[1] A. M. Stasto, K. Golec-Biernat, and J. Kwiecinski *Phys. Rev. Lett.* **86** (2001) 596–599, hep-ph/0007192.

[2] K. Golec-Biernat and M. Wusthoff *Phys. Rev.* **D59** (1999) 014017, hep-ph/9807513.

[3] K. Golec-Biernat and M. Wusthoff *Phys. Rev.* **D60** (1999) 114023, hep-ph/9903358.

[4] J. Bartels, K. Golec-Biernat, and H. Kowalski *Phys. Rev.* **D66** (2002) 014001, hep-ph/0203258.

[5] K. Golec-Biernat and S. Sapeta *Phys. Rev.* **D74** (2006) 054032, hep-ph/0607276.

[6] E. Iancu, K. Itakura, and L. McLerran *Nucl. Phys.* **A708** (2002) 327–352, hep-ph/0203137.

[7] K. Golec-Biernat, L. Motyka, and A. M. Stasto *Phys. Rev.* **D65** (2002) 074037, hep-ph/0110325.

[8] J. Kwiecinski and A. M. Stasto *Phys. Rev.* **D66** (2002) 014013, hep-ph/0203030.

[9] S. Munier and R. Peschanski *Phys. Rev. Lett.* **91** (2003) 232001, hep-ph/0309177.

[10] S. Munier and R. Peschanski *Phys. Rev.* **D70** (2004) 077503, hep-ph/0401215.

[11] E. Iancu and D. N. Triantafyllopoulos *Nucl. Phys.* **A756** (2005) 419–467, hep-ph/0411405.

[12] E. Iancu, A. H. Mueller, and S. Munier *Phys. Lett.* **B606** (2005) 342–350, hep-ph/0410018.

[13] E. Avsar, G. Gustafson, and L. Lönnblad *JHEP* **07** (2005) 062, hep-ph/0503181.

[14] E. Avsar, G. Gustafson, and L. Lonnblad *JHEP* **01** (2007) 012, hep-ph/0610157.

[15] A. H. Mueller *Nucl. Phys.* **B415** (1994) 373–385.

[16] A. H. Mueller and B. Patel *Nucl. Phys.* **B425** (1994) 471–488, hep-ph/9403256.

[17] A. H. Mueller *Nucl. Phys.* **B437** (1995) 107–126, hep-ph/9408245.

[18] S. Catani, F. Fiorani, and G. Marchesini *Phys. Lett.* **B234** (1990) 339.

[19] M. Ciafaloni *Nucl. Phys.* **B296** (1988) 49.

[20] B. Andersson, G. Gustafson, and J. Samuelsson *Nucl. Phys.* **B467** (1996) 443–478.

[21] G. P. Salam *JHEP* **03** (1999) 009, hep-ph/9902324.

[22] G. P. Salam *Comput. Phys. Commun.* **105** (1997) 62–76, hep-ph/9601220.

[23] G. P. Salam *Nucl. Phys.* **B461** (1996) 512–538, hep-ph/9509353.

[24] G. P. Salam *Acta Phys. Polon.* **B30** (1999) 3679–3705, hep-ph/9910492.

[25] L. H. Orr and W. J. Stirling *Phys. Rev.* **D56** (1997) 5875–5884, hep-ph/9706529.

[26] J. R. Andersen and W. J. Stirling *JHEP* **02** (2003) 018, hep-ph/0301081.

[27] **H1** Collaboration, C. Adloff *et al. Eur. Phys. J.* **C21** (2001) 33–61, hep-ex/0012053.

[28] **ZEUS** Collaboration, J. Breitweg *et al. Phys. Lett.* **B487** (2000) 53–73, hep-ex/0005018.

[29] G. Gustafson and G. Miu *Eur. Phys. J.* **C23** (2002) 267–274, hep-ph/0110143.

[30] F. Gelis, R. Peschanski, G. Soyez, and L. Schoeffel hep-ph/0610435.

[31] G. Gustafson *Acta Phys. Polon.* **B34** (2003) 2963–2988, hep-ph/0306108.

[32] S. Munier *Phys. Rev.* **D66** (2002) 114012, hep-ph/0205319.

[33] V. P. Goncalves and M. V. T. Machado hep-ph/0607125.

[34] **ZEUS** Collaboration, S. Chekanov *et al. Phys. Rev.* **D69** (2004) 012004, hep-ex/0308068.

[35] H. G. Dosch, T. Gousset, and H. J. Pirner *Phys. Rev.* **D57** (1998) 1666–1679, hep-ph/9707264.

[36] S. Munier hep-ph/0609161.

IV

On the Dipole Swing and the Search for Frame Independence in the Dipole Model

Emil Avsar

Dept. of Theoretical Physics, Sölvegatan 14A, S-223 62 Lund, Sweden

Submitted to JHEP, arXiv:0709.1371, LU-TP 07-09.

Small-x evolution in QCD is conveniently described by Mueller's dipole model which, however, does not include saturation effects in a way consistent with boost invariance. In this paper we first show that the recently studied zero and one dimensional toy models exhibiting saturation and explicit boost invariance can be interpreted in terms positive definite $k \to k+1$ dipole vertices. Such $k \to k+1$ vertices can in the full model be generated by combining the usual dipole splitting with $k-1$ simultaneous dipole swings. We show that, for a system consisting of N dipoles, one needs to combine the dipole splitting with at most $N-1$ simultaneous swings in order to generate all colour correlations induced by the multiple dipole interactions.

IV.1 Introduction

The small-x region in QCD can be described by the well known, linear, BFKL equation which predicts a power-like growth in x for the gluon density. Such a fast growth is problematic since it breaks the unitarity bound at high energies. As the gluon density becomes large, non-linear effects cannot be ignored and it was early suggested that effects from parton saturation should tame the growth of the gluon density, in accordance with unitarity [1].

Starting the evolution from a colour singlet quark-antiquark pair, a colour dipole, Mueller [2,3] formulated a dipole model in transverse coordinate space which reproduces the BFKL equation to leading order. The transverse coordinate formulation also allows one to go beyond the BFKL equation since it is here easier to take into account multiple interactions. This is so because the transverse coordinates of the partons are frozen during the evolution, and it is therefore rather easy to sum the multiple scattering series in an eikonal approximation. This was exploited by Mueller, who was thus able to obtain a unitarised formula for the scattering amplitude.

Within the dipole formalism, Balitsky [4] derived an infinite hierarchy of equations for the dipole scattering amplitudes. Kovchegov [5] derived a closed equation for the amplitude using a mean field approximation, and this equation is referred to as the Balitsky-Kovchegov (BK) equation. The same hierarchy of equations also follows from the JIMWLK equation [6–9] which is the master equation of the Color Glass Condensate (CGC) formalism [10] and describes the non-linear evolution of dense hadronic matter in the presence of saturation effects.

In Mueller's model the multiple dipole interactions correspond to multiple pomeron exchange, and in the Lorentz frame where the collision is studied these multiple interactions lead to the formation of pomeron loops. However, these loops cannot be formed during the evolution of the dipole cascade since this evolution is linear. Thus only those loops which are cut in the specific Lorentz frame used for the calculation are accounted for, while none of the remaining loops is included. This implies that the model is not frame independent. To minimize the error, the optimal frame to use is the one where the colliding dipole cascades are of the same density, since multiple scatterings then become important at rapidities where one may still neglect saturation effects in the evolving dipole cascades.

In order to obtain a frame independent formalism it is necessary to include saturation effects also in the evolution of each dipole cascade. There have been various attempts to include such saturation effects in a consistent manner, but no explicitely frame independent formalism has yet been presented.

To gain insight and possible hints towards a solution, a simple 1+0 dimensional (rapidity constitutes the only dimension) toy model in which transverse

coordinates are neglected was constructed in [3, 11]. This model has been further studied in [12, 13], and the resulting frame independent evolution can be interpreted as a coherent emission of new "dipoles" from the multi-"dipole" state.

In [14] we developed a dipole cascade model for DIS and pp collisions based on Mueller's model but also including effects of energy-momentum conservation. This model was further extended in [15] to include saturation effects in the cascade evolution through the so called dipole swing mechanism [15,16], which gives an additional $2 \to 2$ transition during the evolution. Monte Carlo (MC) simulations show that the evolution is almost frame independent, and the model results are in good agreement with inclusive and diffractive data from HERA and the Tevatron [17].

In this paper we will first show that the explicitely frame independent evolution in the toy model mentioned above, and also in its 1+1 dimensional generalization in [18], can be given a probabilistic interpretation in terms of positive definite $k \to k+1$ dipole vertices. Such $k \to k+1$ transitions can in the full model be generated by combining the dipole splitting with the dipole swing.

In case each individual dipole is restricted to single scattering only, we show that one needs to combine the dipole splitting with at most one swing at a time in order to generate the necessary colour correlations. As remarked in [12], the toy model evolutions mentioned above describe the multiple scatterings of individual dipoles, and we will here show that one can in the real model generate the correlations induced by the dipole scatterings by combining a splitting with several simultaneous swings. For a system consisting of N spatially uncorrelated dipoles, it is easy to see that one needs to combine the dipole splitting with at most $N-1$ simultaneous swings. In a process where one splitting is combined with $k-1$ swings, k dipoles are replaced by $k+1$ dipoles, thus giving a $k \to k+1$ transition.

However, starting the evolution from a single $q\bar{q}$ pair, one obtains dipoles which are connected in chains, and in this case not all swings are allowed. It is here important to keep track of the correct topology of the dipole state. While this is never a problem in the original formulation which only contains the $1 \to 2$ splitting, it is here very important to avoid the formation of unphysical states. Although it has been checked for a large number of cases, a formal proof that it is always enough with $N-1$ swings is not avaliable, and the result is a conjecture.

The paper is organized as follows. In the next section we shortly review Mueller's dipole model and the question of frame independence in the evolution. In section IV.3 we will review the toy models in zero and one transverse dimensions formulated in [11, 18], and show how these can be interpreted in terms of the $k \to k+1$ transitions mentioned above. Then in section IV.4 we

consider the evolution in the full model and argue that also in this case the correct evolution can be formulated in terms of $k \to k+1$ vertices. In section IV.5 we go on to study the colour topology of the evolution, and we show how one can generate the needed colour correlations using the dipole swing. Finally, in section IV.6, we present our conclusions.

IV.2 Approaches Towards a Frame Independent Formalism

In Mueller's model [2, 3] for onium-onium scattering a colour dipole formed by a colour charge at transverse coordinate x and an anticharge at y can split into two dipoles by emitting a soft gluon at position z with the following probability

$$\frac{d\mathcal{P}}{dY} = \frac{\bar{\alpha}}{2\pi} d^2z \frac{(x-y)^2}{(x-z)^2(z-y)^2} \equiv d^2z \mathcal{M}(x,y,z), \tag{IV.1}$$

$$\bar{\alpha} \equiv \frac{\alpha_s N_c}{\pi} \text{ and } Y \equiv \ln \frac{1}{x_{Bj}}. \tag{IV.2}$$

We refer to $\mathcal{M}$ as the dipole kernel and to Y as the rapidity, which here acts as the time variable in which the evolution proceeds. A dipole cascade is then formed when each dipole splits repeatedly. When two such cascades collide, a right-moving dipole (x_i, y_i) and a left-moving dipole (x_j, y_j) interact with a probability

$$f_{ij} = f(x_i, y_i | x_j, y_j) = \frac{\alpha_s^2}{8} \left[\log \left(\frac{(x_i - y_j)^2 (y_i - x_j)^2}{(x_i - x_j)^2 (y_i - y_j)^2} \right) \right]^2. \tag{IV.3}$$

All dipole interactions are assumed to be independent, and the S-matrix element is given by $S = \exp(-\sum_{ij} f_{ij})$.

In this formalism, saturation effects occur only due to multiple scatterings while the evolution of the dipole cascade satisfies the usual BFKL equation. This implies that the formalism is not frame independent and in order to obtain a frame independent formalism such saturation effects must be properly included in the cascade evolution.

Different approaches have been proposed to obtain this. It was noted that the CGC formalism is not complete in the sense that it does not contain any gluon splittings, or gluon number fluctuations. This problem comes from the fact that the Balitsky-JIMWLK (B-JIMWLK) equations[1], which can schematically be written as

$$\partial_Y \langle T^k \rangle = \mathcal{M} \otimes \{ \langle T^k \rangle - \langle T^{k+1} \rangle \}, \tag{IV.4}$$

[1] Throughout this paper, we will only consider the large-N_c version of these equations.

only couples the $k-$dipole scattering amplitude T^k to the $(k+n)$-dipole amplitudes with $n = 0, 1, \ldots$. From the view of target[2] evolution, this means that one includes all gluon merging diagrams, while the gluon splitting diagrams are absent. Gluon splittings are equivalent to dipole splittings, and the dipole model has been used to add fluctuations into the formalism. The modified B-JIMWLK equations then read

$$\partial_Y \langle T^k \rangle = \mathcal{M} \otimes \{\langle T^k \rangle - \langle T^{k+1} \rangle\} + \mathscr{K} \otimes \langle T^{k-1} \rangle, \tag{IV.5}$$

where $\mathscr{K}$ is a kernel representing the fluctuations in the target.

Viewed in the opposite direction, the fluctuation effects in the target correspond to saturation effects in the projectile evolution. Given the form of the modified B-JIMWLK equations above, it may seem natural to include a $2 \to 1$ vertex in the dipole evolution. Such an interpretation has, however, the drawback that it cannot be interpreted as a classical evolution process since the $2 \to 1$ vertex is not positive definite, as was shown by Iancu et al. [19]. In [16] Kozlov et al. calculated directly the $4 \to 2$ gluon merging vertex within the dipole language and were led to the conclusion that one should include a $2 \to 4$ dipole vertex which is composed of a splitting and a swing.

In [15] we included the $2 \to 2$ dipole "swing", in addition to the $1 \to 2$ dipole splitting, in the evolution. If we have two dipoles (x_i, y_i) and (x_j, y_j), the swing will replace them by (x_i, y_j) and (x_j, y_i). The dipole swing can be interpreted in two ways. First, as a way to approximate colour quadrupoles as two independent dipoles formed by the closest charge–anti-charge pairs, in which case the swing is naturally suppressed by N_c^2. Secondly, we may view it as the result of a gluon exchange between the dipoles, which results in a change in the colour flow. In this case the swing would be proportional to α_s^2, which again, compared to $\bar{\alpha}$, is formally suppressed by N_c^2.

The dipole swing is related to the pomeron interactions studied by Bartels and Ryskin [20, 21]. Here a pomeron is interpreted as two gluons in a colour singlet state. In a four gluon system with two singlet pairs, gluon exchange can give a transformation (a "switch" or "swing") $(12) + (34) \to (13) + (24)$, where a parenthesis denotes two gluons in a singlet state.

We note that the swing is here not a vertex in the same sense as the splitting process since, unlike the splitting, the swing is not proportional to dY but rather happens instantaneously. In the MC implementation we assign a "colour" to each dipole and two dipoles are allowed to swing if their colour

[2] In the CGC approach, it is usually assumed that the target is a dense hadron while the projectile is an elementary colour dipole.

indices match[3]. The swing is then determined by the weight

$$P(\text{swing}) \propto \frac{(x_1 - y_1)^2(x_2 - y_2)^2}{(x_1 - y_2)^2(x_2 - y_1)^2}. \quad \text{(IV.6)}$$

Here the two initial dipoles are determined by the coordinates (x_1, y_1) and (x_2, y_2), and the new by (x_1, y_2) and (x_2, y_1). This form favours the formation of small dipoles. It also preserves one of the results in Mueller's original formulation, namely that the total weight for a dipole chain is given by the product $\prod_i \frac{1}{r_i^2}$, where r_i is the size of dipole i and the product runs over all "remaining" dipoles in the cascade.

In our formalism the total number of dipoles does not decrease. For each event, many of the dipoles will not interact and these have to be considered as being virtual. In this case saturation effects do not have to decrease the total number of dipoles but rather only the number of interacting, or "real", dipoles. The dipole swing has this property since it is more likely that two dipoles are replaced by two smaller dipoles, as can easily be seen from (IV.6), and smaller dipoles have smaller interaction probabilities. Thus the number of interacting dipoles will actually decrease, and in pomeron language this means that the swing generates pomeron mergings.

An essential feature of our formalism is that the dipoles in the cascade form connected chains[4], rather than a collection of uncorrelated dipoles, as in a reaction-diffusion type of formalism. A dipole chain cannot end in a gluon, and it is not possible to remove a dipole without reconnecting its neighbors. A generic $2 \to 1$ vertex is therefore not possible in this formalism[5], and the dipole swing gives the simplest process from which one can form closed chains during the evolution.

IV.3 The Toy Models

IV.3.1 The 1+0 dimensional toy model

In this section we will review the toy model which was studied in detail in [12] (see also [13]). This model was first presented by Mueller [3] and it is interesting since, besides having some structural aspects similar to the dipole model, it offers analytical solutions which have been very hard to obtain for the full model.

[3] The number of effective colours is N_c^2 which is the number of possible colour configurations for a given colour–anti-colour pair.

[4] In Mueller's original formulation this is not relevant since there the dipoles evolve truly independently. However, in our implementation of energy-momentum conservation, neighboring dipoles affect each other and it is then relevant that the cascade is formulated as a dipole chain.

[5] The only allowed merging process is in case two neighboring dipoles merge.

The model is defined such that at any rapidity Y the system is specified only by the number of dipoles. The probability to find the system in the n-dipole state at time Y is denoted by $P_n(Y)$. Here transverse coordinates are completely neglected and Y defines the only coordinate in the model.

If we let $\boldsymbol{\mathcal{H}}$ denote the Hamiltonian of the system we have

$$\mathcal{H}_{nm} = \langle m|\boldsymbol{\mathcal{H}}|n\rangle = \mathcal{R}(n)(\delta_{m,n+1} - \delta_{m,n}). \tag{IV.7}$$

$\mathcal{R}(n)$ is so far an unspecified function, which determines the splitting rate of the n dipole state. The probability $P_n(Y)$ evolves according to

$$\partial_Y P_n = \mathcal{H}_{mn} P_m. \tag{IV.8}$$

With S_{nm} we denote the S-matrix for the scattering of two dipole states of n and m dipoles respectively. If we assume that each dipole scatters independently with a probability τ, we have $S_{nm} = (1-\tau)^{nm}$. We here assume that $\tau << 1$ and if this is not the case, one should replace $1-\tau$ by $\exp(-\tau)$. The physical $S-$matrix, $\mathcal{S}$, is obtained by taking an average over all possible events. Using matrix notation we have

$$\mathcal{S}(Y_1 + Y_2) = \boldsymbol{p}^T(Y_1)\boldsymbol{S}\boldsymbol{q}(Y_2). \tag{IV.9}$$

Here $\boldsymbol{p}^T(Y_1) = (P_1(Y_1), P_2(Y_1), \dots)$ is the row vector of the configuration probabilities for the right moving onium (evolved up to Y_1) while $\boldsymbol{q}$ denotes the column vector of configuration probabilities for the left moving onium (evolved up to Y_2).

In (IV.9) we have anticipated that $\mathcal{S}$ depends only on the total rapidity interval $Y_1 + Y_2$, which defines boost invariance. This implies that we have $(\partial_{Y_1} - \partial_{Y_2})\mathcal{S} = 0$, and requiring this in (IV.9) one obtains

$$\boldsymbol{p}^T(Y_1)\boldsymbol{\mathcal{H}}\boldsymbol{S}\boldsymbol{q}(Y_2) - \boldsymbol{p}^T(Y_1)\boldsymbol{S}\boldsymbol{\mathcal{H}}^T\boldsymbol{q}(Y_2) = 0. \tag{IV.10}$$

A sufficient condition for a solution is to require that

$$\boldsymbol{\mathcal{H}}\boldsymbol{S} = \boldsymbol{S}\boldsymbol{\mathcal{H}}^T \tag{IV.11}$$

which means that $\boldsymbol{\mathcal{H}}\boldsymbol{S}$ is symmetric (since $\boldsymbol{S}$ is symmetric). It is now easily seen that the condition (IV.11) requires $\mathcal{R}(n)$ in (IV.7) to be given by

$$\mathcal{R}(n) = c\,(1 - (1-\tau)^n) \tag{IV.12}$$

where c is a constant, $c = \mathcal{R}(1)/\tau$. By rescaling Y, we might as well assume c to equal 1.

IV.3.2 Stochastic evolution with $k \to k+1$ vertices

We note that (IV.12) can be rewritten as

$$\mathcal{R}(n) = c \sum_{k=1}^{n} \binom{n}{k} (-1)^{k-1} \tau^k. \tag{IV.13}$$

This suggests that we can interpret the evolution in terms of $k \to k+1$ transitions with weights $(-1)^k \tau^k$. However, the alternating signs implies that one cannot interpret these vertices in a probabilistic formulation.

We will now show that one can nevertheless interpret the evolution in terms of positive definite $k \to k+1$ vertices. Thus the evolution can still be formulated as a stochastic process, but we will also see that the probabilistic interpretation of the evolution implies that it cannot be reduced into a formalism which describes a system of incoherent particles.

Assume we have a system of n particles X, which we also refer to as dipoles, satisfying the following rules. Each isolated X can emit a new X with a probability per unit time (rapidity) given by τ, *i.e.* we have a reaction $X \to X + X$ which occurs with probability $\tau > 0$. In addition to this, k isolated dipoles can undergo a transition $kX \to (k+1)X$ with probability τ^k.

The evolution of the probabilities $P_n(Y)$ for these X then satisfies

$$\partial_Y P_n(Y) = -\sum_{k=1}^{n} \mathcal{R}^{(n)}_{k\to k+1} P_n(Y) + \sum_{k=1}^{n-1} \mathcal{R}^{(n-1)}_{k\to k+1} P_{n-1}(Y) \tag{IV.14}$$

where $\mathcal{R}^{(n)}_{k\to k+1}$ is the splitting rate for the process where k dipoles are replaced by $k+1$ dipoles in a state containing n dipoles.

Now, the splitting rate $\mathcal{R}^{(n)}_{k\to k+1}$ is not simply given by $\binom{n}{k}\tau^k$ as one could expect naively, but it is instead given by

$$\mathcal{R}^{(n)}_{k\to k+1} = \binom{n}{k} \tau^k (1-\tau)^{n-k}, \tag{IV.15}$$

since for each $k \to k+1$ we must also multiply with the probability that no more than k dipoles were involved in the emission of the new dipole. Obviously, k must run from 1 to n, and summing all contributions we obtain the total splitting rate as

$$\sum_{k=1}^{n} \mathcal{R}^{(n)}_{k\to k+1} = \sum_{k=1}^{n} \binom{n}{k} \tau^k (1-\tau)^{n-k} = (1 - (1-\tau)^n) = \mathcal{R}(n) \tag{IV.16}$$

where $\mathcal{R}(n)$ was defined in (IV.12). The positive definite transition rates in (IV.15) thus give a boost invariant evolution as before. Note also that in this

case the $k \to k+1$ transitions are not universal since they depend on n, unlike the rates in (IV.13). The $k \to k+1$ splitting vertex therefore not only depends on the state of the k emitters, but it does also depend on the rest of the dipoles in the cascade. We will in the forthcoming sections see that the dipole swings give a very similar evolution in the full model.

We also note that the $k \to k+1$ transitions can be made manifest by writing down the Hamiltonian

$$\boldsymbol{\mathcal{H}} = \sum_{k=1}^{\infty} \frac{\tau^k}{k!} (\boldsymbol{N}^{-1/2} \boldsymbol{a}^\dagger - \mathbf{1}) (\boldsymbol{a}^\dagger)^k \boldsymbol{a}^k \prod_{l=k+1}^{\infty} (1-\tau) \sum_{m=l}^{\infty} |m\rangle\langle m|, \tag{IV.17}$$

where $\boldsymbol{a}^\dagger$ and $\boldsymbol{a}$ are dipole creation and annihilation operators respectively, and $\boldsymbol{N} = \boldsymbol{a}^\dagger \boldsymbol{a}$.

IV.3.3 Evolution equations

In this section we will first show that the evolution equations for the scattering amplitudes derived in [12] are described *exactly* by the $k \to k+1$ transitions in (IV.15). We will then go on to point out that there is a fundamental structural reason for the fact that the attempts to interpret the full model evolution given in (IV.5) in a probabilistic manner have run into problems. We will see that it is not possible to interpret this equation using a probabilistic $2 \to 1$ vertex even in the toy model. However, we note that it is not necessary to include a $2 \to 1$ vertex to obtain saturation. In fact any $2 \to n$ vertex where only one of the n dipoles interact also corresponds to a $2 \to 1$ transition, and this will be discussed more later.

First we write the S-matrix given in (IV.9) as

$$\mathcal{S}(Y_1 + Y_2) = \boldsymbol{p}^T(Y_1) \boldsymbol{s_q}(Y_2), \quad \boldsymbol{s_q} \equiv \boldsymbol{S q} \tag{IV.18}$$

where the nth component of the vector $\boldsymbol{s_q}(Y_2)$ is the S-matrix element of a projectile, evolved up to Y_1, made up from n dipoles scattering against a generic target, which is evolved up to Y_2. It is then easy to see that $(\boldsymbol{s_q})_n \equiv \langle s^n \rangle$ satisfies the following evolution equation [12]

$$\partial_Y \langle s^n \rangle = \mathcal{R}(n) \{ \langle s^{n+1} \rangle - \langle s^n \rangle \}. \tag{IV.19}$$

Using the relation $s = 1 - t$, where t denotes the scattering amplitude, one can similarly derive the equations obeyed by $\langle t^n \rangle$. Since τ is assumed to be small, one can expand $\mathcal{R}(n)$ in each equation and drop contributions which are negligible in all regimes (dilute and dense systems). Doing this, the authors in [12] arrived at the following evolution equations for $\langle t \rangle$, $\langle t^2 \rangle$ and

$\langle t^3\rangle$,

$$\partial_Y\langle t\rangle = \langle t\rangle - \langle t^2\rangle, \tag{IV.20}$$
$$\partial_Y\langle t^2\rangle = 2(\langle t^2\rangle - \langle t^3\rangle) + \tau\langle t(1-t)^2\rangle, \tag{IV.21}$$
$$\partial_Y\langle t^3\rangle = 3(\langle t^3\rangle - \langle t^4\rangle) + 3\tau\langle t^2(1-t)^2\rangle + \tau^2\langle t(1-t)^3\rangle. \tag{IV.22}$$

If one neglects all terms proportional to τ, then it is seen that the resulting hierarchy corresponds to the large N_c version of the B-JIMWLK hierarchy.

Let us now see how equations (IV.20)-(IV.22) arise from the transition rates $\mathcal{R}^{(n)}_{k\to k+1}$. The evolution of the S-matrix elements are given by

$$\partial_Y\langle s\rangle = \mathcal{R}^{(1)}_{1\to 2}\{\langle s^2\rangle - \langle s\rangle\}, \tag{IV.23}$$
$$\partial_Y\langle s^2\rangle = (\mathcal{R}^{(2)}_{1\to 2} + \mathcal{R}^{(2)}_{2\to 3})\{\langle s^3\rangle - \langle s^2\rangle\}, \tag{IV.24}$$
$$\partial_Y\langle s^3\rangle = (\mathcal{R}^{(3)}_{1\to 2} + \mathcal{R}^{(3)}_{2\to 3} + \mathcal{R}^{(3)}_{3\to 4})\{\langle s^4\rangle - \langle s^3\rangle\}. \tag{IV.25}$$

It is then straightforward to obtain the following equations for the scattering amplitudes

$$\partial_Y\langle t\rangle = \mathcal{R}^{(1)}_{1\to 2}\{\langle t\rangle - \langle t^2\rangle\} = \langle t\rangle - \langle t^2\rangle, \tag{IV.26}$$
$$\begin{aligned}\partial_Y\langle t^2\rangle &= 2\mathcal{R}^{(1)}_{1\to 2}(\langle t\rangle - \langle t^2\rangle) - \mathcal{R}^{(2)}_{1\to 2}\langle t(1-t)^2\rangle - \mathcal{R}^{(2)}_{2\to 3}\langle t(1-t)^2\rangle \\ &= 2(\langle t^2\rangle - \langle t^3\rangle) + 2\tau\langle t(1-t)^2\rangle - \tau\langle t(1-t)^2\rangle.\end{aligned} \tag{IV.27}$$

We indeed see that the first equation is equal to (IV.20) and that the second equation is equal to (IV.21). It is also straightforward to see that the equation for $\langle t^3\rangle$ agrees with (IV.22).

Next, we comment on the structure of the equation given in (IV.5). Assume we wish to view the process as a stochastic evolution with a $1\to 2$ splitting vertex, $f_{1\to 2}$, and a $2\to 1$ merging vertex, $k_{2\to 1}$. We here assume the total splitting rate to be the incoherent sum of the individual splitting rates. For the evolution of the $2-$dipole state we have

$$\partial_Y\langle s^2\rangle = f^{(2)}_{1\to 2}\{\langle s^3\rangle - \langle s^2\rangle\} + k^{(2)}_{2\to 1}\{\langle s\rangle - \langle s^2\rangle\} \tag{IV.28}$$

which gives

$$\begin{aligned}\partial_Y\langle t^2\rangle &= 2f^{(1)}_{1\to 2}\{\langle t\rangle - \langle t^2\rangle\} + k^{(2)}_{2\to 1}\langle t(1-t)\rangle - f^{(2)}_{1\to 2}\langle t(1-t)^2\rangle \\ &= (2f^{(1)}_{1\to 2} - f^{(2)}_{1\to 2} + k^{(2)}_{2\to 1})\langle t\rangle + \\ &+ (-2f^{(1)}_{1\to 2} + 2f^{(2)}_{1\to 2} - k^{(2)}_{2\to 1})\langle t^2\rangle - f^{(2)}_{1\to 2}\langle t^3\rangle \\ &= k^{(2)}_{2\to 1}\langle t\rangle + (f^{(2)}_{1\to 2} - k^{(2)}_{2\to 1})\langle t^2\rangle - f^{(2)}_{1\to 2}\langle t^3\rangle.\end{aligned} \tag{IV.29}$$

We thus see that the $2 \to 1$ contribution not only generates the "fluctuation" term, $k^{(2)}_{2\to 1}\langle t\rangle$, but it does also modify the $\langle t^2\rangle$ term. If this term is to be unaffected by the additional vertex, as in (IV.5), then we have to set $k^{(2)}_{2\to 1} = 0$. This is actually very similar to what happens in the full model. In that case the integral over the proposed $2 \to 1$ vertex has to be zero, which implies that the vertex cannot be positive definite, as was noted in [19]. We can also try to add another vertex such that the total contribution to the $\langle t^2\rangle$ term cancels. Assume for example the existence of an additional $2 \to 0$ vertex $g_{2\to 0}$. We then get

$$\partial_Y\langle t^2\rangle = (k^{(2)}_{2\to 1} + 2g^{(2)}_{2\to 0})\langle t\rangle + (f^{(2)}_{1\to 2} - k^{(2)}_{2\to 1} - g^{(2)}_{2\to 0})\langle t^2\rangle - f^{(2)}_{1\to 2}\langle t^3\rangle \quad \text{(IV.30)}$$

from which we conclude that

$$k^{(2)}_{2\to 1} + g^{(2)}_{2\to 0} = 0 \quad \text{(IV.31)}$$

which means that either $k^{(2)}_{2\to 1}$ or $g^{(2)}_{2\to 0}$ has to be negative. Thus we conclude that this approach has big problems, as one must choose $k^{(2)}_{2\to 1}$ either to be 0, or it must be negative, which means that one cannot obtain a probabilistic formulation.

IV.3.4 The 1+1 dimensional toy model

A somewhat more complicated 1+1 dimensional model is presented in [18]. The structure of this model is very similar to the 1+0 dimensional model, but the difference is that this time a dipole state is not only specified by the total number of dipoles, but it also depends on the distribution of these dipoles along some additional transverse axis.

We denote the position of a dipole along this axis with x_i, and the generic n-dipole state is denoted $|\{x_i\}\rangle = |x_1, \ldots, x_n\rangle$. The assumption in [18] is that the dipole state evolves *only* by the addition of a single new dipole at some position x_{n+1}. In that case the frame independence equation in (IV.11) can easily be solved, and the simplest solution for the total splitting rate $\mathcal{R}_i(\{n\})$ is given by [18]

$$\mathcal{R}(\{x_i\} \to \{x_i\} + x_{n+1}) = \frac{1 - \prod_{i=1}^{n}(1 - \tau(x_i|x_{n+1}))}{\tau}. \quad \text{(IV.32)}$$

Here τ is a constant which can, by a redefinition of Y, set to be equal to 1.

We now show that the evolution can once again be formulated as a probabilistic process in terms of coherent $k \to k+1$ transitions as in sec IV.3.2. In this case we assume we have a system of dipoles, X_i, which live on a one dimensional spatial axis. We assume this axis to represent the position of the

"point-like" dipoles. This axis is assumed to be continuous, so that the index i actually represents a continuous label x_i. An isolated dipole X_i can then emit another dipole X_j at position x_j with a probability $\tau_{ij} = \tau(x_i|x_j)$. However, in the presence of more than one X_i, the new X_j can also be emitted coherently from several dipoles with a probability given by the product of the individual emission probabilities. For a system of n dipoles located at positions $x_1, \ldots, x_n$, the total $k \to k+1$ splitting rates $\mathcal{R}^{(n)}_{k\to k+1}(\{x_i\} \to \{x_i\} + x_{n+1})$ are then given by

$$\mathcal{R}^{(n)}_{k\to k+1}(\{x_i\} \to \{x_i\} + x_{n+1}) = \frac{1}{k!} \sum_{i_1 \neq \cdots \neq i_k}^{n} \tau_{i_1,n+1} \ldots \tau_{i_k,n+1} \prod_{m \neq 1,\ldots,k}^{n} (1 - \tau_{i_m,n+1}), \tag{IV.33}$$

and their sum satisfies

$$\sum_{k=1}^{n} \mathcal{R}^{(n)}_{k\to k+1}(\{x_i\} \to \{x_i\} + x_{n+1}) = 1 - \prod_{i=1}^{n}(1 - \tau_{i,n+1}). \tag{IV.34}$$

which is equal to (IV.32). Note that once again the positive definite splitting rates do not only depend on the state of the emitting dipoles, but also on the state of the other dipoles in the cascade. This is unavoidable if one wants to obtain a probabilistic evolution.

The $k \to k+1$ splitting rates in (IV.33) are very similar in structure to the processes generated by the dipole swing, to be discussed in the forthcoming sections. Anticipating the discussion there, we can interpret (IV.33) as a process where the newly produced dipoles swing multiply with the rest of the dipoles in the cascade (a concrete example of this is shown in fig IV.5). Note that in the toy models both the splitting and the scatterings of the dipoles are determined by the quantities τ_{ij}. If we would assume that these also determine the swing probability, then the $k \to k+1$ splitting rates in (IV.33) would describe processes where the newly produced dipole i swings with $k-1$ dipoles from the cascade, and the factor $\prod_j(1 - \tau_{ij})$ could then be interpreted as the probability that i swings with no more than $k-1$ dipoles.

One difficulty is, however, that the swing in its form in the full model cannot really provide saturation in the toy models since the dipoles have no size here [6]. This follows from the fact that both toy models have trivial topologies, in the sense that the dipole state is assumed to evolve only by the addition of a new dipole without changing the emitting state. In the toy models saturation occurs because k dipoles emit a single dipole with the same strength as

[6] In [18], the spatial axis was interpreted as being related to the dipole size while we feel a more close analogy is to interpret it as a spatial coordinate where dipoles of some fixed size live. Irrespective of the interpretation, however, direct comparison with the full model is made difficult by the assumption that the toy model state only evolves by the addition of a single dipole.

a single dipole. In our implementation of the dipole swing however, saturation occurs because the swing decreases the sizes of the dipoles, and smaller dipoles have a smaller probability to interact.

IV.4 Evolution in the full model

We will here argue that the evolution in the full model also can be formulated as a probabilistic process in terms of $k \to k+1$ transitions.

The S-matrix is in the full model given by

$$\begin{aligned} S_Y &= \sum_{N,M} P_N(Y_0) P_M(Y - Y_0) \prod_{i=1}^{N} \prod_{j=1}^{M} \Big(1 - f(x_i, y_i | x_j, y_j) \Big). \\ &= \left\langle \prod_{i=1}^{N} \prod_{j=1}^{M} (1 - f_{ij}) \right\rangle. \end{aligned} \tag{IV.35}$$

where f_{ij} is given by (IV.3).

Let us consider the evolution initiated by a pair of oppositely moving $q\bar{q}$ pairs. We then consider generic dipole states $\mathscr{A}_N$, containing $N-1$ gluons, which at each rapidity step can evolve into states $\mathscr{A}_{N+1}$ containing N gluons. The splitting rate is denoted $\mathcal{R}(\mathscr{A}_N \to \mathscr{A}_{N+1})$.

The scattering between the states $\mathscr{A}_N$ and $\mathscr{B}_M$ is then frame independent if

$$\begin{aligned} &\sum_{\mathscr{A}_{N+1}} \int_z \mathcal{R}(\mathscr{A}_N \to \mathscr{A}_{N+1}) \Big\{ 1 - \prod_{j \in \mathscr{B}_M} \{ 1 - (\sum_{i \in \mathscr{A}_{N+1} \setminus \mathscr{A}_N} - \sum_{i \in \mathscr{A}_N \setminus \mathscr{A}_{N+1}}) f(i|j) \} \Big\} = \\ &\sum_{\mathscr{B}_{M+1}} \int_z \mathcal{R}(\mathscr{B}_M \to \mathscr{B}_{M+1}) \Big\{ 1 - \prod_{i \in \mathscr{A}_N} \{ 1 - (\sum_{j \in \mathscr{B}_{M+1} \setminus \mathscr{B}_M} - \sum_{j \in \mathscr{B}_M \setminus \mathscr{B}_{M+1}}) f(i|j) \} \Big\}. \end{aligned} \tag{IV.36}$$

The notations in this equation are as follows. The integral $\int_z$ denotes the integration over the transverse position of the Nth emitted gluon. In $\prod_{j \in \mathscr{B}_M}$, the index j runs over all dipoles in the state $\mathscr{B}_M$. The set denoted by $\mathscr{A}_{N+1} \setminus \mathscr{A}_N$ consists of those new dipoles produced in the last step of the evolution. Similarly, $\mathscr{A}_N \setminus \mathscr{A}_{N+1}$ denotes the set of all dipoles which are present in $\mathscr{A}_N$, but not in $\mathscr{A}_{N+1}$, *i.e.* those dipoles which were removed from the cascade in the last step of the evolution. Finally, $f(i|j)$ stands for the scattering amplitude between the dipoles i and j, *i.e.* the expression f_{ij} in (IV.3) and (IV.35). The sum $\sum_{\mathscr{A}_{N+1}}$ is over all N gluon states which can be reached from $\mathscr{A}_N$ in one step.

In the toy model analogy, the difference $\sum_{i\in\mathscr{A}_{N+1}\setminus\mathscr{A}_N} - \sum_{i\in\mathscr{A}_N\setminus\mathscr{A}_{N+1}}$ consists of only the newly produced dipole, i, since all others dipoles are assumed to be unaffected by the evolution. In that case eq (IV.36) reduces to

$$\begin{aligned}&\sum_i \mathcal{R}(\mathscr{A}_N \to \mathscr{A}_N + i)\left\{1 - \prod_{j\in\mathscr{B}_M}(1 - f(i|j))\right\}\\ &= \sum_i \mathcal{R}(\mathscr{B}_M \to \mathscr{B}_M + i)\left\{1 - \prod_{j\in\mathscr{A}_M}(1 - f(i|j))\right\}.\end{aligned} \tag{IV.37}$$

The most simple solution is given by

$$\mathcal{R}(\mathscr{A}_N \to \mathscr{A}_N + i) = 1 - \prod_{j\in\mathscr{A}_N}(1 - f(i|j)), \tag{IV.38}$$

which we recognize from (IV.32). We will now see that the evolution in the full model can be formulated probabilistically in terms of $k \to k+1$ vertices as in the toy models. At first we will formulate the evolution as in eq (IV.13) which implies that the $2 \to 3$ transition will appear to have negative sign. However, we know from above how to treat these signs, and thus give the evolution a probabilistic interpretation. We will also see how one can interpret these vertices in terms of the dipole swing.

To this end, we consider first the situation where $N = 2$ and $M = 1$. The state $\mathscr{A}_2$ must consist of two connected dipoles since we know that a single, isolated dipole (the state $\mathscr{A}_1$) evolves by a dipole splitting (assuming the evolution is initiated by a single $q\bar{q}$ pair). We then denote the two dipoles in $\mathscr{A}_2$ with a and b, and the single dipole in the state $\mathscr{B}_1$ is denoted by l. We can then write (IV.36) as

$$\begin{aligned}\sum_{\mathscr{A}_3}\int_z \mathcal{R}(a,b \to \mathscr{A}_3)\Big(\sum_{i\in\mathscr{A}_3\setminus\mathscr{A}_2} - \sum_{i\in\mathscr{A}_2\setminus\mathscr{A}_3}\Big) f(i|l) = \int_z \mathcal{R}(l \to (l_1,z)+(z,l_2)) \times\\ \times\Big(\mathscr{F}(l,a,z) + \mathscr{F}(l,b,z) - \mathscr{F}(l,a,z)\mathscr{F}(l,b,z)\Big)\end{aligned} \tag{IV.39}$$

where

$$\mathscr{F}(l,a,z) = f(l_1,z|a) + f(z,l_2|a) - f(l|a). \tag{IV.40}$$

Here l_1 and l_2 denote the transverse positions of the partons of dipole l. From studying the case $N = M = 1$ (the scattering between two elementary dipoles), we know that each isolated dipole evolves by a $1 \to 2$ splitting. We therefore

write $\sum_{\mathscr{A}_3} \mathcal{R}(a,b \to \mathscr{A}_3)$ as

$$\sum_{\mathscr{A}_3} \mathcal{R}(a,b \to \mathscr{A}_3) = \mathcal{R}^{(1)}(a \to (a_1,z)+(z,a_2)) + \mathcal{R}^{(1)}(b \to (b_1,z)+(z,b_2)) + \sum_{\mathscr{A}_3^{(2)}} \mathcal{R}^{(2)}(a,b \to \mathscr{A}_3^{(2)}). \tag{IV.41}$$

Here $\mathscr{A}_3^{(2)}$ denotes the set of all 2 gluon states which can be reached from $\mathscr{A}_2 = \{a,b\}$ via the vertex $\mathcal{R}^{(2)}$. Now, we know from [11] that the incoherent contributions, $\mathcal{R}^{(1)}$, above are equal to the first order contributions (in $f(i|j)$) in (IV.39). Thus we are left with the equation

$$\sum_{\mathscr{A}_3^{(2)}} \int_z \mathcal{R}^{(2)}(a,b \to \mathscr{A}_3^{(2)}) \Big(\sum_{i \in \mathscr{A}_3^{(2)} \setminus \mathscr{A}_2} - \sum_{i \in \mathscr{A}_1 \setminus \mathscr{A}_3^{(2)}} \Big) f(i|l) = = -\int_z \mathcal{R}(l \to (l_1,z)+(z,l_2)) \Big(\mathscr{F}(l,a,z) \cdot \mathscr{F}(l,b,z) \Big). \tag{IV.42}$$

In the toy model, where the dipole state evolves by the addition of a single dipole i only, we know that $\mathcal{R}^{(2)}(a,b \to \mathscr{A}_3^{(2)}) = -f(i|a)f(i|b)$ (in case we use the formulation in (IV.13)). Indeed in that case we see that both sides in (IV.42) equals $-\sum_i f(i|a)f(i|b)f(i|l)$. It is then clear that we must have a $2 \to 3$ transition.

By similarly studying the case where $N = 3$ and $M = 1$, we would conclude that we need an additional $3 \to 4$ dipole vertex and so on. We are thus led to a picture where the dipole state evolves by $k \to k+1$ transitions. If these transitions can be generated by combining the dipole splitting with the dipole swing, as we will argue in the next sections, we furthermore obtain a probabilistic interpretation of the evolution, as was discussed in the end of sec IV.3.4.

Before we going on, we also note that care has to be taken to the fact that the frame independence equation in (IV.36) may contain divergences. In the original dipole model, these divergences arise from the dipole splitting kernel in (IV.1), but the frame independence equation is still finite since the expressions in the brackets in (IV.36) vanish at these singular points. This is both due to the topology of the dipole splitting and also to the colour transparency of small dipoles. Any new vertex to be introduced into the model must retain this property since otherwise equation (IV.36) would not make any sense.

IV.5 The Colour Topology of the Evolution

Although we are not able to explicitely write down the splitting rate $\mathcal{R}^{(3)}(a, b \to \mathscr{A}_3^{(2)})$ in the full model, we will in this section argue that the correct topology of the evolution is the one induced by the dipole swing.

We first write eq (IV.36) in Mueller's original formulation,

$$\sum_{i=1}^{N} \int_z \mathcal{M}(i|z) \left\{ 1 - \prod_{j=1}^{M} (1 - (\sum_{k \in new} - \sum_{k \in old}) f(k|j)) \right\} =$$
$$= \sum_{i=1}^{M} \int_z \mathcal{M}(i|z) \left\{ 1 - \prod_{j=1}^{N} (1 - (\sum_{k \in new} - \sum_{k \in old}) f(k|j)) \right\}. \qquad \text{(IV.43)}$$

Here $\mathcal{M}(i|z)$ is the usual dipole kernel in (IV.1) for a dipole i emitting a gluon at position z, and for simplicity we denote with $\sum_{k \in new(old)}$ the sum over the dipoles produced (destroyed) in the last step.

In case the newly produced dipoles only scatter against one target dipole, eq (IV.43) linearizes, and in that case the equality is known to hold [11]. Note that this case does not restrict us to one pomeron exchange, it is only the dipoles produced in the last step which should scatter against a single dipole. There may be still be several scatterings between dipoles produced earlier, with the restriction that each dipole only scatters once. In such events, the colour topology may be described by open chains stretching between the target and the projectile. An example is shown in fig IV.1. Here, the simple $1 \to 2$ splitting is sufficient for producing all possible colour configurations.

In case the newly produced dipoles scatter off two or more target dipoles, however, more complicated topologies are formed, and the simple $1 \to 2$ splitting is not sufficient anymore. Let us first consider the case where each dipole is restricted to single scattering only. In this case, the newly produced two dipoles can at most scatter off two target dipoles. An example is shown in fig IV.2 where three different colour configurations are formed (there are three more configurations which can be formed by reversing the colour flow in each line). Here two right-moving dipoles (x_1, y_1) and (x_2, y_2), are connected to a single left-moving dipole (u, v). With the restriction that each dipole scatters only once, the dipole (u, v) can obviously not be connected to more than two oppositely moving dipoles. In this case one can produce all colour configurations by combining the dipole splitting with only one swing. This is in agreement with the findings in [16]. In fig IV.3 we show how the three configurations in fig IV.2 can be generated from a dipole split and one swing, by first forming the configuration in fig IV.3(A). Figure IV.3 can be compared to eq (IV.42) where the right hand side of that equation describes the evolution and the scattering of the dipole (u, v) (l in (IV.42)). The vertex $\mathcal{R}^{(2)}$ on the left

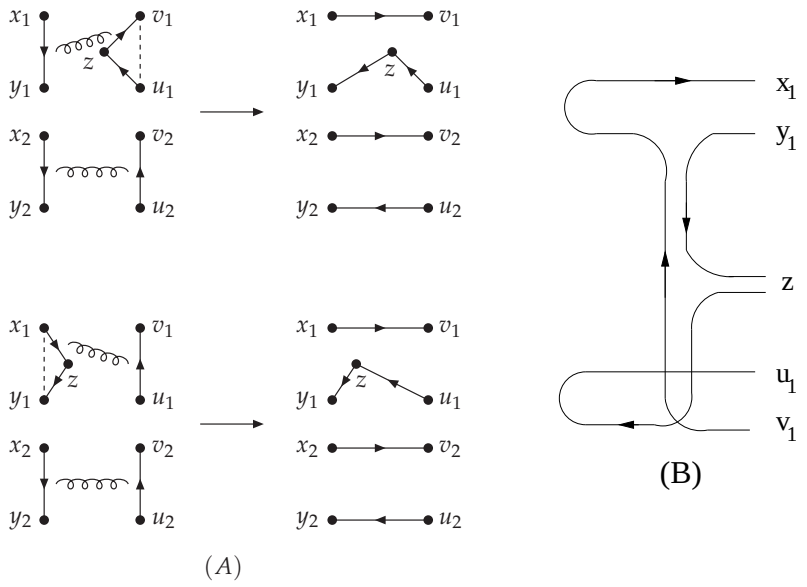

Figure IV.1: A process where the newly produced dipoles exchange only a single gluon with the target. In this case the colour correlations can be generated by the dipole splitting only. Here the position of z is integrated over and is therefore not fixed, and we only show one possible colour flow. Note that each interaction implies a change in the colour flow, which goes from colour to anticolour as indicated by the arrows. It is not important whether there are also other interactions or not. In fig (A) we assume an additional interaction between (x_2, y_2) and (u_2, v_2). In fig (B) we show the same colour flow in the corresponding Feynman diagram.

hand side would then correspond to the diagrams showing the evolution of (x_1, y_1) and (x_2, y_2) into the three dipoles (x_1, z), (z, y_2) and (x_2, y_1).

We conclude that in an approximation where multiple scatterings are allowed, but with the restriction that *each dipole scatters only once*, the maximal correlation induced between the dipoles is that between a pair, and such a correlation can be generated by a simple swing.

Actually, in this approximation, explicit frame independence in zero transverse dimensions can be achieved by including a $2 \to 1$ vertex in addition to the usual $1 \to 2$ splitting. This reflects the fact that the maximal correlation induced is that between a pair of dipoles. Note also that, in the situation described above, it is always only one out of the three dipoles produced via the combination of the dipole splitting and the swing which interacts with the target. In that sense the swing corresponds to a $2 \to 1$ transition. We can thus obtain an effective $2 \to 1$ transition without actually decreasing the number

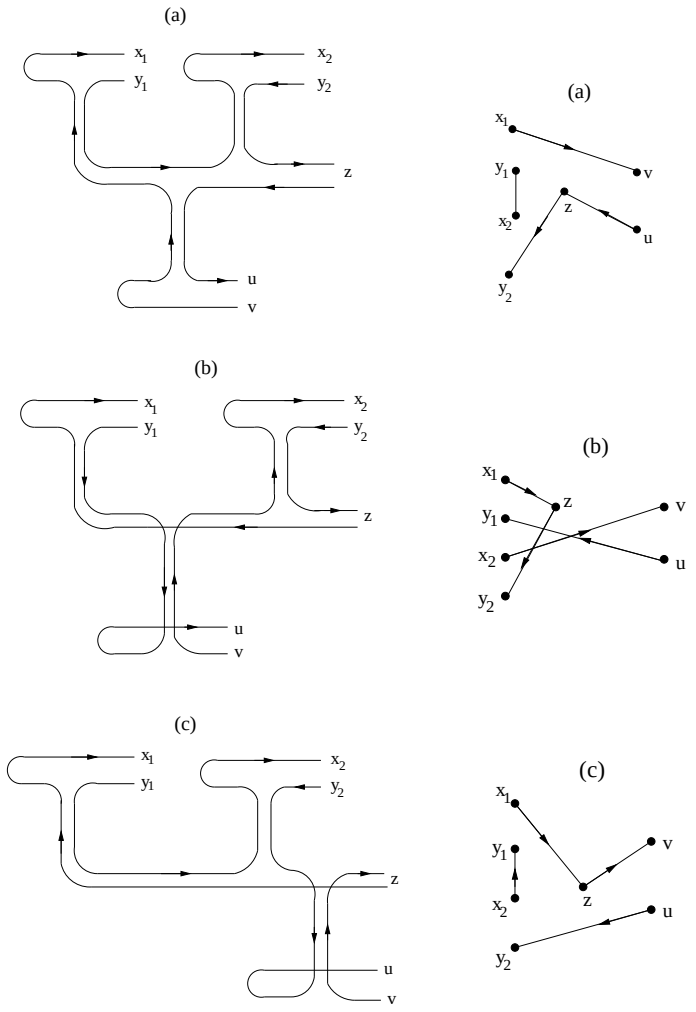

Figure IV.2: The colour flow in a process where two right-moving dipoles (x_1, y_1) and (x_2, y_2) are linked to a single left-moving dipole (u, v). Three different configurations, (a), (b) and (c), are shown.

of dipoles.

If a single dipole can *scatter multiply*, one swing will not be enough. In this case one dipole can for example split into two new dipoles, and these two dipoles can then interact with more than two target dipoles, inducing higher order correlations. Before going on, we note that there is an ambiguity in the

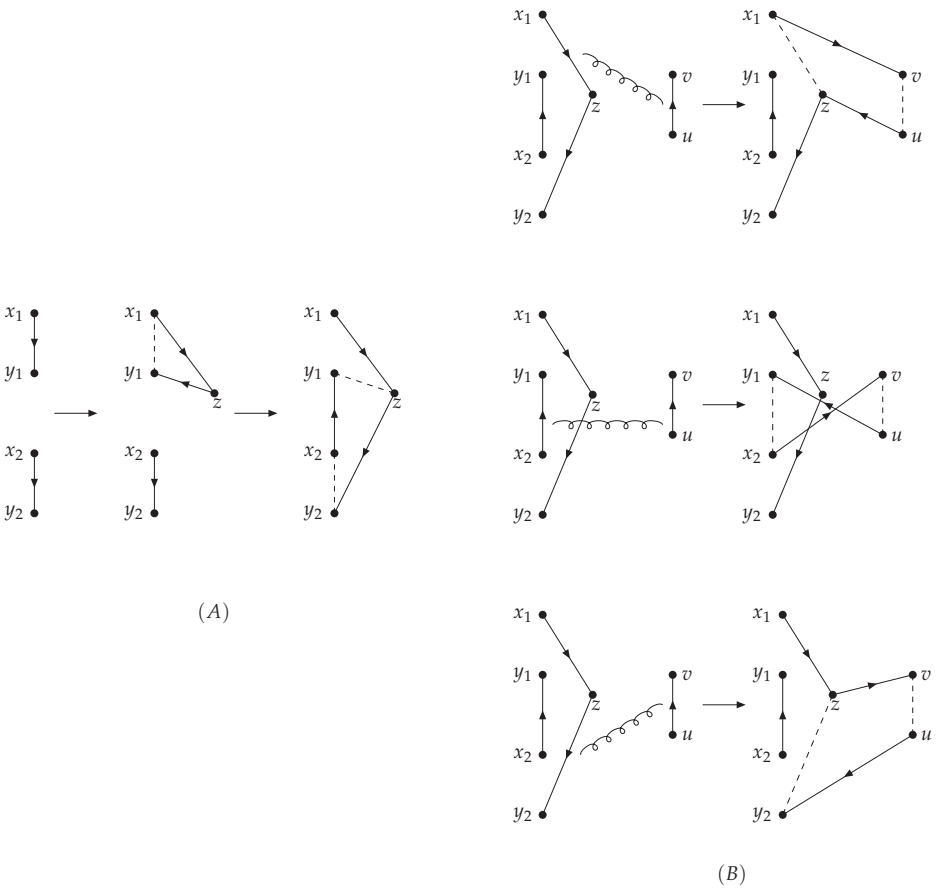

Figure IV.3: The three configurations marked by (a), (b) and (c) in fig IV.2 can all be generated when the dipole (u, v) interacts with one of three dipoles from the configuration shown in fig (A). This is illustrated in fig (B). As illustrated, the configuration in fig (A) can in turn be generated via the dipole swing.

statement that one dipole scatters multiply. Since each scattering implies a recoupling of the colour flow, a dipole which interacts is replaced by a new dipole. What we rather mean here is that the partons of the dipole can exchange multiple gluons.

Consider the diagrams shown in fig IV.4. Here a single left-moving dipole (u, v) is linked to three right-moving dipoles (x_1, y_1), (x_2, y_2) and (x_3, y_3), as shown in the figure. The two colour configurations shown in the figure can then be generated as illustrated in fig IV.5: First one generates the configuration $\{(x_3, y_2), (x_2, y_1), (x_1, z), (z, y_3)\}$ by combining a dipole splitting with two

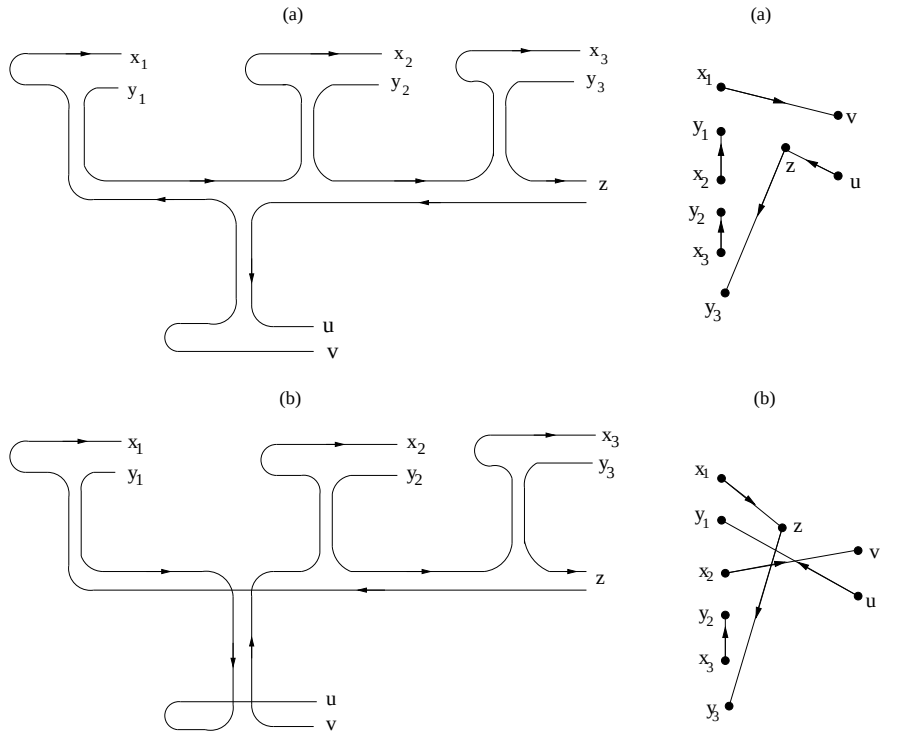

Figure IV.4: The colour flow in a process where three right-moving dipoles (x_1, y_1), (x_2, y_2) and (x_3, y_3) interact with a single left-moving dipole (u, v) after the emission of a gluon located at z. For simplicity, we only show two, marked (a) and (b), out of the four possible configurations.

swings as shown in fig IV.5(A) (this is obviously not the only process from which this final configuration can be generated). One of the four dipoles in this state can then collide with the dipole (u, v). If for example (u, v) collides with (x_1, z), the configuration marked by (a) in fig IV.4 is produced.

The same process can also be viewed as an evolution of the dipole (u, v), which then splits into (u, z) and (z, v), and fig IV.5 shows also how the two configurations in fig IV.4 can be generated when the dipoles (u, z) and (z, v) interact with $(x_1, y_1), (x_2, y_2)$ and (x_3, y_3) exchanging now 3 gluons (fig IV.5(C)). Thus at least one of the dipoles (u, z) and (z, v) must scatter multiply in this case, since it would otherwise be impossible to generate the necessary colour correlations. As remarked in [12], the evolution equations in sec IV.3.3 actually describe such events where a newly produced dipole scatters multiply. We can also compare the processes in fig IV.5 to eq (IV.36) where one

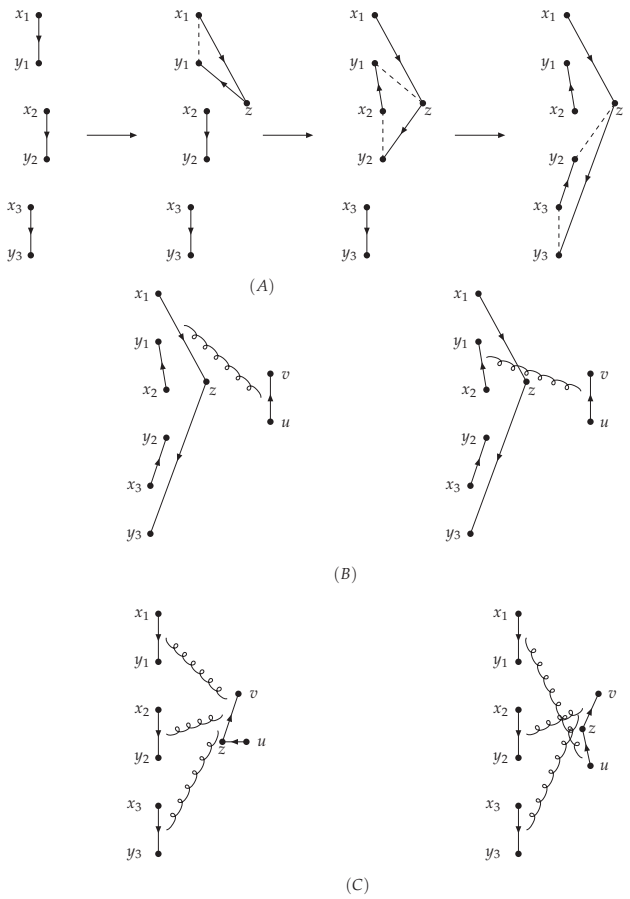

Figure IV.5: The configurations marked by (a) and (b) in figure IV.4 can be generated when the dipole (u, v) interacts with different dipoles from the configuration in fig (A), as illustrated in fig (B). There are two more configurations which can be obtained when (u, v) interacts with the other two dipoles in fig (A). In fig (C) we show how the same configurations can be generated when the evolution is instead put into the dipole (u, v).

side of the equation describes the multiple scatterings of the dipoles (u, z) and (v, z), while the other side describes how the 3-dipole system evolves into a 4-dipole system which then exchanges a single gluon with (u, v).

IV.5.1 Generating arbitrary correlations using at most $N-1$ swings

We might then expect that the correlation induced by the scattering between a single left-moving dipole and k right-moving dipoles can be generated by a splitting followed by $k-1$ swings in the right-moving system. Note that such a process gives a $k \to k+1$ transition. In the example above this was possible since we were able to form the configuration $\{(x_3, y_2), (x_2, y_1), (x_1, z), (z, y_3)\}$ by combining one splitting with two swings. This will always be possible if, given an arbitrary set of N dipoles we always can generate all possible $(N+1)$-dipole states, by combining a splitting with at most $N-1$ dipole swings. We will below argue that this is indeed the case. In case we have N spatially disconnected dipoles, the proof is easy. However, starting from a single $q\bar{q}$ pair, the evolution does not generate spatially disconnected dipoles, and in this case the result is a conjecture.

Spatially disconnected dipoles

As a warm up, we first show the statement in case we have N spatially disconnected dipoles $\{(x_i, y_i)\}_{i=1}^N$. We then wish to evolve this state into some arbitrary $N+1$ dipole state,

$$\prod_i (x_i, y_i) \to (x_k, z)(z, y_j) \prod_{i \neq k, p(i) \neq j} (x_i, y_{p(i)}), \tag{IV.44}$$

using at most $N-1$ dipole swings. Here $p(i)$ is a permutation of $i = 1, \ldots, N$. We first start by emitting gluon z from the dipole (x_k, y_k),

$$\prod_i (x_i, y_i) \to (x_k, z)(z, y_k) \prod_{i \neq k} (x_i, y_i). \tag{IV.45}$$

The result then follows if we can show that, for an arbitrary permutation $p(i)$, we can with $N-1$ swings always make the transformation

$$\prod_{i=1}^N (x_i, y_i) \to \prod_{i=1}^N (x_i, y_{p(i)}). \tag{IV.46}$$

To this end, we perform the following swings in the indicated order,

1 $(x_N, y_N)(x_{p(N)}, y_{p(N)}) \to (x_N, y_{p(N)})(x_{p(N)}, y_N)$

2 $(x_{N-1}, y_{N-1})(x_{p(N-1)}, y_{p(N-1)}) \to (x_{N-1}, y_{p(N-1)})(x_{p(N-1)}, y_{N-1})$

etc. Then, after at most $N-2$ swings we are either finished, or we have

$$(x_1, y_{p(2)})(x_2, y_{p(1)}) \prod_{i=3}^N (x_i, y_{p(i)}). \tag{IV.47}$$

We then need only one more swing $(x_1, y_{p(2)})(x_2, y_{p(1)}) \to (x_1, y_{p(1)})(x_2, y_{p(2)})$, and so after at most $N-1$ swings we are finished.

The problem is that generally the dipoles are not spatially independent, and one then has to be careful in performing swings, since they might generate zero size dipoles, *i.e.* colour singlet gluons which cannot be allowed.

Dipole states initiated by a $q\bar{q}$ dipole

Representation of the dipole states and the swing in terms of permutations

Consider the evolution initiated by a $q\bar{q}$ colour dipole. In the original formulation of the dipole model, the dipole state at each rapidity Y consists of an open chain, $\mathcal{C}$, of colour dipoles which are linked together via the gluons. Note the dual role played by the gluons and the dipoles, each gluon links together two dipoles, and each dipole links together two gluons.

The inclusion of the dipole swing generates closed dipole loops, $\mathcal{L}$, in addition to the open chain, $\mathcal{C}$. The swing induces the transformations

$$\mathcal{C} \leftrightarrow \mathcal{C}' + \mathcal{L}, \tag{IV.48}$$

$$\mathcal{L} \leftrightarrow \mathcal{L}_1 + \mathcal{L}_2. \tag{IV.49}$$

In what follows, we will denote each N-dipole state as an element of the permutation group $\mathcal{P}_N$. For simplicity we suppress the transverse coordinates in the notation, and each gluon is denoted by a number indicating the order in which it was emitted, the first emitted gluon is denoted 1, the second 2 and so on. The initial $q\bar{q}$ pair is simply denoted by 0. A generic N-dipole state containing $N-1$ gluons, with $k_0 - 1$ gluons in the open chain, and the rest in m closed loops each containing k_i gluons, is denoted

$$\mathscr{A}_N = (0\,\alpha_1 \dots \alpha_{k_0-1})(\alpha_{k_0} \dots \alpha_{k_0+k_1-1}) \dots (\alpha_{\sum_{i=0}^{m-1} k_i} \dots \alpha_{N-1}) \in \mathcal{P}_N. \tag{IV.50}$$

Here $\{\alpha_i\}_{i=1}^{N-1}$ is a permutation of $i = 1, \dots, N-1$. The generic dipole state[7] in (IV.50) is illustrated in IV.6. Each arrow indicates the colour flow, and in the group theoretical notation in (IV.50), each gluon α_i points to the gluon to the right of it. The open chain is always represented by the cycle containing the element 0 (the $q\bar{q}$ pair), and each cycle in (IV.50) corresponds to a colour singlet. Since we cannot have colour singlet gluons, the numbers α_i cannot appear as 1-cycles. The only 1-cycle allowed is (0), which corresponds to a dipole formed by the initial $q\bar{q}$ pair.

[7] Note the difference in notation as compared to the previous sections; with (x, y) we always mean a single dipole spanned between the charge–anti-charge pair located at transverse positions x and y respectively.

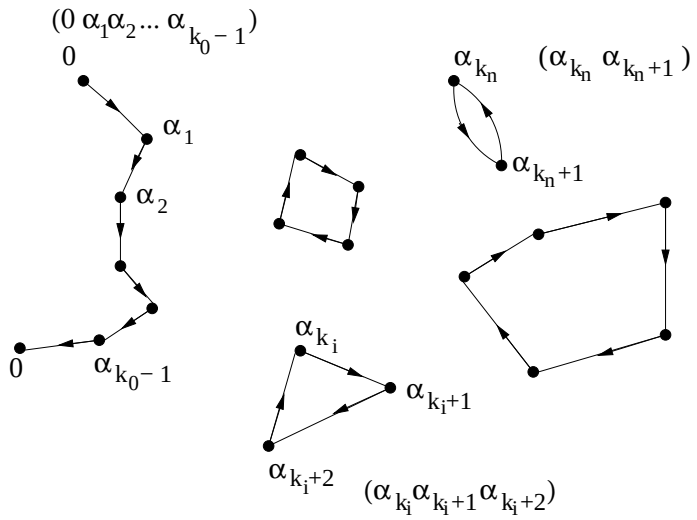

Figure IV.6: A generic dipole state formed after a rapidity evolution of Y, starting from a $q\bar{q}$ pair. The initial quark and the antiquark are both denoted by 0 while the gluons are denoted by α_i as explained in the text and in eq (IV.50). The arrows on the dipoles indicate the colour flow, which goes from colour to anti-colour as before.

Every element in the group $\mathcal{P}_N$ belongs to a certain class, which is determined by the cyclic structure of the element. The group $\mathcal{P}_4$ has 5 classes: 1111, 211, 31, 22 and 4. Here each n-cycle is represented by the number n. The state $\mathscr{A}_N$ in (IV.50) belongs to the class $k_0\, k_1 \ldots k_m$. The identity element is the permutation which takes every number onto itself, and has the cyclic structure $11\ldots1$. A swing operation can be represented by an element of $\mathcal{P}_N$ which consist of one 2-cycle and $(N-2)$ 1-cycles, *i.e.* by an element belonging to the class $211\ldots1$. Thus for example, the swing illustrated in fig IV.7 is represented by $S(\alpha_i,\alpha_j) = (\alpha_i\alpha_j)\prod_{k\neq i,j}(\alpha_k)$, and we have

$$\begin{aligned} S(\alpha_i,\alpha_j)\otimes(\ldots\alpha_{i-1}\alpha_i\ldots\alpha_{j-1}\alpha_j\ldots) &= (\alpha_i\alpha_j)\prod_{k\neq i,j}(\alpha_k)\otimes(\ldots\alpha_{i-1}\alpha_i\ldots\alpha_{j-1}\alpha_j\ldots) \\ &= (\ldots\alpha_{i-1}\alpha_j\ldots)(\alpha_i\ldots\alpha_{j-1}). \end{aligned} \tag{IV.51}$$

Here $\otimes$ denotes the group multiplication. The action of $S(\alpha_i,\alpha_j)$ makes α_{i-1} point at α_j, and α_{j-1} point at α_i, leaving all other α_k unchanged as shown in the figure.

Due to the fact that not every swing leads to a physically acceptable state, the number of allowed swings for a state containing N dipoles is not simply $\frac{1}{2}N(N-1)$. This would e.g. be the the number of pairs in a reaction-diffusion

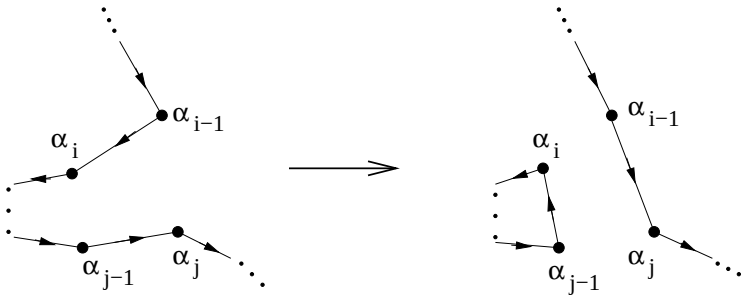

Figure IV.7: Illustration of eq (IV.51).

type of formalism. In most formulations this is not taken into account, but we here wish to emphasize the importance of keeping track of the correct topology of the evolution. While this is not important in the original formulation of the dipole model where the dipole state evolves through the $1 \to 2$ splitting only, it is very necessary for transitions involving more than one initial dipole. In the appendix we show that the the number of physically possible states $\mathcal{N}_D$, and the number of possible swings $\mathcal{N}_S$ are for N dipoles given by

$$\mathcal{N}_D(N) = (N-1)! \sum_{l=0}^{N-1} \frac{(-1)^l}{l!}(N-l), \tag{IV.52}$$

$$\mathcal{N}_S(N) = \frac{1}{2}(N-1)(N-2) + n_2, \tag{IV.53}$$

where n_2 is the number of closed loops containing 2 dipoles.

Multiple swings in the $N \to N+1$ evolution

The classes of the group $\mathcal{P}_N$ are connected to each other via the swing as illustrated in fig IV.8, where each line means that two elements from the respective classes can be transformed into one another using one swing. Note that the longest distance is that between 4 and 1111, which requires 3 swings. In $\mathcal{P}_5$, we need 4 swings to go from 11111 to 5, as is also shown in fig IV.8.

Generally, for $\mathcal{P}_N$, any element in the class N can be reached from the identity element using $N-1$ swings. Explicitely, we can write the N-cycle $(j_1 \dots j_N)$ as $\prod_{i=1}^{N-1}(j_1 j_{i+1})$. This also implies that, given any arbitrary element $a \in \mathcal{P}_N$, we can reach any other element $b \in \mathcal{P}_N$ using at most $N-1$ swings. This is so since we can always find $N-1$ swings such that their product equals ba^{-1}.

However, not all classes fall into the subset of physically acceptable states,

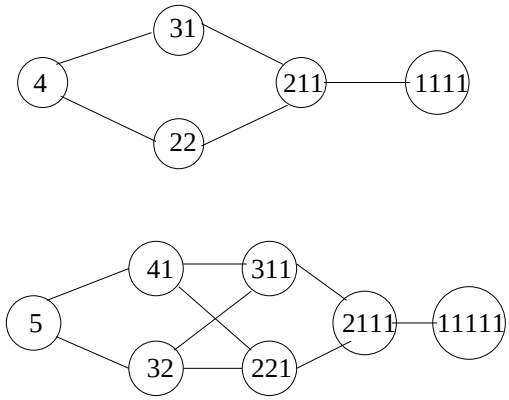

Figure IV.8: Class diagrams for $\mathcal{P}_4$ and $\mathcal{P}_5$.

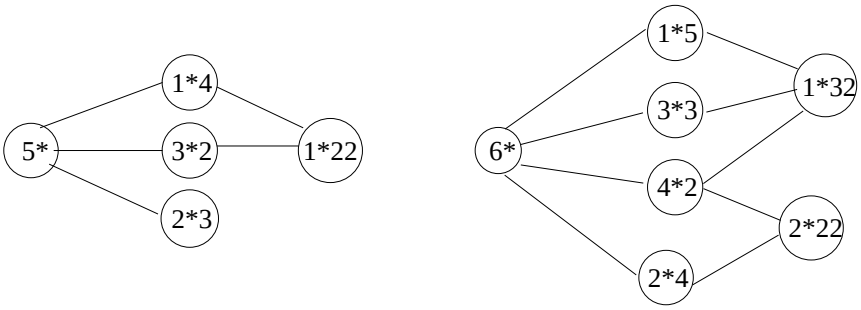

Figure IV.9: Class diagrams for the subset of physical states of $\mathcal{P}_5$ and $\mathcal{P}_6$. The open chain is marked by $*$.

which in particular does not contain the identity element. Therefore we cannot a priori say whether or not the result above also holds for this subset. In fig IV.9, we show the class diagrams of physically acceptable states for $\mathcal{P}_5$ and $\mathcal{P}_6$. Here n^* denotes the open chain containing $n-1$ gluons. Thus using this notation we would say that $\mathscr{A}_N$ in (IV.50) belongs to the "class" $k_0^* k_1 \dots k_m$. With a slight abuse of nomenclature, we will for simplicity continue to refer to these quantities as "classes", even though they do not constitute classes in the group theoretical sense.

Actually, the dipole splitting can be represented by the same class of elements as the dipole swing. Assume we are in the state $\mathscr{A}_N$. We then regard the splitting as a two-step process; first, we add the Nth gluon as a 1-cycle into

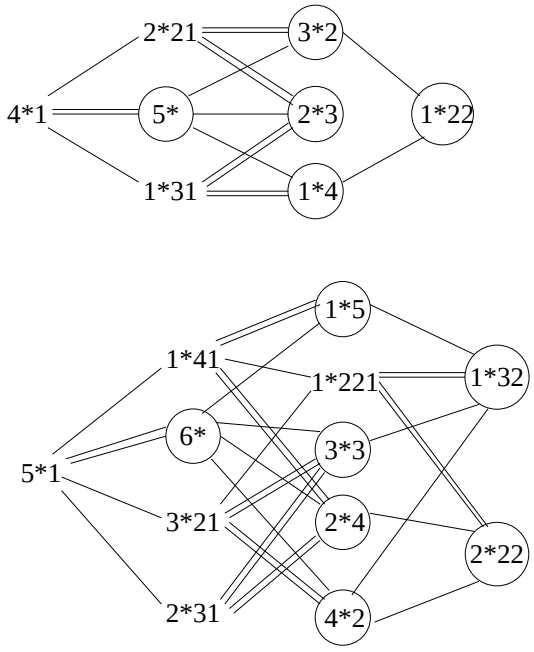

Figure IV.10: Class diagrams representing the evolutions $N = 4 \to N = 5$, and $N = 5 \to N = 6$. Here the double lines represent the dipole splitting. Note that for these we can only go in one direction, from an un-circled class to a circled one.

the state $\mathscr{A}_N$, formally writing $\mathscr{A}_N$ as an element of $\mathcal{P}_{N+1}$,

$$\bar{\mathscr{A}}_N = (0\,\alpha_1 \dots \alpha_{k_0-1})(\alpha_{k_0} \dots \alpha_{k_0+k_1-1}) \dots (\alpha_{\sum_{i=0}^{l-1} k_i} \dots \alpha_{N-1})(N) \in \mathcal{P}_{N+1}. \tag{IV.54}$$

We put a bar on $\bar{\mathscr{A}}_N$ since, written in this way, it is not a physically acceptable state. Then, in the second step, we represent the emission of N from the dipole spanned between α_i and α_{i+1} by operating on $\bar{\mathscr{A}}_N$ with $S(N, \alpha_{i+1})$ (see eq (IV.51)), since in that case $(\dots \alpha_i\, \alpha_{i+1} \dots)$ is replaced by $(\dots \alpha_i\, N\, \alpha_{i+1} \dots)$.

The class diagrams for the generic $N \to N+1$ evolution can be drawn in a similar fashion as before. In fig IV.10, we show examples for $N = 4$ and $N = 5$. Here only the circled classes are physically acceptable, and it is one of these that we must end up in, starting from one of the un-circled ones. The maximal distance between any two circled classes in an $N \to N+1$ evolution is 2 for $N = 3$, 3 for $N = 4$, and also 3 for $N = 5$. Thus in this case this distance is not equal to $N-1$ for a N-dipole state. This does, however, not automatically imply that we can reach any given state in less than $N-1$ swings.

We here conjecture that one can also for the subset of physical states go from $\mathscr{A}_N$ to any $\mathscr{A}_{N+1}$ by combining a dipole splitting with at most $N-1$ swings. In the appendix we show explicitely that this statement is true for $N = 4$ (the cases $N = 1, 2$ are trivial, and $N = 3$ can be checked very easily). We have also checked this result for $N = 5$, $N = 6$ and $N = 7$, but we will for simplicity not present the calculations for these cases. In a process where $k-1$ swings take place, k dipoles in the cascade get replaced by $k+1$ dipoles, thus giving a $k \to k+1$ transition.

The only exception to the statement above is when there are states containing an isolated triangle. For example, if we wish to go from the state $(0)(1\,2\,3)(4)$ in 1^*31, to the state $(0\,4)(1\,3\,2)$ in 2^*3, we need 5 steps totally, 1 splitting and 4 swings. Thus for these states, $N-1$ swings are not enough (one needs $N+1$ swings). This is directly related to the fact that the physical set of states does not allow the steps: $(1\,2\,3) \to (1)(2\,3) \to (1\,3\,2)$. Therefore we need to use 4 swings rather than only 2 swings, which implies that we generally need $N+1$ swings for these states. Note, however, that this problem does not appear for higher order cycles. The 4-cycle $(1\,2\,3\,4)$ can for example be transformed into $(1\,4\,3\,2)$ easily: $(1\,2\,3\,4) \to (1\,4)(2\,3) \to (1\,4\,3\,2)$.

However, we also note that the only difference between the configurations $(1\,2\,3)$ and $(1\,3\,2)$ is in the orientation of the dipoles. Moreover, the states $\mathscr{A}_N = (\alpha_1\,\alpha_2\,\alpha_3)\mathscr{B}_{N-3}$ and $\mathscr{A}'_N = (\alpha_1\,\alpha_3\,\alpha_2)\mathscr{B}_{N-3}$ have exactly the same weights in the cascade evolution. They are therefore always produced equally, and it is therefore not a problem if we cannot go between them using $N-1$ swings. Finally, we note that the semi-classical approximation represented by the cascade evolution cannot take into account all quantum-mechanical interference effects. The quantum-mechanical states corresponding to the configurations $(\alpha_1\,\alpha_2\,\alpha_3)$ and $(\alpha_1\,\alpha_3\,\alpha_2)$ have colour factors $\mathrm{Tr}(T^aT^bT^c)$ and $\mathrm{Tr}(T^aT^cT^b)$ respectively, and for finite N_c these states are not orthogonal. Although the interference is suppressed by $1/N_c^2$, it is enhanced in for example the decay process $\Upsilon \to 3g$, and is in this case quite large [22], which is also confirmed experimentally.

IV.6 Conclusions

Mueller's dipole model gives a simple picture of the small-x evolution which is also very suitable to use in a MC simulation. While it is known that it gives the correct evolution for dilute systems, a fully consistent version for dense systems, where saturation effects during the evolution cannot be neglected, is not known. There have been some attempts to interpret these saturation effects in terms of dipole mergings but it has not been possible to present a consistent probabilistic formulation.

A consequence of neglecting the saturation effects during the dipole evolution is that the model is not frame independent. In a previous paper [15] (see also [17] for a more detailed account) we demonstrated that approximate frame independence can be achieved by including a so called dipole swing in the evolution (the swing was also suggested in [16] as a mechanism to generate pomeron loops). Based on this, we constructed a phenomenological model which, implemented in a MC simulation, gives an almost frame-independent formalism.

It has been quite difficult to analytically derive the relevant dipole interactions which would give rise to saturation effects in the dipole model in a way consistent with boost invariance. A very simplified treatment of the dipole evolution is offered by the toy model introduced in [3, 11], and later also studied in [12, 13]. In this model it is possible to modify the evolution so that the formalism is explicitely frame independent. The evolution proceeds here by the addition of a new dipole at each step, in such a way that the total splitting rate saturates as the dipole occupation number gets large. As discussed in [12], this is actually quite similar to the way saturation occurs in the CGC formalism.

In this paper we have first shown that it is possible to give a probabilistic interpretation to the toy model evolutions in terms of positive definite $k \to k+1$ transitions. These transitions describe the coherent evolution of the dipoles, which is an unavoidable consequence of the requirement that the transition rates be positive definite. The evolution can also be formulated in a more close analogy with a standard reaction-diffusion picture, where the $k \to k+1$ transition rates only depend on the k dipoles involved in the transition. In this case, however, these rates appear with alternating signs which implies that a probabilistic treatment is not possible.

In the real dipole model such positive definite vertices can be generated by combining the dipole splitting with the dipole swing. In a $k \to k+1$ transition, a splitting is combined with $k-1$ simultaneous swings. In the approximation where each single dipole only scatters once, we have seen that it is enough to combine each splitting with a single swing in order to generate the necessary colour correlations.

When each single dipole is allowed to scatter multiply, one needs to include more than one simultaneous swing. In this case the evolution proceeds by the $k \to k+1$ transitions as in the toy models mentioned above, and we have further shown that for a system of N dipoles, one needs at most $N-1$ simultaneous swings in order to generate all colour correlations induced by the multiple dipole interactions. We therefore obtain a close analogy with the toy model evolutions, and the dipole swing furthermore gives a probabilistic interpretation of the evolution. This is easy to show for spatially disconnected dipoles, but there are strong arguments that this is also the case in the more

relevant situation when the dipoles are connected in chains.

This statement is strictly speaking not true for states containing a triangular loop, where only one orientation of this loop can be reached using at most $N-1$ swings. This is, however, not a problem because the two possible orientations always appear with the same weight.

Acknowledgments

I would like to thank Gösta Gustafson for valuable discussions and critical reading of the manuscript. I am also thankful to Leif Lönnblad for useful comments, and to Bo Söderberg for useful discussions on mathematical issues.

IV.A The Number of Dipole States

In this section we will demonstrate that the number of possible states for a system containing $N-1$ gluons, together with the initial $q\bar{q}$ pair, is given by formula (IV.52).

We start by considering n gluons in a closed topology, *i.e.* a state containing one or more closed dipole loops. If all n gluons are in the same loop we obviously have $(n-1)!$ possible states. Next we might have n gluons in two loops. The number of such states is given by the number of elements in $\mathcal{P}_n$ which consists of one k- and one $(n-k)$-cycle. There are $\frac{1}{2}\binom{n}{k}(k-1)!(n-k-1)!$ such elements. The symmetry factor $1/2$ comes from the fact that we can write the k-cycle either to the left or the right of the $(n-k)$-cycle. For a closed topology consisting of m loops, each containing k_i dipoles, the number of possible states is given by

$$\frac{1}{m!}\prod_{j=1}^{m-1}\binom{\sum_{i=j}^{m}k_i}{k_j}\prod_{i=1}^{m}(k_i-1)! = \frac{1}{m!}\frac{n!}{\prod_{i=1}^{m}k_i}, \tag{IV.A1}$$

where

$$\sum_{i=1}^{m}k_i = n. \tag{IV.A2}$$

For each fixed closed topology with n gluons we also have $(N-1-n)!$ possible states in the open chain. To write down the total number of states it is convenient to introduce a generating function $G(z)$ whose series expansion

give the dipole state multiplicity. We have

$$\begin{aligned} G(z) &= \binom{N-1}{n}(N-1-n)!n!\sum_{m=0}^{\infty}\frac{1}{m!}\left(\sum_{k=2}^{\infty}\frac{z^k}{k}\right)^m\sum_{k_0=0}^{\infty}z^{k_0}, \\ &= (N-1)!\frac{e^{-z}}{(1-z)^2} \end{aligned} \tag{IV.A3}$$

where k_0 is the number of gluons in the open chain. We also demand that each closed loop contain at least 2 dipoles as we do not allow colour singlet gluons. The constraint $\sum_{i=0}^{m}k_i = N-1$ is automatically ensured since we are looking for the $(N-1)$th coefficient in the expansion of G. The expansion of G gives

$$G(z) = (N-1)!\sum_{M=0}^{\infty}\sum_{l=0}^{M}\frac{(-1)^l}{l!}(M-l+1)z^M. \tag{IV.A4}$$

We then immediately see that the $M = N-1$ coefficient is equal to eq (IV.52). Notice also that for large N the number of states approaches $\frac{N!}{e}$. This can be compared to the number of possible states for N dipoles formed by N spatially independent charge–anti-charge pairs, which is $N!$, and to the number of states in a system consisting of a single open dipole chain, as in the original formulation of the dipole model, which is $(N-1)!$.

IV.B The Number of Possible Swings

In this section we demonstrate that the number of possible swings for a system containing $N-1$ gluons, together with the initial $q\bar{q}$ pair, is given by eq (IV.53).

Assume again that we have m closed loops each containing k_i dipoles ($i = 1,\ldots,m$) with $k_i \geqslant 2$. The open chain contains k_0 gluons, and thus $\sum_{i=0}^{m}k_i = N-1$. Within each closed loop we then have

$$\frac{1}{2}\sum_{i=1}^{m}k_i(k_i-3)\theta(k_i \geqslant 3) \tag{IV.B1}$$

swings. The theta function takes into account the fact that we cannot have any swings in a loop containing only two or three dipoles. The number of swings between the closed loops is given by

$$\frac{1}{2}\sum_{i\neq j}^{m}k_ik_j \tag{IV.B2}$$

since there are no restrictions in this case. The number of swings between the open chain and the closed loops is given by

$$\sum_{i=1}^{m}(k_0+1)k_i, \tag{IV.B3}$$

and finally, the number of swings within the open chain is given by

$$\frac{k_0(k_0-1)}{2}. \tag{IV.B4}$$

The total number of swings is then given by

$$\begin{aligned}
&\frac{1}{2}\Big\{\sum_{i=1}^{m}\{k_i(k_i-3)-k_i(k_i-3)\delta_{k_i 2}\}+\sum_{i\neq j}^{m}k_ik_j+2(k_0+1)(N-1-k_0)+\\
&+k_0(k_0-1)\Big\}\\
&=\frac{1}{2}\Big\{(N-1-k_0)^2-3(N-1-k_0)+2n_2+2(k_0+1)(N-1-k_0)+\\
&+k_0(k_0-1)\Big\}\\
&=\frac{1}{2}(N-1)(N-2)+n_2
\end{aligned} \tag{IV.B5}$$

where n_2 is the number of closed loops containing 2 dipoles.

IV.C More Details on the $N \longrightarrow N+1$ Evolution

In this last appendix, we will explicitely prove that $N-1$ swings are enough to reach any arbitrary state for $N=4$. We have also explicitely checked the cases $N=5$, but we will for simplicity not present these calculations. We will very briefly try to sketch the case when $N=7$. The cases $N=1,2$ are trivial, and we also omit the case $N=3$ which is very easy to work out.

IV.C.1 $N=4$

For this case, the class diagram is shown in fig IV.10. Assume first that we are in the class 4^*1. An arbitrary element in this class is given by $(0p_1\,p_2\,p_3)(4)$, for some permutation $\{p(i)\}$. We must reach any arbitrary element using at most 3 swings, and thus using at most 4 steps, counting the splitting as one step.

4*1 → 1*22: We see from fig IV.10 that we have to reach any element in 1^*22 using at most 3 steps (or else we would need at least 5 steps). An arbitrary element in 1^*22 can be written $(0)(p_1'\,p_2')(p_3'\,p_4')$ where $\{p'(i)\}$ is some other permutation. Without any loss of generality we might as well assume $p_4'=4$. Then we can always start by putting 4 next to p_3' in the step $4^*1 \rightarrow 5^*$. In the next step we can then always isolate $(p_3'4)=(p_3'p_4')$ in a 2-cycle.

We then have an element $(0\pi(1)\pi(2))(p'_3\,p'_4)$ where $(\pi(1),\pi(2)) = (p'_1,p'_2)$ or (p'_2,p'_1). Finally we can separate$(0\pi(1)\pi(2)) \to (0)(\pi(1)\pi(2))$ to reach $(0)(p'_1\,p'_2)(p'_3\,p'_4)$. To summarize, we can go through the following steps

$$4^*1 \to 5^* \to 3^*2 \to 1^*22, \tag{IV.C1}$$

and reach any element in 1^*22 using at most 3 steps.

4*1 → 3*2: Here we can go in either 2 or 4 steps. We then want to go to an element $(0p'_1\,p'_2)(p'_3\,p'_4)$. Again we start by putting 4 to the right of the number which appears to the left of it in $(0p'_1\,p'_2)(p'_3\,p'_4)$. If this number is 0 (*i.e.* if $p'_1 = 4$), we can go from 5^* to 2^*3, putting 0 and 4 in 2^*. Then we just go back to 5^* to obtain $(0p'_1\,p'_2\,p'_3\,p'_4)$ or $(0p'_1\,p'_2\,p'_4\,p'_3)$. In either we case we can split this chain into $(0p'_1\,p'_2)(p'_3\,p'_4)$. Thus we go through

$$4^*1 \to 5^* \to 2^*3 \to 5^* \to 3^*2. \tag{IV.C2}$$

If $p'_1 \neq 4$, we go from 5^* to 3^*2, isolating 4 and its partner in 2. If the three elements in 3^* are not in the right order, we can split 3^* into 1^*2 and then go back to 3^*. Thus we can go through the steps

$$4^*1 \to 5^* \to 3^*2 \to 1^*23 \to 3^*2. \tag{IV.C3}$$

4*1 → 2*3: We here want to go to the element $(0p'_1)(p'_2\,p'_3\,p'_4)$. Again we start by putting 4 together with its final partner (4 is always put to the right of its partner). If its partner is 0, we can first go from 5^* to 3^*2 and then go back to 5^* so that the elements $(p'_2\,p'_3\,p'_4)$ have the correct permutation. Then we can in one step go the final configuration, and thus complete the process

$$4^*1 \to 5^* \to 3^*2 \to 5^* \to 2^*3. \tag{IV.C4}$$

If 4 is in the 3-cycle in the final element, we can go from 5^* to 3^*2 and then to 5^* again to put all the elements together in the correct positions. This is possible since all three elements in the final 3-cycle must have the correct permutation. Then we can finish by going from 5^* to 2^*3. Thus we can choose the path

$$4^*1 \to 5^* \to 3^*2 \to 5^* \to 2^*3. \tag{IV.C5}$$

Here the 2-cycle in 3^*2 contains 4 and its partner.

4*1 → 1*4: Here we want to reach an element $(0)(p'_1\,p'_2\,p'_3\,p'_4)$. Since we always put 4 (without loss of generality we can assume $p'_4 = 4$) next to its partner in the first step, all we need to do is to isolate them (p'_3 and p'_4) in a 2-cycle by going from 5^* to 3^*2. Then we go to 1^*22, after which we can simply join 22 to 4, to obtain any desired state. We thus have the path

$$4^*1 \to 5^* \to 3^*2 \to 1^*22 \to 1^*4. \tag{IV.C6}$$

4*1 → 5*: We can here use at most 3 steps. The final element we want to reach has the form $(0p_1' \, p_2' \, p_3' \, p_4')$. There are two cases, either 4 and its partner are linked to 0, or they are not. If they are, we can split 5^* into 3^*2 where 3^* contains 0, 4 and its partner. Then the other two elements can always be put back in 5^* in the right position, so that we reach any 5^* element by

$$4^*1 \to 5^* \to 3^*2 \to 5^*. \tag{IV.C7}$$

In the second case, 4 and its partner are not linked to 0 (they are p_2' and p_3'). Then we can split 5^* into 2^*3 where 3 contains 4, its partner and one of the other two elements. They will automatically have the correct permutation, and we can then get the desired state by joining 3 and 2^* into 5^*. Then we have used the path

$$4^*1 \to 5^* \to 2^*3 \to 5^*. \tag{IV.C8}$$

We have thus seen that we can reach any arbitrary state in $N = 5$ from 4^*1 by combining at most 3 swings with a splitting.

Below we list the cases where we start from 2^*21. In this case we have an initial element $(0p_1)(p_2 \, p_3)(4)$. By using a splitting first, we can either go to 3^*2, or to 2^*3.

2*21 → 5*: First we fix 4 and its partner as usual. If the partner is p_1, we can separate $(0p_1 \, 4)$ into $(0)(p_1 \, 4)$, and then we can join $(p_1 \, 4)$ with $(p_2 \, p_3)$ to obtain an element in 1^*4. Then in one step we can go to the desired 5^* state. If its partner is 0, and the other three elements do not have the correct permutation, we can isolate two of them in a 2-cycle (after putting 3^* and 2 into 5^*), and then put them back into the 5^* state in the correct position. Thus we can through the two paths

$$2^*21 \to 3^*2 \to 1^*22 \to 1^*4 \to 5^*, \tag{IV.C9}$$

$$2^*21 \to 3^*2 \to 5^* \to 3^*2 \to 5^*. \tag{IV.C10}$$

If the final partner of 4 is either p_2 or p_3, we first go to 2^*3. Then it is easily seen that the two paths,

$$2^*21 \to 2^*3 \to 5^* \to 3^*2 \to 5^* \tag{IV.C11}$$

$$2^*21 \to 2^*3 \to 5^* \to 2^*3 \to 5^*, \tag{IV.C12}$$

can take us to any arbitrary element in 5^*.

2*21 → 1*4: If 4 is next to either p_2 or p_3, we can directly from 2^*3 go to 5^*, and then to 1^*4. If 4 is next to p_1, we can from 3^*2 go to 1^*22 and then in one more step we can reach any 1^*4 state. Thus we can follow the paths

$$2^*21 \to 2^*3 \to 5^* \to 1^*4 \tag{IV.C13}$$

$$2^*21 \to 3^*2 \to 1^*22 \to 1^*4, \tag{IV.C14}$$

to reach any state in 1^*4 in maximum 3 steps.

2*21 → 1*22: If 4 is next to p_1 we can finish in 2 steps, $2^*21 \to 3^*2 \to 1^*22$. If 4 is next to either p_2 or p_3, we can first join 2^*3 into 5^*, and then isolate 4 and its partner in the 2-cycle in 3^*2. Then we need only one more step. We thus have the steps

$$2^*21 \to 2^*3 \to 5^* \to 3^*2 \to 1^*22. \tag{IV.C15}$$

2*21 → 3*2: If p_1 is partner to 4, we need at most go to 1^*22 from 3^*2, and then back to 3^*2 to finish. If 4 is next to 0, we can first go to 5^* from 3^*2, and then split 5^* into the desired 3^*2 state. If 4 is next to p_2 or p_3, we can again go to 5^* and then directly to 3^*2. Thus we have the steps

$$2^*21 \to 3^*2 \to 1^*22 \to 3^*2 \tag{IV.C16}$$
$$2^*21 \to 3^*2 \to 5^* \to 3^*2 \tag{IV.C17}$$
$$2^*21 \to 2^*3 \to 5^* \to 3^*2. \tag{IV.C18}$$

2*21 → 2*3: If 4 is in the final 2-cycle (*i.e.* next to 0), all we need to do is to join 3^*2 into 5^*, after which we can extract the final 3-cycle in one step. If one the other hand 4 is in the final 3-cycle, we are after one step either finished, or we can from 2^*3 go to 5^*, putting 0 and its final partner together, after which we can split 5^* split into 2^*3, obtaining the desired state. Thus we can go choose one of the paths,

$$2^*21 \to 3^*2 \to 5^* \to 2^*3 \tag{IV.C19}$$
$$2^*21 \to 2^*3 \to 5^* \to 2^*3. \tag{IV.C20}$$

Finally, we check the case when we start from 1^*31.

1*31 → 1*22: Here we only need two steps:

$$1^*31 \to 1^*4 \to 1^*22 \tag{IV.C21}$$

which can be easily seen.

1*31 → 1*4: This case is almost trivial, and we can see that we need at most three steps:

$$1^*31 \to 1^*4 \to 1^*22 \to 1^*4. \tag{IV.C22}$$

1*31 → 3*2: If 4 appears in the 2-cycle in 3^*2, all we need is to take the steps

$$1^*31 \to 1^*4 \to 1^*22 \to 3^*2. \tag{IV.C23}$$

In the second step we here isolate 4 and its partner in one of the 2-cycles. If 4 instead appears in 3^*, we can go through either $1^*31 \to 1^*4 \to 5^* \to 3^*2$, or $1^*31 \to 2^*3 \to 5^* \to 3^*2$, depending whether or not 4 appears next to 0 in the final configuration.

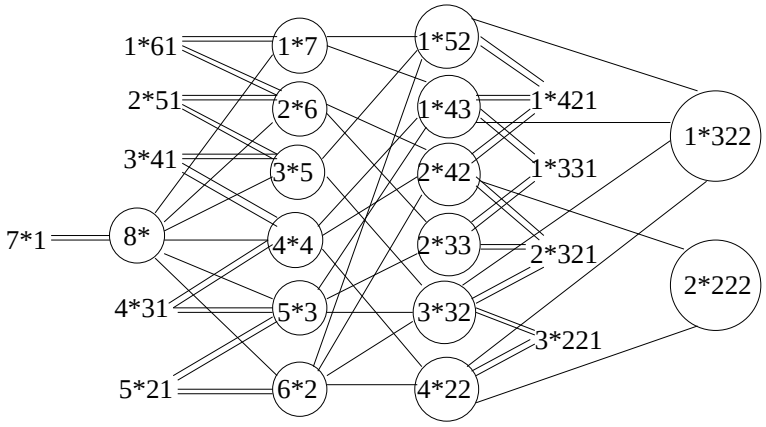

Figure IV.C1: Class diagrams for the evolution $N = 7 \to N = 8$. Here for simplicity we do not draw lines between the un-circled classes.

1*31 → 5*: Here we can again have 4 either to the right of 0 or not. If not, we just take the steps $1^*31 \to 1^*4 \to 1^*22 \to 3^*2 \to 5^*$. If it is next to 0, we instead take the steps $1^*31 \to 2^*3 \to 5^* \to 3^*2 \to 5^*$.

1*31 → 2*3: If 4 appears in 3, we can just go through $1^*31 \to 1^*4 \to 5^* \to 2^*3$ and finish. However, if 4 is next to 0, $N - 1$ swings are not enough to go to $(04)(p_1\, p_3\, p_2)$ as we have already discussed in the main text. We have also already noted that this is not a problem for the frame independence. With this remark we finish the case $N = 4$.

IV.C.2 $N = 7$

As a more complicated case, consider the evolution $N : 7 \to 8$. The class diagram for the evolution is shown in fig IV.C1. Here it is obviously quite tedious to explicitely check all possible connections. However, one can now use the results from the previous cases to simplify the analysis. For example, let us consider the case where we want to go from 7^*1 to 1^*322. If 7 appears in the final 2-cycle, we can pull it out together with its partner after 2 steps, and the question is then whether we can go from 6^* to 1^*32 in 5 steps, and we know from the case $N = 5$ that this is indeed possible. If 7 appears in the final 3-cycle, we can after 4 steps isolate it with its partners, and then we need to go from 5^* to 1^*22 in 3 steps, which we also know is possible. Another example is if we want to go to a final configuration in 2^*42, where 7 appears in 2. After 2 steps, 7 and its partner can again be isolated, and we then need to go from 6^* to 2^*4 in 5 steps. Again we know that this is indeed possible. We can similarly

work out the rest of the cases. It is also interesting to note that we can here go from 1*331 to 2*33 in 7 steps, even if the initial and final states differ by the orientations of the two triangular loops.

IV References

[1] L. V. Gribov, E. M. Levin, and M. G. Ryskin *Phys. Rept.* **100** (1983) 1–150.

[2] A. H. Mueller *Nucl. Phys.* **B415** (1994) 373–385.

[3] A. H. Mueller *Nucl. Phys.* **B437** (1995) 107–126, hep-ph/9408245.

[4] I. Balitsky *Nucl. Phys.* **B463** (1996) 99–160, hep-ph/9509348.

[5] Y. V. Kovchegov *Phys. Rev.* **D60** (1999) 034008, hep-ph/9901281.

[6] J. Jalilian-Marian, A. Kovner, A. Leonidov, and H. Weigert *Nucl. Phys.* **B504** (1997) 415–431, hep-ph/9701284.

[7] J. Jalilian-Marian, A. Kovner, A. Leonidov, and H. Weigert *Phys. Rev.* **D59** (1999) 014014, hep-ph/9706377.

[8] E. Iancu, A. Leonidov, and L. D. McLerran *Phys. Lett.* **B510** (2001) 133–144, hep-ph/0102009.

[9] H. Weigert *Nucl. Phys.* **A703** (2002) 823–860, hep-ph/0004044.

[10] E. Iancu, A. Leonidov, and L. McLerran hep-ph/0202270.

[11] A. H. Mueller and G. P. Salam *Nucl. Phys.* **B475** (1996) 293–320, hep-ph/9605302.

[12] J. P. Blaizot, E. Iancu, and D. N. Triantafyllopoulos *Nucl. Phys.* **A784** (2007) 227–258, hep-ph/0606253.

[13] A. Kovner and M. Lublinsky *Nucl. Phys.* **A767** (2006) 171–188, hep-ph/0510047.

[14] E. Avsar, G. Gustafson, and L. Lönnblad *JHEP* **07** (2005) 062, hep-ph/0503181.

[15] E. Avsar, G. Gustafson, and L. Lonnblad *JHEP* **01** (2007) 012, hep-ph/0610157.

[16] M. Kozlov, E. Levin, and A. Prygarin hep-ph/0606260.

[17] E. Avsar, G. Gustafson, and L. Lönnblad arXiv:0709.1368 [hep-ph].

[18] E. Iancu, J. T. de Santana Amaral, G. Soyez, and D. N. Triantafyllopoulos *Nucl. Phys.* **A786** (2007) 131–163, hep-ph/0611105.

[19] E. Iancu, G. Soyez, and D. N. Triantafyllopoulos *Nucl. Phys.* **A768** (2006) 194–221, hep-ph/0510094.

[20] J. Bartels and M. G. Ryskin *Z. Phys.* **C62** (1994) 425–430.

[21] J. Bartels and M. G. Ryskin *Z. Phys.* **C60** (1993) 751–756.

[22] G. Gustafson *Z. Phys.* **C15** (1982) 155–160.

V

Diffractive Excitation in DIS and pp Collisions

Emil Avsar, Gösta Gustafson and Leif Lönnblad

Dept. of Theoretical Physics, Sölvegatan 14A, S-223 62 Lund, Sweden

Submitted to JHEP, arXiv:0709.1368 LU-TP 07-25.

We have in earlier papers presented an extension of Mueller's dipole cascade model, which includes subleading effects from energy conservation and running coupling as well as colour suppressed effects from pomeron loops via a "dipole swing". The model was applied to describe the total cross sections in pp and $\gamma^* p$ collisions. In this paper we present a number of improvements of the model, in particular related to the confinement mechanism. A consistent treatment of dipole evolution and dipole–dipole interactions is achieved by replacing the infinite range Coulomb potential by a screened potential, which further improves the frame-independence of the model. We then apply the model to elastic scattering and diffractive excitation, where we specifically study the effects of different sources for fluctuations. In our formalism we can take into account contributions from all different sources, from the dipole cascade evolution, the dipole–dipole scattering, from the impact-parameter dependence, and from the initial photon and proton wavefunctions. Good agreement is obtained with data from the Tevatron and from HERA, and we also present some predictions for the LHC.

V.1 Introduction

In high energy pp scattering the cross section for parton–parton subcollisions becomes larger than the total cross section. This means that on average there are more than one subcollision in a single event, and it was early suggested that hard subcollisions dominate the features of high energy scattering and are the cause of the rising cross section. This is also the basic assumption in the model by Sjöstrand and van Zijl [1] implemented in the PYTHIA event generator, which is able to describe many features of high energy collisions.

That perturbative dynamics dominate high energy collisions is also supported by the large intercept of the BFKL pomeron. Via unitarity and the AGK cutting rules, the large subcollision cross section and high probability for multiple collisions have also strong implications for diffraction. Hard diffraction was first observed by the UA8 collaboration at the CERN Sp$\bar{\text{p}}$S collider [2], and has later been studied in much more detail both at the Tevatron (see eg. [3, 4]) and at HERA (see eg. [5, 6]).

Multiple collisions, unitarity and saturation are conveniently studied in terms of dipoles in transverse coordinate space. The dipole model by Golec-Biernat and Wüsthoff (GBW) [7, 8] has successfully described both F_2 and diffraction in DIS. Mueller's dipole cascade model [9–11] reproduces the leading log (linear) BFKL equation, and includes also multiple collisions and satisfies the unitarity constraint. The multiple collisions correspond to pomeron loops. Mueller's model includes, however, only such loops which are cut in the particular Lorentz frame used in the calculation, but not loops which are fully contained in one of the individual dipole cascades. Many attempts (see for example [12,13] and references therein) have been presented including *e.g.* $2 \to 1$, $2 \to 4$ or more complicated dipole vertices, but so far no explicitly frame-independent formalism has been presented.

An important part of the NLL corrections to the BFKL equation are related to energy conservation [14], and in a series of papers [15, 16], we have developed Mueller's model to include both effects of energy–momentum conservation and effects of pomeron loops and saturation inside the cascade evolution via a $2 \to 2$ dipole transition, called a dipole swing. The swing does not reduce the number of dipoles, rather the saturation effect is achieved as the "new" dipoles are smaller, and therefore have smaller cross sections. Although not explicitly frame independent, the numerical result is almost independent of the frame used for the calculations. With a simple model for the proton in terms of three dipoles, the Monte Carlo implementation also reproduces the total cross section both for DIS at HERA and for pp scattering from ISR energies to the Tevatron.

In this paper we will first make some technical improvements related to confinement, and then use the model to study diffractive scattering at HERA

and the Tevatron. The perturbative calculation has some problems in the IR region, especially with a running coupling, and a cutoff for large dipoles is essential for the frame independence and the good agreement with data. We here propose to treat this effect of confinement by everywhere replacing the Coulomb colour-electric potential by a screened Yukawa potential.

Both the screening length and the size of the initial proton wave function are determined by the confinement mechanism. In the MC implementation these two quantities are assumed to be of the same size. This implies that for pp-collisions and DIS at high Q^2 the model has only two tunable parameters; besides Λ_{QCD} only the confinement scale denoted by r_{max}. For smaller Q^2 the result is, however, also sensitive to the quark masses in the virtual photon wave function. The value of r_{max} turns out to be very important in order to obtain the correct normalization for σ_{tot} in pp collisions, but the increase of σ_{tot} with the center of mass energy is found to be much less sensitive to this parameter. Once $r_{\max}$ is fixed to obtain the correct normalization for σ_{tot} in pp scattering, the DIS cross section is obtained without any further changes.

Our treatment of elastic scattering and diffractive excitation is based on the eikonal approximation and the Good and Walker picture [17]. The result is determined by the fluctuations in the collision process originating from the initial wave functions of the proton and the virtual photon, from the dipole cascades and from the dipole–dipole scattering probability. In our formalism all these different components give important contributions. One result of this is that the impact parameter profile is less steeply falling, *i.e.* less black and white and more "grey", than in models where the dominant fluctuations are assumed to come from fluctuations in the impact parameter, b.

The distribution in the mass, M_X, of the diffractive state can be obtained by a study of the collision in different Lorentz frames, as discussed by Hatta et al. [18]. (It is here essential that we have a frame-independent formalism.) However, in addition to the fluctuations included in this reference and in the GBW approach, we also include fluctuations in the evolution of the proton target.

In section V.2 we review briefly the dipole cascade model, discuss the modification of the confinement effect, and demonstrate the frame independence of the model. In section V.3 we discuss the formalism for elastic and diffractive scattering, and the effects of the different sources of fluctuations in the collision process. Our results are presented in section V.4, and the conclusions in section V.5.

V.2 Dipole Model and Frame Independence

We will in this section briefly discuss the cascade model presented in refs. [15, 16], describe the modified treatment of confinement, and demonstrate the

frame independence by showing some quantitative examples.

V.2.1 Mueller's cascade model

The model is based on Mueller's dipole formalism [9–11] in which the small-x evolution is interpreted in terms of a dipole cascade. The probability per unit rapidity Y that a dipole $(\boldsymbol{x},\boldsymbol{y})$ emits a gluon at position $\boldsymbol{z}$ is here given by

$$\frac{d\mathcal{P}}{dY} = \frac{\bar{\alpha}}{2\pi} d^2\boldsymbol{z} \frac{(\boldsymbol{x}-\boldsymbol{y})^2}{(\boldsymbol{x}-\boldsymbol{z})^2(\boldsymbol{z}-\boldsymbol{y})^2}, \tag{V.1}$$

and the evolution of the cascade agrees with the leading order BFKL evolution. As a consequence, the total number of dipoles grows exponentially. This also implies a strong growth for the total cross section which, however, is tamed by taking multiple dipole interactions into account. The scattering probability between two elementary colour dipoles with coordinates $(\boldsymbol{x}_i,\boldsymbol{y}_i)$ and $(\boldsymbol{x}_j,\boldsymbol{y}_j)$ respectively, is given by

$$f_{ij} = f(\boldsymbol{x}_i,\boldsymbol{y}_i|\boldsymbol{x}_j,\boldsymbol{y}_j) = \frac{\alpha_s^2}{8}\left[\log\left(\frac{(\boldsymbol{x}_i-\boldsymbol{y}_j)^2(\boldsymbol{y}_i-\boldsymbol{x}_j)^2}{(\boldsymbol{x}_i-\boldsymbol{x}_j)^2(\boldsymbol{y}_i-\boldsymbol{y}_j)^2}\right)\right]^2. \tag{V.2}$$

Since Mueller's model is formulated in transverse coordinate space, multiple scatterings can be included in an eikonal approximation, and a unitarised expression for the total scattering amplitude can be obtained as

$$T(\boldsymbol{b}) = 1 - \exp\left(-\sum_{ij} f_{ij}\right). \tag{V.3}$$

V.2.2 Energy conservation

The fast growth in leading order BFKL is much reduced by NLL effects. A large fraction of these corrections is related to energy-momentum conservation [14]. Using the similarities between Mueller's cascade model and the Linked Dipole Chain (LDC) model [19, 20], we implemented energy-momentum conservation in the dipole cascade in ref. [15]. The $p_\perp$ of the partons was here associated with the dipole sizes in coordinate space. Although the number of dipoles still increases exponentially, the growth is significantly reduced and the onset of saturation is delayed.

V.2.3 Initial proton and photon wave functions

Photon

The splitting $\gamma^* \to q\bar{q}$ can be calculated perturbatively, and we use the well known leading order results for longitudinally and transversely polarized

photons:

$$|\psi_L(z,r)|^2 = \frac{6\alpha_{em}}{\pi^2}\sum_f e_f^2 Q^2 z^2(1-z)^2 K_0^2\left(\sqrt{z(1-z)Q^2+m_f^2}\,r\right)$$
$$|\psi_T(z,r)|^2 = \frac{3\alpha_{em}}{2\pi^2}\sum_f e_f^2\Big\{[z^2+(1-z)^2](z(1-z)Q^2+m_f^2)\times$$
$$K_1^2\left(\sqrt{z(1-z)Q^2+m_f^2}\,r\right)+m_f^2K_0^2\left(\sqrt{z(1-z)Q^2+m_f^2}\,r\right)\Big\}. \tag{V.4}$$

Here z is the negative light-cone momentum fraction of the photon carried by q, and r is the transverse separation between q and $\bar{q}$, and we consider four active quark flavours, with an effective light quark mass of 60 MeV and a charm mass of 1.4 GeV, as described in [21].

Although the wave functions in (V.4) are well known, there are still ambiguities in the initial phase of the evolution of the dipole cascade. This problem is an unavoidable consequence of the difficulty to reconcile the fundamentally quantum mechanical process with the semiclassical approximation represented by the cascade evolution.

For a given W in DIS, the total rapidity range available for final state particles is given by $Y = \ln W^2/m_0^2$, where m_0 is of the order of[1] 1 GeV. We use a Lorentz frame such that an interval Y_0 is on the photon side and the remaining interval $Y - Y_0$ is on the proton side. The kinematics is illustrated in figure V.1, which shows the phase-space diagram for a DIS event in the $\ln p_\perp, y$-plane. Here the positions of the q and $\bar{q}$ are also indicated. Their distance in rapidity from the photon end are given by $\ln p_\perp/z$ and $\ln p_\perp/(1-z)$ respectively, where $p_\perp$ is the transverse momentum of the quark and the antiquark.

In the simulations we have assumed that gluon emission is possible only at rapidities larger than the rapidity of both q and $\bar{q}$. We also identify $p_\perp$ with its typical value $2/r$. As can be seen from figure V.1, this implies that the interval allowed for the photon-initiated cascade is given by

$$Y_\gamma^{eff} = Y_0 - \ln\left(\frac{p_\perp}{\min(z,1-z)}\right) = Y_0 - \ln\left(\frac{2}{r\min(z,1-z)}\right). \tag{V.5}$$

Thus Y_γ^{eff} depends on both variables r and z. The total range for the evolution

$$Y_p + Y_\gamma^{eff} = \ln W^2 - \ln\left(\frac{2}{r\min(z,1-z)}\right) \tag{V.6}$$

[1] In the following the scale $m_0 = 1$ GeV will be omitted in writing logarithms.

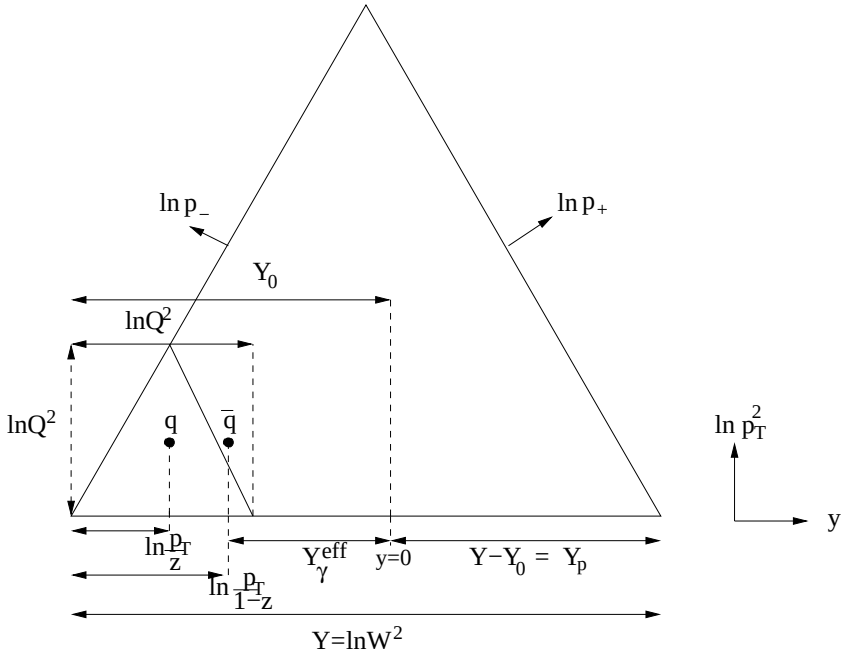

Figure V.1: The available phase space for gluon emission in DIS. We have here for simplicity assumed that $z > 1 - z$. The vertical dashed line labeled $y = 0$ denotes the Lorentz frame in which the collision is studied.

may be larger or smaller than $\ln 1/x \approx \ln W^2 - \ln Q^2$. One could also imagine other choices, but we want to emphasize that the difference is subleading in $\ln W^2$, and therefore the optimal choice cannot be determined from QCD with present techniques.

Anticipating the discussion in the following sections, we want in connection to figure V.1 mention that a calculation of the diffractive cross section corresponds to events which have a gap at $y = 0$ in this particular Lorentz frame. This means that the diffractively excited photon is confined within the rapidity range Y_0 corresponding to a mass limited by $M^2_{X,max} \approx \exp Y_0$.

Proton

The initial proton wavefunction can obviously not be determined by perturbation theory, but has to be specified by a model. Our assumption is that the initial proton can be described by three dipoles in a triangular configuration, where the corners could be associated with the three valence quarks. We ad-

mit that this model has deficiencies, and it should not be used to study the particle distribution in the proton fragmentation regions. The corner connecting two dipoles in a triangle corresponds to an octet colour charge, and not a quark triplet, and an alternative model could be three dipoles connected by a junction in a Y-shaped configuration. This would imply the need for extra assumptions about the behaviour of the colour-neutral junction, and we also believe that the enhanced radiation from the three colour octets might mimic radiation from gluon contributions present in the proton structure also at low virtuality.

We have tried two different triangular shapes. In the first one the triangle is assumed to be equilateral. In this case the size of the dipoles is assumed to be distributed according to a Gaussian

$$dP_1(\boldsymbol{r}) = \mathcal{N}_1\, d^2\boldsymbol{r} \exp\left(-\frac{r^2}{r_{max}^2}\right). \tag{V.7}$$

We found in ref. [16] that this simple model gives a very good agreement with data on cross sections for both pp scattering and DIS. To test the sensitivity to this simple assumption, we have now also studied a model where the triangle is not equilateral, but has an arbitrary shape. Also here the distribution is given by a Gaussian in the sizes of the three sides, r_1, r_2 and r_3,

$$dP_2(\boldsymbol{r}_1,\boldsymbol{r}_2,\boldsymbol{r}_3) = \mathcal{N}_2\, d^2\boldsymbol{r}_1 d^2\boldsymbol{r}_2 d^2\boldsymbol{r}_3 \exp\left(-\frac{r_1^2+r_2^2+r_3^2}{r_{max}^2}\right)\delta(\boldsymbol{r}_1+\boldsymbol{r}_2+\boldsymbol{r}_3). \tag{V.8}$$

The results of the two models are very similar, and we will therefore in the following mainly present results obtained with the simple model given by $dP_1(\boldsymbol{r})$.

The parameter r_{max}, which determines the initial dipole size in the proton, is here assumed to be the same as the confinement scale in the cascade evolution and the dipole-dipole scattering (see section V.2.5 below). Along with Λ_{QCD}, it is one of the essentially two free parameters of our model. We note, however, that the variation of these two parameters have similar effects. Thus an increased value for r_{max} can be compensated by a reduced value for Λ_{QCD} (and *vice versa*), leaving the cross sections unchanged as seen in figure V.2. We note in particular that the energy dependence is rather insensitive to the parameters chosen.

The probability for a three-body system to contract to a single point should be zero, and we have therefore also tested a wavefunction where small r-values are suppressed but where $\langle r^2 \rangle$ has the same value. We then find essentially the same results for total cross sections, but the reduced initial fluctuations imply that the cross sections for elastic scattering and single diffractive excitation become larger. This feature will be further discussed in sections V.3.2 and V.4.

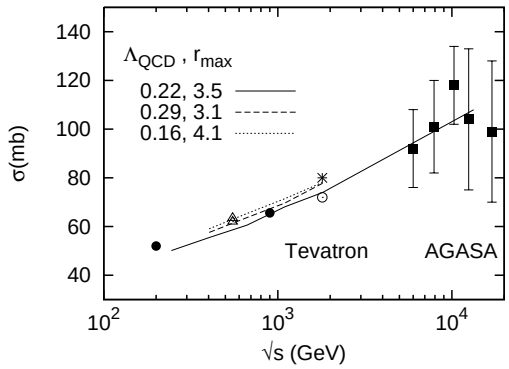

Figure V.2: The total pp cross section as a function of collision energy for various values of r_{max} and Λ_{QCD} in units of GeV^{-1} and GeV respectively.

V.2.4 Dipole swing

One problem with Mueller's model is the fact that saturation effects are not included inside the individual dipole cascades. Thus only pomeron loops which are cut in the particular Lorentz frame used are taken into account, and the result is not frame independent. Non-linearities due to multiple interactions are included, but the evolution of the dipole cascades obey the linear BFKL equation.

We argued in ref. [16] that the missing saturation effects can be taken into account by including the so-called dipole swing in the evolution. Although there is no analytical proof that this would give a frame independent formalism, numerical simulations in a MC implementation showed that the resulting evolution is approximately frame independent. We will show this in more detail in subsection V.2.6.

The swing is a process in which two dipoles $(\boldsymbol{x}_i, \boldsymbol{y}_i)$ and $(\boldsymbol{x}_j, \boldsymbol{y}_j)$ are replaced by two new dipoles $(\boldsymbol{x}_i, \boldsymbol{y}_j)$ and $(\boldsymbol{x}_j, \boldsymbol{y}_i)$. The process can be interpreted in two ways. First, as a way to approximate colour quadrupoles as two independent dipoles formed by the closest charge–anti-charge pairs. Here the swing is naturally suppressed by N_c^2, and it should be more likely to replace two given dipoles with two smaller ones. Secondly, we may see it as the result of a gluon exchange between the dipoles, which results in a change in the colour flow. In this case the swing would be proportional to α_s^2, which again is formally suppressed by N_c^2, compared to the splitting process in (V.1), which is proportional to $\bar{\alpha} = N_c \alpha_s / \pi$.

In the MC implementation each dipole is randomly given one of N_c^2 possi-

ble colours. Only dipoles with the same colour can swing, and the weight for a swing $(\boldsymbol{x}_1,\boldsymbol{y}_1),(\boldsymbol{x}_2,\boldsymbol{y}_2) \to (\boldsymbol{x}_1,\boldsymbol{y}_2),(\boldsymbol{x}_2,\boldsymbol{y}_1)$ is determined by a factor proportional to

$$\frac{(\boldsymbol{x}_1-\boldsymbol{y}_1)^2(\boldsymbol{x}_2-\boldsymbol{y}_2)^2}{(\boldsymbol{x}_1-\boldsymbol{y}_2)^2(\boldsymbol{x}_2-\boldsymbol{y}_1)^2}. \tag{V.9}$$

This implies that the swing favours the formation of smaller dipoles. The number of dipoles is not reduced by the swing, but the fact that smaller dipoles have smaller cross sections gives the desired suppression of the total cross section.

The swing is instantaneous in Y for both the colour multipole and gluon exchange interpretations. It is therefore not a vertex in the sense of the dipole splitting whose probability is proportional to ΔY. In the MC implementation the swing is formulated as if it was proportional to ΔY, but its strength is adjusted so that it is effectively instantaneous. In ref. [22] it is shown that combining the dipole splitting and the dipole swing, one can reproduce all colour correlations induced from the multiple dipole interactions. This is a necessary condition for the formalism to be frame independent. In case each dipole is restricted to single scattering, one can combine a splitting with one swing at a time to reproduce all correlations, but without this restriction, the maximum number of simultaneous swings needed in combination with a splitting, for a system consisting of N dipoles, is $N-1$.

V.2.5 Consistent treatment of confinement

As the dipole model is formulated within perturbative QCD, confinement effects are naturally not included. Obviously, one cannot let the dipoles in the cascade become too large, and it is then natural to introduce a scale, such as our r_{max} parameter, so that large dipoles are suppressed.

Similarly, the scattering of dipoles is calculated perturbatively, and the interaction range is therefore longer than what we would expect from confinement. The formula for f_{ij} in (V.2) is just the two dimensional Coulomb potential which for large distances behaves as

$$f_{ij} \sim \frac{\alpha_s^2}{8}\frac{(\boldsymbol{x}_i-\boldsymbol{y}_i)^2(\boldsymbol{x}_j-\boldsymbol{y}_j)^2}{\boldsymbol{b}^4}, \tag{V.10}$$

where $\boldsymbol{b} = \frac{1}{2}((\boldsymbol{x}_i+\boldsymbol{y}_i)-(\boldsymbol{x}_j+\boldsymbol{y}_j))$ is the impact parameter of the dipole-dipole collision. Thus the scattering probability falls off only as a power of $\boldsymbol{b}$, and not as an exponential as one would expect from a confining field. The expression for f_{ij} can be written as

$$f(\boldsymbol{x}_i,\boldsymbol{y}_i|\boldsymbol{x}_j,\boldsymbol{y}_j) = \frac{g^4}{8}(\Delta(\boldsymbol{x}_i-\boldsymbol{x}_j)-\Delta(\boldsymbol{x}_i-\boldsymbol{y}_j)-\Delta(\boldsymbol{y}_i-\boldsymbol{x}_j)+\Delta(\boldsymbol{y}_i-\boldsymbol{y}_j))^2 \tag{V.11}$$

where $\Delta(\boldsymbol{r})$ is the Green's function given by

$$\Delta(\boldsymbol{r}) = \int \frac{d^2\boldsymbol{k}}{(2\pi)^2}\frac{e^{i\boldsymbol{k}\cdot\boldsymbol{r}}}{\boldsymbol{k}^2}. \tag{V.12}$$

To take confinement into account we can replace the infinite range Coulomb potential with a screened Yukawa potential. This implies that the Coulomb propagator $1/\boldsymbol{k}^2$ in eq. (V.12) is replaced by $1/(\boldsymbol{k}^2 + M^2)$, where $M = 1/r_{max}$ is the confinement scale. In this case the integral in (V.12) is replaced by

$$\int \frac{d^2\boldsymbol{k}}{(2\pi)^2}\frac{e^{i\boldsymbol{k}\cdot\boldsymbol{r}}}{\boldsymbol{k}^2 + M^2} = \frac{1}{2\pi}K_0(rM) \tag{V.13}$$

where K_0 is a modified Bessel function. The expression in (V.2) is then replaced by

$$f_{ij} \to \frac{\alpha_s^2}{2}\Big(K_0(|\boldsymbol{x}_i - \boldsymbol{x}_j|/r_{max}) - K_0(|\boldsymbol{x}_i - \boldsymbol{y}_j|/r_{max}) - \\ -K_0(|\boldsymbol{y}_i - \boldsymbol{x}_j|/r_{max}) + K_0(|\boldsymbol{y}_i - \boldsymbol{y}_j|/r_{max})\Big)^2. \tag{V.14}$$

For small separations where $r << r_{max}$, the function $K_0(r/r_{max})$ behaves like $\ln(r_{max}/r)$ and we then immediately get the result in (V.2). For large separations where $r >> r_{max}$, $K_0(r/r_{max})$ falls off exponentially $\sim \sqrt{\frac{\pi r_{max}}{r}}e^{-r/r_{max}}$, as expected from confinement.

To be consistent we should then also modify the dipole splitting kernel accordingly. The dipole splitting probability in eq. (V.1) can be written in the form

$$\frac{d\mathcal{P}}{dY} = \frac{\bar{\alpha}}{2\pi}d^2\mathbf{z}\frac{(\boldsymbol{x}-\boldsymbol{y})^2}{(\boldsymbol{x}-\boldsymbol{z})^2(\boldsymbol{z}-\boldsymbol{y})^2} = \frac{\bar{\alpha}}{2\pi}d^2\mathbf{z}\left(\frac{\boldsymbol{x}-\boldsymbol{z}}{(\boldsymbol{x}-\boldsymbol{z})^2} - \frac{\boldsymbol{y}-\boldsymbol{z}}{(\boldsymbol{y}-\boldsymbol{z})^2}\right)^2. \tag{V.15}$$

The two terms in this expression are each obtained from the integration

$$\int \frac{d^2\boldsymbol{k}}{(2\pi)^2 i}\frac{\boldsymbol{k}e^{i\boldsymbol{k}\cdot\boldsymbol{r}}}{\boldsymbol{k}^2} = -\boldsymbol{\nabla}\int \frac{d^2\boldsymbol{k}}{(2\pi)^2}\frac{e^{i\boldsymbol{k}\cdot\boldsymbol{r}}}{\boldsymbol{k}^2}. \tag{V.16}$$

Once again making the change $1/\boldsymbol{k}^2 \to 1/(\boldsymbol{k}^2 + M^2)$, and noting that

$$\boldsymbol{\nabla}K_0(r/r_{max}) = -\frac{\boldsymbol{r}}{r\cdot r_{max}}K_1(r/r_{max}), \tag{V.17}$$

we may replace (V.15) by

$$\frac{d\mathcal{P}}{dY} \to \frac{\bar{\alpha}}{2\pi}d^2\mathbf{z}\left(\frac{1}{r_{max}}\frac{\boldsymbol{x}-\boldsymbol{z}}{|\boldsymbol{x}-\boldsymbol{z}|}K_1(|\boldsymbol{x}-\boldsymbol{z}|/r_{max}) - \\ -\frac{1}{r_{max}}\frac{\boldsymbol{y}-\boldsymbol{z}}{|\boldsymbol{y}-\boldsymbol{z}|}K_1(|\boldsymbol{y}-\boldsymbol{z}|/r_{max})\right)^2. \tag{V.18}$$

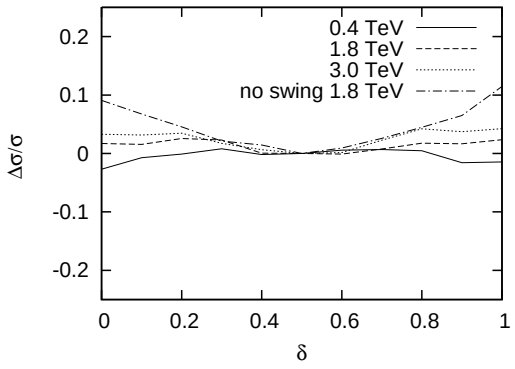

Figure V.3: The quantity $\Delta\sigma/\sigma = (\sigma(Y_0, Y) - \sigma(Y/2, Y))/\sigma(Y/2, Y)$ plotted as a function of $\delta = Y_0/Y$ for different collision energies: full line $\sqrt{s} = 0.4$ TeV, dashed line $\sqrt{s} = 1.8$ TeV and dotted line $\sqrt{s} = 3.0$ TeV. Also shown is the result excluding the dipole swing for $\sqrt{s} = 1.8$ TeV (dash-dotted line).

For small arguments $K_1(r/r_{max}) \approx \frac{r_{max}}{r}$, from which get back the result in (V.15), while for large arguments $K_1(r/r_{max}) \sim \sqrt{\frac{\pi r_{max}}{r}} e^{-r/r_{max}}$, and so once again we obtain an exponentially decaying field.

V.2.6 Frame independence

We will in this subsection demonstrate the frame independence by showing some explicite results obtained using the MC implementation.

The cross section obtained when the right-moving (left-moving) cascade is evolved a rapidity distance Y_0 ($Y - Y_0$) is denoted $\sigma(Y_0, Y)$, and in figure V.3 we show the relative difference $\Delta\sigma/\sigma = (\sigma(Y_0, Y) - \sigma(Y/2, Y))/\sigma(Y/2, Y)$ plotted *vs* $\delta = Y_0/Y$. The figure shows results both including the dipole swing and without the swing. Without the swing the cross section is too large when $\delta \to 0$ or $\delta \to 1$. As expected, the degree of frame dependence is increasing for larger $\sqrt{s}$, when the saturation effects within cascades become more important. When we include the swing, we see that the cross section is (within errors) independent of the Lorentz frame used.

Figure V.4 shows similar results for DIS. Here the cross section is not exactly frame independent, with a tendency of getting larger as we give more of the total rapidity interval to the evolution of the photon. (This may not be very clear from the figures shown but it can be seen more clearly for dipole-proton scattering where we do not have ambiguities in choosing the Y interval as in DIS.) There seems to be two causes for this behaviour, and neither of them

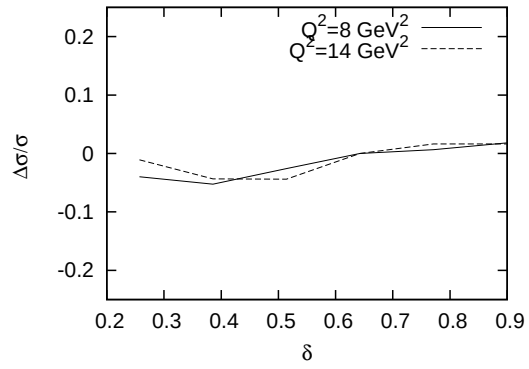

Figure V.4: The quantity $\Delta\sigma/\sigma = (\sigma(Y_0, Y)) - \sigma(0.64Y, Y))/\sigma(0.64Y, Y)$, plotted as a function of $\delta = Y_0/Y$ in DIS for $W = 220$ GeV and $Q^2 = 8$ GeV^2 (solid line) and $Q^2 = 14$ GeV^2 (dashed line).

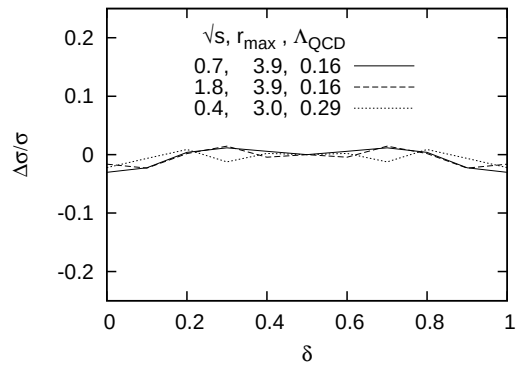

Figure V.5: The quantity $\Delta\sigma/\sigma$ (as defined in figure V.3) as a function of δ for different values of collision energy, r_{max} and Λ_{QCD} (in units of TeV, GeV^{-1} and GeV respectively) in pp scattering.

are related to saturation or the dipole swing. The first cause is the running of the coupling, especially when the dipole–dipole scattering amplitudes are calculated (see next subsection). The second cause is the treatment of energy conservation in the dipole–dipole scattering. In case we use a fixed coupling when calculating the scattering amplitude (but still using a running coupling in the evolution), the result appears to be more frame independent. These issues need to be handled more carefully, and we intend to look at them in

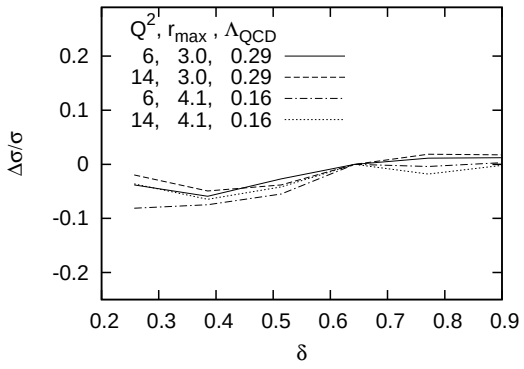

Figure V.6: The quantity $\Delta\sigma/\sigma$ (as defined in figure V.4) as a function of δ in DIS for $W = 220$ GeV for different values of Q^2, r_{max} and Λ_{QCD} (in units of GeV^2, GeV^{-1} and GeV respectively).

forthcoming publications. Note however that the difference is less than 10 percent for both Q^2 values, and it is also not dependent on the energy. As our model is not expected to have a better accuracy than this, we can consider the model to be essentially frame independent also for DIS.

In figures V.5 and V.6 we also show the same diagrams for different values of the parameters r_{max} and Λ_{QCD}, and we can see that a similar behaviour as in the previous figures. The frame independence of the model is therefore not dependent on the precise values of these parameters.

Naturally also the elastic cross section must be frame independent. Diffraction and elastic scattering will be studied in sections V.3 and V.4, and the numerical result for σ_{el} is actually also independent of the Lorentz frame used.

V.2.7 Running Coupling

In our simulations we use a running α_s both in the dipole splitting and in the dipole–dipole scattering probability. Recent NLO studies of the dipole evolution [23,24] have revealed a fairly complicated structure for the running of α_s. However, in [25] this was shown to simplify in the strongly ordered limits, implying that the relevant scale in the dipole splitting is determined by $\min(r, r_1, r_2)$, where r is the mother dipole which splits into r_1 and r_2. This is also the scale we have been using in our simulations.

For the dipole–dipole scattering, the situation is more complicated. We have two powers of α_s and there are six different scales involved. With the two colliding dipoles $(\boldsymbol{x}_i, \boldsymbol{y}_i)$ and $(\boldsymbol{x}_j, \boldsymbol{y}_j)$, we have besides their sizes, also

the distances $|\boldsymbol{x}_i - \boldsymbol{x}_j|$, $|\boldsymbol{x}_i - \boldsymbol{y}_j|$, $|\boldsymbol{y}_i - \boldsymbol{x}_j|$ and $|\boldsymbol{y}_i - \boldsymbol{y}_j|$ (cf. (V.11) and (V.14)). Here we have tried two alternatives. In the first case the scale of α_s for both powers is determined by $\min(|\boldsymbol{x}_i - \boldsymbol{y}_i|, |\boldsymbol{x}_j - \boldsymbol{y}_j|, |\boldsymbol{x}_i - \boldsymbol{y}_j|, |\boldsymbol{y}_i - \boldsymbol{x}_j|)$. In the second case, we associate one α_s to each of the colliding dipoles and choose the scales $\min(|\boldsymbol{x}_i - \boldsymbol{y}_i|, |\boldsymbol{x}_i - \boldsymbol{x}_j|, |\boldsymbol{x}_i - \boldsymbol{y}_j|, |\boldsymbol{y}_i - \boldsymbol{x}_j|, |\boldsymbol{y}_i - \boldsymbol{y}_j|)$ and $\min(|\boldsymbol{x}_j - \boldsymbol{y}_j|, |\boldsymbol{x}_i - \boldsymbol{x}_j|, |\boldsymbol{x}_i - \boldsymbol{y}_j|, |\boldsymbol{y}_i - \boldsymbol{x}_j|, |\boldsymbol{y}_i - \boldsymbol{y}_j|)$ respectively. To avoid divergencies, α_s is frozen below the scale $p_\perp = 2/r_{\max}$.

It turns out that the degree of frame dependence in $\gamma^* p$ is similar in both cases and the results presented in this paper have all been calculated using the first alternative.

V.3 Diffractive and elastic scattering in the dipole model

V.3.1 Formalism

In this section we will describe the formulas we are going to use in calculating the various diffractive and elastic cross sections. We shall rely on the dipole version of the Good and Walker picture of diffraction [17] where the scattering eigenstates are given by the dipole states. The identification of the QCD parton states as the eigenstates of diffraction is due to the work of Miettinen and Pumplin [26]. The situation is complicated by the fact that the states of the proton or the virtual photon depend on the Lorentz frame used, and we will here quite closely follow the formalism presented in [18].

In the Good and Walker picture of diffraction there is a normalized and complete set of real particle states $\{|N\rangle\}$ with fixed quantum numbers. In addition we have eigenstates of the scattering, $\{|n\rangle\}$, which also form a complete set of normalized states. Assume that we have two incoming particles, one right-moving particle $|R\rangle$ and one left-moving particle $|L\rangle$. These particles can then be diffracted onto the various particle states $\{|N\rangle\}$ and $\{|M\rangle\}$, which carry the quantum numbers of $|R\rangle$ and $|L\rangle$ respectively. The incoming wave is given by

$$|\psi_I\rangle = |R, L\rangle = \sum_{n,m} c_n^R c_m^L |n, m\rangle. \tag{V.19}$$

The scattered wave is obtained by operating with $\mathrm{Im}\boldsymbol{T}$ on $|\psi_I\rangle$, where $\boldsymbol{T}$ is the scattering operator. It reads

$$|\psi_S\rangle = \mathrm{Im}\boldsymbol{T}|\psi_I\rangle = \sum_{n,m} c_n^R c_m^L t(n, m)|n, m\rangle. \tag{V.20}$$

The probability for diffractive scattering is given by

$$\langle \psi_S | \psi_S \rangle = \sum_{n,m} P_n^R P_m^L [t(n,m)]^2 = \langle t^2 \rangle_{R,L}. \tag{V.21}$$

We have here identified $|c_n|^2 \equiv P_n$ for both R and L with the probability distribution for the dipole configurations inside the particles. Note that the sum $\sum_n$ actually involves a sum over the dipole occupation number n as well as integrations over the transverse coordinates of each dipole, together with sums over their colour and spin configurations.

Using the completeness of the states $\{|N,M\rangle\}$, the expression in (V.21) can be written in the following form:

$$\langle \psi_S | \psi_S \rangle = |\langle R,L|\psi_S\rangle|^2 + \sum_{N\neq R} |\langle N,L|\psi_S\rangle|^2 + \sum_{M\neq L} |\langle R,M|\psi_S\rangle|^2 + \\ + \sum_{N\neq R}\sum_{M\neq L} |\langle N,M|\psi_S\rangle|^2. \tag{V.22}$$

Here the first term on the RHS corresponds to elastic scattering, where both R and L emerge intact from the collision. The second (third) piece gives the probability of the excitation of R (L) into one of the states N (M) with L (R) remaining intact. This corresponds to single diffractive excitation. Finally, the last term takes into account the fact that *both* R and L may transform into excited states N and M, which thus corresponds to double diffractive excitation.

We note that the different terms in (V.22) correspond to different averages of $t(n,m)^2$. The sum of the single diffractive excitation and the elastic cross section can be calculated as follows

$$\sum_N |\langle N,L|\psi_S\rangle|^2 = \sum_N \left| \sum_{n,m} c_n^{N*}\, c_n^R\, P_m^L\, t(n,m) \right|^2 = \sum_N \sum_{n,n'} c_n^{N*}\, c_n^R\, c_{n'}^N\, c_{n'}^{R*} \langle t(n)\rangle_L^2 \\ = \sum_n P_n^R \langle t(n)\rangle_L^2 = \langle \langle t\rangle_L^2 \rangle_R \tag{V.23}$$

where we used the completeness of the states $\{N\}$,

$$\sum_N c_n^{N*}\, c_{n'}^N = \delta_{nn'}. \tag{V.24}$$

Each of the coefficients c_n above is to be evaluated at a certain rapidity Y_0. The total rapidity interval between R and L is determined by the total cms energy $\sqrt{s}$ of the process. For pp scattering Y is simply given by $\ln(s/M_p^2)$, while the situation is a bit more subtle in DIS. How we determine Y in DIS was discussed above in section V.2.

In Mueller's dipole model the scattering amplitude $t(n,m)$ is given by the eikonal form $1-e^{-F}$, where $F=\sum_{ij} f_{ij}$ is defined in eqs. (V.2, V.3). The different contributions to the diffractive cross section in (V.22) are then given by

$$\frac{d\sigma_{el}}{d^2\boldsymbol{b}} = \left\langle 1-e^{-F}\right\rangle^2_{R,L} \tag{V.25}$$

$$\frac{d\sigma^R_{SD}}{d^2\boldsymbol{b}} = \left\langle \left\langle 1-e^{-F}\right\rangle^2_{L}\right\rangle_R - \left\langle 1-e^{-F}\right\rangle^2_{R,L} \tag{V.26}$$

$$\frac{d\sigma^L_{SD}}{d^2\boldsymbol{b}} = \left\langle \left\langle 1-e^{-F}\right\rangle^2_{R}\right\rangle_L - \left\langle 1-e^{-F}\right\rangle^2_{R,L} \tag{V.27}$$

$$\begin{aligned}\frac{d\sigma_{DD}}{d^2\boldsymbol{b}} = &\left\langle \left(1-e^{-F}\right)^2\right\rangle_{R,L} - \left\langle \left\langle 1-e^{-F}\right\rangle^2_{L}\right\rangle_R - \left\langle \left\langle 1-e^{-F}\right\rangle^2_{R}\right\rangle_L + \\ &+ \left\langle 1-e^{-F}\right\rangle^2_{R,L}.\end{aligned} \tag{V.28}$$

Here σ^R_{SD} (σ^L_{SD}) is the cross section for the diffractive excitation of R (L). Similarly σ_{el} and σ_{DD} stand for the elastic and double diffractive cross sections respectively. Summing these four contributions we get the total diffractive cross section

$$\frac{d\sigma_{diff}}{d^2\boldsymbol{b}} = \langle\psi_S|\psi_S\rangle = \sum_{n,m} P^R_n\, P^L_m\, [t(n,m)]^2 = \left\langle \left(1-e^{-F}\right)^2\right\rangle_{R,L}. \tag{V.29}$$

Assume now that the state R is evolved up to Y_0 while L is evolved up to $Y-Y_0$, with Y the total rapidity interval. The total and elastic cross sections given by

$$\sigma_{tot}(Y) = 2\int d^2\boldsymbol{b}\left\langle 1-e^{-F(\boldsymbol{b})}\right\rangle_{R,L} \text{ and } \sigma_{el}(Y) = \int d^2\boldsymbol{b}\left\langle 1-e^{-F(\boldsymbol{b})}\right\rangle^2_{R,L} \tag{V.30}$$

are necessarily independent of Y_0 due to the requirement of frame independence.

The diffractive cross section in (V.29) is, however, *not* independent of Y_0. This expression gives the probability for diffraction at a particular value of Y_0, *i.e.* the chance that we find a rapidity gap around that particular Y_0. If we calculate *e.g.* σ^R_{SD} at a specific Y_0, we obtain the cross section where the diffractively excited right-moving particle is confined within the rapidity range $(0,Y_0)$. This is approximately equivalent to a maximal diffractive mass given by $M^2_{X,max}\approx e^{Y_0}$. Taking the derivative with respect to Y_0 therefore gives the mass distribution $d\sigma^R_{SD}/dY_0 = d\sigma^R_{SD}/d\ln(M^2_X)$.

For the total diffractive cross section in eq. (V.29) we thus expect, in the case of the symmetric pp collision, a maximum when $Y_0 = Y/2$, and a decrease when either $Y_0 \to 0$ or $Y_0 \to Y$. For asymmetric scattering as in DIS, we expect that it is easier to excite the photon. For a right-moving photon the diffractive cross section should therefore be smallest when $Y_0 \to 0$. This discussion is in accordance with the analysis by Hatta et al. [18]. In this reference the diffractive excitation of the proton is neglected, while in our formalism we can also take the proton excitation into account.

The results obtained for pp collisions and DIS are presented in section V.4.

V.3.2 Importance of fluctuations

The impact of fluctuations upon the small-x evolution has gathered considerable interest lately. As mentioned above, the various expressions for the cross sections in formulas eqs. (V.25)-(V.28) are all obtained by taking different averages of the quantity $(1 - e^{-F})^2$. The diffractive excitation is therefore completely determined by the fluctuations in the colliding systems and the interaction probabilities.

Different sources

There are several sources of fluctuations in the various expressions in eqs. (V.25)-(V.28), related to variations in impact parameter, in the dipole cascades, and in the initial wave functions for the photons and protons. Many analyses include part of the fluctuations, assuming this to give the dominant contribution. Thus the dipole-saturation model by Golec-Biernat and Wüsthoff [7, 8] takes into account fluctuations in the photon wave function and the emission of the first gluon in the photon cascade, while the model of Kowalski and Teaney (KT) [27] emphasizes the fluctuations in the impact parameter. Hatta et al. [18] includes the fluctuations in the photon cascade, but assumes that the fluctuations in the proton cascade can be neglected. As a result fits to data can give different results for the impact parameter profile, and different approaches can give different ratios for the elastic cross section and diffractive excitation. As an illustration we will here compare the fluctuations in our model with those in the Kowalski-Teaney model.

In the KT model the differential dipole-proton cross section in impact parameter space is given by the eikonal

$$\frac{d\sigma_{dp}}{d^2\boldsymbol{b}} = 2(1 - e^{-\Omega(r,b)/2}), \tag{V.31}$$

where r is the dipole size. The opacity Ω is modeled by a factorized form

$$\Omega(r,b) = \frac{\pi^2}{N_c} r^2 \alpha_s(\mu^2) x g(x,\mu^2) T(b), \tag{V.32}$$

where $T(b)$ is the transverse profile function of the proton. In $\Omega(r,b)$ there is also a dependence on $W^2 \propto 1/x$ which is omitted here. To determine the impact parameter profile it is assumed that the t dependence of the diffractive vector meson production cross section is given by an exponential, which in turn implies a Gaussian profile for $T(b)$. The two unknown parameters of this Gaussian are then determined by a fit to diffractive J/ψ production data.

For a virtual photon the only fluctuations are those in the dipole size, r, and impact parameter, b. The diffractive cross section is calculated as

$$\sigma_{diff}^{KT} = \int d^2\boldsymbol{b} \int d^2\boldsymbol{r}\, dz\, \psi_\gamma(r,z,Q^2) \left(1 - e^{-\Omega(r,b)/2}\right)^2, \tag{V.33}$$

where $\psi_\gamma(r,z,Q^2) = |\psi_T(r,z,Q^2)|^2 + |\psi_L(r,z,Q^2)|^2$.

When comparing the two models it may seem natural to compare $\Omega(r,b)/2$ with the average $\langle F \rangle_{d,p}$, where $\langle\rangle_{d,p}$ denotes the averaging over the dipole and proton cascades and the proton wavefunction. The corresponding total and diffractive cross sections would then read

$$\sigma_{tot} = 2 \int d^2\boldsymbol{b} \int d^2\boldsymbol{r}\, dz\, \psi_\gamma(r,z,Q^2) \left(1 - e^{-\langle F(\boldsymbol{r},\boldsymbol{b})\rangle_{d,p}}\right), \tag{V.34}$$

$$\sigma_{diff}^{(1)} = \int d^2\boldsymbol{b} \int d^2\boldsymbol{r}\, dz\, \psi_\gamma(r,z,Q^2) \left(1 - e^{-\langle F(\boldsymbol{r},\boldsymbol{b})\rangle_{d,p}}\right)^2. \tag{V.35}$$

This is, however, not necessarily correct. The opacity Ω is in the KT model determined by a fit to data for the total cross section. What is directly determined is therefore $1 - e^{-\Omega/2}$, rather than Ω itself. Thus a more direct analogy to our model would be the quantity $\langle 1 - e^{-F} \rangle$, which would give the same total cross section as (V.30) and imply the following form for the diffractive cross section:

$$\sigma_{diff}^{(2)} = \int d^2\boldsymbol{b} \int d^2\boldsymbol{r}\, dz\, \psi_\gamma(r,z,Q^2) \left\langle 1 - e^{-F(\boldsymbol{r},\boldsymbol{b})} \right\rangle_{d,p}^2. \tag{V.36}$$

Note that this is not the same as the elastic contribution in (V.25) since in that case also the photon wave function is included in the squared average ((V.25) is meaningless in DIS since the virtual photon cannot scatter elastically).

The expressions in (V.35) and (V.36) should be compared with the results in our model, obtained by integrating (V.29) over $\boldsymbol{b}$:

$$\sigma_{diff} = \int d^2\boldsymbol{b} \int d^2\boldsymbol{r}\, dz\, \psi_\gamma(r,z,Q^2) \left\langle \left(1 - e^{-F(\boldsymbol{r},\boldsymbol{b})}\right)^2 \right\rangle_{d,p}. \tag{V.37}$$

Such a comparison is interesting as a way to gauge the role played by the fluctuations.

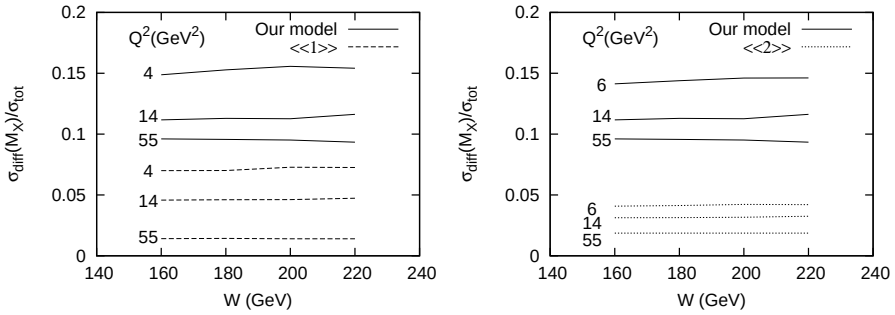

Figure V.7: The ratio of the diffractive cross section to the total cross section for $M_X < 32$ GeV^2. Our results obtained from (V.37) (full lines) are compared to results obtained from both (V.35), marked $\langle\langle 1 \rangle\rangle$ in the left figure (dashed lines), and (V.36), marked $\langle\langle 2 \rangle\rangle$ in the right figure (dotted lines). The total cross section is calculated according to (V.30).

The results obtained from (V.35) and (V.36) are shown in figure V.7, together with the results obtained from (V.37) which includes all fluctuations. We immediately notice the very large effects in our model from the fluctuations in the cascades and the proton wave function. The diffractive cross section calculated from (V.35) is seen to be a factor 2-3 below the result obtained from (V.37), while the result from (V.36) is around a factor 4 lower than (V.37).

We conclude that in our model a large fraction of the fluctuations determining the diffractive cross sections is caused by the dipole cascade evolutions. In order to obtain a similar result in the KT model it is therefore necessary to have larger fluctuations due to the impact parameter dependence, which means an impact parameter profile which is more narrow, *i.e.* more black and white compared to Mueller's dipole cascade model, where the average scattering can be "grey" overall, since the fluctuations in the cascades means that some events are almost black while other are almost white. This can clearly be seen in figure V.8 where we compare the impact parameter profile from the KT model to that obtained from our model. (A similar effect, although less pronounced, is observed in the profile for pp scattering presented in ref. [16]. Also here the profile obtained in our model has a somewhat higher tail for large impact parameters than the Gaussian fit to Tevatron data by Sapeta and Golec-Biernat [28].)

Wave functions

Photon

The photon wave functions in (V.4) for longitudinal and transverse pho-

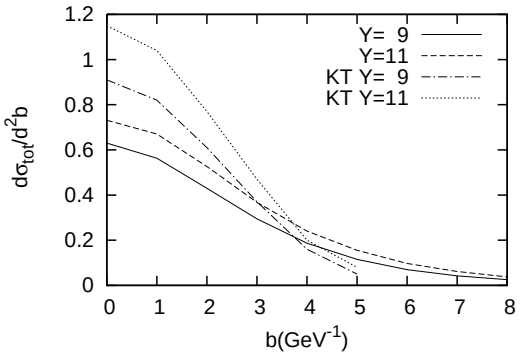

Figure V.8: The impact parameter profile of dipole–proton collisions for an initial dipole size $r = 2\text{GeV}^{-1} \approx 0.4\text{fm}$ at two different energies, $Y = \ln s = 9$ and 11. Our results (solid and dashed lines) are compared to those from the Kowalski–Teaney (KT) model (dot-dashed and dotted lines).

tons are fully determined by pertubation theory. We note that these wave functions are not normalized, even for real photons. This is, however, not in contradiction with the assumption that the states $\{|N\rangle\}$ are normalized. The generic photon state can be written

$$|\gamma(Y_0)\rangle = c_0^\gamma(Y_0)\,|\gamma_d\rangle + \sum_{n=1}^{\infty} c_n^\gamma(Y_0)\,|n\rangle, \tag{V.38}$$

where $|\gamma_d\rangle$ is the component of the photon coupling directly to the quarks. While the state $|\gamma\rangle$ is normalized, the two separate components above are not. Rescattering of the component $|\gamma_d\rangle$ can be neglected, as it is proportional to α_{em}. It is therefore sufficient to only keep the contribution from $|\gamma_h\rangle = \sum_n c_n|n\rangle$, which is not a normalized state.

In DIS it is not meaningful to consider the elastic $\gamma^* p$ scattering, as the virtual photon can never be detected as a real particle. The closest analogies to elastic scattering are given by Deeply Virtual Compton Scattering (DVCS) and the exclusive reactions $\gamma^* p \to Vp$, with V a vector meson. We will return to these processes in a future publication.

Proton

The wave function for the proton is much less well defined. The expressions in eqs. (V.7) or (V.8) ought to be interpreted as probability distributions rather than quantum mechanical wave functions, which can be used to determine the interference effects present in eqs. (V.25)-(V.28). The fluctuations in the wave functions influence the terms in eqs. (V.25)-(V.28) in which the av-

erage of $1 - e^{-F}$ is taken before the square (*i.e.* events containing an elastic proton).

As discussed in section V.2.3 a wave function where three particles can simultaneously be in a single point is not realistic. A Gaussian distribution in impact parameter is usually motivated by the exponential dependence on t for the elastic cross section. However, the constant t-slope is (except possibly for the highest Tevatron energy) only valid for $|t| < 0.15\,\mathrm{GeV}^2$, corresponding to $b > 2/0.4\,\mathrm{GeV}^{-1} \approx 1\,\mathrm{fm}$, and therefore a suppression for small r is still compatible with this constraint. Simulations with such a wave function reduces the fluctuations and increases the cross sections for elastic scattering and single diffractive excitation, while leaving the total and the total diffractive cross sections unchanged, provided the average $\langle r^2 \rangle$ is kept the same.

There is, however, also a more fundamental problem with the proton wave function. In the Good and Walker formalism the hadronic states $\{|N\rangle\}$ form a complete set. This implies that before the cascade has started, there must be other hadron states with wavefunctions orthogonal to the proton wavefunction. This calls for a detailed dynamical scheme describing the relevant degrees of freedom for the hadronic states. With the approximation $M_X^2 \approx \exp Y_0$ these orthogonal states also have the same mass as the proton, which increases the problem further.

Lacking a real quantum-mechanical description of the proton wave function, we can still get an *upper limit* for elastic scattering and single diffraction by removing the contribution from the initial wave function fluctuations. This is obtained if we integrate over the initial wave functions in eqs. (V.25)-(V.28) after taking the squares. Note that the average over different evolutions is still taken before the square, and therefore the fluctuations in the cascade evolution and the impact parameter dependence are still included. Note also that this does not affect the result for the total cross section in (V.30) or the total diffractive cross section in (V.29) (which also includes the elastic cross section).

Non-leading effects

It was early pointed out by Mueller and Salam [29] that there are extremely large fluctuations in the leading order cascade evolution. Expanding the exponential in $\langle 1 - e^{-F} \rangle$ we have

$$\left\langle 1 - e^{-F} \right\rangle = \sum_{k=1}^{\infty} \frac{(-1)^{k-1}}{k!} \langle F^k \rangle. \tag{V.39}$$

Here $\langle F^k \rangle$ could be interpreted as a contribution from the exchange of k pomerons, but such an interpretation may be difficult as it was numerically demon-

strated[2] by Salam [30] that $\langle F^k \rangle \sim (k!)^2$, and therefore this series is strongly divergent. The reason for this is the existence of rare events with a large number of dipoles and large values of F, which make $\langle F^k \rangle$ blow up for large k. On the other hand, these rare events do not contribute much to $\langle 1 - e^{-F} \rangle$, since this expression saturates for large F. Due to these large fluctuations it is therefore possible that one can observe events in which there are large saturation effects, even though the average scattering is still weak. Although such rare events are less important for the total cross section, they are very essential for the diffractive cross section.

In leading order the dipole splitting in (V.1) diverges for small dipoles, and therefore the number of small dipoles depends strongly on the necessary cutoff. As pointed out in [30] a very essential source of the large fluctuations is also the occasional creation of a very large dipole. Such a large dipole has a large probability to split, and the most likely scenario is that it splits into one very small dipole and one dipole which is almost equally large. The process is then iterated and the result is a "jet" of many small dipoles.

We note, however, that the very large fluctuations observed by Mueller and Salam are strongly reduced by non-leading effects. As demonstrated in [15] energy-momentum conservation has a very strong influence. The production of small dipoles is suppressed by the conservation of the positive light-cone momentum p_+, while the large dipoles are suppressed by the conservation of p_-. Another non-leading effect comes from the running coupling α_s. As discussed in section V.2.7, the relevant scale in the dipole splitting is determined by $\min(r, r_1, r_2)$ where r is the mother dipole which splits into r_1 and r_2. This suppresses not only the production of very small dipoles, but also fluctuations where a small dipole splits producing two very large dipoles. We thus conclude that both effects contribute to a suppression of very small or very large dipoles, and therefore also of the abovementioned "jets" radiated from an occasional large dipole. As a result we find in our calculations that $\langle F^k \rangle$ grows like $k!$ rather than $(k!)^2$. The ratios $\langle F^k \rangle / (k \cdot \langle F^{k-1} \rangle)$ for dipole-dipole scattering at $Y = 10$ are approximately equal to 1.2 for all k between 5 and 9 (larger k-values need very high statistics, and are therefore difficult to simulate). However, although the fluctuations in the cascade evolution are strongly tamed by non-leading effects, they are still very important, and have a large effect on the diffractive cross sections, as seen in section V.3.2 and in the results presented in the next section.

[2] The numerical result was anticipated by Mueller [11] who performed analytical calculations on a simple toy model in which transverse coordinates are neglected.

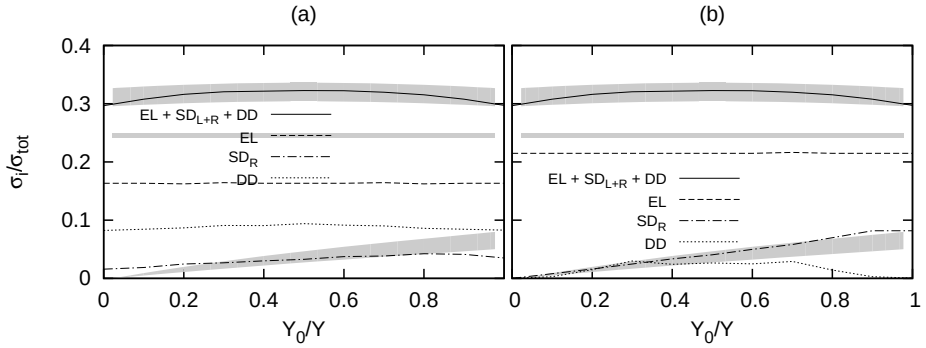

Figure V.9: The ratio between the total diffractive and the total cross section (solid line) together with the contribution from elastic (dashed), single-right (dash-dotted) and double diffractive (dotted) cross sections at 1.8 TeV, obtained including (a) and excluding (b) fluctuations in the initial proton wavefunction. In both cases the lower error band is an estimate from CDF data on single diffraction [31], the middle band is the CDF elastic cross section [32] and the upper is a sum of the two contributions. (Thus the contribution from double diffraction is not included in the CDF result.)

V.4 Results on diffraction and elastic scattering

V.4.1 Diffraction in pp collisions

In figure V.9 we show the ratio of the total diffractive, single diffractive and elastic cross sections to the total cross section at 1.8 TeV as a function of the Lorentz frame used. Figure V.9a shows the result obtained with the initial proton wavefunction in (V.7), while figure V.9b shows the upper limit obtained by integrating over the initial proton wavefunctions after taking the square in eqs. (V.25)-(V.27). In these figures we also show results from the CDF collaboration.

The results in figure V.9a do not agree well with the data. The elastic cross section is too low, and the single diffractive cross section σ_{SD}^R does not go to zero when $Y_0 \to 0$. In this limit $M_X^2 \to m_p^2$ and there should be no phase space for diffractive excitation. The double diffractive excitation is about 9%, which is unrealistically high, and this cross section should also approach zero in the limits $Y_0 \to 0$ or $Y_0 \to Y$. All these features illustrate the problems with our initial proton wave function, discussed above. This formalism presumes that there are other hadronic states which have wavefunctions orthogonal to the proton wavefunction, and which have approximately the same mass. The limiting results in figure V.9b, obtained when the fluctuations in the initial pro-

ton wave function are neglected, do not have this problem. We also see that these results agree quite well with the experimental estimates, supporting the assumption that the initial wavefunction fluctuations have a small effect compared to the fluctuations in the cascade evolution and the impact parameter dependence.

For the elastic cross section we also note (as was claimed above) that it is approximately frame-independent, as it should be. The upper limit shown in figure V.9b is around 22%, which agrees well with the value $(22.02 \pm 0.78)\%$ from E811 [33], while the value from CDF, $(24.6 \pm 0.4)\%$ [32] is a bit larger.

The single diffractive cross section σ_{SD}^R (σ_{SD}^L) is increasing (decreasing) when Y_0 is increased, and in the model we make the identification of the diffractive masses:

$$M_X^{2(R)} = e^{Y_0} \text{ GeV}^2, \quad M_X^{2(L)} = e^{Y-Y_0} \text{ GeV}^2, \tag{V.40}$$

where for 1.8 TeV we have $Y = \ln(s/1\text{GeV}^2) \approx 15$. In figure V.9 we also show results obtained from the CDF parameterization of single diffractive excitation [31]:

$$\frac{d\sigma_{SD}^R}{d\ln M_X^{2(R)}} = \frac{1}{2}\frac{D}{(b_0 + 0.5\ln(s/M_X^{2(R)}))}\left(\frac{s}{M_X^{2(R)}}\right)^{\epsilon} \tag{V.41}$$

with $D = 2.54 \pm 0.43$ mb, $b_0 = 4.2 \pm 0.5$, and $\epsilon = 0.103 \pm 0.017$. Similar results are also presented by the E710 collaboration [34], although with somewhat larger errors. Our results in figure V.9b agree quite well with the data, even if they are a little high for the largest excited masses. Besides not going to 0 when $Y_0 \to 0$, the result in figure V.9a also has a much too slow variation with Y_0, meaning a too low value for $d\,\sigma_{SD}/d\,\ln M_X^2$.

For double diffraction our result for $Y_0 = 7.5$, which corresponds to a central gap, is 2.0 mb. Experimental data exist for 900 GeV from the UA5 collaboration at the CERN Sp$\bar{\text{p}}$S collider [35]. Our result at this energy is 1.8 mb, which is consistent with the experimental result 4.0 ± 2.2 mb. Our results can also be compared to the model of Goulianos [36], who argues that σ_{DD} should decrease with energy, due to saturation effects, from around 1.6 mb at 900 GeV to around 1.3 mb at 1.8 TeV. We also note that our result is consistent with a factorized dependence on the two masses, as expected from Regge formalism:

$$\frac{d\sigma_{DD}}{dM_X^{2(R)}\,dM_X^{2(L)}} = Const. \cdot f(M_X^{2(R)}) \cdot f(M_X^{2(L)}), \tag{V.42}$$

where $f(M_X^2)$ denotes the distribution for single diffraction in (V.41).

As seen in figure V.2 the same total cross section can be obtained with different sets of values for Λ_{QCD} and r_{max}. In figure V.10 we see that varying these parameters, keeping σ_{tot} constant, does modify the elastic cross section somewhat. However, our upper limit is still close to the data, leaving little room for a contribution from the initial proton wave function.

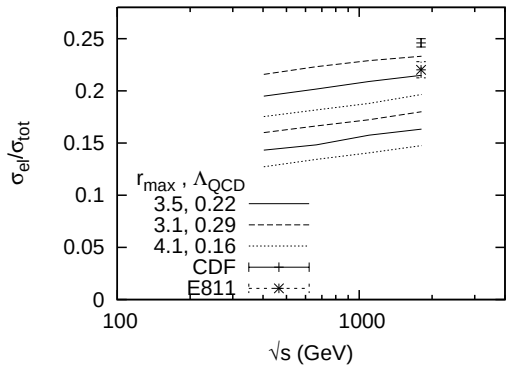

Figure V.10: The ratio of the elastic to the total cross section in pp collisions as a function of $\sqrt{s}$ for various values of $r_{max}(\mathrm{GeV}^{-1})$ and $\Lambda_{QCD}(\mathrm{GeV})$. Lower curves are obtained including fluctuations in the initial proton wavefunction, while the upper curves excludes these fluctuations. The data points are from CDF [32] and E811 [33].

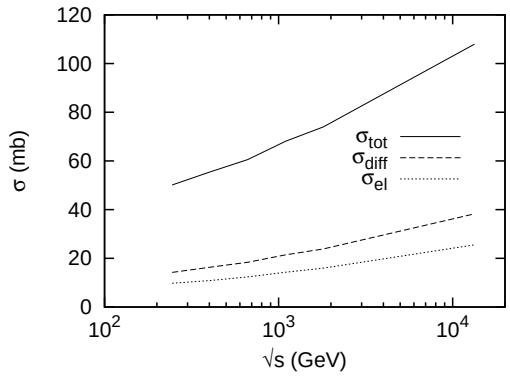

Figure V.11: The total (full line), total diffractive (dashed line) and elastic cross sections (dotted line) as a function of collision energy, $\sqrt{s}$ in pp. Here the diffractive and elastic cross sections are evaluated at $Y_0/Y = 0.5$, *i.e.* with a central gap in the cms.

V

Finally we show in figure V.11 the energy dependence of the total, the total diffractive (including elastic scattering), and the elastic cross sections, including our predictions for the LHC. (The values presented correspond to those in figure V.9b, i.e. to the more realistic results obtained neglecting the fluctuations in the initial proton wave function.) The diffractive cross section is calculated in the cms with $Y_0 = Y/2$, which demands a central gap and implies

that the diffractive excitations are limited by $M_X^2 < \sqrt{s} \cdot 1\text{GeV}$. The values we predict for the LHC are 108, 38, and 26 mb respectively.

V.4.2 Diffraction at HERA

Diffractive excitation has been measured at HERA by the ZEUS [37] and H1 [38] collaborations with two different methods. One is based on an observed rapidity gap. The ZEUS data obtained with this method [37] give the cross section integrated over all diffractively excited protons with mass $M_X^{(p)} < 2.3$ GeV. Assuming that the contribution from events where the proton is excited beyond this limit is small, and can be neglected, the result of this method for $M_X^{(\gamma)} < M_{X,max}^{(\gamma)}$ corresponds to our model calculations for σ_{diff} at $Y_0 = \ln(M_{X,max}^{2(\gamma)})$:

$$\sigma_{diff}(M_{X,max}^{2(\gamma)}) = \int^{\ln M_{X,max}^{2(\gamma)}} d\ln M_X^{2(\gamma)} \frac{d\sigma_{diff}}{d\ln M_X^{2(\gamma)}} = \sigma_{diff}^{(model)}(Y_0 = \ln(M_{X,max}^{2(\gamma)})).$$

The results are shown in figure V.12 and we see a very good agreement with data, although there is a tendency for our cross sections to decrease a bit too slowly with Q^2.

The cross section for single diffractive excitation of the photon can also be calculated in our model, and in figure V.13 we present the ratio wrt. the total diffractive cross section as a function of W for different Q^2 and M_X. In [37] the ZEUS collaboration estimated this ratio to be 0.70 ± 0.03, by comparing a parameterization[3] of their diffractive data to results from their leading proton spectrometer. This results is obtained using the assumption that the ratio is independent of W, Q^2 and M_X. Comparing with figure V.13 we find that our result is consistent with the ZEUS number, but that we predict that the ratio actually does have a small dependence on M_X and Q^2.

V.5 Conclusions and Outlook

We have in earlier papers presented an extension of Mueller's dipole cascade model, which includes subleading effects from energy conservation and running coupling as well as colour suppressed effects from pomeron loops. The model is also implemented in a MC simulation program, which simplifies the comparison between theoretical ideas and experimental data, and allows more detailed studies of important non-leading effects. Calculations of total

[3] Using a modified version of the model in [39].

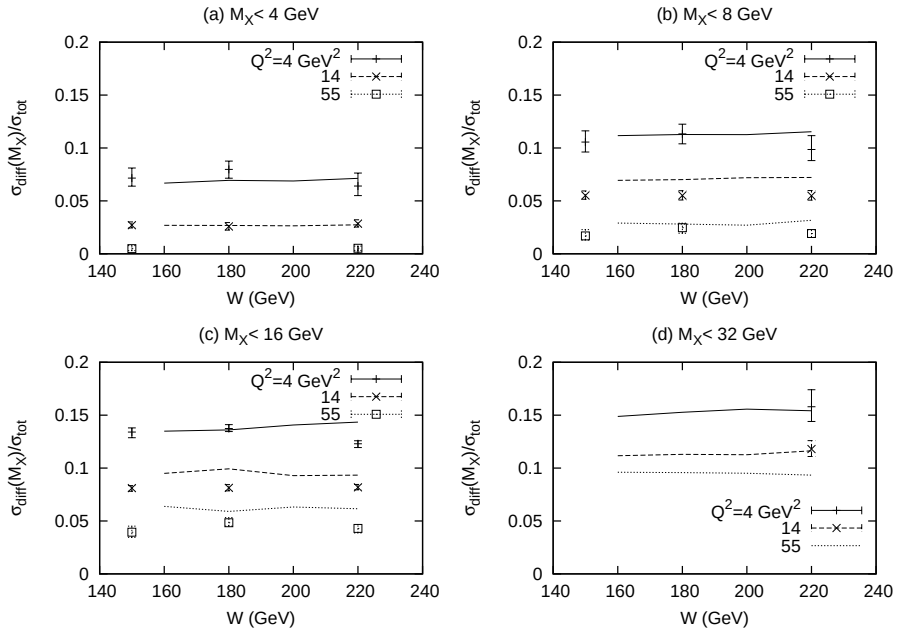

Figure V.12: The ratio of the total diffractive cross section to the total cross section as a function of W, for $M_X < 4$ (a), 8 (b), 16 (c) and 32 GeV (d). Our results are compared to ZEUS data [37] for $Q^2 = 4$ (full lines and + points), 14 (dashed lines and x points) and 55 GeV^2 (dotted lines and open squares).

cross sections agree very well with experimental results for pp collisions and deep inelastic electron scattering.

To gain further insight into small-x evolution and saturation, we have in this paper first presented a number of improvements of the model, in particular related to the confinement mechanism, and thereafter applied the model to elastic scattering and diffractive excitation, where we specifically study the effects of different sources for fluctuations.

A consistent treatment of confinement effects is achieved by replacing the infinite range Coulomb potential in the dipole splitting and in the dipole–dipole scattering with a screened Yukawa potential. By equating the screening length, $r_{\max}$ with the size of the proton entering into its wavefunction, we were able to get a good, boost-invariant description of the pp and $\gamma^\star p$ total cross sections for a wide range of energies, using basically only two parameters, $r_{\max}$ and $\Lambda_{\rm QCD}$. This new treatment of confinement has effects on the boost invariance of the model, further improving the earlier, almost frame in-

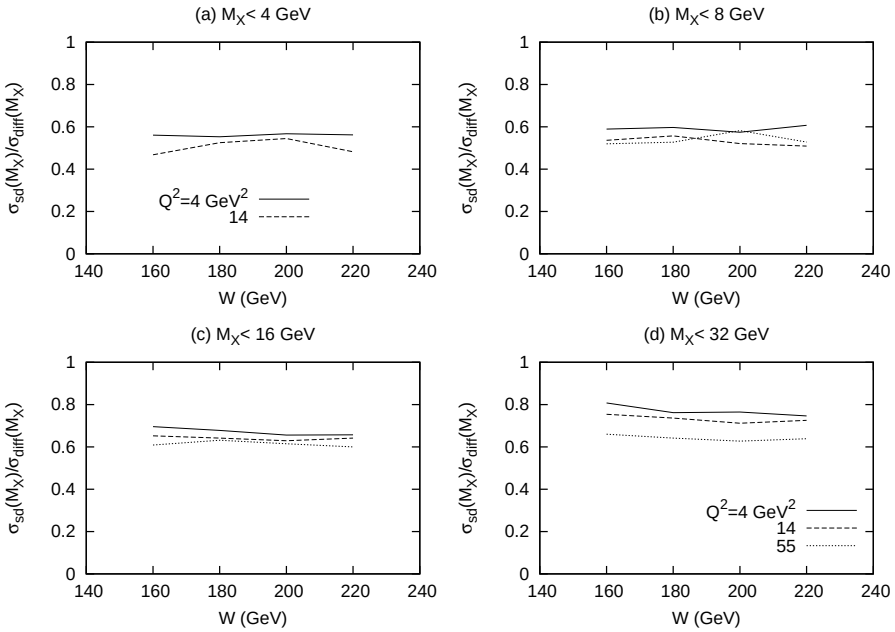

Figure V.13: The ratio of the single diffractive cross section to the total diffractive cross section as a function of W, for $M_X < 4$ (a), 8 (b), 16 (c) and 32 GeV (d) for $Q^2 = 4$ (full lines), 14 (dashed lines) and 55 GeV^2 (dotted lines).

dependent, results.

Our treatment of diffraction is based on the formalism of Good–Walker and Miettinen–Pumplin. The cross sections for elastic scattering and diffractive excitation are here determined by the fluctuations in the interaction probability between different events. Contrary to other calculations, we can in our model easily consider all different sources for such fluctuations; those stemming from the dipole cascade evolution, the dipole–dipole scattering, from the impact parameter dependence, and from the initial photon and proton wavefunctions. We find that all of these sources give important contributions, apart from the initial proton wavefunction, and together they give a very good description of data on elastic and single- and doubly-diffractive scattering in both $\gamma^\star p$ and pp collisions. We must, however, admit that we do not have a realistic quantum-mechanical description of the proton state in terms of dynamical variables. Here data are best reproduced if the contribution from the fluctuations in the initial proton state are small compared to the other contributions.

In a future publication we will use our model to study the quasi-elastic reactions $\gamma^\star p \to Vp$ and deeply inelastic Compton scattering (DVCS). In the future we also want to develop the model further to be able to describe exclusive multi-particle final states. This needs, however, a recipe for how to handle the virtual dipoles, those which do not participate in the collision and therefore cannot come on shell and give final state hadrons. To describe particle production in the proton fragmentation regions would also need a much improved description of the initial proton state.

V References

[1] T. Sjostrand and M. van Zijl *Phys. Rev.* **D36** (1987) 2019.

[2] **UA8** Collaboration, R. Bonino *et al. Phys. Lett.* **B211** (1988) 239.

[3] **CDF** Collaboration, F. Abe *et al. Phys. Rev. Lett.* **79** (1997) 2636–2641.

[4] **D0** Collaboration, B. Abbott *et al. Phys. Lett.* **B531** (2002) 52–60, hep-ex/9912061.

[5] **ZEUS** Collaboration, M. Derrick *et al. Phys. Lett.* **B315** (1993) 481–493.

[6] **H1** Collaboration, T. Ahmed *et al. Nucl. Phys.* **B429** (1994) 477–502.

[7] K. Golec-Biernat and M. Wusthoff *Phys. Rev.* **D59** (1999) 014017, hep-ph/9807513.

[8] K. Golec-Biernat and M. Wusthoff *Phys. Rev.* **D60** (1999) 114023, hep-ph/9903358.

[9] A. H. Mueller *Nucl. Phys.* **B415** (1994) 373–385.

[10] A. H. Mueller and B. Patel *Nucl. Phys.* **B425** (1994) 471–488, hep-ph/9403256.

[11] A. H. Mueller *Nucl. Phys.* **B437** (1995) 107–126, hep-ph/9408245.

[12] E. Iancu, G. Soyez, and D. N. Triantafyllopoulos *Nucl. Phys.* **A768** (2006) 194–221, hep-ph/0510094.

[13] M. Kozlov, E. Levin, and A. Prygarin hep-ph/0606260.

[14] G. P. Salam *Acta Phys. Polon.* **B30** (1999) 3679–3705, hep-ph/9910492.

[15] E. Avsar, G. Gustafson, and L. Lönnblad *JHEP* **07** (2005) 062, hep-ph/0503181.

[16] E. Avsar, G. Gustafson, and L. Lonnblad *JHEP* **01** (2007) 012, hep-ph/0610157.

[17] M. L. Good and W. D. Walker *Phys. Rev.* **120** (1960) 1857–1860.

[18] Y. Hatta, E. Iancu, C. Marquet, G. Soyez, and D. N. Triantafyllopoulos *Nucl. Phys.* **A773** (2006) 95–155, hep-ph/0601150.

[19] B. Andersson, G. Gustafson, and J. Samuelsson *Nucl. Phys.* **B467** (1996) 443–478.

[20] B. Andersson, G. Gustafson, and H. Kharraziha *Phys. Rev.* **D57** (1998) 5543–5554, hep-ph/9711403.

[21] E. Avsar and G. Gustafson *JHEP* **04** (2007) 067, hep-ph/0702087.

[22] E. Avsar arXiv:0709.1371 [hep-ph].

[23] I. Balitsky *Phys. Rev.* **D75** (2007) 014001, hep-ph/0609105.

[24] Y. V. Kovchegov and H. Weigert *Nucl. Phys.* **A789** (2007) 260–284, hep-ph/0612071.

[25] I. Balitsky. Talk presented at the ISMD07, Berkeley, August 2007, see http://www-rnc.lbl.gov/ISMD/.

[26] H. I. Miettinen and J. Pumplin *Phys. Rev.* **D18** (1978) 1696.

[27] H. Kowalski and D. Teaney *Phys. Rev.* **D68** (2003) 114005, hep-ph/0304189.

[28] S. Sapeta and K. Golec-Biernat *Phys. Lett.* **B613** (2005) 154–161, hep-ph/0502229.

[29] A. H. Mueller and G. P. Salam *Nucl. Phys.* **B475** (1996) 293–320, hep-ph/9605302.

[30] G. P. Salam *Nucl. Phys.* **B461** (1996) 512–538, hep-ph/9509353.

[31] **CDF** Collaboration, F. Abe *et al. Phys. Rev.* **D50** (1994) 5535–5549.

[32] **CDF** Collaboration, F. Abe *et al. Phys. Rev.* **D50** (1994) 5550–5561.

[33] **E811** Collaboration, C. Avila *et al. Phys. Lett.* **B445** (1999) 419–422.

[34] **E710** Collaboration, N. Amos *et al. Phys. Lett.* **B301** (1993) 313–316.

[35] **UA5** Collaboration, R. E. Ansorge *et al. Z. Phys.* **C33** (1986) 175.

[36] K. Goulianos *Phys. Lett.* **B358** (1995) 379–388.

[37] **ZEUS** Collaboration, S. Chekanov *et al. Nucl. Phys.* **B713** (2005) 3–80, hep-ex/0501060.

[38] **H1** Collaboration, C. Adloff *et al. Z. Phys.* **C76** (1997) 613–629, hep-ex/9708016.

[39] J. Bartels, J. R. Ellis, H. Kowalski, and M. Wusthoff *Eur. Phys. J.* **C7** (1999) 443–458, hep-ph/9803497.